Modelling the Generation of Toxic Combustion Products and its Transport in Enclosure Fires

Arun Mahalingam

Submitted as partial fulfilment of the requirement for the Degree of
Doctor of Philosophy

October 2007

Fire Safety Engineering Group
Centre for Numerical Modelling and Process Analysis
School of Computing and Mathematical Sciences
The University of Greenwich
Park Row, Greenwich SE10 9LS

Abstract

Combustion products generated in enclosure fires can be transported throughout the enclosure causing death and injury to occupants and a great deal of damage to property and the environment. The ability to estimate the generation and transport of toxic combustion products in real fire scenarios involving common building materials is of great importance to fire protection engineers in producing detailed quantified risk assessment and in the design of fire-safe buildings. Most common building materials are polymer based. Thus toxic products evolving from burning polymers is the single most important factor in fire fatalities. Fire hazard calculations require modelling of heat generation, toxic combustion products generation and its transport in realistic building scenarios involving common building materials. However, the thermal decomposition, combustion behaviour and chemical kinetics for common polymers like wood, plastics, rubber and textiles are extremely complex. In the present study, a methodology (**STEM-LER**: the **S**calar **T**ransport **E**quation based **M**odel using the **L**ocal **E**quivalence **R**atio concept) based on solving separate transport equations for the species and using the yield correlations obtained from bench-scale experiments to model the source terms is proposed to predict the products generation and its transport during enclosure fires. Modelling of complex solid phase degradation and chemical kinetics of polymers is bypassed by measuring the product yields as a function of equivalence ratio by burning the samples in a bench-scale combustion apparatus called Purser furnace. Since the accuracy of prediction depends upon the quality of the yield data obtained from the Purser furnace, attempts were also made to numerically investigate this bench-scale toxicity test method in order to understand its modus operandi.

Also, large-scale fire tests were carried out involving combustible cable materials to generate the validation data for the combustion and toxicity models developed in the current work. Simulations were carried out using the proposed methodology to simulate the large-scale cable fires and validated with the experiments. Irrespective of the errors involved in approximating the complex physical and chemical processes, the **STEM-LER** methodology is able to model the combustion products generation near the fire and its transport to distant locations with reasonable accuracy.

Finally, a preliminary assessment on the effect of cable fires on building evacuation for the simulated fire scenarios were carried out using a sophisticated evacuation model.

Acknowledgements

I sincerely wish to thank my supervisors Dr. Mayur Patel, Dr. Fuchen Jia and Prof. Ed Galea for giving me the opportunity, resources and excellent support to complete my PhD work at the Fire Safety Engineering Group (FSEG).

I would also like to thank Mr. Krzysztof Lebek and Dr. Richard Hull who were at CMRI, University of Bolton for helping me to understand the Purser furnace experiment. Borealis AB, Austria is acknowledged for their financial support and Mr. James Robinson and Dr. Bernt-Åke Sultan are acknowledged for being kind through out the project and making the regular project progress meeting informal.

Large-scale experiments were pivotal to my PhD research and would not have been possible without the fantastic technicians at SP Fire Technology, Sweden. Special thanks go to Mr. Henry Persson who was the head of the experimental team for his help during my stay at SP, Sweden.

Definitely, I cannot forget to thank Dr. Zhaozhi Wang (FSEG) with whom I had several wonderful and thought provoking technical discussions. Thank-you to my examiners, Prof. Koulis Pericleous (internal) and Prof. Jennifer Wen (external), for managing to read the whole thing so thoroughly, and for a surprisingly enjoyable Viva. I would also like to thank my friends, colleagues and all the rest of the academic and support staff of the School of Computing and Mathematical Sciences, University of Greenwich.

Last but not the least I am gratefully indebted to my parents and my wonderful wife Veena who supported me all through this work and being patient with me when I was not available to them or generally absent-minded.

Nomenclature

a	Coefficient of Oxygen in a chemical reaction equation
A	Eddy-break Up constant
Ar	Area [m^2]
b	Coefficient of Carbon monoxide in a chemical reaction equation
c	Coefficient of Carbon dioxide in a chemical reaction equation
c_p	Specific heat capacity [kJ/(K kg)]
d	Coefficient of water vapour in a chemical reaction equation
D_r	Radiative denominator
FIH_c	Convective heat hazard attribute
FIH_r	Radiative heat hazard attribute
FIN	Toxic gas hazard attribute
g	Acceleration due to gravity [m^2/s]
h	Enthalpy [J]
k	Turbulent kinetic energy
$\dot{m}_{fuel}$	Mass of the gas in upper layer derived from the fuel
$\dot{m}_{air}$	Mass of the gas that is introduced from the ambient air
Pr	Pressure [Pa]
q	Radiative flux [kW/m^2]
R_f	Fuel burning rate [kg/s]
S_{co}	Source term for CO transport equation [kg/s]
S_{co2}	Source term for CO_2 transport equation [kg/s]
So_2	Source term for O_2 transport equation [kg/s]
S_{h2o}	Source term for H_2O transport equation [kg/s]
St	Stoichiometric
t	Time in [s] or [min] (depending on the specific application)
T	Temperature in [K] or [^0C] (depending of the specific application)
Δh_c	Heat of combustion [MJ/kg]
u	Velocity along a coordinate axis [m/s]
V	Velocity [m/s]

Y_{co}	Mass fraction of CO
Y_{co2}	Mass fraction of CO_2
Yo_2	Mass fraction of O_2
Y_{fuel}	Mass fraction of fuel
Y_{h2o}	Mass fraction of H_2O

Greek symbols

α	Yield correlation coefficient
β	Yield correlation coefficient
ξ	Mixture fraction
ζ	Yield correlation coefficient
ϕ	Any dependant flow variable
ϕ_c	Compartment equivalence ratio
ϕ_g	Global Equivalence Ratio
ϕ_{local}	Local Equivalence Ratio
ϕ_p	Plume equivalence Ratio
ϕ_{ul}	Upper layer equivalence ratio
ρ	Density [kg/m^3]
ν	Stoichiometric air to fuel ratio
κ	Karman constant
ε	Dissipation rate of turbulent kinetic energy
μ_{lam}	Laminar viscosity
ν_t	Turbulent viscosity
Γ_ϕ	Diffusive coefficient of a flow variable ϕ

Subscripts

i	Species i or X co-ordinate direction (depending on the application)
j	Y co-ordinate direction
f	fuel
t	Turbulent

List of Figures

Figure 1.1 Deaths by cause, UK 2005 1

Figure 1.2 Total economic cost of fire in UK and US 4

Figure 1.3 Total civilian deaths 4

Figure 2.1 Schematic of the two-layer system created in hood experiments of Beyler 13

Figure 2.2 CO yields as a function of ϕ_p for various fuels studied by Beyler 14

Figure 2.3 Mole fractions of CO 15

Figure 2.4 Mole fractions of O_2 15

Figure 2.5 Chemical kinetics model calculated species concentration vs time for ϕ_g = 1.36 at temperature 1000 K 20

Figure 2.6 Comparison of normalized CO yield correlations obtained for hexane fires between the compartment fires of Gottuk [1992b] (shown in circles) and Beyler's hood experiments 23

Figure 2.7 Scheme of the Real-Scale Test Rig used by Fei et al. 26

Figure 2.8 Cross-section of a power cable showing the components 27

Figure 2.9 Compartment/hallway experimental setup used by Ewens [1994]. 31

Figure 2.10 Layout of the first level of the experimental building-fire facility, instrumentation and fuel configuration 32

Figure 3.1 Illustration of Field Modelling Concept 41

Figure 3.2 State relations for Polypropylene (C_3H_6) 48

Figure 3.3 Staggered Grid arrangement for Velocity Components and Pressure ...51

Figure 4.1 CO and CO_2 yields for NYM 62

Figure 4.2 CO and CO_2 yields for NHMH 63

Figure 4.3 CO and CO_2 yields for RZ1-K 64

Figure 4.4 Comparison of state relationship for NHMH (C_3H_6) 67

Figure 5.1 Purser furnace 73

Figure 5.2 Purser furnace photos 77

Figure 5.3 Tube furnace geometry 83

Figure 5.4 Computational geometry and grid details 84

Figure 5.5 Wall temperature distribution of tube furnace hot zone (Primary air flow = 15 l/min). 85
Figure 5.6 Wall temperature distribution of tube furnace hot zone (Primary air flow = 4 l/min). 85
Figure 5.7 Thermocouple measuring locations (details given in Table 5.3) 88
Figure 5.8 Temperature Distribution (K) for 750 ^{0}C, 4 litres/min primary air flow without sample burning. 89
Figure 5.9 Velocity vectors across the Purser furnace 89
Figure 5.10 Distribution of k and ε inside the Purser furnace 92
Figure 5.11 CO distribution inside tube furnace (NHMH) 92
Figure 5.12 CO distribution inside tube furnace (NYM) 92
Figure 6.1 Basic Layout (without the soffits) 96
Figure 6.2 Temperature contours (^{o}K) along the fire corridor (Inlet vent is at the bottom right of the figures) 98
Figure 6.3 Layout with the soffits 99
Figure 6.4 CO_2 (% volume) distribution and velocity vectors along the fire corridor (a) 100% inlet (b) 25% inlet (c) with inlet closed (d) with inlet closed and 1 m weir 99
Figure 6.5 Details of the labyrinth 100
Figure 6.6 Overview of corridor construction with the first corridor to the right and the third corridor and the calorimeter hood to the left.....100
Figure 6.7 Photographs of the large scale labyrinth construction 102
Figure 6.8 Photos taken during one of the fire test. 104
Figure 6.9 Summary of the arrangement of gas analysis instruments and position (×) for CO (yellow), CO_2 (red) and O_2 (green) measurements. 104
Figure 6.10 Load cell measurement of mass loss in kg (Test 5) 107
Figure 6.11 Temperature above horizontal tray and vertical tray (Test 5) 108
Figure 6.12 Total Heat Release Rate measured at exhaust hood by oxygen calorimetry (Test 5) 108
Figure 6.13 Load cell measurement of mass loss in kg (Test 7) 109
Figure 6.14 Temperature above horizontal tray and vertical tray (Test 7) 110

Figure 6.15 Total Heat Release Rate measured at exhaust hood by oxygen calorimetry (Test 7) 110
Figure 6.16 Load cell measurement of mass loss in kg (Test 8) 111
Figure 6.17 Temperature above horizontal tray and vertical tray (Test 8) 112
Figure 6.18 Total Heat Release Rate measured at exhaust hood by oxygen calorimetry (Test 8) 112
Figure 6.19 Load cell measurement of mass loss in kg (Test 10) 113
Figure 6.20 Temperature above horizontal tray and vertical tray (Test 10) 114
Figure 6.21 Total Heat Release Rate measured at exhaust hood by oxygen calorimetry (Test 10) 114
Figure 7.1 Computational domain and grid (Grid I) 117
Figure 7.2 CO volume fraction at location 5 124
Figure 7.3 CO volume fraction at location 9 124
Figure 7.4 CO volume fraction at location 15 125
Figure 7.5 Computed temperature distributions along the corridor 125
Figure 7.6 Positions of location 5, 9 and 15 highlighted by red dots 128
Figure 7.7 CO concentration at location 9 (Test 8) 128
Figure 7.8 CO_2 concentration at location 9 (Test 8) 129
Figure 7.9 Temperature profile at location 9 (Test 8) 129
Figure 7.10 CO concentration at location 15 (Test 8) 130
Figure 7.11(a) CO_2 concentration at location 9 (Test 8) 130
Figure 7.11(b) Temperature profile at location 15 (Test 8) 131
Figure 7.12(a) Variation of $s(\phi)$ as function of Equivalence ratio for NHMH cable 132
Figure 7.12(b) Temperature above the fire (above horizontal tray) 132
Figure 7.13 (a) Schematic of Borealis cable fire test compartment (b) Heat Release Rate during the NYM cable fire 133
Figure 7.14 (a) Accumulative CO during the NYM cable fire (b) Accumulative CO_2 during the NYM cable fire 135
Figure 7.15 (a) Mass loss rate curve (Test 8) (b) Heat Release Rate curve (HRR) during Test 8 136
Figure 7.16 CO concentration at location 5 (Test 8) 138
Figure 7.17 CO_2 concentration at location 5 (Test 8) 138

Figure 7.18 Temperature profile at location 5 (Test 8) 138
Figure 7.19 CO concentration at location 9 (Test 8) 139
Figure 7.20 CO_2 concentration at location 9 (Test 8) 139
Figure 7.21 Temperature profile at location 9 (Test 8) 140
Figure 7.22 CO concentration at location 15 (Test 8) 141
Figure 7.23 CO_2 concentration at location 15 (Test 8) 141
Figure 7.24 Temperature profile at location 15 (Test 8) 141
Figure 7.25 (a) Mass loss rate curve (Test 10) (b) Heat Release Rate curve (HRR) during Test 10 143
Figure 7.26 CO concentration at location 5 (Test 10) 143
Figure 7.27 CO_2 concentration at location 5 (Test 10) 144
Figure 7.28 CO_2 concentration in the first corridor (X = 7.5 m) 145
Figure 7.29 Temperature profile at location 5 (Test 10) 146
Figure 7.30 CO concentration at location 9 (Test 10) 147
Figure 7.31 CO_2 concentration at location 9 (Test 10) 147
Figure 7.32 Temperature profile at location 9 (Test 10) 148
Figure 7.33 CO concentration at location 15 (Test 10) 148
Figure 7.34 CO_2 concentration at location 15 (Test 10) 149
Figure 7.35 Temperature profile at location 15 (Test 10) 149
Figure 7.36 (a) Mass loss rate curve (Test 5) (b) Heat Release Rate curve (HRR) during Test 5 151
Figure 7.37 HCl release rate (Test 5) 151
Figure 7.38 CO concentration at location 5 (Test 5) 152
Figure 7.39 CO_2 concentration at location 5 (Test 5) 152
Figure 7.40 Temperature profile at location 5 (Test 5) 152
Figure 7.41 HCl concentration at location 4 (h = 2.2 m) 153
Figure 7.42 CO concentration at location 9 (Test 5) 154
Figure 7.43 CO_2 concentration at location 9 (Test 5) 154
Figure 7.44 Temperature profile at location 9 (Test 5) 154
Figure 7.45 CO concentration at location 15 (Test 5) 154
Figure 7.46 CO_2 concentration at location 15 (Test 5) 155
Figure 7.47 Temperature profile at location 15 (Test 5) 157
Figure 7.48 (a) Mass loss rate curve (Test 7) (b) Heat Release Rate curve (HRR) during Test 7 157

Figure 7.49 CO concentration at location 5 (Test 7) 158
Figure 7.50 CO_2 concentration at location 5 (Test 7) 158
Figure 7.51 Temperature profile at location 5 (Test 7) 159
Figure 7.52 CO yields vs Equivalence ratio for RZ1-K cables 159
Figure 7.53 CO concentration at location 9 (Test 7) 160
Figure 7.54 CO_2 concentration at location 9 (Test 7) 161
Figure 7.55 Temperature profile at location 9 (Test 7) 161
Figure 7.56 CO concentration at location 15 (Test 7) 161
Figure 7.57 CO_2 concentration at location 15 (Test 7) 162
Figure 7.58 Temperature profile at location 15 (Test 7) 162
Figure 8.1 EXODUS zones and a hypothetical scenario 169
Figure 8.2 Onset of flashover during the NHMH cable fire (Test 8) 171
Figure 8.3 Death locations for response time of 900 seconds 175
Figure 8.4 EXODUS zones and a hypothetical scenario 176
Figure 8.5 Incapacitation location during NYM cable fire
(Response time = 540 sec) 178

List of Tables

Table 1.1 Carbon monoxide physiological effects on Humans 2
Table 3.1 Turbulence Model Constants 45
Table 5.1 Classification of fire types and correlation with parameters needed to predict CO yields [Richard et al., 2002]. 79
Table 5.2 Boundary conditions for simulations without sample burning 86
Table 5.3 Temperature inside mixing chamber (750 ^{0}C, 4 litres/min primary air flow with empty boat) 88
Table 5.4 Temperature inside mixing chamber (750 ^{0}C, 15 litres/min primary air flow with empty boat) 89
Table 5.5 Boundary conditions for simulations without sample burning 90
Table 5.6 Comparison of yields for NYM and NHMH 93
Table 6.1 Summary of data for the cables used during tests 102
Table 6.2 Summary of the main test programme and the test conditions for each test. 102
Table 7.1 Grid Sensitivity Analysis – Peak CO and CO_2 volume fractions at location 9 and 15 (Test 8). 119
Table 7.2 Comparison of peak CO, CO_2 concentrations and CO_2/CO at location 15 130
Table 7.3 Yield correlation constants for PVC 134
Table 7.4 Comparison of peak CO, CO_2 concentrations and CO_2/CO at location 15 140
Table 7.5 LER at location 5 159
Table 8.1 Average hazard attribute values of response time of 500 seconds 172
Table 8.2 Average hazard attribute values of response time of 700 seconds 172
Table 8.3 Average hazard attribute values of response time of 900 seconds 172
Table 8.4 Effect of variation in temperature on the Incapacitation times 173
Table 8.5 Zone temperatures for measured and computed fire hazard (pre-flashover) 173
Table 8.6 Zone temperatures for measured and computed fire hazard (flashover) 173

Table 8.7 Zone temperatures for measured and computed fire hazard (post-flashover) 174
Table 8.8 Various times at which flashover starts 176
Table 8.9 Average values of hazard effect attributes for a response time of 540 second 177

Contents

Abstract

Acknowledgements

Nomenclature

List of Figures

List of Tables

1. Introduction 1

1.1. Project Motivation 2

1.1.1. Carbon Monoxide– **'The Invisible Killer'** 2

1.1.2. Building Industry 3

1.1.3. Electro-Technical Industry 5

1.1.4. The Euro-classification of Cables 6

1.2. Research Objectives and Questions 7

1.3. Layout of Thesis 9

2. Literature Review 11

2.1. Introduction 11

2.2. Small-Scale Experiments on Species Generation in Fires 11

2.2.1 Hood Experiments and the Global Equivalence Ratio (GER) Concept 11

2.2.2 Summary of Conclusions Based on Hood Experiments 17

2.3. Detailed Chemical-Kinetic Modeling of Upper-Layer Reaction Behavior ...18

2.4. Thermodynamic calculations of upper-layer composition 19

2.5. Compartment Fire Experiments 21

2.5.1 Compartment Fire Experiments Involving Cables 25

2.6. Experiments on Species Production and Transport in Real-Scale Fires 28

2.7. Mathematical Modelling of Fires 33

2.7.1 Zone Modelling 33

2.7.2 Field Modelling 34

2.8. Concluding Remarks 39

3. Field Modelling of Enclosure Fires 40

3.1. Introduction 40

3.2. Field Modelling 40

3.3. Theoretical Basis for Field Models 41

3.3.1 Conservation of Mass 42

3.3.2 Conservation of Momentum 42

3.3.3 Conservation of Energy 43

3.3.4 Conservation of Chemical Species 43

3.3.5 Turbulence Modelling 44

3.3.6 Radiation Modelling 46

3.3.7 Combustion Modelling 47

3.3.7.1 Eddy Break-Up Model (EBU) 49

3.4. Discretisation Concept 49

3.4.1 Staggered Grid 50

3.5. Solution Algortihm for Pressure – Velocity Coupling 51

3.5.1 SIMPLEC Algorithm 52

3.6. Concluding Remarks 53

4. Methodology to Predict Toxic Species Generation and Transport 54

4.1. Introduction 54

4.2. Basic Definitions 55

4.3. LER Concept 56

4.4. Numerical Model 59

4.5. STEM – LER Model 65

4.5.1 Modelling of source term in scalar transport equation for Y_{fuel}, S_{fuel} 65

4.5.2 Modelling of source terms in transport equations for $\mathbf{Y_{CO}}$, $\mathbf{Y_{CO2}}$, $\mathbf{Y_{oxidant}}$ **and** $\mathbf{Y_{H2O}}$ 69

4.6. Concluding Remarks 70

5. Purser Furnace Toxicity Test Method 72

5.1. Introduction 72

5.2. Previous Research on Purser Furnace 74

5.3. Purser Furnace Toxicity Test Method 76

5.3.1 Experimental Setup 76
5.3.2 Operating Procedure 76
5.3.3 Experimental Data 78
5.4. Simulation of Purser (Tube) Furnace Test Method 80
5.4.1 Toxicity Model 81
5.4.2 Numerical Details 82
5.4.3 Simulation of Purser Furnace without Cable Burning 85
5.4.3.1 Results and Discussion 86
5.4.4 Simulation of Purser Furnace with NYM and NHMH Cable Burning 90
5.4.4.1 Results and Discussion 91
5.5. Conclusions 93

6. Large-Scale Fire Tests 94

6.1. Introduction 94
6.2. Objectives 94
6.3. Preliminary Simulations to Study the Layout for Large-scale Fire Tests 95
6.4. Experimental Layout 100
6.5. Measurements and Recordings 103
6.5.1 Gas Analysis 103
6.5.2 Temperature Measurements 105
6.5.3 Heat Release Rate and Mass Loss 105
6.6. Test Procedure 105
6.7. Results and Discussions 105
6.7.1 NYM Cable Fire (Test 5) – Inlet closed and 1m Weir placed
6.7.2 RZ1-K Cable Fire (Test 7) – Inlet open and no Weir placed
6.7.3 NHMH Cable Fire (Test 8) – Inlet open and 1m Weir placed
6.7.4 NHMH Cable Fire (Test 10) – Inlet closed and 1.5m Weir placed
6.8. Concluding Remarks 115

7. Simulation of Large-Scale Tests 116

7.1. Introduction 116
7.2. Numerical Details 116

7.3. Grid Sensitivity Analysis 118
7.4. Simulation of large-scale cable fire tests 119
7.4.1 Modelling of CO oxidation 120
7.4.2 Modified Eddy Break-Up Combustion model (EBU) 126
7.5. Validation of the STEM-LER model 132
7.5.1 Simulation of the Borealis small room cable fire test.....133
7.5.2 Simulation of Test 8 – NHMH cables 136
7.5.3 Simulation of Test 10 – NHMH cables 142
7.5.4 Simulation of Test 5 – NYM cables 149
7.5.5 Simulation of Test 7 – RZ1-K cables 156
7.6 Concluding Remarks 162

8 Preliminary Assessment on the Effect of Cable Fires on Building Evacuation.....164

8.1. Introduction.....164
8.2. The buildingEXODUS evacuation software 165
8.3. Comparison between the Effect of Computed and Experimental Fire Environment on Building Evacuation.....168
8.3.1 Simulation of a NHMH Cable Fire Scenario using Computed and Experimental Fire Hazard Data.....168
8.4. Preliminary Assessment of Cable Fires on Building Evacuation.....175
8.5. Concluding Remarks.....178

9 Conclusions 181

9.1 Summary 181
9.2 Conclusions 183

10 Future Work 189

Appendix A 192

References 215

Chapter 1

Introduction

This chapter is dedicated to provide an overview on this project along with the justifications for its execution. Fire can be described as an exothermic oxidative process or as undesirable and hazardous combustion phenomenon. Combustion products are evolved during enclosure fires and are eventually transported throughout the building causing a great deal of damage to property and the environment, and can even cause death or injury to people. The ability to estimate the toxic hazards of combustion gases in real fire scenarios is of great importance to the fire protection engineers to design more fire-safe buildings. This chapter discusses about the significance, motivation and objectives of the project. Finally a brief description about the structure of this thesis is provided.

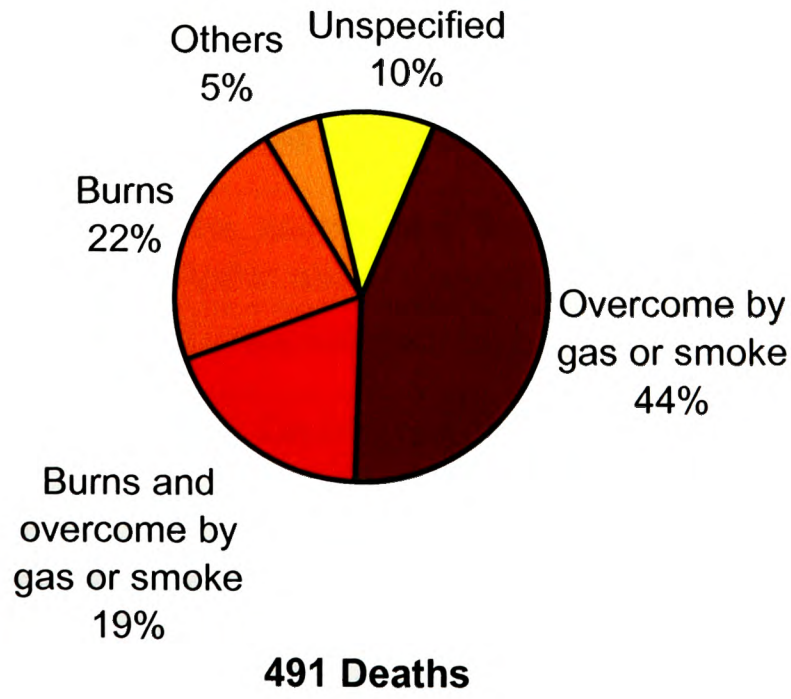

Figure 1.1 Deaths by cause, UK 2005 (components are rounded)

1.1 Project Motivation

1.1.1 Carbon Monoxide – 'The Invisible Killer'

The most common identified cause of death during the fire incidents is being overcome by gas or smoke (Figure 1.1) [ODPM Report, 2007]. Fire statistics have consistently shown that the majority of fatalities resulting from enclosure fires are due to smoke inhalation and roughly two-thirds can be attributed to the Carbon monoxide (CO) poisoning [Hall 1997; Hirschler et al., 1993; Gann et al., 1994; ODPM Report, 2007]. In addition, two-thirds of the smoke inhalation victims were found at locations remote from the room of fire origin [Gann et al., 1994]. CO is an odourless, colourless gas that kills people by blocking the oxygen carrying capacity of the blood. This is due to the fact that the haemoglobin in the blood has 3000 times greater affinity towards CO than that for oxygen. The physiological effects of increased CO levels in the body include incapacitation, asphyxiation, and death [Wieczorek, 2003]. The physiological effects of CO levels with exposure time on humans are listed in Table 1.1 [NFPA Report, 2000].

Table 1.1 Carbon monoxide physiological effects on Humans

Level	Physiological Effect
50 ppm	Threshold limit value for no adverse effects
200 ppm	Possible mild headache after 2-3 hours
400 ppm	Headache and nausea after 1-2 hours
800 ppm	Headache, nausea, and dizziness after 45 minutes; collapse and possible unconsciousness after 2 hours
1000 ppm	Loss of consciousness after 1 hour
1600 ppm (0.16 %)	Headache, nausea, and dizziness after 20 minutes
3200 ppm (0.32 %)	Headache and dizziness after 5-10 minutes; unconsciousness after 30 minutes
6400 ppm (0.64 %)	Headache and dizziness after 1-2 minutes, unconsciousness and danger of death after 10-15 minutes
12,800 ppm (1.28 %)	Immediate physiological effects; unconsciousness and danger of death after 1-3 minutes

Generation of toxic combustion products like CO is a complex function of air availability, nature of mixing, fuel and oxidant properties, temperature etc. despite the fact that it is a relatively stable molecule [Kuo 1986; Drysdale 1998; Karlsson et al. 2001; Tuovinen 1995]. The fatality statistics on CO poisoning clearly indicate the need for models that can accurately predict the generation and transport of CO during real fires.

1.1.2 Building Industry

Fire hazard calculations require modelling of heat generation, toxic combustion products generation and its transport in realistic building scenarios. The species of interest to the fire safety engineer would most often be CO, CO_2, and O_2, but concentrations of other combustion products may also be of interest; for example, Hydrogen Chloride (HCl) can cause corrosion leading to the failure of critical electronic components, and can be directly linked to mobility of people evacuating [Galea et al., 2004]. For decades, statistics have consistently shown that the key factor in fire fatalities is smoke inhalation, not only in the fire enclosure but also in areas remote from the fire compartment.

The following description of two such incidents is taken from Lattimer et al. [1997]. On October 5, 1989 at the Hillheaven Nursing Home in Norfolk, Virginia, US, a fire in a patient's room resulted in the death of 13 people. Each victim died of CO poisoning with 12 of the victims found in a room or position down the hallway from the room containing the fire. Twenty-three (23) patients resided along the wing containing the burning room. Nine (9) of the victims were found in rooms on the opposite side of the hallway from the burning room while 1 victim was found on the burning room side of the hallway. A similar type fire in a Southern Michigan hospice, US on December 15, 1985 claimed the lives of 8 people. Six (6) victims died of CO poisoning and were found in rooms down the hallway from the burning room.

Besides loss of life, fires cost billions of pounds worldwide, from damage to property, loss of business etc. Figure 1.2 gives the economic cost of fire for the period 2000-05 in UK and US [ODPM Report, 2007; Karter, 2006]. The total cost of fire in UK includes the costs incurred in anticipation of fire, such as fire protection measures in

buildings. The figures for UK are in pounds and the figures for US are in dollars. The US figures shows only the direct property loss due to fires. The figure for US during 2001 includes $ 33.44 billion in property loss that occurred from the events of 9/11/2001.

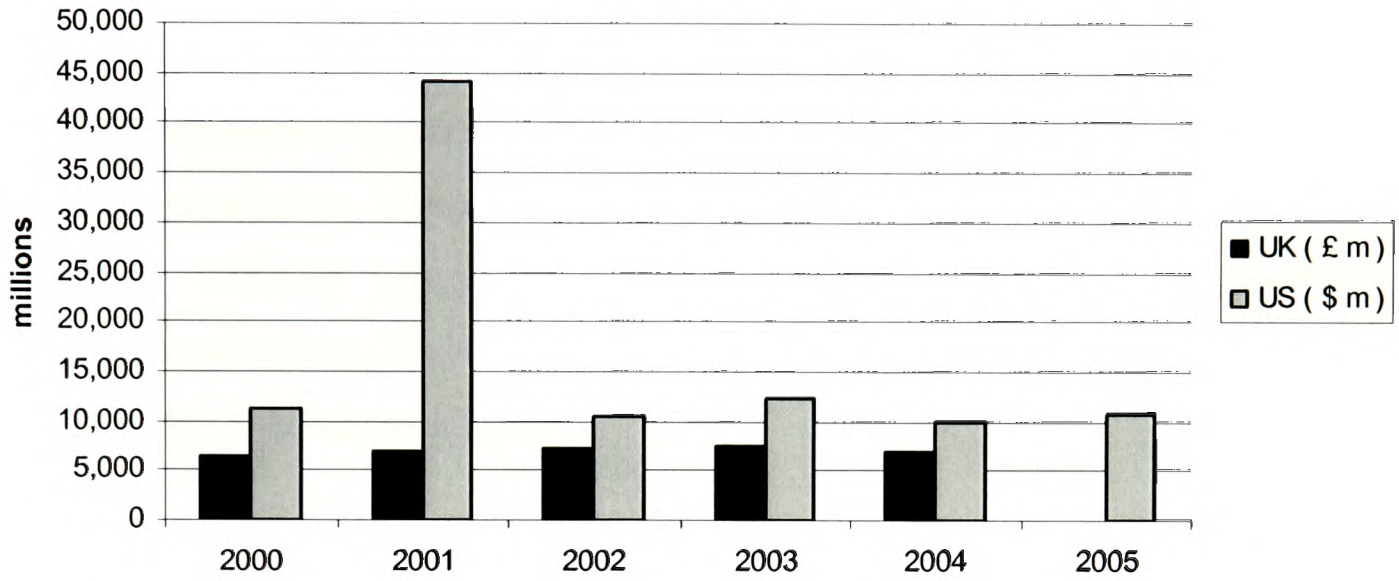

Figure 1.2 Total economic cost of fire in UK and US (based on the current prices and the UK data for 2005 not available)

Figure 1.3 gives the number of civilian deaths in fires reported for the period 2000-05 in UK and US [Fire statistics monitor UK, 2006; Karter, 2006]. The US figure during 2001 includes the 2,451 civilian deaths from the events of 9/11/2001.

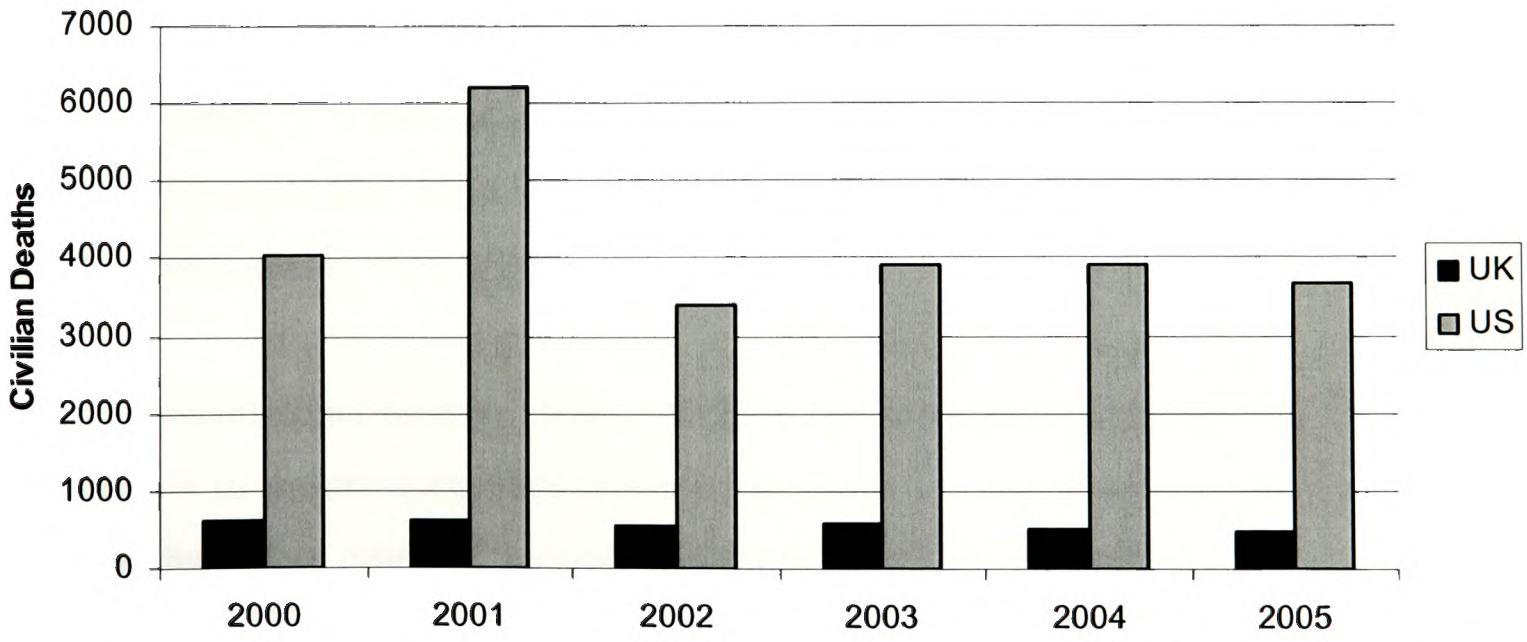

Figure 1.3 Total civilian deaths

Fire safety engineering analysis of buildings includes some degree of assessment of the tenability by occupants in the event of fire. These assessments include estimates of the time available for people to escape a burning facility or find refuge within. Performance based life safety building design depends on a comparison between the time required for escape (Required Safe Egress Time – RSET) and the time to loss of tenability (Available Safe Egress Time – ASET). The time to incapacitation or the ASET during a fire is determined by the integrated exposure of a person to the fire effluent components. Calculation of integrated exposure of the fire environment on evacuating population requires the distribution (both spatial and temporal) of temperature, radiation fluxes and combustion product gases etc. throughout the building. Computational Fluid Dynamics (CFD) can be utilised to generate the data required for the evacuation analysis.

1.1.3 Electro-technical Industry

The world's annual consumption of plastic materials has increased from around 5 million tonnes in the 1950s to nearly 100 million tonnes today. In the global plastic materials market, the cable segment reflects the sale of power and telecoms cables. In 2005 the global cable market generated total revenues of $ 29.4 billion.

In most scenarios, the combustible materials fuelling unwanted fires are organic based polymers which may sometimes include flame retardant additives. Toxic products evolving from burning polymers is the single most important factor in fire fatalities [Hull et al. 2000]. The thermal decomposition, combustion behaviour and chemical kinetics for polymers like wood, plastics, rubber and textiles are complex [Sultan and Paul 2002; Hermansson et al. 2003].

The toxic species concentration varies with time and space during an evolving fire as the generation of products depends on both the yields i.e., the amount of each toxic product produced per unit fuel burned, and the local vitiation condition. The former are commonly obtained using a bench-scale combustion apparatus. There are a number of ways in which the toxicity information can be obtained [Gann, 2004]. Purser furnace is one such apparatus which is able to reproduce burning of samples

under various decomposing conditions occurring in different types and stages of real fires. These data are often used in toxic hazard calculations and chemical analyses of the toxic potency of products. The chemical analyses of the products is further utilised to improve the fire properties of polymer used in electro-technical products such as power cables, communication cables and plastics. The accuracy of the hazard calculations depends on the accuracy of the yield data obtained from the bench-scale apparatus. The geometry, test method, experimental procedure and the operating parameters can affect the performance of bench-scale toxicity test methods. Fire field models which are based on CFD technique can be used to simulate the fire environment inside the bench-scale combustion apparatus to validate the physical models. Simulations can further be used to get some insights on working of some bench-scale toxicity test methods for e.g. Purser furnace.

1.1.4 The Euro-Classification of Cables

In 1988, the European Commission released the 'Construction Product Directive (CPD)' [Evans, 1998; Leoz Arguelles, 1999]. The main objective of this directive is to 'remove technical barriers to trade arising from national laws and regulations in Member States of the EU, thus enabling the single European market in construction products'. Hence, the purpose of the CPD is trade liberalisation. In the same year it was decided that fixed cables within buildings should be regarded as one of the construction products. Euro-classification rates the cables in terms of a number of parameters viz., fire growth, heat release, flame spread, dripping and smoke. These parameters for any cable products are normally assessed by prescriptive standards such as single and bunched vertical burning. Essentially these tests concern fire propagation on a pass/fail basis [Robinson, 1999].

Cable producing companies are working on a mission to change the CPD regulations towards performance based Euro-classification. In order to change the regulations such as CPD, real and quantifiable benefits needs to be brought out [Robinson, 2006]. The principal perceived benefit of Low Smoke Zero Halogen (LSZH) cable technology is the reduction in fire effluent toxicity and irritancy giving improved fire safety in terms of building evacuation. Assessment of the impact of cable fire

environment on building evacuation can be utilised to rate the cables based on their overall performance.

In summary, some important applications of the CFD fire simulation are as follows:

- Designing of 'fire-safe' buildings.
- Analyse the effect of toxicity of the materials on people in the event of fire. The input can be used to suggest 'safer' materials.
- Classification of combustible materials based on their overall performance.
- Analysis of toxicity test methods and experiments to improve their performance and accuracy which are conducted to measure the toxicity of materials.

1. 2 Research Objectives and Questions

During recent years, there has been growing concern about the potential of fires in residential, public facilities, transportation etc. due to growing amount of combustible materials inside these enclosures. In order to perform quantified risk assessments and to design 'fire-safe' buildings, performance based toxic hazard calculations are necessary. CFD based fire field modelling is a viable choice to carry out fire hazard calculations. The main aim of the present study is to extend the fire field model generally used, i.e. the volumetric heat source model and the Eddy-BreakUp approach, to include the capability of predicting the production of toxic combustion products and transport to distant locations from the fire origin. The objectives set to be achieved in the development of the toxicity model during the present research are as follows:

1. Conduct literature survey in order to gain present understanding on the formation mechanisms of CO and other toxic combustion products and their transport in fires through hood experiments, compartment fire experiments and full-scale experiments. Emphasis should be given on combustible polymers like wood, plastics etc. Literature review should also focus on the available

toxicity models for the simulation of toxic combustion product formation in fires involving complex solid fuels.

2. Develop a simple, yet sophisticated model to predict the final levels of CO and other toxic products generated and transported to distant locations from the fire origin.
3. Identify the appropriate and corresponding toxicity data required for the materials to be considered in the present study as inputs to the toxicity model from the bench scale experiments.
4. Literature survey on the available large-scale experimental data for combustible polymers to validate the combustion, toxicity and the transport model.
5. Conduct large scale fire tests and obtain comprehensive set of fire data for the purpose of validating the above toxicity model.
6. Validation of the methodology developed in the present study to predict the final levels of CO and other toxic products generated and transported to distant locations from the fire origin.
7. Validation of the experimental data (yield correlations) obtained from the bench-scale tests (Purser furnace) in predicting the large-scale fires.

The following research questions will be attempted to answer vis-à-vis the development of the toxicity model within the CFD fire field modelling framework:

- How can the species generation and transport in real-scale fires be predicted using the yield data obtained from the Purser furnace bench-scale tests (IEC 60695-7-50 and ISO/CD 19700)?
- Can CFD simulate the thermal and flow conditions inside bench-scale experiments like Purser furnace? How CFD can be used as a design tool to improve the performance of the Purser furnace?
- How are the combustion models important in predicting the species concentrations at distant locations? Eddy Break-Up model [Magnussen and Hjertager, 1977] under predicts the combustion rate in fuel-rich regions, how this model can be modified to improve the prediction?

- How does the fire environment affect the movement of people during the evacuation process? Can the computed fire environment in real-scale building scenarios be used to provide good engineering judgements such as the 'survivability' and 'suitability of materials'?

1. 3 Layout of Thesis

In Chapter 2, literature review on (a) experiments describing the characteristics of the species production, (b) transport of species from compartment fires, and (c) modelling of generation and transport of combustion products during fires are provided.

The theoretical basis for the fire field modelling approach is presented in detail in chapter 3. In addition, the turbulence model, radiation model and the basic combustion model used in the present investigation are also discussed.

For the prediction of CO and CO_2 concentrations and their final levels that are transported to distant locations, a new model, **S**calar **T**ransport **E**quations based **M**odel using the **L**ocal **E**quivalence **R**atio concept (**STEM-LER**) is proposed and discussed in detail in chapter 4. The model utilises the yield data obtained from the bench-scale tests to model the source terms for CO and CO_2 to simulate real-scale fires. A modified Eddy Break-Up (MEBU) model is also described which takes into consideration the CO generation. This MEBU is used along the STEM-LER model to model the fuel burning rate.

Purser furnace is a bench-scale tube furnace toxicity test method in which the polymer samples are decomposed under various vitiation conditions occurring in different types and stages of real fire. The yields of CO and CO_2 for the various samples are measured as a function of equivalence ratio. The yield correlations obtained from this bench-scale experiment will be used to model the source terms in the STEM-LER model. Chapter 5 describes the previous research on Purser furnace experiments, experimental setup and the operating procedure. Numerical investigations were also carried out to demonstrate the ability of CFD to simulate the purser furnace and to get some insights on the working of the toxicity test method.

In Chapter 6, the experimental details and results of the large scale cable fire tests conducted at SP, Sweden during October 2005 are provided and discussed. The objective of the large scale tests is to provide a comprehensive fire data to validate the STEM-LER model.

Chapter 7 is devoted to the simulations of large scale cable fire tests selected from the series of fire tests discussed in Chapter 6 involving three different power cables. The simulations were carried out using the STEM-LER model. The simulation results of CO, CO_2 and temperature at various locations along the corridor are validated with the experimental results.

In Chapter 8, the effect of experimental fire hazard data is compared with the simulated fire hazard data for a hypothetical evacuation scenario. Also, a preliminary assessment on the effect of simulated cable fire environments on the evacuation is performed.

Finally, a summary on the research work carried out during this project and the important conclusions are presented in Chapter 9 with some remarks on future directions in further improving the methodology given in Chapter 10.

Chapter 2

Literature Review

2.1 1ntroduction

A complete building fire hazard assessment requires the knowledge of toxic chemical species production and its transport to remote locations from the fire. Typically, the combustion products generated during real fires involving common building materials include chemical species such as acid gases, CO, CO_2, HCN, NO_x, SO_2, unburned hydrocarbons, soot, polycyclic aromatic hydrocarbons (PAH), volatile organic compounds (VOC) and formaldehyde to name a few [Andersson et al., 2004]. This chapter discusses previous research on the current understanding of species production near the fire and transport of these gases from the fire origin to adjacent areas.

2.2 Small-Scale Experiments on Species Generation in Fires

2.2.1 Hood Experiments and the Global Equivalence Ratio (GER) Concept

Significant progress has been made on identifying the various formation mechanisms for combustion product species such as CO within an enclosure containing fire. Pitts [1995] in his article gives an extensive review summarising research on CO formation in fires up to 1994. In a typical compartment fire, a two-layer system is formed in which the upper

layer consists of hot combustion products that collect below the ceiling, and the lower layer consists of primarily the ambient air that is entrained into the base of the fire. Much of the progress in understanding CO formation mechanisms in real-scale fires are built on a series of 'hood' experiments. Beyler [1986a; 1986b] was the first to propose that it might be possible to correlate the species yields and species production rates to an overall fuel-to-air ratio(equivalence ratio). The experiments performed consisted of placing a burner underneath a 1 m diameter insulated hood which resulted in the formation of a layer of combustion products in the hood similar to that found in a two-layer compartment fire. The schematic of the two-layer system created in the hood experiments of Beyler is shown in Figure 2.1. By varying the fuel supply rates and the distance between the burner and the layer interface, and, consequently, the air entrainment rate, a range of equivalence ratios was obtained. Beyler's results [1986a; 1986b] showed that the species yields correlate very well with the plume equivalence ratio (ϕ_p) in his experiments which is equivalent to the Global Equivalence Ratio (GER) under steady state conditions. The GER, defined in equation 2.1, indicates whether a fire is fuel or ventilation controlled.

$$\phi_g = \frac{\left[\frac{\dot{m}_{fuel}}{\dot{m}_{air}}\right]}{\left[\frac{\dot{m}_{fuel}}{\dot{m}_{air}}\right]_{St}} \tag{2.1}$$

where $\dot{m}_{fuel}$ is the mass of the gas in the upper layer derived from the fuel, $\dot{m}_{air}$ is the mass of the gas that is introduced from air and $\left[\frac{\dot{m}_{fuel}}{\dot{m}_{air}}\right]_{St}$ is the stoichiometric mass ratio that is required for complete burning of the fuel to fully oxidized products.

Beyler presented the results of CO yields for gaseous, liquid, and solid fuels as a function of the plume equivalence ratio which is shown in Figure 2.2 [Gottuk and Roby, 1995]. Beyler concluded that below an equivalence ratio of 0.6 a constant minimal CO production was observed. Above $\phi_p = 0.6$, CO yield increases with ϕ_p and, for most fuels,

tends to level out at $\phi_p > 1.2$. When presented as unnormalised yields, the data clearly indicates fuel type independence; however, Beyler reported that if presented as a normalized yield, the CO production can be ranked by chemical structure according to oxygenated hydrocarbons > hydrocarbons > aromatics.

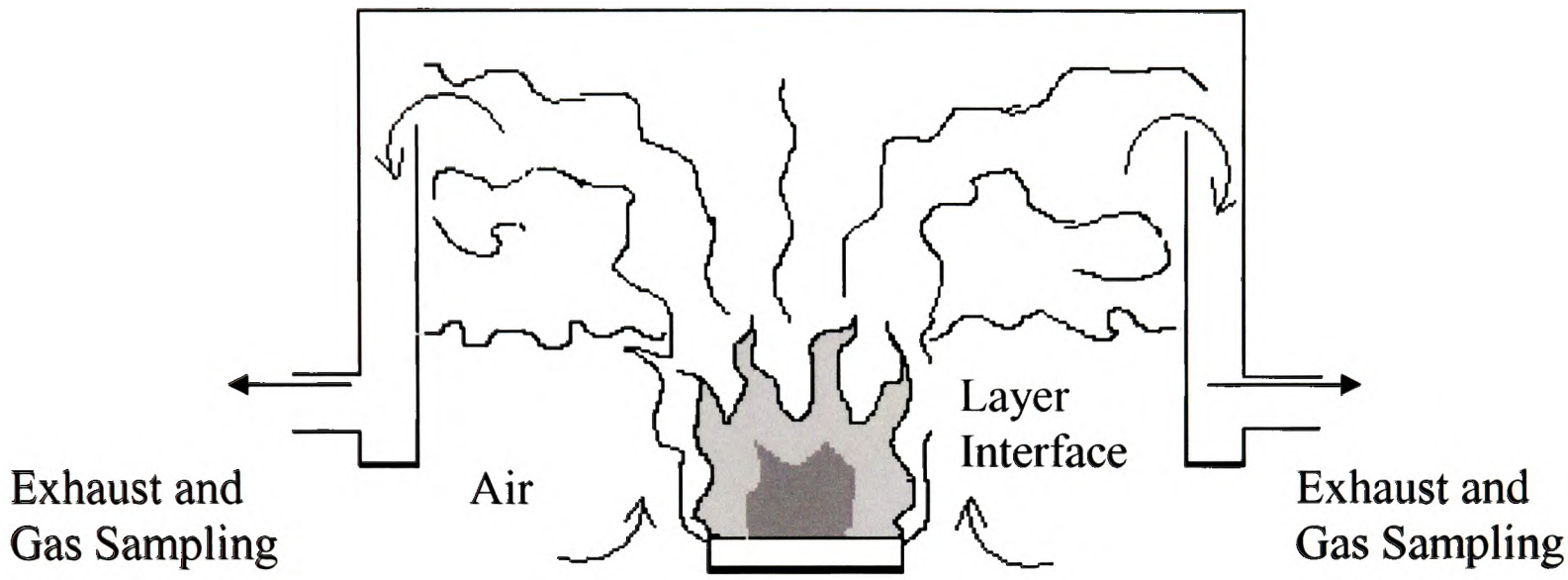

Figure 2.1 Schematic of the two-layer system created in hood experiments of Beyler [1986a; 1986b]

Cetegen [1982] investigated the entrainment into the buoyancy-driven fire plume using a modified hood design. Instead of sampling the gases directly from within the hood, as was done by Beyler, the combustion gases were allowed to spill out beneath the inner hood and into a second hood from which they were exhausted from the laboratory. As a result of this arrangement, the interface region became thinner and the layer interface was located very close to the bottom of the first or catcher hood making it to be better defined. Cetegen used natural gas as the fuel and his measurements were consistent with the observations of Beyler for a range of other fuels. For rich conditions, upper-layer temperatures were on the order of 850 K.

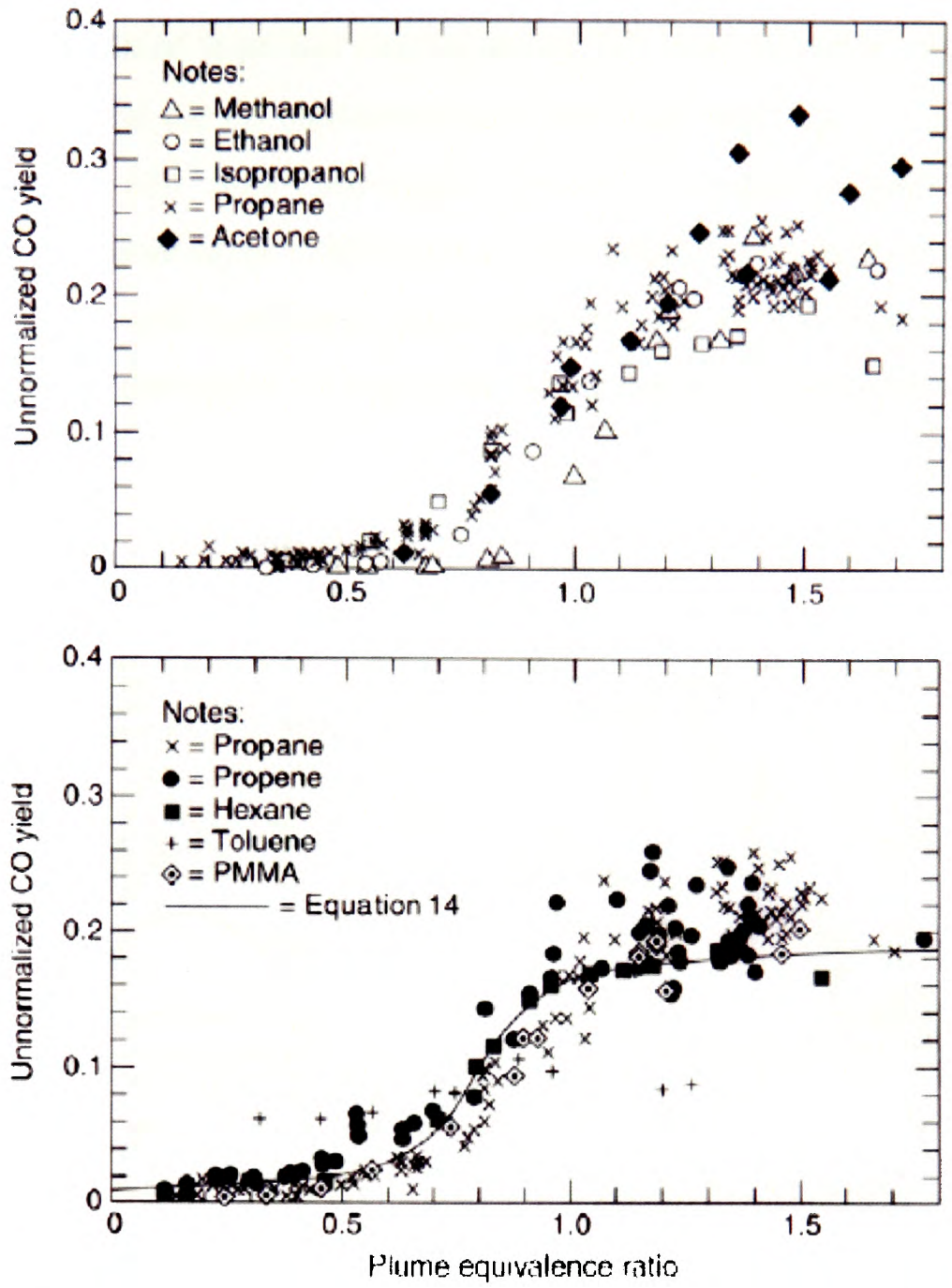

Figure 2.2 CO yields as a function of ϕ_p for various fuels studied by Beyler (Reproduced from Gottuk and Roby 1995)

In a later work, Lim [1985] used the same hood experimental facility with natural gas fuel to make more careful measurements. The observed upper-layer temperatures were in the range of 450-850 K. Figures 2.3 and 2.4 show the results of CO and O_2 yields. All the above hood experimental measurements have good qualitative and quantitative agreement between them. The solid lines in Figures 2.3 and 2.4 correspond to chemical-equilibrium calculations assuming natural gas and air mixtures at the given GER (ϕ_g) and are allowed to come into chemical equilibrium at the temperatures indicated. By the

Figure 2.3, Lim [1985] demonstrated and suggested that chemical-equilibrium calculations can be utilized to predict reasonably the CO concentrations for a temperature range of 750-800 K and the O_2 concentration in fuel-lean areas ($\phi_g < 1.0$). However, it seems that there is still some uncertainty involved in their calculations for the recommended temperature range (750-800 K). Lim [1985] concluded that the difference between experimental and theoretical values may be due to: (1) the accuracy of the instruments; (2) their assumption of negligible soot formation; (3) equilibrium not being established in the hood.

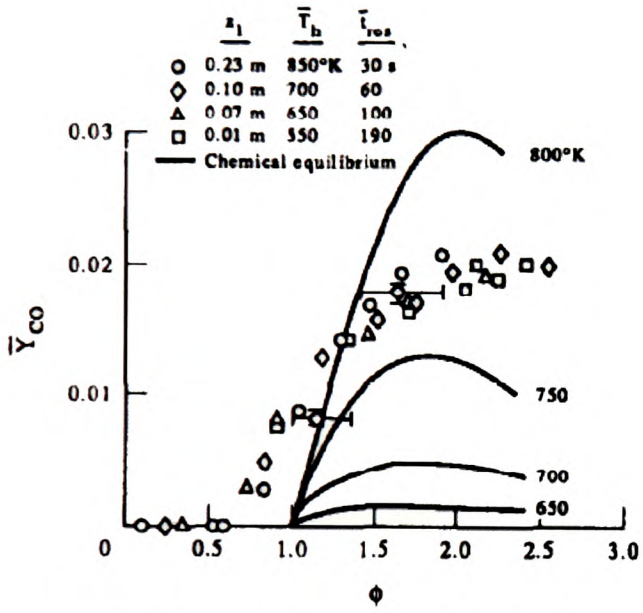

Figure 2.3 Mole fractions of CO
(Reproduced from Lim [1985])

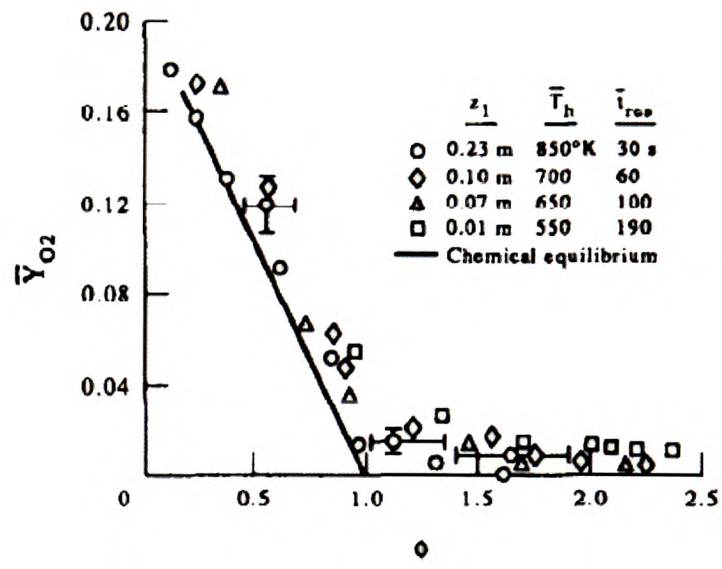

Figure 2.4 Mole fractions of O_2
(Reproduced from Lim [1985])

Tonner et al. [1987] and Zukoski et al. [1991] carried out similar hood experiments with a different experimental setup. The hood used was a 1.2 m cube box, insulated on the inside with ceramic fiber insulation board. Gas samples were drawn using an uncooled stainless-steel probe inserted into the layer. They replaced the individual gas analysers used by earlier researchers with a gas chromatography system, which allowed accurate concentration measurements of a large number of species in the upper layer contained within the inner hood. This made it possible to measure the concentrations for a sufficient number of species more accurately. The upper layer equivalence ratio (ϕ_{ul}) was determined from conservation of atoms using the chemical species measurements, the composition of fuel, and the fuel flow rate. Natural gas was used as the fuel and upper

layer temperatures ranged from 490 to 870 K. It was concluded that the species concentrations were well correlated to the upper layer equivalence ratio, ϕ_{ul}, and insensitive to temperatures for the range studied.

Morehart et al. [1990] performed a series of hood experiments with a new hood facility, but utilized the same gas analysis procedures developed by Toner. The new hood was considerably larger (1.8 x 1.8 x 1.2 m) than the earlier facility. Steady-state burning conditions were established by keeping the burner-to-layer interface height and the fuel burning rate as constant. Near the top of the hood, a series of tubes with perforation is located to inject additional air into the upper layer at a known flow rate until a new steady state is achieved. This procedure established the condition ϕ_{ul} lower than ϕ_p, since ϕ_p is based on the ratio of the fuel mass burning rate to the mass of air entrained into the plume from room air below the layer interface. By varying the air supply rate to the upper layer, a range of ϕ_{ul} was established while maintaining a constant ϕ_p.

Although the CO and CH_4 correlations obtained by Morehart et al. [1990] followed similar trends, it deviated from those obtained by Toner et al. For well-ventilated conditions Morehart et al. [1990] observed higher CO and CH_4 yields. For under-ventilated conditions, Morehart et al. observed lower CO, CO_2 and H_2O yields and higher CH_4 and O_2 concentrations than Toner et al. The upper layer temperature ranged from 488 to 675 K. Morehart et al. attributed the deviation to the fact that the layer temperatures were 120 to 200 K lower than in the experiments conducted by Toner et al.

Morehart et al. [1990] also studied the effect of increasing temperature on layer compositions. They observed that an increase in the upper layer temperature resulted in more fuel being combusted to products of complete combustion and additional CO.

Pitts [1995] extensively reviewed the experimental investigations carried out to charaterise the CO production mechanism. Pitts [1995] noted that the focus of the hood experiments on changes in upper-layer composition was solely on the temperature dependence. Pitts [1995] also postulated that the average residence time for the

combustion products in the upper-layer have some effects too on the final composition of the upper-layer. He further expanded the GER concept and postulated that the final CO concentration levels depend on the following processes [Pitts, 1997]:

a. Quenching of a turbulent fire plume upon entering a rich upper layer
b. Direct introduction of additional oxygen in to the high-temperature, vitiated upper layer.
c. Pyrolysis of wood in the high-temperature, fuel rich upper layer.
d. Approach to equilibrium by the combustion products.

All the above mechanisms results in the formation of additional CO.

2.2.2 Summary of Conclusions Based on Hood Experiments

a. The hood experimental measurements discussed above demonstrated that the composition of upper layers in hoods above the fires correlate well by plotting the concentrations in terms of GER.
b. The correlations are independent of fuel supply rate and the layer interface height from the fuel source.
c. However, the correlations depend on the fuel type and the upper layer temperature.
d. For upper layer temperatures < 500 K, the reaction rates are very slow, and the correlations are independent of temperature.
e. For the temperature range 500 – 800 K, changes in the upper layer composition of the products are observed. The hood experimental data suggest that the shifts in the upper layer composition are the result of oxidation of additional fuel to produce CO, CO_2 and H_2O. Concentrations of H_2 appear to be relatively insensitive to the temperature effect.
f. For upper layer temperatures > 800 K, the O_2 concentrations in the upper layer approaches zero.
g. The average residence time in the upper layer is also an important variable that has an effect on modification in the upper layer gases concentration along with the temperature.

2.3 Detailed Chemical-Kinetic Modeling of Upper-Layer Reaction Behavior

Toner et al. [1987] compared the measured species concentrations to the calculated equilibrium composition of reactants and products at constant temperature and pressure. They found that the chemical equilibrium calculations were able to model quite well the layer composition for very well-ventilated conditions and not for under-ventilated conditions. Following their observation of CO production for $\phi_{ul} > 1.0$ at the expense of CO_2 production, they suggested that the CO oxidation was 'frozen out' before completion i.e., at low temperatures, there is insufficient energy for CO to oxidize to CO_2. Since the experimental measurements were independent of temperature for the range studies (490 to 870 K), Toner et al. [1987] concluded that, if a freeze-out temperature for CO existed, it must be higher than 900 K.

Morehart [1990] performed detailed chemical-kinetic calculations of a plug-flow reactor for a fuel rich mixture typical of the upper layer conditions observed in the hood experiments of Morehart [1990] to address the effect of temperature on upper-layer reactivity. The calculations showed that such mixtures did become reactive for temperatures > 700 K in agreement with his experimental findings, but the calculated changes in upper-layer composition were not consistent with the differences between the Toner and Morehart's experiments.

Pitts [1992] reported calculations using similar experimental concentrations of combustion gases observed by Morehart. Calculations were performed over a range of temperatures (700 – 1300 K), $0.5 < \phi_g < 2.83$, and residence times from 0 to 20 seconds. Effects of mixing behavior and heat loss variation were also investigated by considering two possible extremes: infinitely fast (Perfectly Stirred Reactor Model) and infinitely slow (Plug-Flow Reactor) mixing models. The detailed chemical-kinetic calculations were performed using CHEMKIN subroutines [Kee et al., 1980].

The conclusions based on the investigation are summarized below:

- Upper-layer gases are unreactive for temperatures less than 700 K.
- Upper-layer combustion gases become reactive for temperatures > 800 K.
- Reaction rates increase with temperature. For the lowest temperatures, residence times of 10 seconds were required for complete reaction, while periods of < 1 second were required at 1300 K.
- The products generated varied for lean and rich conditions and with temperature. For lean conditions products of complete combustion (i.e. CO_2 and H_2O) were formed. For rich conditions, CO was produced in preference to CO_2. At lower temperatures (< 1100 K) H_2O was generated in preference to hydrogen (H_2), but for temperatures greater than 1100 K, H_2 was the main product. Since hydrogen does not require an oxygen atom, more oxygen was available for oxidation of fuel and higher concentrations of CO were formed at the higher temperatures.

2.4 Thermodynamic calculations of upper-layer composition

Zukoski et al. [1987] attempted to understand the temperature dependence of the hood experiments based on thermodynamic arguments which assumes that the combustion gases in a hood come into thermodynamic equilibrium at the temperature of the hood gases. However, concentrations of the various species under the hood were inconsistent with this assumption.

Gottuk et al. [1995] carried out a detailed study to assess the effect of temperature on CO production in compartment fires in order to resolve the applicability of GER-Yield correlations obtained in simplified upper layer environments in predicting realistic compartment fires. Gottuk et al. [1995] studied the chemical reactivity of upper layer gas composition using a detailed chemical kinetics model to get insights into the effect of temperature on CO production. Based on the study, the effect of change in temperature on upper-layer composition of a compartment fire is twofold:

1. Generation of intermediate species like CO in the fire plume depends upon the quenching of the fire plume by the upper layer. Quenching of the fire plume at

various heights has significant effect on the final CO levels from the fire plume. Also as the compartment temperature increases, the fire plume temperature increases resulting in more complete oxidation of the fuel to CO_2 and H_2O within the plume thus reducing the final CO levels from the fire plume.

2. Oxidation of post-flame gases in the upper layer is also affected. Upper-layer temperatures > 900 K allow near complete oxidation of CO to CO_2 when $\phi_g < 1.1$. However, for the upper-layer temperatures < 800 K, no CO oxidation is reported which indicates that the upper layer is fairly un-reactive.

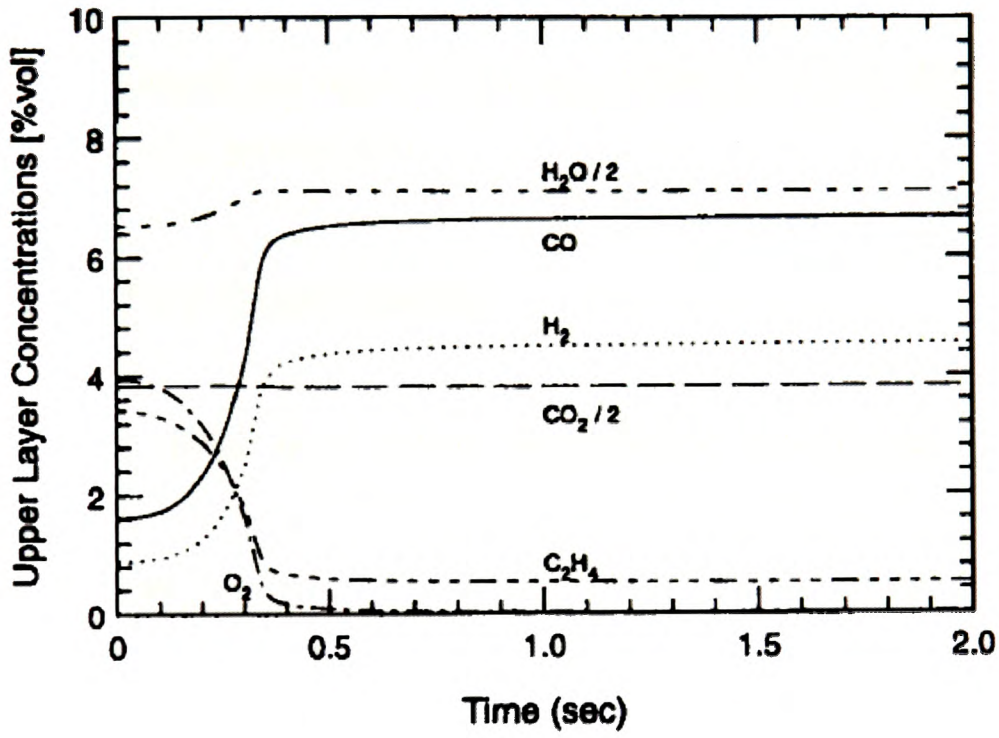

Figure 2.5 Chemical kinetics model calculated species concentration vs time for $\phi_g = 1.36$ at temperature 1000 K (Figure taken from Gottuk et al. 1995)

Figure 2.5 shows the calculated major species concentrations plotted versus time for an under-ventilated case, $\phi = 1.36$, at an upper layer temperature of 1000 K. At upper layer temperatures characteristic of compartment fires, the upper layer gases are quite reactive. The figure also shows that for under-ventilated fires, the CO level rises quickly as the fuel (C_2H_4) is being oxidized. However, the oxygen is depleted before all the fuel is oxidized resulting in high CO concentrations and residual fuel. Hence, carbon dioxide levels remain virtually unchanged. From the above thermodynamic calculations of Gottuk et al. [1995] (see Figure 2.5), it is evident that the hydrocarbon oxidation to CO

and H_2 is much faster than CO and H_2 oxidation to CO_2 and H_2O, respectively. This is due to the preferential combination of free radicals, such as OH, with hydrocarbons over CO. Carbon monoxide is oxidised almost exclusively by OH radical to CO_2 [Warnatz, 1984]. Therefore, it is not until the hydrocarbons are consumed that free radicals are able to oxidise CO to CO_2. The above mechanisms results in the increase of final CO levels transported to remote locations. If additional air is introduced to this high-temperature fuel-rich upper layer, complete oxidation of fuel and CO takes place which are exothermic reactions. This above mechanism results in reduction of final CO levels transported to remote locations. Thus the upper-layer temperature dictates post-flame oxidation in the upper-layer. Chemical kinetics results of Zukoski et al. [1989] and Gottuk et al. [1995] indicated that upper layer temperatures of 850 to 900 K or higher are needed for the layer gases to be reactive.

2.5 Compartment Fire Experiments

The hood experiments differ from actual compartment fires in the following ways [Gottuk et al., 1995]:

1. The hood setup allowed heat losses through considerable radiation to the lab space below. However, in real compartment fires, the heat loss through radiation results in higher wall and upper-layer temperatures.
2. Under hood setup, the plume is fed from an infinite supply of air which is neither vitiated nor heated. In real compartment fires, the hot vitiated air containing products is entrained in to the plume.
3. The hood experiments did not include any significant ceiling and wall flame jets. These dynamic flame structures enhance mixing of the upper layer in actual compartment fires and extend the flame zone beyond the plume.
4. The hood experiment correlations were developed from sustained steady state burning conditions. Actual fires of interest evolve with time, and, thus are more transient in nature.

Mulholland [1990] reviewed a number of large-scale fire tests which were conducted at National Institute of Standards and Technology (NIST) in Gaithersburg, USA. He recommended the values for post flashover yields of CO, CO_2 and O_2 depletion to be 0.2, 1.5, and 1.8 g/g fuel respectively for enclosure fires involving materials commonly found in a computer work place. Pitts [2001] presented a brief summary on some of the post 1995 real-scale experimental efforts to characterise CO formation. He identified that majority of experimental investigations focused on CO formation within the room and the need for further studies to understand the subsequent reaction and transport of these gases to predict accurate engineering hazard estimates.

Tewarson [1993] performed detailed studies on generation rates of fire products for various fire ventilation conditions using the Flammability Apparatus at Factory Mutual Research Corporation (FM). Tewarson [1995] presented the data as a ratio of species yields for ventilation controlled to well ventilated fires. Tewarson [1995] developed generalised relationships to calculate chemical, convective and radiative heats of combustion and yields of combustion products at various equivalence ratios for halogenated and non-halogenated polymers. Tewarson concluded that the ratios of oxygen and carbon dioxide were independent of the chemical composition of the materials, while the ratios of carbon monoxide and hydrocarbons did exhibit a dependence on the chemical structure of the materials as reported by Beyler.

Tewarson [1984] reported the CO and CO_2 yields and O_2 depletion for wood crib fires conducted in a special small-scale test apparatus at Factory Mutual Research Corporation (FM Global) along with results from three other studies. The three studies consisted of burning cellulosic based fiberboard and pine wood cribs in various compartment geometries, ranging in volume from 0.21 to 21.8 m^3. Tewarson [1984] concluded that the yields correlated well with the air-to-fuel stoichiometric ratio and that the GER was a useful parameter for the correlation of species yields for equivalence ratio between 0 to 5. The air entrainment rate in to the compartment was estimated using a ventilation parameter, $Arh^{1/2}$, where Ar is the cross-sectional area and h is the height of the vent.

Gottuk et al. [1992a] and Gottuk [1992b] conducted reduced-scale compartment fire experiments to determine the yield-equivalence ratio correlations for hexane, PMMA, spruce, and flexible polyurethane foam. The test compartment (1.2 m x 1.5 m x 1.2 m high) was specially designed with a two-ventilation path system to measure directly the air entrainment rate and the fuel volatilisation rate. Measurements of species concentrations using an uncooled stainless steel probe and temperature at several locations showed a well-mixed, uniform layer.The correlations of these experiments were in qualitative agreement with those observed during Beyler's hood experiments. However, some significant quantitative differences in the rise of CO yield exist between the two studies. Figure 2.6 shows the comparison of CO yields for hexane fires in the compartment setup of Gottuk [1992b] and under hood apparatus of Beyler. An offset exists between the rise in normalised CO yield for the two studies. For the Beyler's hood experiment, the CO yield is negligible until $\phi_p = 0.5$ and then the CO yield rise to a peak value of 0.09 at around $\phi_p = 1.0$. During the Gottuk's compartmental fire experiment, the CO yield is negligible until $\phi_p = 1.0$ and then the CO yield rise to a peak value of 0.11 at around $\phi_p = 1.3$. Gottuk et al. [1992a] explained the differences in terms of temperature effects.

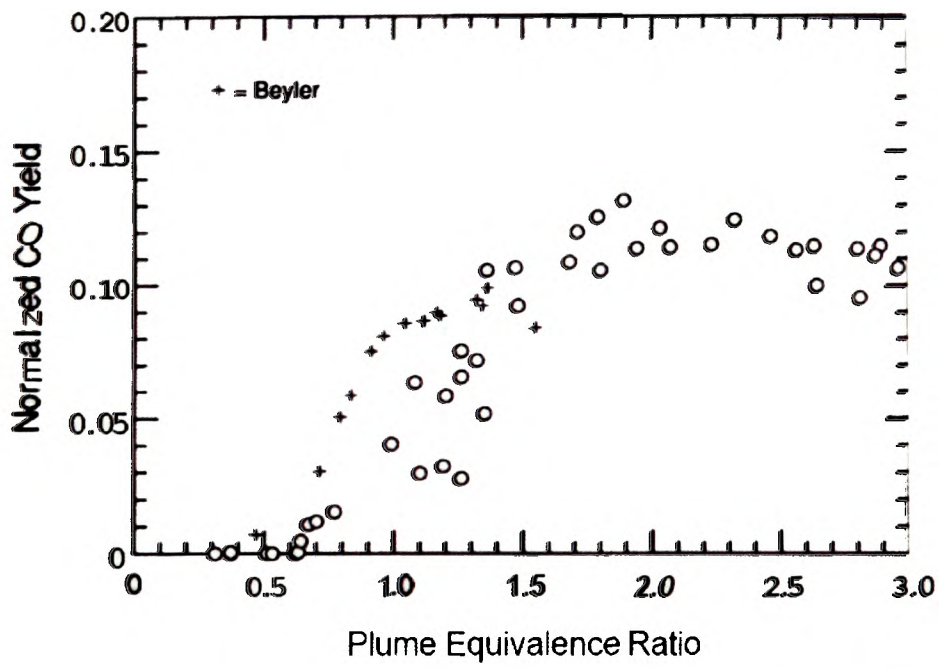

Figure 2.6 Comparison of normalized CO yield correlations obtained for hexane fires between the compartment fires of Gottuk [1992b] (shown in circles) and Beyler's hood experiments (Figure reproduced from Gottuk [1992b])

For the region of discrepancy between ϕ_p = 0.5 and 1.5, the upper layer temperatures in Beyler's hood experiments were typically below 850 K, whereas temperatures for the hexane compartment fires of Gottuk were above 920 K which is typically associated with postflashover fires.

Bryner et al. [1994] reported measurements of combustion gases within a 40 % reduced scale model of a ISO 9705 standard compartment, measuring 0.98 x 1.46 x 0.98 m. A single doorway was located in the centre of the short wall measuring 0.4 m wide x 0.81 m high. The fire source was a 15 cm diameter natural gas burner, located 15 cm above the floor in the centre of the compartment having a heat release rate range between 10 to 670 kW. The corresponding GERs ranged between 0.1 to 1.5. Both horizontal and vertical measurements of the species were taken within the compartment. The results showed that the horizontal variations in the species concentration exists within the compartment. Data for vertical variations in the species levels were reported for 250 kW and 600 kW fires. The data indicated vertical variations in the species levels within the compartment, as opposed to the typically assumed uniform composition of the upper layer.

Bryner et al. [1995] reported measurements in a full-scale ISO 9705 standard compartment using natural gas as the fuel and compared the measurements with the results of the 40% reduced-scale enclosure results. For underventilated burning conditions, the concentrations of CO in the full-scale room were observed to grow with time, reaching levels considerably higher than observed in the 40% reduced-scale ISO 9705 standard room. Bryner et al. [1994, 1995] observed that the upper-layer gas concentrations can vary significantly over a small vertical and horizontal distances. Therefore, Bryner et al. [1994, 1995] concluded that the concentrations within the compartment could not be correlated to a single global equivalence ratio for the compartment, instead a local equivalence ratio would be required.

Lönnermark et al. [1997] and Blomqvist and Lönnermark [2001] performed experiments in a ISO 9705 room with solid and liquid fuel sources at the Swedish National Testing and Research Institute, SP. The compartment ventilation was varied by changing the

soffit height and keeping the door width as constant. Five fuel sources were used in the study, viz., Polypropylene (PP), Nylon 66 (Ny), Tetramethylthiuram monosulfide (TMTM), Chlorobenzene (CB), and Chlorornitrobenzoic acid (CNBA). The average species concentrations at the exit plane were performed using a probe with seven equally spaced holes; the probe was positioned diagonally across the exiting flow of the opening. The species measurements included O_2, CO_2, CO. NO_x, THC, HCL, HCN, NH_3, and soot. Vitiation condition was measured using the phi-meter at a single point. Data was presented as species yields versus the global equivalence ratio. The data covers a range of equivalence ratios upto 1.4. Based on the discussion by Blomqvist and Lönnermark [2001] on the correlation, they believed that it would have been more appropriate to report the data as local species levels versus local equivalene ratio since only single point measurements using the phi-meter were made.

2.5.1 Compartment Fire Experiments Involving Cables

One of the sources of fire is attributed to electrical faults [Cullis and Hirschler, 1981]. Also a neighbouring fire could give out sufficient energy to ignite electrical cables. Once ignited, the fire not only propagates but may also intensify, owing to the fact that electrical cables have an insulation layer which is flammable and may decompose to produce combustible gases at high temperature. Notorious examples of fires which involved electrical cables are Kings Cross underground station in London, HMS Sheffield in the Falklands conflict and Dusseldorf Airport in Germany. There is thus a strong motivation for investigating the flammability of electrical cables [Leung et al., 2000].

The amount of power and communication cables involved in buildings increases day by day fueled by rapid advancement in the field of Information Technology. For building wiring applications, almost all cable insulation coverings are made of plastics. Polyvinylchloride (PVC) is more widely used than other polymers such as polypropylene, polyethylene, and synthetic rubbers. It is well known that burning of these plastics produces combustion products which are toxic and corrosive. Fires involving cables and

the effects thereof have increasingly been in focus in recent years largely due to the fact that the effects of cable fires can be very large (both in terms of people and property loss), and the damages they cause correspondingly are high for insurance companies.

Fei et al. [2003] performed series of fire tests simulating cable fires in plenum caused by exposed and aged combustible cables in a real-scale flatlet model containing burn room, ceiling plenum, and target room. A special communication cable type insulated with High Density Polyethylene (HDPE) and sheathed with Linear Low Density Polyethylene (LLDPE) was utilized. A related fire reference scenario was designed to simulate how cables in plenum were involved in a fire from potential fire loads to substantial fuel by the role of an external flaming source and to characterize related fire issues. The geometrical details of the combustion flatlet model are shown in Figure 2.7.

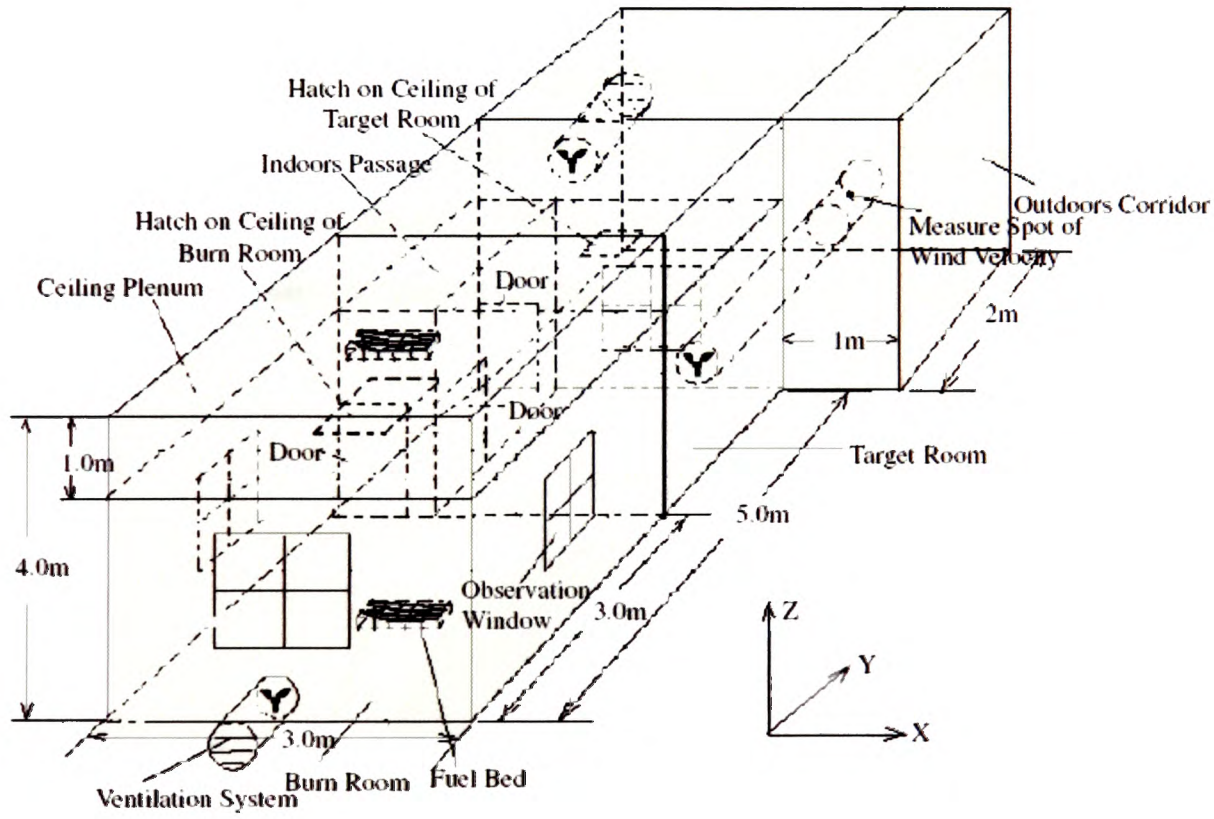

Figure 2.7 Scheme of the Real-Scale Test Rig used by Fei et al. [2003]

Apart from temperature, smoke obscuration and heat release rate measurements, gas sampling to detect the concentration of CO, CO_2, O_2, HCN, HCl, and SO_2 were carried out both at the plenum of burn room and target room. Major concerns were as to that how

various amounts, various ignition means, construction and different ventilation rates impact on fire performances (heat release rate, smoke temperature, smoke obscuration, combustion products, and toxicity) of cables in plenum. It was found that influences of these parameters are obvious. The burning of exposed tested cables in plenum easily poses a high potential of fire hazard even at a relatively low fire load.

Andersson et al. [2004] conducted a series of small scale (using the DIN 53436 tube furnace) and large scale experiments (using the IEC 60332-3 rig) to measure the toxicity for two types of power transmission cables used in buildings. The two types of cables are: PVC sheathed cable with PVC insulation around the individual wires and a cable sheathed with Casico material with Casico insulation. The cross-section of the power cables exhibiting various parts in the cable is shown in Figure 2.8. The PVC used was a non-flame retarded, flexible PVC formulation and the main components of Casico material are $CaCO_3$, a silicon gum and an ethylene butylene acrylater (EBA) copolymerised with polyethylene. The experimental results of the gas composition under different fire conditions were unique in that they identified a wide variety of organic and inorganic species. The main focus of their work is to provide information concerning quantitative organic species evolution from cable fires which was lacking in the open literature until then.

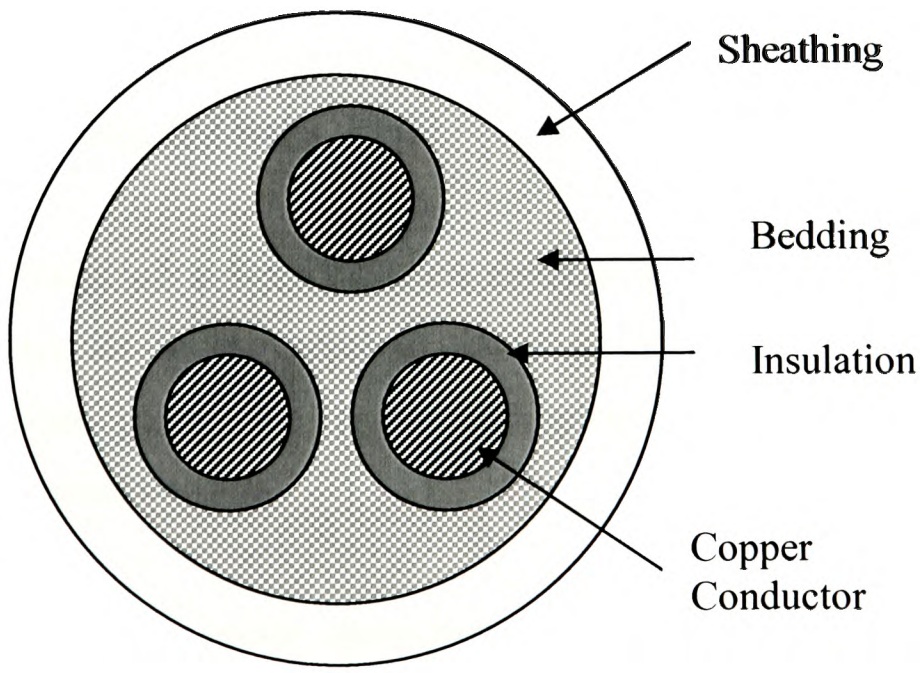

Figure 2.8 Cross-section of a power cable showing the components

Sung et al. [2004] performed full-scale burning tests on PVC electric cables at post-flashover stages. A room calorimeter of size similar to that in the ISO 9705 standard test compartment was built. The room is of length 3.6 m, width 2.4 m, and height 2.4 m with a door of height 2 m and width 0.8 m. An exhaust hood was constructed outside to measure the heat release rates by oxygen consumption method. Combustion gases such as CO, CO_2, and O_2 were measured at the hood. The main objective of Sung et al. [2004] was to measure the net heat release rate curve on burning the cables inorder to assess the fire hazard and its devastating side effects. They suggest to utilise this additional heat release curve to fire models to give a better assessment on the consequences of burning the plastic combustibles.

2.6 Experiments on Species Production and Transport in Real-Scale Fires

The previous sections of this chapter have dealt with measuring the production of combustion species using hood setup (lab scale experiments) and in standard compartments (reduced scale experiments) under various fire conditions. In practicality, real-scale fires are also dependent on building geometry. Since CO is an odorless and colourless gas, the transport of this toxic gas to regions remote from the fire also poses a serious threat. Some studies have been conducted to investigate the generation and transport of toxic combustion products in real-scale building scenarios, but there is still much more work to be done [Gottuk and Roby, 1995].

During the post-flashover stage of a fire, fuel-rich exhaust gases escape from the compartment. If the ambient air in the adjacent space is entrained into the high temperature fuel-rich exhaust gases, the exhausting gases starts burning. This phenomenon is termed as 'external burning'.

Fardell et al. [1986] conducted large-scale experiments with a burning compartment having a 2 m high doorway exhausting perpendicular to the axial direction of a 11.4 m long, 1.2 m wide corridor with full-height walls. The study investigated the species levels

just outside of the doorway, and at the end of the corridor, for burning of four fuels: pine wood, polymethylmethacrylate (PMMA), polypropylene homopolymer (PP), and expanded polystyrene (EPS). Experiments were conducted for two different doorway widths, i.e., for 0.76 m and 0.2 m wide openings. The doorway provided the single ventilation path between the burning compartment and the corridor for both airflow into the compartment and exhaust gas flowing out of the compartment. Fardell et al. [1986] focused their attention in investigating the toxicity of the environment produced at the two sampled locations.Between 20 to 40 hydrocarbon compounds, including oxygenated organincs, saturated and unsaturated hydrocarbons, and aromatic hydrocarbons were identified during the analysis of spot samples. Overall Fardell et al. [1986] found that the CO was the most significant gas, in concentration and toxicity, at both locations sampled.

Morikawa et al. [1993] conducted experiments with a fire resistant two-storey house with the ground floor burning compartment vented to the open atmosphere and to a hallway attached to stairs leading to the first floor. The room in the first floor had a door opening whose size was varied for different experiments. The burn room was fully furnished with typical room contents, representing a wide range of materials. Continuous monitoring of CO, CO_2, and O_2 was performed in the ground floor hallway just outside of the burn room, and in the first floor room, at both high and low locations. Spot sampling of gases allowed chromatographic analysis of hydrogen cyanide (HCN) and acrolein concentration levels at the same sampling locations. The results indicated, as with Fardell et al. [1986], that CO was the dominant toxic gas with the most significant concentration in the fire exhaust. However, HCN will also have a significant contribution to the lethal toxicity of the atmoshpere.

Gottuk et al. [1992c] and Lönnermark et al. [1997] investigated the effect of open-jet external burning, on the burning of exhaust gases from a compartment fire as they exhaust to the open atmosphere. Gottuk et al. [1992c] compared the gas composition inside the compartment during similar fires of Gottuk et al. [1992a] to determine the efficiency of external burning in oxidising CO and soot. A summary of these studies is given below [Gottuk and Roby, 1995]

- Two distinct types of external flames were observed during the compartment fires. First, external flame jets appeared as ceiling jets extended from the main fire plume within the compartment, and out through the exhaust vent. Secondly, during significantly underventilated fires in the compartment, external flames occurred when the exhausting flammable gases from the compartment mixed with a sufficient amount of ambient air, and were ignited causing external burning.
- Overventilated fires never produced external burning, because the excess oxygen in the compartment completely oxidised all of the fuel inside the compartment.
- Compartment fires that produced a 'quasi-steady-state' average plume equivalence ratio equal to or greater than 1.7 produced sustained external burning. The occurrence of sustained external burning was the only form of external burning observed to reduce CO and soot levels significantly.

Ewens et al. [1994] investigated the evolution of compartment fire exhaust gases during transport through a 3.66 m long hallway for underventilated conditions (Figure 2.9). The fuel-rich plume exhausting from the compartment, into an adjacent enclosed space, when mixed with ambient air can result in oxidation of toxic combustion gases to less threatening CO_2 and water, provided correct conditions exist. Ewens et al. [1994] focussed on the effect of hallway fluid dynamics on the oxidation process by varying the hallway inlet and exit soffit heights. Ewens et al. [1994] concluded that the oxidation of exhaust plume in the adjacent space was a function of the hallway fluid dynamics, the stoichiometry of the gases entering the hallway, gas temperatures, and the fuel volatilasation rate inside the compartment. Ewens noted that unburned hydrocarbons were oxidised more completely than CO or soot, and attributed this to the low hallway gas temperatures.

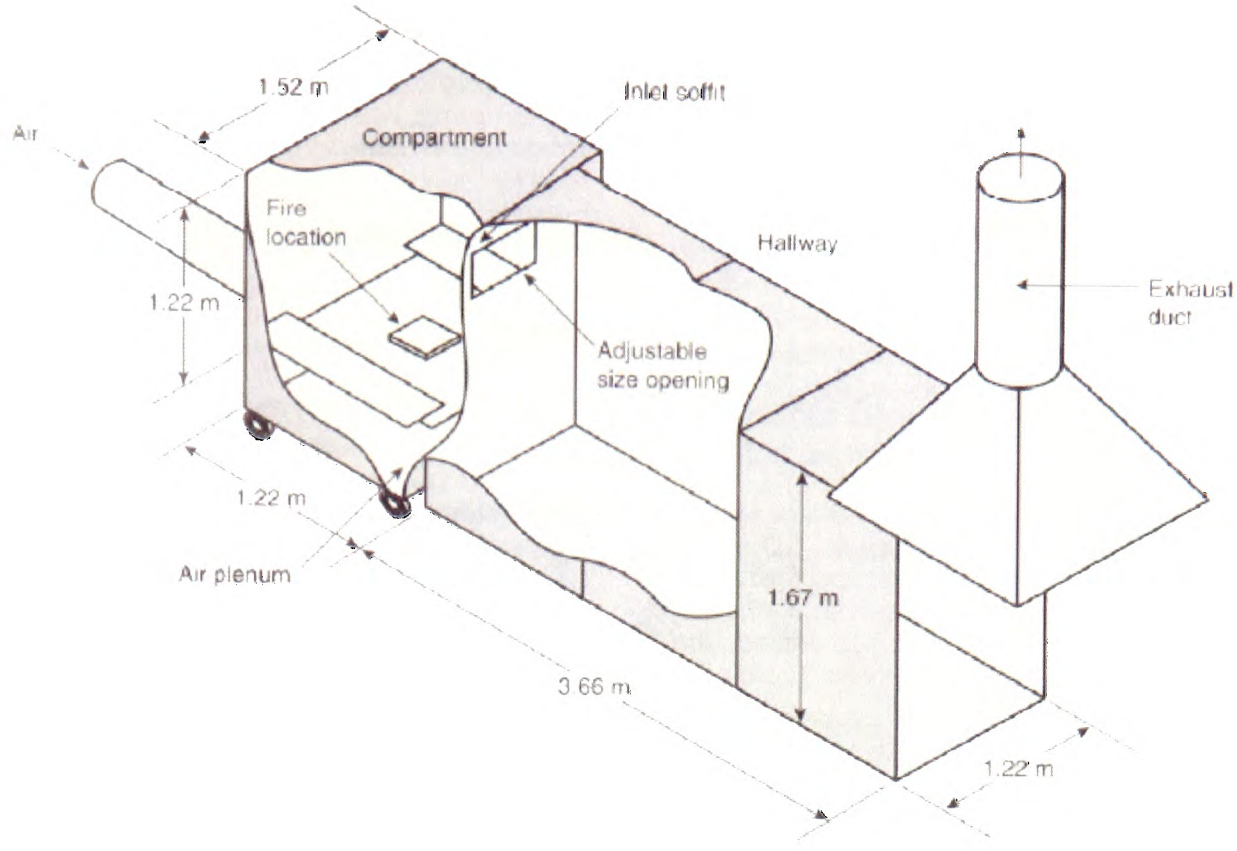

Figure 2.9 Compartment/hallway experimental setup used by Ewens [1994]. (Image reproduced from Gottuk and Lattimer [2002])

Luo and Beck [1994, 1997] conducted full-scale tests in a multi-enclosure, multi-storey building having the basic structure of 21 x 15 x 12 m high steel and concrete frame. A schematic plan-view of the multi-room fire compartment building is shown in Figure 2.10. The objective was to obtain a comprehensive set of experimental data including flame spread velocity, mass release rate, gas temperature, radiation heat flux and gas analysis. Polyurethane foam was used as the fuel to generate non-flashover and flashover fires. Based on the measured gas compositions of CO, CO_2 and O_2, the total fraction of incapacitating dose (FID) at the center of the room 101 (R101) and 1.9 m above the floor, reached 0.17 for the non-flashover fire and 0.7 for the flashover fire in 5 min. In room 102 (the burn room) the temperature reached 400^0 C in 3 min for the non-flashover fire; in the case of the flashover fire the temperature reached 600^0 C during the same period. The time to incapacitation based on the CO, CO_2, low O_2 and heat exposure in the burn room is much shorter (< 1 min) compared with that in room 101 for both types of fires. This comprehensive set of experimental data was used as the validation cases for CFAST

two-zone model and the computational fluid dynamics model, CESARE-CFD [Luo and Beck, 1996; Luo et al., 1997].

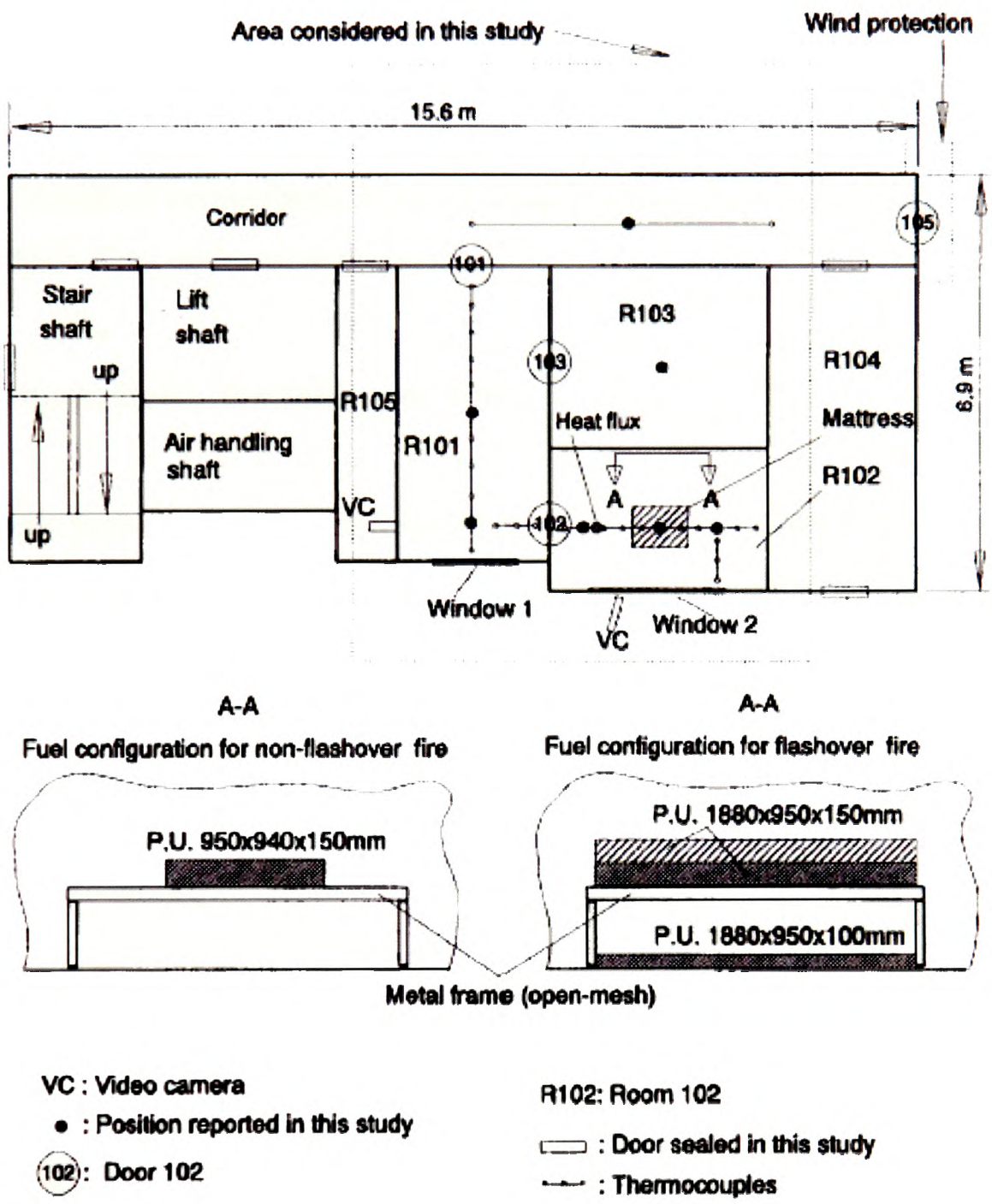

Figure 2.10 Layout of the first level of the experimental building-fire facility, instrumentation and fuel configuration (Reproduced from Luo and Beck, 1996)

The main objective of this PhD research is to develop a methodology to predict levels of CO and other toxic products generated and transported to distant locations during real-scale fires involving complex solid fuels. It was necessary to review bench-scale experiments like hood experiments, compartment fire experiments and full-scale

experiments dealing with CO and other toxic combustion products generation to gain the present understanding on the formation mechanism of CO and other toxic combustion products generation and their transport in fires. Emphasis was given on combustible polymers like wood, plastics etc. The review also focussed on the available large-scale experimental data for combustible polymers to validate the combustion, toxicity and the transport models. Based on the literature survey on fire experiments, it is evident that there is a dearth of comprehensive set of experimental data on real-scale fires involving complex fuels like combustible plastics.

2.7 Mathematical Modelling of Fires

It is evident from the experimental investigations on compartment fires discussed above that the upper layers in real fires are far from homogeneous [Bryner et al., 1994] and that the upper layer may be reactive. The advent of mathematical modelling started from semi-emprical and analytical models. There are two basic strategies in mathemetical modelling of fires: zone and field modelling.

2.7.1 Zone Modelling

The evolution of early semi-emprical and analytical methods led to the development of zone models: the first generation of computer fire models. As the name implies, the fire compartment is divided into at least two distinct regions such as hot upper layer and a cool lower layer. These two zones are considered representative of two control volumes and gas properties are assumed to be constant. Zone models have been widely used to simulate a variety of fires, thanks to its simplicity and low computational expenses [Kawagoe 1958, Emmons 1978, Rockett 1976, Luo et al. 1997, Mitler 1991]. Zone modelling relies heavily on empirical data and much work has been carried out to generate these data [Steckler et al. 1982, Peacock et al. 1991]. Zone models have the following intrinsic disadvantages.

a. Zone model heavily relies on empirical data.

b. Cannot predict the distribution of concentration of toxic gases and temperature in the upper layer.
c. Not applicable to complex geometries [Beard, 1996].

2.7.2 Field Modelling

Fire field models based on CFD techniques have the ability to resolve spatial variation of fire environment. This approach is based on applying local conservation laws for physical quantities such as mass, momentum, energy and species in a flow domain. Over the last two decades, revolutionary progress has been made in the field of Computational Fluid Dynamics (CFD) and the computational power has increased enormously and computational resources have become cheaper. Such progress manifests itself in building codes, regulations and standards through gradual movement away from prescriptive-based to performance-based flexible methodologies. This coincides with the dramatic shift from zone models to field models in fire modelling. Field models are not as sensitive as zone models to geometry and can describe the fire plume and upper layer behaviours to a higher resolution. The CFD approach is considered to be fundamental to the future development of fire modelling which can provide the basis for the development of performance-based fire safety regulations. Cox [1995] reviewed both zone and field models used in the simulation of compartment fires and Novozhilov [2001] provides a comprehensive review on the mathematical modelling techniques, currently available for compartment fires.

One of the stated objectives of this work is to develop a model for toxic combustion gases production and transportation in realistic building scenarios. To do so requires a review of current modeling techniques of carbon monoxide production in fires. The widely used models to simulate real-scale fires are

- Eddy Break-Up (EBU) based models.
- Flamelet concept based models.
- Equivalence ratio concept based models

Eddy Break-Up model (EBU) is the most widely used combustion model with much success. The model originated from the works of Spalding [1971] and is based on the assumption that chemical time scales are fast compared to the turbulence scales. Bilger [1976] showed that a conserved bounded scalar mixture fraction can be used to formulate state relationships for a variety of flame properties (i.e. species mass fraction, temperature and enthalpy). Thus the flamelet models calculated the temperature, density and species concentrations by the correlation between these variables and the mixture fraction. These correlations are either evaluated from the detailed calculations of the laminar, stagnation point diffusion flame or from the most common opposed jet laminar flame experiments.

Luo et al. [1997] simulated non-flashover and flashover polyurethane slab fires in a prototype multi-room, multi-storey building using a field model, called CESARE-CFD fire model. Gas phase combustion phenomena were modeled using the mixture fraction concept. The basic concept is that the combustion reaction rate is determined by the gas mixing rate of fuel with air under infinitely fast reaction assumption. For combustion of polyurethane foam, CO and CO_2 were assumed to be the products of combustion calculated by the chemical reaction equation given as follows [Tsuchiya, 1995]:

$$CH_{1.91}O_{0.263}N_{0.055} + (0.5b + c + 0.346 + 0.028x)O_2 \rightarrow bCO + cCO_2 + 0.955H_2O + 0.055NO_x \qquad (2.2)$$

Emprical relationships for polyurethane foam given by Takeda and Yung [1992] were used to calculate the local CO and CO_2 concentrations as follows:

$$\frac{Y_{CO}}{Y_{CO2}} = \frac{28b}{44c} \quad \text{and} \quad \frac{44c}{28b} = \frac{60Y_{O_2}}{23} \qquad (2.3)$$

Where Y_j is the mass fraction of species j (j = CO, CO_2 and O_2); b and c are constants. In general CESARE-CFD fire model gave reasonable qualitative predictions for non-

flashover fire and gave conservative results for flashover fire. The authors explained the differences by the limitation of fire growth model and the combustion model.

Yeoh et al. [2003] validated the CFD based fire model using laminar flamelet method by simulating an enclosure fire in a single level multi-room building[Luo and Beck, 1994]. The state relationships for individual species as a function of mixture fraction were taken from the curves fitted against laminar flame measurements. The authors found the laminar flamelet combustion model to perform reasonably well in predicting the CO and CO_2 concentrations within the burn room against the experimental data obtained.

Wen and Huang [2000] predicted confined jet fires under ventilation-controlled conditions using three different combustion models, viz., the laminar flamelet model, the constrained equilibrium method and the eddy break-up model. They found that all the three combustion models were able to predict the trends of distributions for velocity, temperature, soot, and CO. Due to the lack of detailed experimental data on species concentrations, no conclusions were drawn on the models capability in predicting species distributions.

Wen et al. [2001] studied the effect of microscopic and global radiative heat exchange on the field predictions of compartment jet fires. Laminar flamelet calculations were performed using the RUN-1DL code developed by Rogg and co-workers [Rogg, 1998]. For the chemical reactions, a detailed reaction mechanism for propane oxidation developed by Peters [1992] was used. It consisted of 112 reactions and 37 species. Radiation was included in the flamelet calculations by DTRM [Liu and Rogg, 1996]. The predicted vertical distributions of CO, CO_2 and OH at two locations near the fire were in good agreement with the steady state experimental profiles. It was also observed by Wen et al. [2001] that microscopic radiation has significant effect on the predictions of soot and OH and negligible effect on the predicted concentrations of CO, CO_2 and H_2O. This was attributed to the fact that the mixing processes have more dominant effects on their formation than chemical kinetics. In consistent with the general belief, they also found

that the global radiative heat exchange had significant effect on the temperature predictions.

Welch [2002] attempted to model a corner façade fire scenario involving plastic and cellulosic materials by means of a non-adiabatic laminar flamelet model. For this purpose, flamelets were generated using the CHEMKIN code [Kee et al., 1996] for heptane fuel by a detailed chemical kinetic mechanism (160 species/1540 reactions). A reasonable quantitative match was achieved between the predicted and the experimental CO concentrations for the scenario involving plastics. The predicted CO concentrations were over-predicted for the case involving wood volatiles. Welch [2002] postulated that the over-prediction for this case derives from the heptane chemistry underlying the flamelet combustion model, which is clearly inappropriate for wood volatiles. He concluded that further work is needed to examine the model's performance for a wider range of materials and test cases. In addition, the existing flamelet library requires extension, in particular to achieve a better representation of the wood chemistry to model the CO concentrations more accurately.

Hyde [2000] conducted a series of experiments to investigate the evolution of CO formation in low momentum turbulent vitiated flames, typical of a well developed compartment fire. Experimental results for ethylene, showed that the CO yield is dependent on ambient temperature and the ambient oxygen level, producing a maximum yield at the highest temperature and oxygen levels. It was also illustrated in his thesis that given the timescales involved it seems most unlikely that equilibrium levels would be reached in the hot upper layer of the compartment fire and that elevated levels of CO were due to flame quenching and continued reaction at the interface between the two layers. A Flamelet model using the laminar flame data and several modified EBU models were incorporated into a finite volume fire research code, SOFIE, for evaluation. Simulations of the experimental flames and representative compartment fire scenarios using the above models were reported. Hyde [2000] concluded that in general EBU models tends to underpredict the CO yields whereas the laminar flamelet approach shows

more promise particularly in the rich regions of the flame arguably typical of hot upper layers.

Hyde and Moss [2002] compared the strategies based on laminar flamelet relationships, derived from computations of vitiated laminar diffusion flames, and a simplified two-step EBU for the modeling of CO production in vitiated compartment fires. A flamelet library was constructed incorporating the parametric variation of ambient oxygen concentration and temperature. Both the strategies were implemented in SOFIE, a CFD based fire modeling code. CFD simulations of ventilation controlled compartment fires using the SOFIE code suggest that both modeling approaches offer the prospect of reliable CO prediction, given a measure of calibration.

Jason and Kevin [2007] proposed a new mixture fraction based framework wherein the mixture fraction is decomposed into constitute parts that represent the products of different reactions (two-step chemistry). Jason and Kevin [2007] suggest that the mixture fraction needs to be decomposed into three components to account for local flame extinction and also the production/destruction of CO. The proposed new mixture fraction approach was validated against three sets of experimental data of varying scale: a slot burner, a hood experiment and a compartment fire experiment. All three sets of experiments involve relatively clean burning fuels. Jason and Kevin [2007] concluded that the new method tends to over-predict CO formation because of its assumption that the first step of the reaction was infinitely fast and believe that there is room for improvement to the current approach.

The primary aim of this subsection was to conduct a brief review on the state-of-the-art combustion and toxicity models in modelling of the complex solid fuels burning in real-scale fires. The Global Equivalence Ratio concept, developed for zone modelling, is found to be a useful tool to describe the fire conditions within compartments. Also the generation of CO is well correlated to the GER for both the hood experiments and the reduced room fires [Gottuk, 1992b; Beyler, 1986a; Beyler, 1986b; Pitts, 1994; Wang et

al., 2001; Wang 2006]. Various field modelling approaches using the equivalence ratio concept will be discussed in detail in the Chapter 4.

2.8 Concluding Remarks

Based on the literature survey on fire experiments, it is evident that there is a dearth of comprehensive set of experimental data on real-scale fires involving complex fuels like combustible plastics. Hence it was decided to perform full-scale fire experiments involving cables in collaboration with Swedish National Fire Technology and University of Bolton and conduct detailed measurements of the toxic combustion gases as part of the present research. The author was involved in preliminary assessment of the labyrinth design, construction of the labyrinth, setting up of the analysers, thermocouples, lasers, etc. The author was also involved in the monitoring of the real-time test data and post-processing of the test data. The comprehensive set of experimental data thus obtained will be utilized to validate toxicity models used to simulate the generation and transport of combustion species in real-scale fires involving combustible plastics.

Real fire incidents involve complex fuels such as combustible plastics. Almost all of the investigators modelling the cable fires have targeted their research on predicting the mass loss rate, flame spread or heat release rate [Grayson et al., 2000; Green, 2001; Dey, 2001; Moss, 2001]. Majority of the investigations on modelling of CO and CO_2 during fires deals with liquid or gaseous fuels which have simpler molecular structure and are often easy to conduct combustion experiments. It is important to model the real fires involving realistic fuels to improve the toxic gas hazard modelling.

Given the benefit of fire field models over the zone models, the new methodology that will be developed later in the thesis will be under the field modelling framework. Hence, the basic concepts and sub-models of the field modelling approach will be presented in detail in the next chapter.

Chapter 3

Field Modelling of Enclosure Fires

3.1 Introduction

The rapid progress in the understanding of fire processes and their interaction with building structures and layout has resulted in the development of a wide variety of models that are used to simulate enclosure fires. This chapter gives a detailed description about the Field modelling approach.

3.2 Field Modelling

Field models are the most sophisticated computer models for simulating enclosure fires and are often described as 'CFD' (Computational Fluid Dynamics) models. Over the last two decades, the use of computer models for simulating enclosure fires have increased dramatically. This is due to many factors, including the increased complexity of building design, rapid progress made in understanding the fire and flow phenomena, and the advances made in computer technology. Fire field models based on CFD techniques have the ability to resolve spatial variation of fire environment. Recently, there is a dramatic shift from zone models to field models in fire modelling. Such transformation manifests itself in building codes, regulations and standards through gradual movement away from prescriptive-based to performance-based flexible methodologies. The CFD approach is

considered to be fundamental to the future development of fire modelling which can provide the basis for the development of performance-based fire safety regulations [Novozhilov, 2001; Yeoh et al., 2003].

Using field modeling, the domain of interest is divided into a large number of small control volumes and the basic laws of mass, momentum, and energy conservation are applied to each control volume. Figure 3.1 shows a schematic diagram of how this may be done for a compartment fire.

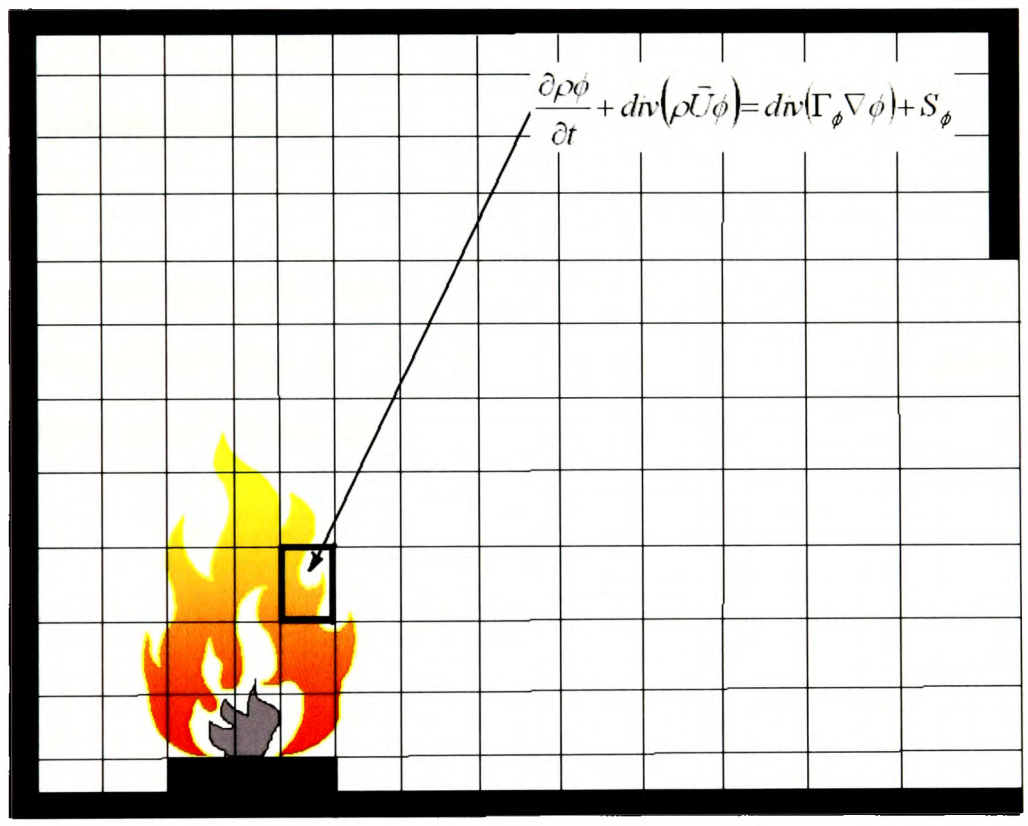

Figure 3.1 Illustration of Field Modelling Concept

3.3 Theoretical Basis for Field Models

Fires and other combustion processes fall in the area of turbulent chemically reacting flows, which are modeled by a set of conservation equations describing the flow, the chemical species mass fraction, and the enthalpy. The CFD fire field modelling software SMARTFIRE [Galea et al., 1999; Ewer et al., 2004] is used in the present investigation to

simulate the detailed thermal and fluid flow. The basic set of conservation equations consists of the classical Navier-Stokes, mass, momentum and energy transport equations. Due to random fluctuations, and wide spectrum of time and length scales of eddies present in turbulent flows, the balance equations are averaged to describe only the mean flow field. The Favre averaged equations of continuity, momentum and scalar variables are given below. Generally, a Favre averaged (mass weighted) quantity, Q is represented by $\tilde{Q}$ with the tilde over the variable and the time averaged quantity by $\overline{Q}$ with a superposed bar. For simplicity, the tilde over any single variable and the superposed bars over the tensor product are omitted. In the following discussion, the product of a variable and a vector indicate Favre averages.

3.3.1 Conservation of Mass

The mass conservation equation, also called the mass continuity equation or simply the continuity equation, implies that for any flow situation, the rate of increase of mass in the control volume must equal the net rate of inflow across its faces.

$$\frac{\partial \rho}{\partial t} + \frac{\partial \rho u_j}{\partial x_j} = 0 \tag{3.1}$$

3.3.2 Conservation of Momentum

Newton's second law of motion states that the rate of change of momentum of a fluid particle equals the sum of all forces acting on the fluid particle. The momentum conservation equation is given by

$$\frac{\partial \rho u_i}{\partial t} + \frac{\partial \rho u_j u_i}{\partial x_j} = -\frac{\partial \Pr}{\partial x_i} + \frac{\partial (\mu_{eff} \operatorname{grad} u_i)}{\partial x_j} - \frac{\partial \rho u_j' u_i'}{\partial x_j} + S_u \tag{3.2}$$

3.3.3 Conservation of Energy

The energy conservation equation is derived from the first law of thermodynamics which states that the rate of change of energy of a fluid particle is equal to the rate of heat addition to the fluid particle plus the rate of work done on the particle. The enthalpy form of the energy equation is given by

$$\frac{\partial \rho h}{\partial t}+\frac{\partial \rho u_j h}{\partial x_j}=\frac{\partial}{\partial x_j}\left\{\left(\frac{k}{c_p}+\frac{\rho \nu_t}{\sigma_T}\right)\mathrm{grad}(h)\right\}+S_h \qquad (3.3)$$

The static enthalpy, h is defined as follows:

$$h=\left(\int_0^T c_p(T)\,dT-h_0\right)+m_f H \qquad (3.3a)$$

Where $c_p(T)$ is the specific heat of the gas mixture, T is the temperature and h_0 is the enthalpy of air in its standard state at 0 K. Under the assumption of a constant and equal specific heat for all components, the temperature can be evaluated from the expression

$$T=\frac{h+h_0-m_f H}{c_p} \qquad (3.3b)$$

3.3.4 Conservation of Chemical Species

$$\frac{\partial}{\partial t}(\rho Y_{fuel})+\mathrm{div}(\rho u Y_{fuel})=\mathrm{div}(\Gamma_{fuel}\,\mathrm{grad}(Y_{fuel}))-S_{fuel} \qquad (3.4\ a)$$

$$\frac{\partial}{\partial t}(\rho Y_{Oxidant})+\mathrm{div}(\rho u Y_{Oxidant})=\mathrm{div}(\Gamma_{Oxidant}\,\mathrm{grad}(Y_{Oxidant}))-S_{Oxidant} \qquad (3.4\ b)$$

$$\frac{\partial}{\partial t}(\rho Y_{CO})+\mathrm{div}(\rho u Y_{CO})=\mathrm{div}(\Gamma_{CO}\,\mathrm{grad}(Y_{CO}))+S_{CO} \qquad (3.4\ c)$$

$$\frac{\partial}{\partial t}\left(\rho Y_{CO_2}\right)+\mathrm{div}\left(\rho u Y_{CO_2}\right)=\mathrm{div}\left(\Gamma_{CO_2}\,\mathrm{grad}(Y_{CO_2})\right)+S_{CO_2} \qquad (3.4\ \mathrm{d})$$

$$\frac{\partial}{\partial t}\left(\rho Y_{H_2O}\right)+\mathrm{div}\left(\rho u Y_{H_2O}\right)=\mathrm{div}\left(\Gamma_{H_2O}\,\mathrm{grad}(Y_{H_2O})\right)+S_{H_2O} \qquad (3.4\ \mathrm{e})$$

The basic reactions assumed in the present study and how the source terms are calculated based on the yields and fuel reaction rate (R_f) are described in detail in Chapter 4 (section 4.5).

3.3.5 Turbulence modeling

In most practical combustion scenarios the flow is turbulent. Turbulent flows are characterized by irregularity and three-dimensionality. The main objective of turbulence modeling is to propose closure for the unknown quantities appearing in the Favre averaged conservation equations such as, $\frac{\partial \rho u_j' u_i'}{\partial x_j}$ (Reynolds stress) and $\frac{\partial \rho u_j' Y_i'}{\partial x_j}$ (Reynolds flux). The standard k-ε turbulence model [Launder and Spalding, 1974] or its variants are the most widely used turbulence models. The k-ε turbulence model is based on *eddy viscosity hypothesis* and solves for two additional variables k, the turbulent kinetic energy, and ε, the dissipation rate to model directly the Reynolds stress and Reynolds flux. As diffusion flames accompanying fires are essentially buoyancy-driven flows, additional production of turbulence due to buoyancy needs to be taken into account. The transport equations for buoyancy modified two-equation, k-ε turbulence model [Hossain and Rodi, 1982; Rodi, 1985] are given as

$$\frac{\partial k}{\partial t}+\frac{\partial \rho u_j k}{\partial x_j}=\frac{\partial}{\partial x_j}\left\{\left(\mu_{lam}+\frac{\rho \nu_t}{\sigma_k}\right)\mathrm{grad}(k)\right\}+P+G-\rho\varepsilon \qquad (3.5)$$

and

$$\frac{\partial \varepsilon}{\partial t}+\frac{\partial \rho u_j \varepsilon}{\partial x_j}=\frac{\partial}{\partial x_j}\left\{\left(\mu_{lam}+\frac{\rho \nu_t}{\sigma_\varepsilon}\right)\mathrm{grad}(\varepsilon)\right\}+\frac{\varepsilon}{k}\left[C_{1\varepsilon}\left(P+C_3\max(G,0)\right)-C_{2\varepsilon}\rho\varepsilon\right] \quad (3.6)$$

where P represents the turbulent production rate

$$P=2\rho\nu_t\left\{\left(\frac{\partial u}{\partial x}\right)^2+\left(\frac{\partial v}{\partial y}\right)^2+\left(\frac{\partial w}{\partial z}\right)^2\right\}+\rho\nu_t\left\{\left(\frac{\partial u}{\partial y}+\frac{\partial v}{\partial x}\right)^2+\left(\frac{\partial u}{\partial z}+\frac{\partial w}{\partial x}\right)^2+\left(\frac{\partial w}{\partial y}+\frac{\partial v}{\partial z}\right)^2\right\} \quad (3.7)$$

and G represents the buoyancy term, given by

$$G=-\beta g\rho\nu_t\frac{\partial T}{\partial y} \quad \text{or} \quad G=-g\nu_t\frac{\partial \rho}{\partial y} \quad (3.8)$$

where g is the acceleration due to gravity and

$$\beta=-\frac{1}{\rho}\frac{\partial \rho}{\partial T} \quad (3.8a)$$

The turbulent viscosity is evaluated by using the expression

$$\nu_t=C_\mu\frac{k^2}{\varepsilon} \quad (3.8b)$$

where $C_\mu, \sigma_k, \sigma_\varepsilon, C_{1\varepsilon}, C_{2\varepsilon}$ and C_3 are turbulence model constants. The default values for these constants as incorporated in SMARTFIRE are given in the table below:

C_μ	σ_k	σ_ε	$C_{1\varepsilon}$	$C_{2\varepsilon}$	C_3
0.09	1.0	1.22	1.44	1.92	1.0

Table 3.1 Turbulence Model Constants

3.3.6 Radiation Modelling

Radiative heat transfer plays a very important role in fires. In many combustion systems it is the dominant mode of heat transfer particularly near the fire source. Radiation contributes significantly to ignition of distant objects and flame spread. The conservation equation for the radiative heat transfer in a medium is described by

$$\frac{d}{dl}I(\Omega,r) = -(a+s)I(\Omega,r) + aI_b(r) + \frac{s}{4\pi}\int_{\Omega'=4\pi} I(\Omega',r)\phi(\Omega'-\Omega)d\Omega' \qquad (3.9)$$

where Ω is a specified direction; l represents the physical path length along Ω; r is the position of a point; $I(\Omega,r)$ stands for radiation intensity along Ω at position r; a and s are absorption and scattering coefficients of the medium respectively; $I_b(r)$ is the blackbody radiation intensity; and $\phi(\Omega' - \Omega)$ is the scattering phase function. In many engineering applications, the effect of scattering is negligible and when the scattering is neglected, the Equation (3.9) is simplified as follows:

$$\frac{d}{dl}I(\Omega,r) = -aI(\Omega,r) + aI_b(r) \qquad (3.10)$$

The two widely used computational methods to solve the radiant heat transfer equation are the *Flux* and the *Discrete Transfer* methods. Since the six-flux radiation model [Hamaker, 1947] is employed in this study, it is outlined in detail.

The Six-Flux radiation model available within SMARTFIRE solves for six equations, one in each co-ordinate direction (both positive and negative directions). In the modified Six-Flux radiation model, heat fluxes R_i, are calculated by solving the additional conservation equations in each component direction which have the following form:

$$\frac{dI}{dx} = -(\alpha+s)I + \alpha E + \frac{s}{6}(I+J+K+L+M+N) \qquad (3.11a)$$

$$\frac{dJ}{dx} = (\alpha + s)J - \alpha E - \frac{s}{6}(I + J + K + L + M + N) \tag{3.11b}$$

$$\frac{dK}{dy} = -(\alpha + s)K + \alpha E + \frac{s}{6}(I + J + K + L + M + N) \tag{3.11c}$$

$$\frac{dL}{dy} = (\alpha + s)L - \alpha E - \frac{s}{6}(I + J + K + L + M + N) \tag{3.11d}$$

$$\frac{dM}{dz} = -(\alpha + s)M + \alpha E + \frac{s}{6}(I + J + K + L + M + N) \tag{3.11e}$$

$$\frac{dN}{dz} = (\alpha + s)N - \alpha E - \frac{s}{6}(I + J + K + L + M + N) \tag{3.11f}$$

where α is the absorption coefficient, s is the scattering coefficient, E is the black body emissive power of the fluid and I, J, K, L, M, and N are the six coordinates direction radiative fluxes.

Transfer of heat through radiation leads to a source in the enthalpy equation given by

$$S_{six\text{-}flux} = \alpha\,((1\text{-}E) + (K\text{-}E) + (M\text{-}E) + (J\text{-}E) + (L\text{-}E) + (N\text{-}E)) \tag{3.12}$$

3.3.7 Combustion modeling

Combustion phenomenon is a mass and energy conversion process during which chemical bond energy is transformed to thermal energy. Fuel reacts with oxygen available in the air to form products such as CO_2 and H_2O which have lower chemical bond energy than the reactants. To define turbulence in a non-reacting flow, at least two quantities; a velocity and a length scale are required. In chemically reacting flows, such as in turbulent combustion, some more time scales such as chemical time scale and diffusive time scale etc. needs to be determined to calculate the turbulence-chemistry interaction and its influence on the flow field. A non-dimensional parameter which is used to characterize the combustion regime is Damköhler number. It is defined as the ratio of flow time to the chemical time. Two limit cases important for non-premixed

turbulent combustion are: pure mixing without combustion (Da → 0) and infinitely fast chemical reaction rate (Da → ∞). In most practical cases, turbulent flames correspond to high values of Damköhler number. Since the time scales of the convective processes are much larger than time scales of the combustion reaction process, infinite reaction rate chemistry assumption is justified in most real fire scenarios. Under the *fast chemistry* assumption, fuel and oxygen cannot co-exist and the instantaneous species concentrations are the functions of the conserved scalar at that instant only. One such scalar parameter that is widely used with much success is the mixture fraction, ξ. The state relations for both reactants and products derived by considering complete combustion reaction for polypropylene (C_3H_6) is shown in Figure. 3.2.

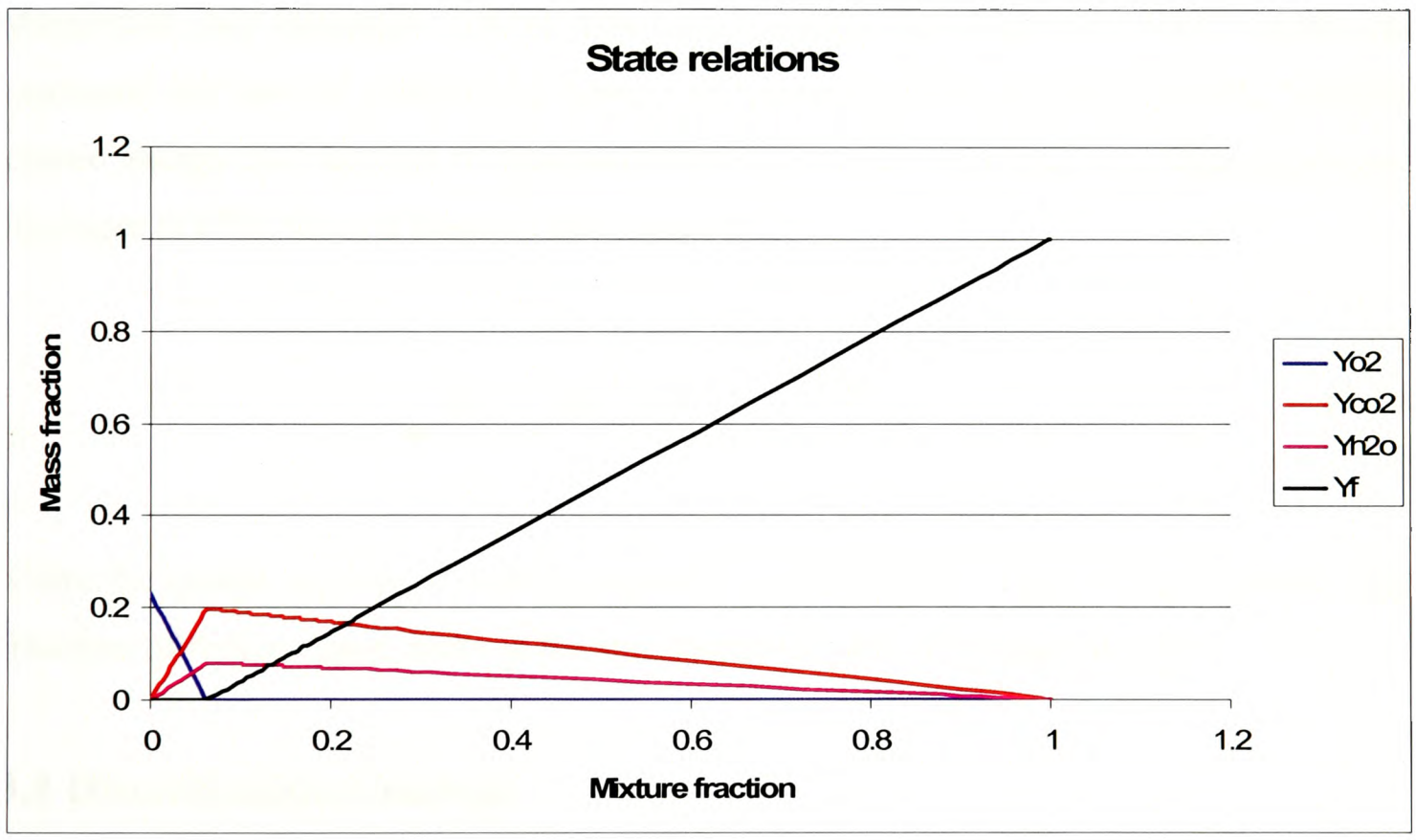

Figure 3.2 State relations for Polypropylene (C_3H_6)

Thus the crux of the problem in modeling turbulent reacting flows with non-premixed reactants lies in the handling of the mean chemical species production term and in the chemistry-turbulence interaction.

3.3.7.1 Eddy Break-Up Model

Eddy Break-Up model (EBU) is the most widely used combustion model with much success. The model originated from the works of Spalding [1971] and is based on the assumption that chemical time scales are fast compared to the turbulence scales. He proposed that the reaction rate may be directly related to the time required for the reactants to mix at molecular level. In turbulent flows, this mixing time depends on the rate of break-up of the eddies by the action of turbulence, and therefore, the rate is proportional to a mixing time defined by the turbulent kinetic energy, k, and the dissipation rate, ε.

Magnussen and Hjertager [1977] have subsequently developed the EBU model and expressed the rate of reaction by mean concentration of a reacting species, turbulent kinetic energy and the rate of dissipation of this energy. According to Magnussen and Hjertager [1977], the fuel burning rate is given by

$$R_f = -A\rho\frac{\varepsilon}{k}\min\left\{Y_f, \frac{Y_{Oxygen}}{\nu}\right\} \tag{3.14}$$

where the model constant A usually takes the value of 4.0. Y_f and Y_{Oxygen} are the mass fractions of fuel, oxygen, and ν is the stoichiometric ratio of oxygen to fuel.

3.4 Discretisation Concept

All the dependent variables of interest obey a generalised conservation principle. The starting point of any numerical method is the mathematical model. In CFD fire modelling, it is the set of governing partial differential equations for the dependent variables and their associated boundary conditions. After selecting the mathematical model, one has to choose a suitable discretisation method, i.e. a method of approximating the differential equations by a system of algebraic equations for the variables at some set of discrete locations in space and time [Ferziger and Perić, 2002]. Variety of discretisation

techniques such as Finite Differencing Method (FDM), Finite Volume Method (FVM), Finite Element Method (FEM), and spectral methods are available. FVM is currently adopted in the present work. In FVM, the calculation domain is divided into a number of non-overlapping control volumes such that there is one control volume surrounding each grid point [Patankar, 1980]. The advantage of using control volume formulation is that it is easy to understand and lends itself to direct physical interpretation. The differential equation is integrated over each control volume assuming piecewise profiles for the variation of any dependant variable between grid points to evaluate the required integrals. The result is a set of discretised equations containing the values of dependant variables at a group of neighboring grid points.

3.4.1 Staggered Grid

The FVM method begins with discretisation of the flow domain and of the relevant transport equations. It seems logical to define and store flow variables and scalar variables at the same location. However, difficulties arise where the velocity or pressure at alternative grid points are equal. As a consequence a highly non-uniform pressure field can behave like a uniform field in the discretised momentum equations. This situation is popularly known as 'checker-board' pressure field. A remedy to this problem is to use a 'Staggered Grid' for the velocity components and evaluate scalar variables, such as pressure, density, temperature etc. at nodal points [Harlow and Welch, 1965]. The arrangement for a two-dimensional flow calculation is shown in Figure 3.3.

Although the staggered grid storage arrangement for the velocity components in each coordinate direction has been the most widely used technique for pressure based solution schemes, it has been recognised that the storage requirements for such schemes is very large. In SMARTFIRE, a collocated grid arrangement, where velocity components in each coordinate direction are stored at the cell-centre, is used. This approach reduces the storage requirements for geometrical related quantities. To alleviate the problem of predicting the 'checker-board' pressure fields, SMARTFIRE uses the Rhie and Chow's interpolation technique [Rhie and Chow, 1982] to predict the flux at the cell-faces, where

they are needed, by means of an algorithm that is free from the checker-board oscillations. Thus the face velocity depends on the pressure values prevailing at the cell centers of the neighboring cells (without using interpolation), and interpolated values of the other quantities used within the momentum equation [Ewer et al., 2004].

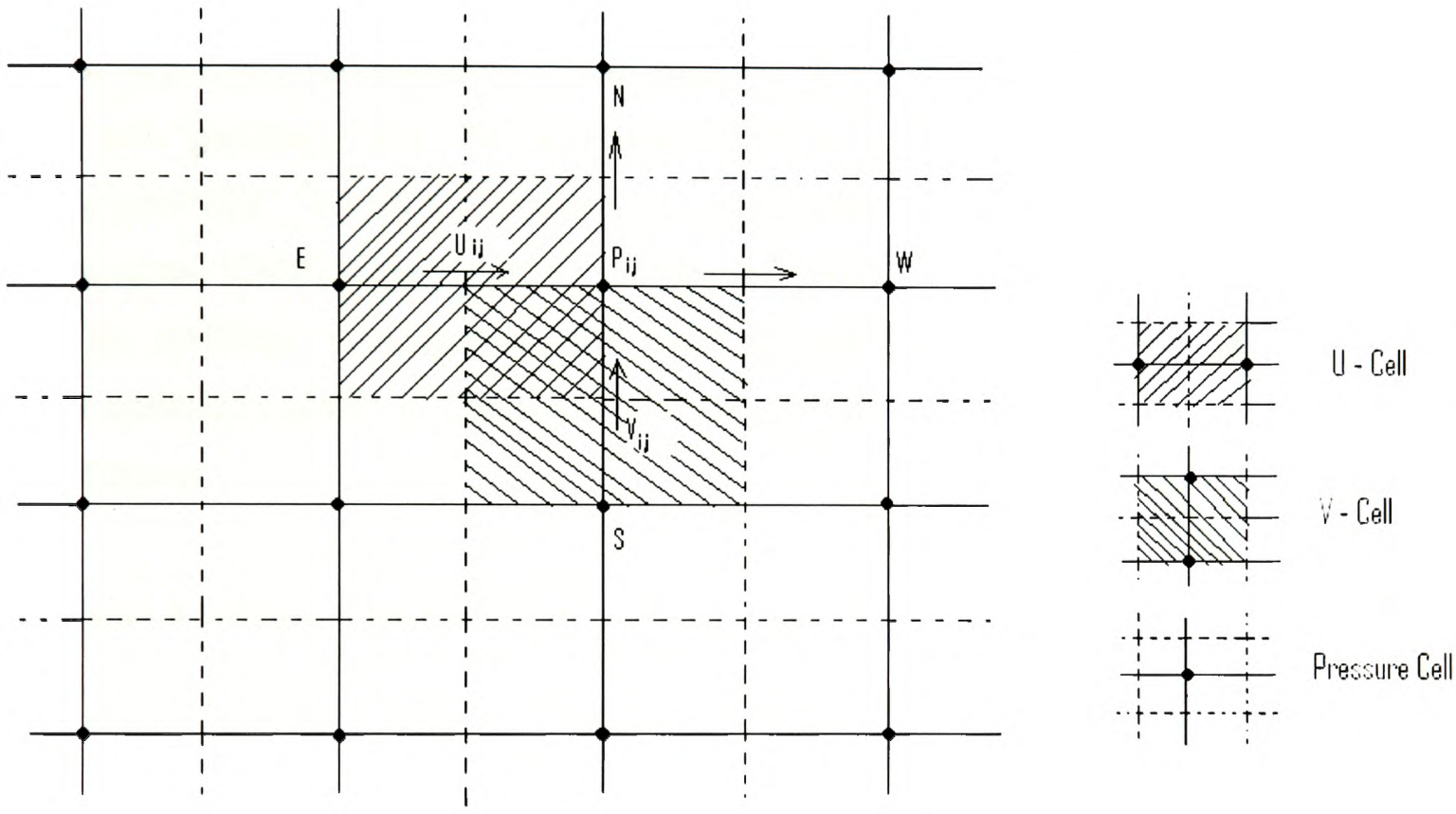

Figure 3.3 Staggered Grid Arrangement for Velocity Components and Pressure

3.5 Solution Algortihm for Pressure – Velocity Coupling

The convection of a scalar variable ϕ, depends on the magnitude and direction of the local velocity components. In general the velocity field is not known in the begining of the calculation and the solution process starts with a guessed velocity field. The velocity and the pressure field emerges as part of the overall solution process along with all other flow variables. The pressure gradient term in the momentum equations is the dominant

momentum source in most flow of engineering importance. The real obstacle in the calculation of the velocity field lies in the unknown pressure field.

3.5.1 The SIMPLEC Algorithm

In 1972, Semi-Implicit Method for Pressure-Linked Equations (SIMPLE) algorithm was proposed by Patankar and Spalding which is essentially an iterative procedure for the calculation of pressure and velocities on the staggered grid arrangement described above [Patankar and Spalding, 1972]. In the present work a modified version of SIMPLE, known as SIMPLEC (SIMPLE-Consistent) is used. SIMPLEC algorithm follows the same steps as the SIMPLE algorithm, except that the momentum equations are modified such that the SIMPLEC velocity correction equations omit terms that are less significant than those omitted in SIMPLE. The solution procedure for SIMPLEC in sequential steps is outlined below.

Step 1: Guess the initial pressure field p^*, velocity field (u^*, v^*, w^*) and scalar field ϕ^* etc.

Step 2: Solve the momentum equations with the guessed pressure field to obtain the velocity field.

Step 3: Solve for the pressure correction equation, p'.

Step 4: Calculate the new pressure field.

Step 5: Correct the velocity field using SIMPLEC- velocity correction equation.

Step 6: Solve the other conserved quantities i.e. Enthalpy, Temperature, Turbulence, Concentration, Radiation, Density, Viscosity, Species mass fractions, etc.

Step 7: Update the corrected pressure, velocity etc. as the latest values and return to Step 2.

Step 8: Repeat Steps 2 to 7 until the solution has converged.

Step 9: Repeat Steps 2 to 8 for the next time step.

3.6 Concluding Remarks

This chapter described the governing conservation laws and various sub-models to model the turbulence, radiation, combustion phenomenon in the CFD modelling approach. Having described the basics of the field modelling approach, the new methodology based on solving separate transport equations for species and using LER concept and yield correlations from the Purser furnace bench-scale experiments to model the source terms will be presented in detail in the next chapter.

Chapter 4

Methodology to Simulate Toxic Species Generation and Transport

4.1 Introduction

The production and transport of combustion products during fires can affect people, property, equipment, and operations. In fact, a relatively small fire can produce enough soot to damage items very far from the source, and the seemingly benign smoldering fire can produce enough Carbon monoxide (CO) to incapacitate people at a remote location. Other combustion products, e.g., HCl, can cause corrosion leading to the failure of critical components, and is directly linked to the mobility of evacuating people [Purser, 1995]. Although combustion products generated during real fires include a vast number of chemical species, in practical circumstances the product gas mixture can be charaterised by a small number of species. Results from several fire fatality studies [Hall 1997; Hirschler et al., 1993; Gann et al., 1994] have demonstrated that CO is the dominant toxic combustion product responsible for the smoke inhalation fatalities. Hence, in the present study, carbon monoxide (CO), carbon dioxide (CO_2), water (H_2O), are assumed to represent the most common combustion products for any organic fuels and the only combustion products simulated to demonstrate the methodology proposed in this chapter. The methodology can be extended to predict various other toxic combustion products which might require additional experimental data similar to that of CO, CO_2.

Modelling the generation of combustion products involves a detailed knowledge of their chemistry. Burning behaviour of most fuels is complex in nature, and the kinetic mechanisms are not well defined if not least understood. To allow an estimation of the fire hazard, the amount of each toxic product produced per unit fuel burned must be assessed, i.e., the species yield must be estimated. Such estimates are possible using data from small-scale or large-scale experiments. Since the large-scale experiments are very expensive, the alternative approach is to obtain the species yield from bench-scale experiments. Developing an effective and simple strategy for incorporating chemistry and thermal degradation into the combustion model was one of the main objectives of this work. To model accurately the generation of combustion products locally, and the transport of products to remote locations, species transport equations for fuel, CO, CO_2, O_2 and H_2O need to be solved. Fortunately, with rapid advancement in computer processing power, computational times have been substantially reduced and solving a few more transport equations have become feasible.

In this chapter, a **S**calar **T**rasport **E**quation based **M**odel using the **L**ocal **E**quivalence **R**atio (**STEM-LER** Model) to model the species source terms is proposed and disscussed.

4.2 Basic Definitions

Equivalence ratio – The ratio of the available fuel mass to the mass of available oxygen (or air), divided by ν, the stoichiometric fuel to oxygen (or air) mass ratio.

Fuel mixture fraction (ξ) – The mass of atoms that originally were from fuel divided by the total mass of the gaseous mixture.

Yield of species (y_i) – The mass of species i produced per unit mass of gaseous fuel.

Mass fraction of a species (Y_i) – The mass of species i divided by the total mass of the gaseous mixture.

Local Equivalence Ratio, ϕ_{local} – The ratio of the available fuel mass to the mass of available oxygen (or air) in a control volume, divided by ν, the stoichiometric fuel mass to oxygen (or air) mass ratio.

4.3 LER Concept

Beyler [1986a; 1986b] and Cetegen [1982] were the first to propose that it might be possible to correlate the species yields and species production rates to the mean upper layer equivalence ratio. This upper layer mean equivalence ratio is widely referred in the literature as Global Equivalence Ratio (GER) [Pitts, 1994; Pitts, 1995]. The GER is defined as the mass of gas in the upper layer derived from the fuel divided by that introduced from air normalised by the stoichiometric ratio.

Gottuk et al. [1992a] conducted reduced scale experiments where he measured both the air inflow and exhaust gases and confirmed that species production inside the compartment are very well correlated with the compartment equivalence ratio, ϕ_C, defined as,

$$\phi_c = \nu \left(\frac{\dot{m}_{fuel}}{\dot{m}_{air,c}} \right) \tag{4.1}$$

where $\dot{m}_{fuel}$ is the mass loss rate of fuel, $\dot{m}_{air,c}$ is the mass flow rate of air into the compartment, and ν is the stoichiometric air-to-fuel ratio.

Lattimer et al. [2005] have defined a modified GER to predict the transported CO, CO_2, O_2 and unburned hydrocarbons to remote locations from a post-flashover compartment fire. The modified GER termed as Control Volume Equivalence Ratio (ϕ_c) is defined as the ratio of the mass loss rate of fuel inside the compartment to the air flow into the compartment plus the air entrained into compartment fire gases flowing along the

hallway. Their study indicated a strong correlation between the species levels in the hallway with the ϕ_c.

Pitts [1997] postulated that there are at least four mechanisms responsible for CO formation in enclosure fires and concluded that GER concept captures only the quenching of fire plume upon entering a rich upper layer. The various concepts based on GER, which were developed mainly for zone modelling, are of great useful tool to describe the fire conditions within compartments and may be used to give a rough estimate on the combustion products leaving the compartment. However, the main shortfall of this technique is that the methodology might predict similar upper layer CO concentrations for reduced-scale and full-scale compartment fires when ventilation conditions (GER) are the same. In reality, the distribution of gases in the upper layer for reduced-scale, full-scale compartments and a long corridor can be quite different [Tuovinen, 1995; Peters, 1984; Wang et al., 2001].

Luo and Beck [1997], introduced a modified combustion model based on the stoichiometric combustion model with the mixture-fraction concept and an oxygen threshold assumption to simulate the combustion process. In their study, they predicted the CO_2 concentration based on mass balance of consumed carbon in the fuel and CO concentration from empirical correlation between the yields of CO and CO_2. In spite of the overall agreement between experimental and the predicted results, the authors concluded that significant discrepancies still exist and attributed the poor performance of the model to the mixture-fraction based formulation.

Floyd et al.[2003] modified the traditional mixture fraction based model to allow for a reaction zone of finite thickness. The modification provided a framework for the inclusion of minor combustion species like CO and Soot in the mixture fraction state relationship using the production of CO and Soot in terms of the mixture fraction.

Recently, Wang et al. [2007] defined the LER over a small control volume as the ratio of mass in the volume that originated from fuel sources to the mass in the same volume that

originated from the natural air stream divided by the stoichiometric fuel-to-air ratio. Wang et al.[2007] calculated the LER from the mixture fraction ξ using the relationship [Tuovinen, 1995; Peters, 1984],

$$\phi_{l,wang} = \frac{\xi \nu}{1-\xi} \tag{4.2}$$

Then the mass fractions of combustion products are expressed with the mixture fraction by the following equations

$$Y_{CO} = y_{CO}(\phi_l)\xi \tag{4.3}$$

$$Y_{CO_2} = y_{CO_2}(\phi_l)\xi \tag{4.4}$$

where $y_{CO}(\phi_l)$ and $y_{CO_2}(\phi_l)$ are yields of CO and CO_2 in g/g of fuel at local equivalence ratio $\phi_{l,wang}$.

One of the main factors influencing the CO and CO_2 generation locally, during fires, is the local vitiated condition, which is represented in this study by the 'Local Equivalence Ratio (LER)'. In the present methodology, the local vitiated condition or the LER is described by the local fuel-to-air ratio neglecting the effect of products and oxygen concentration on the combustion rate [Brohez et al., 2004]. Hence, the LER is defined as follows:

$$\phi_{local} = \frac{\left(\frac{\text{Fuel}}{\text{Oxygen}}\right)_{\text{control volume}}}{\left(\frac{\text{Fuel}}{\text{Oxygen}}\right)_{\text{stoichiometric}}} \tag{4.5}$$

Thus to model accurately the generation of intermediate combustion products like CO, species transport equations for CO, CO_2, O_2, & H_2O need to be solved.

4.4 Numerical Model

The CFD fire field modelling software SMARTFIRE [Galea et al., 1999; Ewer et al., 2004] is used in the present investigation to simulate the detailed thermal and fluid flow. Three-dimensional transport equations based on conservation of mass, momentum, species and enthalpy are solved iteratively. The governing transport equations for all fluid variables can be expressed in a general form [Patankar, 1980; Versteeg and Malalasekera, 1995; Ferziger and Perić, 2002]

$$\frac{\partial}{\partial t}(\rho\phi_i)+\mathrm{div}(\rho u\phi_i)=\mathrm{div}(\Gamma_i\,\mathrm{grad}(\phi_i))+S_{\phi_i} \tag{4.6}$$

Where S_{ϕ_i} is the source term. The dependent variable ϕ_i represents any of the following: three velocity components (u,v,w), pressure (p), enthalpy (h), turbulent kinetic energy (k), dissipation rate of turbulent kinetic energy (ε) or mass fraction of fuel, oxygen, CO, CO_2 & H_2O. Formation of CO during fires is a consequence of incomplete combustion and mainly influenced by the local conditions like vitiation conditions, insufficient temperature to drive the chemical reaction, less residence time in the flame zone.

Production rates of CO and CO_2 in g/g of polymer consumed under various vitiation conditions (GER) were obtained using a tube furnace called Purser furnace [Purser, 1994; Hull et al., 2005]. This bench scale experimental apparatus was developed to enable the study of smoke and toxic combustion product evolution from polymers under the different stages and types of fire. It is assumed that each control volume is similar to a miniature combustion apparatus [Wang et al., 2001; Wang et al., 2007]. The combustion conditions within a control volume and the associated LER are assumed approximately equivalent to that in the Purser furnace with the same value of GER. The correlation

between yields of CO & CO_2 and GER obtained from the Purser furnace tests is then used in this study to model source terms in the transport equations for CO and CO_2. Thus by equating GER in the correlation with the LER in each control volume, generation rates and concentration of species can be estimated.

Tewarson [1994; 1995] has developed generalised relationships to calculate chemical, convective & radiative heats of combustion, and yields of combustion products at various equivalence ratios for halogenated and non-halogenated polymers. The generalised correlation function developed between product yields and equivalence ratio is given as

$$fp_v = fp_\infty \left[1 + \frac{\alpha}{\exp(\phi/\beta)^{-\zeta}} \right] \qquad (4.7)$$

where fp is the product yield, α, β, and ζ are the correlation coefficients characteristics of the chemical composition of the polymers, subscript v represents the condition with restricted amount of air available and ∞ represents the condition with infinite amount of air available.

Purser furnace experiments were carried out at Fire Materials Laboratories CMRI, University of Bolton [Lebek and Hull, 2005; Hull et al., 2005] and yields data were collected during the experiments. In the present study, Tewarson's [1995] correlation function was used to obtain a mathematical fit to the Purser furnace data. The CO and CO_2 yield data for various equivalence ratios obtained from the Purser furnace and the correlation curve fit for NYM, NHMH and RZ1-K power cables are shown in the Figures 4.1 to 4.3. The correlation function with constants for the yields of CO and CO_2 in g/g of polymer consumed for the three cables considered in the present investigation, are given as follows:

NYM:

$$y_{CO} = 0.0911 * \left[1 + \frac{4.23}{\exp(\phi_{local} / 1.2)^{-1.7}} \right] \tag{4.8}$$

$$y_{CO_2} = 1.849 * \left[1 - \frac{0.7912}{\exp(\phi_{local} / 0.8)^{-3.8}} \right] \tag{4.9}$$

NHMH:

$$y_{CO} = 0.00917 * \left[1 + \frac{33.5}{\exp(\phi_{local} / 0.9)^{-4.5}} \right] \tag{4.10}$$

$$y_{CO_2} = 3.24909 * \left[1 - \frac{0.67735}{\exp(\phi_{local} / 1.0)^{-2.5}} \right] \tag{4.11}$$

RZ1-K:

$$y_{CO} = 0.00887 * \left[1 + \frac{18.2}{\exp(\phi_{local} / 0.8)^{-11}} \right] \tag{4.12}$$

$$y_{CO_2} = 2.445 * \left[1 - \frac{0.4167}{\exp(\phi_{local} / 0.6)^{-11}} \right] \tag{4.13}$$

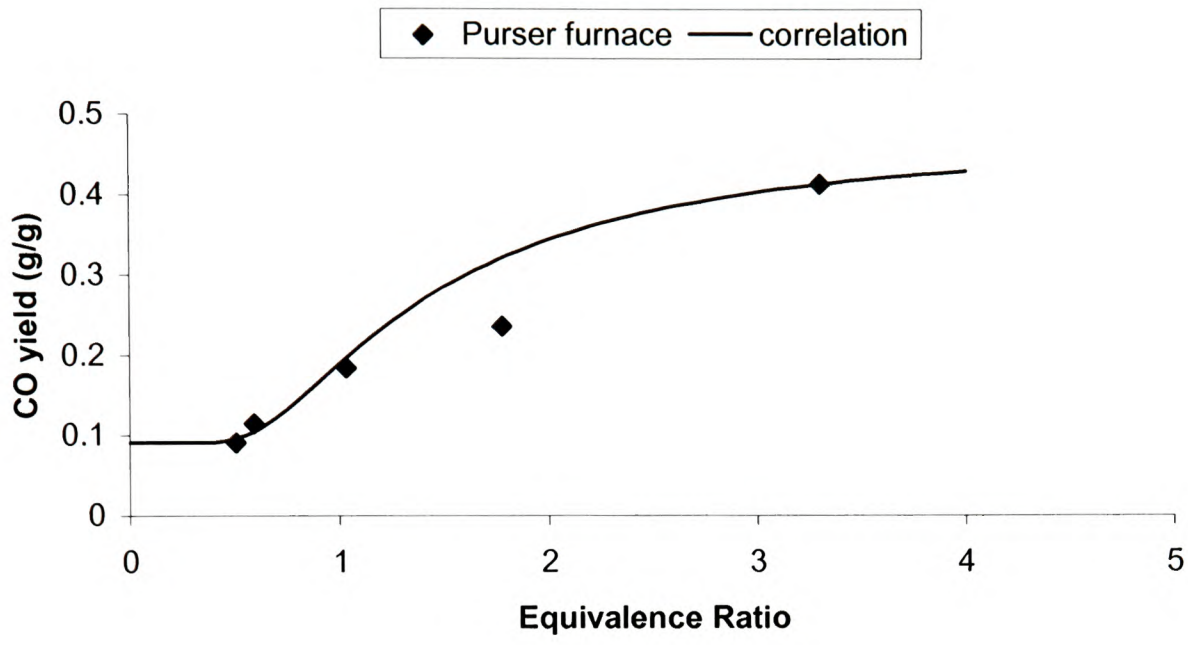

(a)

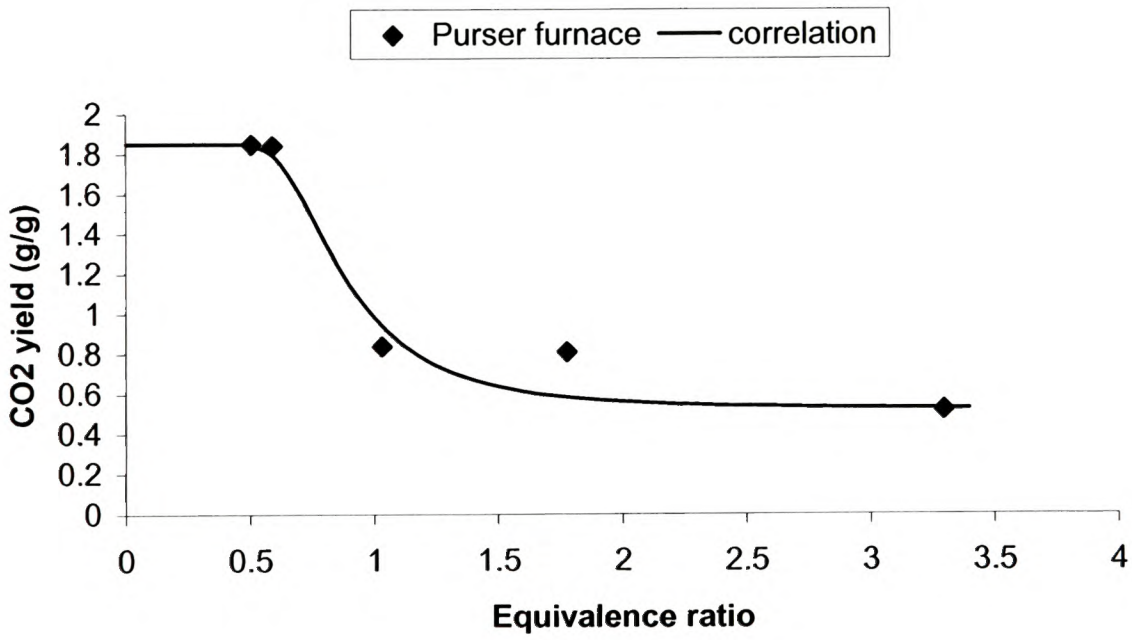

(b)

Figure 4.1 CO and CO_2 yields for NYM

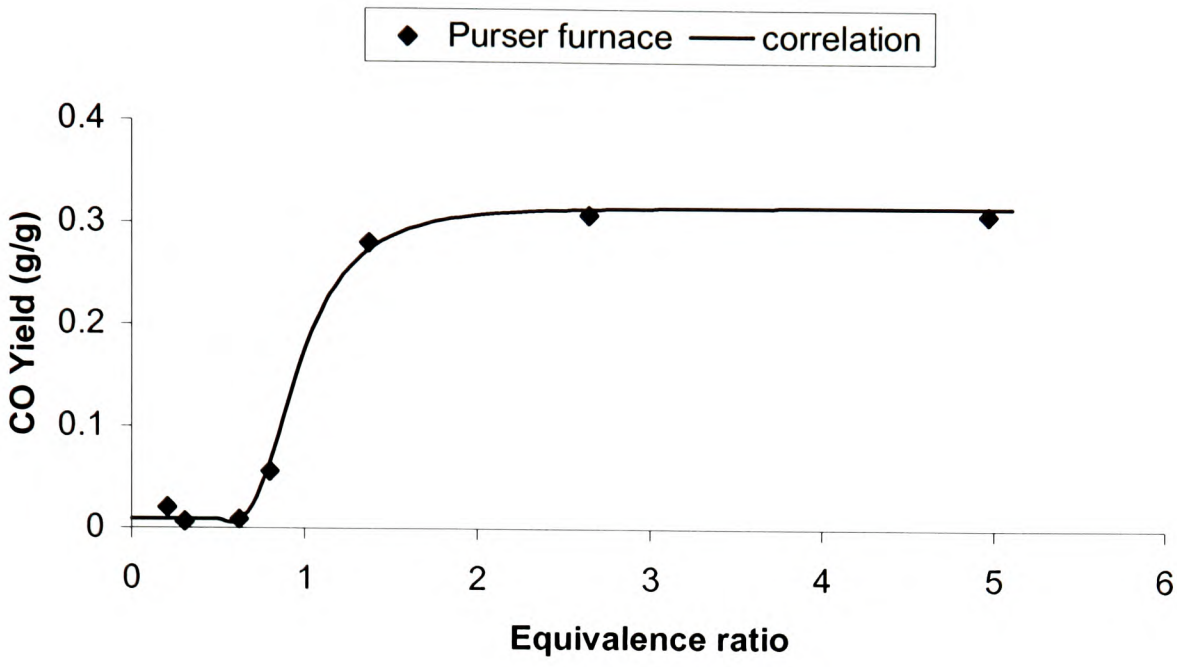

(a)

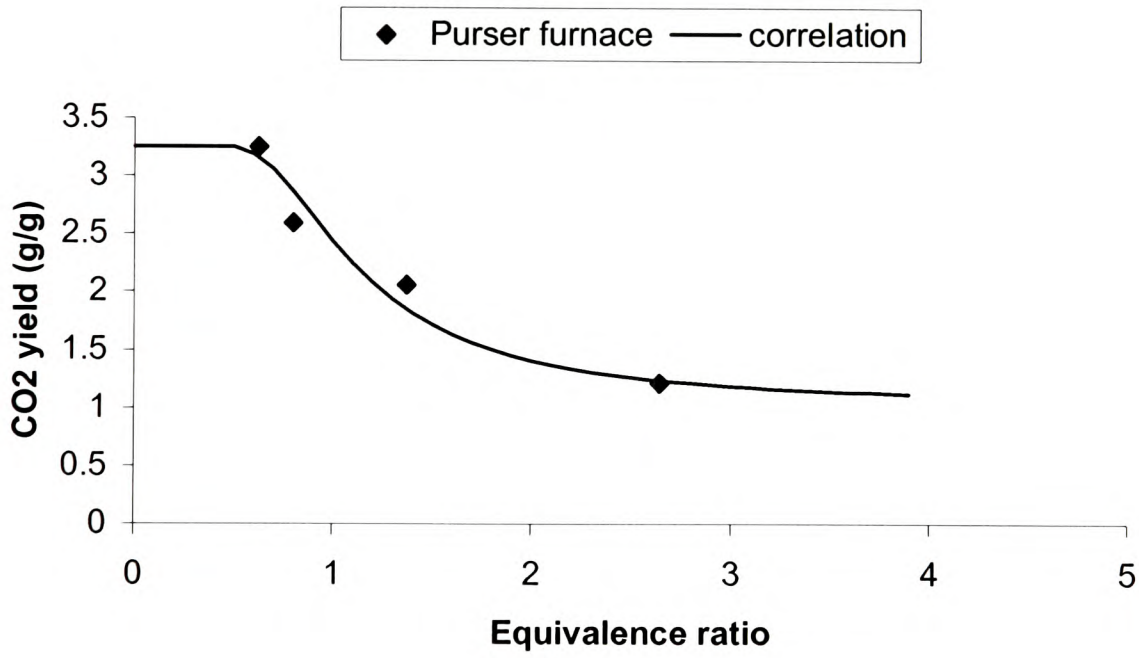

(b)

Figure 4.2 CO and CO_2 yields for NHMH

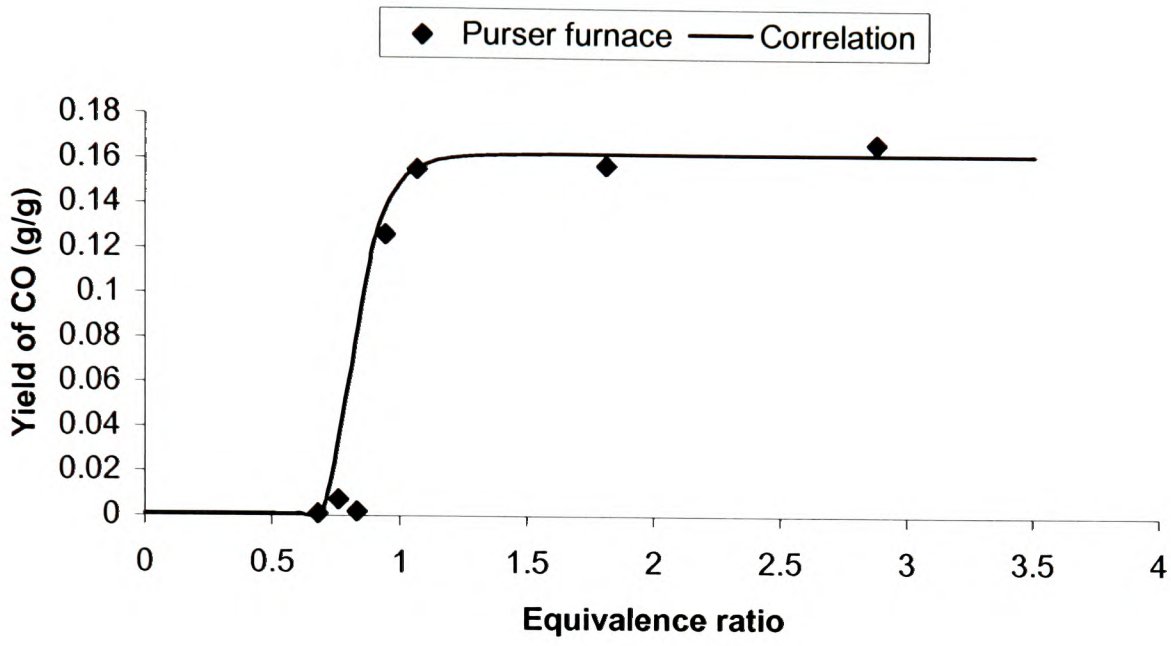

(a)

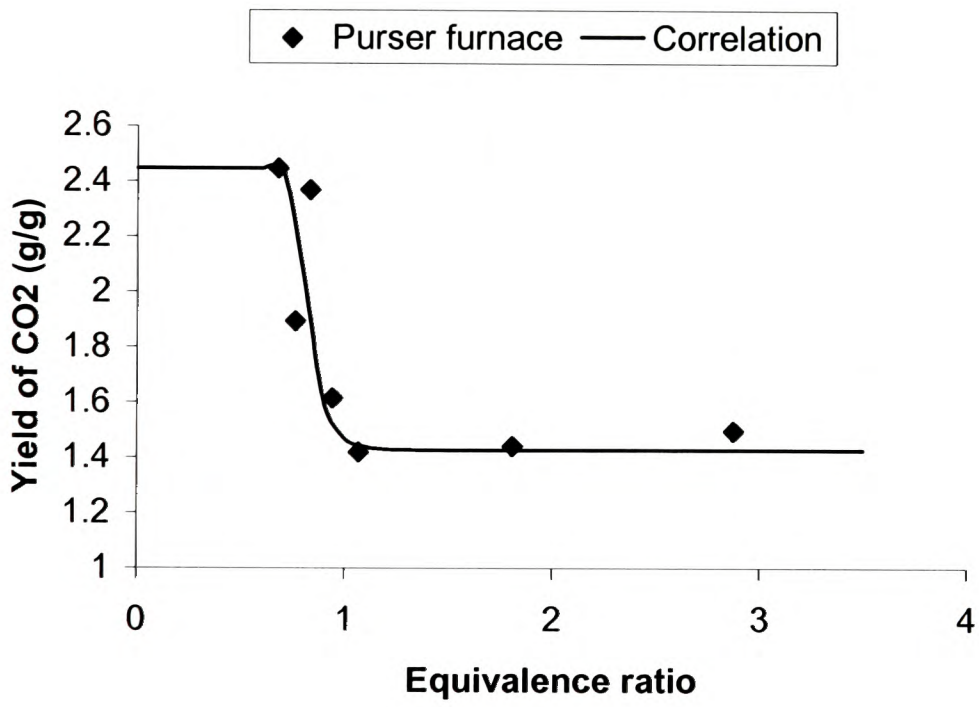

(b)

Figure 4.3 CO and CO_2 yields for RZ1-K

4.5 STEM – LER Model

4.5.1 Modelling of the source term (S_{fuel}) in scalar transport equation for Y_{fuel}

In the EBU described in Chapter 3, the fuel and oxygen are assumed to be consumed in their stoichiometric proportions with some stable intermediate species like CO being ignored. In fuel-rich areas, the standard EBU model under-predicts the combustion rate assuming that no CO is generated [Fletcher et al. 1994; Chow, 1995]. According to EBU hypothesis, in fuel-rich regions, the combustion rate is limited by the rate of dissipation of the oxygen containing eddies as they show the most marked intermittence. Since significant CO is generated in the fire plume, for a given oxygen concentration, the actual fuel involved in the combustion process is more than that is predicted by the standard EBU. In the present investigation, the standard EBU is modified to calculate the actual fuel involved in the fuel-rich combustion region. The actual fuel involved in the combustion can be calculated using the yield vs equivalence ratio correlations for CO and CO_2 obtained from the Purser furnace and the oxygen concentration. Following is a simple state relationship calculation for the NHMH cable using the Purser furnace data. The mixture fraction, ξ corresponding to an equivalence ratio is calculated from the relation given by Equation 4.2. The amount of CO_2 and CO generated for 1 kg of fuel and air mixture at any mixture fraction (or equivalence ratio) is given by

$$Y_{CO} = Y_f * y_{CO}(\xi) \tag{4.14}$$

$$Y_{CO_2} = Y_f * y_{CO_2}(\xi) \tag{4.15}$$

and state relation for Y_f is calculated from the carbon balance considering only the products CO and CO_2.

The state relations for NHMH cable material is compared with their corresponding state relations for their basic molecular structure, C_3H_6, under ideal complete combustion

situation and are shown in Figure 4.4. The stoichiometric mixture fraction, ξ_{st} for C_3H_6 is 0.0672. It is evident from the Figure 4.4, that the fuel consumption is more for $\xi > 0.08$ which was based on the yields of CO and CO_2 obtained from Purser furnace.

Hence, in the present version of EBU, the rate of fuel burning, R_f is modified as follows

$$R_f = A\rho\frac{\varepsilon}{k}\min\left\{Y_f, \frac{Y_{air}}{s(\phi_{local})}\right\} \tag{4.16}$$

where $\frac{Y_{air}}{s(\phi_{local})}$ is the amount of fuel that can be consumed by the available air at the vitiation condition ϕ_{local} and $s(\phi_{local})$ takes into consideration the amount of CO generated. The following sub-section is devoted to describe how the yield data from small-scale experiments can be used to calculate the combustion rate better.

For the NYM type power cable, the basic molecular structure is C_2H_3Cl (PVC). The combustion products for NYM include CO, CO_2, H_2O, HCl and unburned hydrocarbons. The chemical reaction equation for the NYM cable considered is

$$C_2H_3Cl + a\,O_2 \rightarrow b\,CO + c\,CO_2 + d\,H_2O + HCl + e\,CH\,(UHC) \tag{4.17}$$

For the NHMH and RZ1-K type power cables, the basic molecular structure is assumed to be C_3H_6 (Polypropylene). The combustion products include CO, CO_2, H_2O and unburned hydrocarbons. The chemical reaction equation for the NHMH and RZ1-K type cables considered is

$$C_3H_6 + a\,O_2 \rightarrow b\,CO + c\,CO_2 + d\,H_2O + e\,CH\,(UHC) \tag{4.18}$$

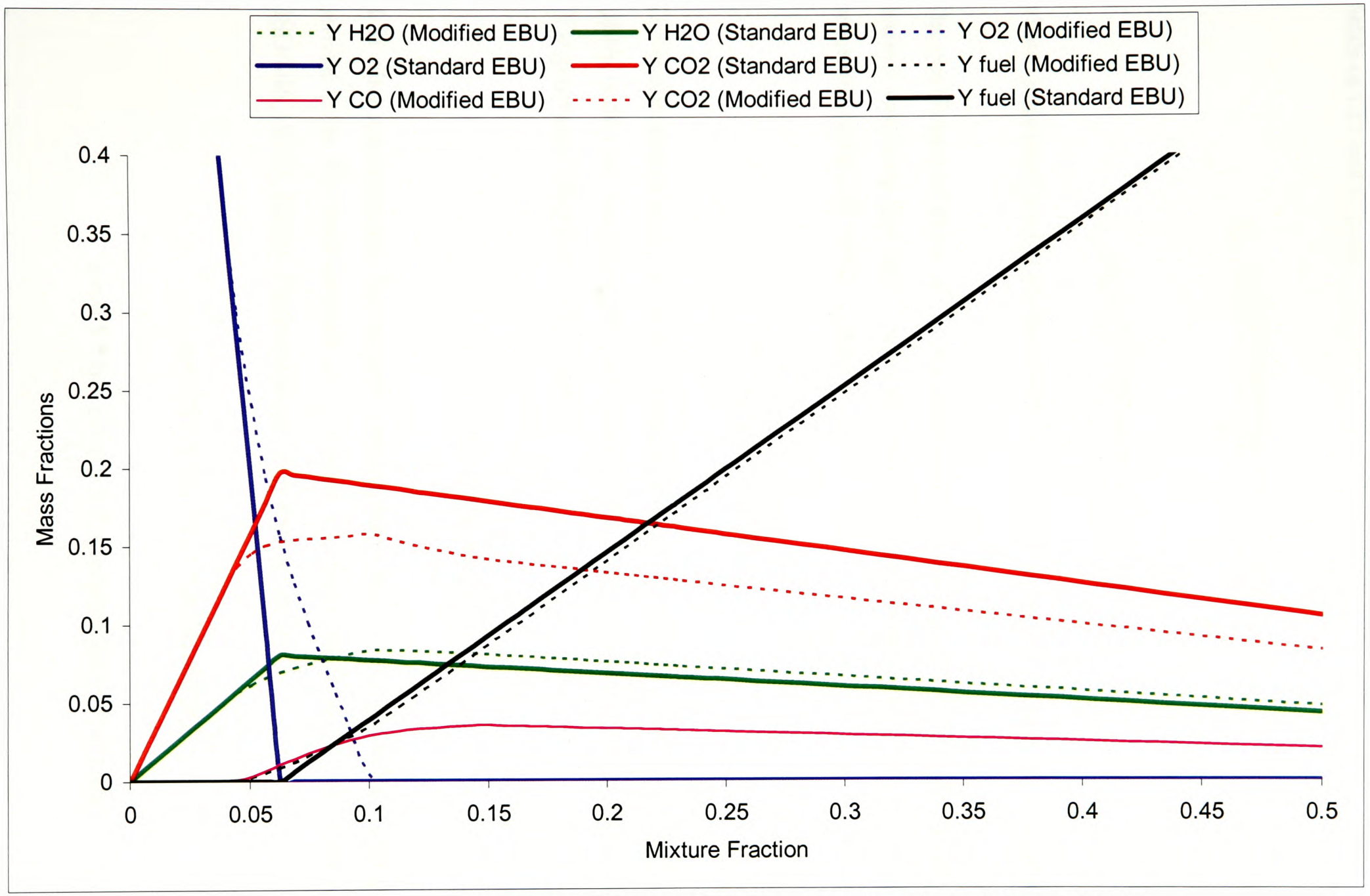

Figure 4.4 Comparison of state relationship for NHMH (C_3H_6)

The coefficients b and c in equations 4.15 and 4.16 are evaluated from their respective yields of CO and CO_2 as

$$b = \frac{y_{CO}(\phi) * \text{molecular wt. of fuel}}{28} \tag{4.19}$$

$$c = \frac{y_{CO_2}(\phi) * \text{molecular wt. of fuel}}{44} \tag{4.20}$$

where $y_{co}(\phi)$ and $y_{co2}(\phi)$ are the yields of CO and CO_2 in g/g of polymer consumed.

The coefficient of H_2O, 'd' in the combustion reaction equation 4.17 for NYM cable is derived assuming that half a mole of H_2O is generated for every mole of CO and CO_2 generated [ISO/DIS 19703, 2004].

$$d = (b + c)/2 \text{ (for NYM)} \tag{4.21}$$

The coefficient of H_2O, 'd' in the combustion reaction equation 4.18 for NHMH and RZ1 cables is derived assuming that one mole of H_2O is generated for every mole of CO and CO_2 generated [ISO/DIS 19703, 2004].

$$d = b + c \text{ (for NHMH and RZ1)} \tag{4.22}$$

It is also assumed that the oxygen consumption from the surrounding atmosphere is derived from the total amount of combined oxygen contained in CO, CO_2 and H_2O [ISO/DIS 19703, 2004]. The coefficient 'a' is then given by

$$a = 0.5 * b + c + 0.5 * d \text{ (for NYM)} \tag{4.23}$$

$$a = 0.5 * b + c + 0.5 * d \text{ (for NHMH and RZ1-K)} \tag{4.24}$$

Hence the dynamic air to fuel ratio, $s(\phi)$ is evaluated as a function of LER as

$$s(\phi) = \frac{4.34 * 32 * a}{\text{molecular wt. of fuel}} \tag{4.25}$$

The factor, 4.34 in the above equations converts the 'oxygen to fuel ratio' to 'air to fuel ratio' assuming that the oxygen mass fraction in the air as 23 %. The effect of calculating the variable $s(\phi)$ is evident from the comparison of state relationships (Figure 4.4), where the fuel consumption under fuel rich conditions is more than the fuel consumption based on standard EBU. The modified EBU gives higher temperature in the fire plume than the standard EBU, but the temperatures out of the fire plume and at distant locations is predicted better. This is discussed in detail in Chapter 7, with an example showing the improvement in temperature predictions at far locations.

4.5.2 Modelling of source terms in transport equations of Y_{CO}, Y_{CO2}, $Y_{oxidant}$ and Y_{H2O}

The Eddy Break-up model and Eddy Dissipation Model are based on the assumption that the chemical reactions occur at the smallest eddy level, i.e. where the molecular transfer process is more significant than the heat conduction and chemical reaction process. Thus under infinitely fast chemistry assumption, Magnussen and Hjertager postulated that the combustion process is dominated by eddy mixing process. So, "the combustion rate can be determined by the rate of intermixing on a molecular scale of fuel and oxygen eddies, in other words, by the rate of dissipation of eddies" [Magnussen and Hjertager, 1977].

Given that the yields of CO and CO_2 obtained from the purser furnace are in g/g of polymer consumed, the source terms S_{CO}, S_{CO2}, S_{H2O} and $S_{oxidant}$ in the transport equations for CO, CO_2, H_2O and Oxidant in kg/(m^3s) (the units correspond to the discretised form of the species conservation equations) can be calculated as follows:

$$S_{CO} = y_{CO}(\phi_{local}) * R_f \tag{4.26}$$

$$S_{CO_2} = y_{CO_2}(\phi_{local}) * R_f \tag{4.27}$$

$$S_{H_2O} = 0.5 * 18 * \left(\frac{S_{CO}}{28} + \frac{S_{CO_2}}{44} \right) \text{ (for NYM)} \tag{4.28}$$

$$S_{H_2O} = 18 * \left(\frac{S_{CO}}{28} + \frac{S_{CO_2}}{44} \right) \text{ (for NHMH and RZ1-K)} \tag{4.29}$$

$$S_{Oxygen} = 32 * \left(0.5 \frac{S_{CO}}{28} + \frac{S_{CO_2}}{44} + 0.5 \frac{S_{H_2O}}{18} \right) \tag{4.30}$$

where $y_{CO}(\phi_{local})$ and $y_{CO_2}(\phi_{local})$ are yields of CO and CO_2 in g/g of polymer consumed at local equivalence ratio of ϕ_{local}. Using the equations 4.16, 4.26-4.30, the source terms in the species conservation equations (Equations 3.4a – 3.4e) are evaluated. Hence, the distribution of species such as fuel, CO, CO_2, O_2 and H_2O during enclosure fires involving complex combustibles can be computed by the above methodology using the yields of CO and CO_2 obtained from the bench-scale tests (Purser furnace).

4.6 Concluding Remarks

Modelling the generation of combustion products involves a detailed knowledge of their chemistry. Burning behaviour of most fuels is complex in nature, and the kinetic mechnisms are not well defined if not least understood. To allow an estimation of the fire hazard, the amount of each toxic product produced per unit fuel burned must be assessed, i.e., the species yield must be estimated. The species yields correlate well with the Global Equivalence Ratio (GER) in small-scale combustion apparatus. Purser furnace (IEC 60695-7-50) is one such small-scale toxicity test method which was successfully demonstrated in obtaining species yield correlations by burning samples under well controlled decomposing conditions equivalent to that occuring in different types and stages of real fire.

To model accurately the generation of combustion products locally, and the transport of products to remote locations, species transport equations for fuel, CO, CO_2, O_2 and H_2O needs to be solved. Hence in the present methodology, a **S**calar **T**ransport **E**quation based **M**odel using the **L**ocal **E**quivalence **R**atio (**STEM-LER** Model) to model the species source terms is proposed which solves separate transport equations with individual source terms for the species. The fuel consumption rate or the combustion rate is calculated by a modified EBU model which calculates the fuel consumption in fuel rich areas based on the yields of CO and CO_2. The source terms for CO and CO_2 transport equations are calculated based on their yield correlations obtained from the Purser furnace and the Local Equivalence Ratio (LER) in each control volume. The source term for H_2O transport equation is calculated based on the generation of CO and CO_2 and finally, the source term for Oxidant transport equation is calculated based on the oxygen consumed in the generation of CO, CO_2 and H_2O. Thus, the distribution of species such as fuel, CO, CO_2, O_2 and H_2O during enclosure fires involving complex combustibles can be computed by the above methodology using the yields of CO and CO_2 obtained from the bench-scale tests (Purser furnace).

The next chapter will describe the Purser furnace experimental setup, operating procedure and some CFD simulations of thermal and flow field inside the furnace to gain some insights into how the bench-scale experiments work.

Chapter 5

Purser Furnace Toxicity Test Method

5.1 Introduction

Manufacturers, suppliers, specifiers, regulators and those who model fires involving electro-technical products are often faced with the need to generate toxicity data from decomposition tests on materials. These data are often used in toxic hazard calculations and chemical analyses of the toxic potency of products. Toxic potency data can be derived from real-scale burning of commercial furnishing and building products. However, given the number of such products in use in residential, public facilities, transportation, etc., the cost of such testing would be inordinate. An alternative approach is to obtain the data needed by burning small specimens cut from commercial products in a bench-scale apparatus. Numerous devices have been developed for this purpose [Gann, 2004]. Babrauskas [1992] presented a method whereby the bench-scale toxic potency measurements were computationally corrected to better approximate the toxic potencies measured in real-scale, post-flashover room fires since underestimation of CO yields was typical of small-scale tests until then. Later, Purser [Purser, 1994] developed an improved version of DIN 53436 test method using a tube furnace with a moving sample decomposing at different temperatures and air flow rates, designed to reproduce the decomposition conditions of a range of fire types as characterised in ISO TR 9122-1 [1989]. A schematic diagram of Purser furnace is shown in Figure 5.1.

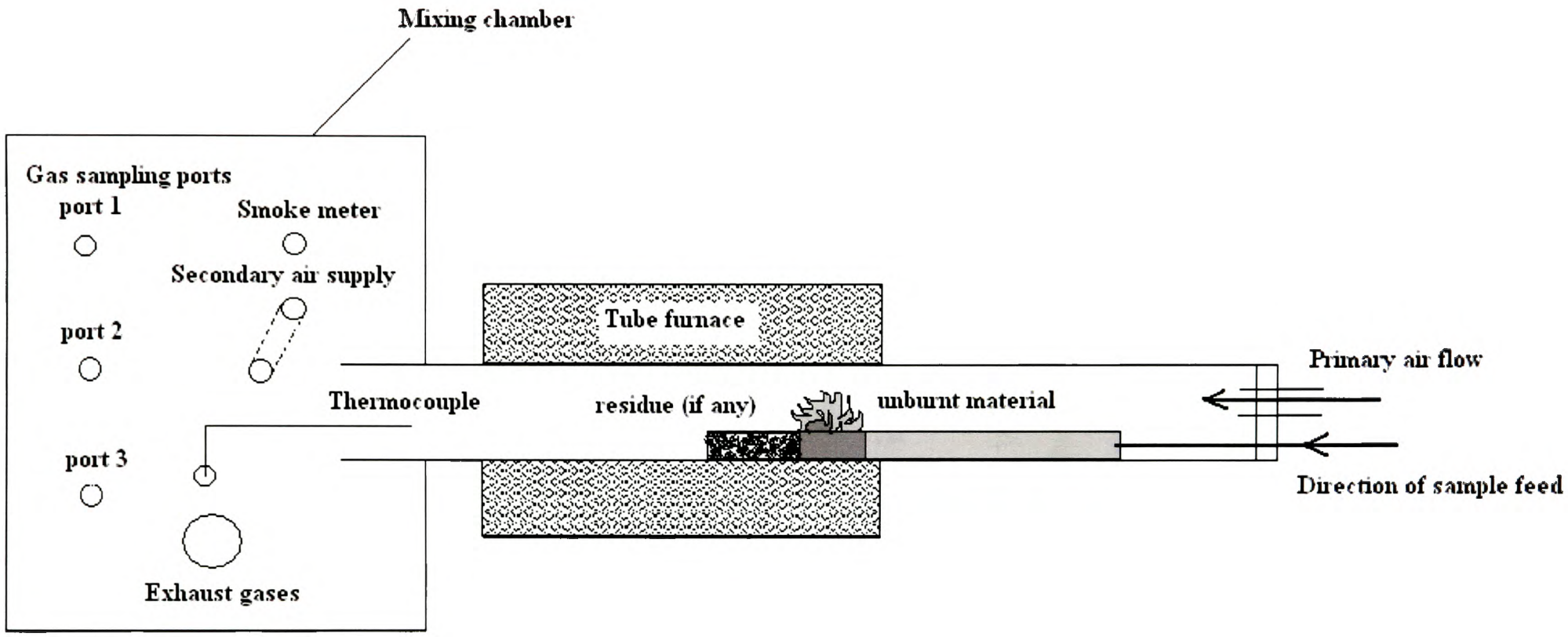

Figure 5.1 Purser furnace

IEC 60695-7-50 [2002] describes a test method for the generation of fire effluent and the identification and measurement of its constituent combustion products under the guidance of ISO TC 92 SC3. This method involves the decomposition of materials or products under various decomposing conditions occurring in different types and stages of real fire.

Simulations of flow and fire condition inside the tube (Purser) furnace have been carried out and validated with the measurements in this study. The objective is to demonstrate the validity of using Computational Fluid Dynamics (CFD) technique in predicting the fire environment inside the tube furnace. These numerical investigations are also used to verify critical experimental operating parameters that affect the performance of the Purser furnace and also to get some insights into the working of Purser furnace toxicity method.

5.2 Previous Research on Purser Furnace

Carman et al. [2000] carried out a systematic assessment of the experimental parameters that affect the performance of the Purser furnace. The parameters considered were

- Equivalence ratio ϕ_g, derived from the sample mass and primary air flow-rate
- Furnace temperature
- Sample feed-rate
- Secondary air flow.

Based on their findings, an optimum value for the sample feed-rate and the secondary air supply rate was suggested in order to create steady-state combustion conditions within the Purser furnace.

Hull et al. [2000; 2002] measured the concentrations of combustion products for various polymers and fire retarded polymers using the Purser furnace under a range of equivalence ratios varying from 0.5 to 1.5. The CO yields reported in their study were around 0.2 g/g which corresponds to the CO yields in full-scale flashover fires. The

CO yields under fuel-rich conditions disproved the general opinion that all small-scale fire tests under-predict CO yields does apply to the Purser furnace. They also reported a strong correlation between the CO_2/CO ratio with equivalence ratio for non-oxygen containing polymers like Polypropylene (PP), Polystyrene (PS) and Low Density Polyethylene (LDPE).

Fardell et al. [2004] studied fires under oxygen starved conditions using full-scale (based on the ISO 9705 room) and bench-scale (based on the BRE tube furnace BS 7990:2003) tests. They developed a prototype empirical predictive model based on the tube furnace yield data to predict toxic gas yields in real-scale vitiated fires and then validated the model with a full-scale test. Fardell et al. [2004] also demonstrated the use of 'Global Equivalence Ratio' ϕ as a basis for comparing species yields in small and large scale test.

Hull et al. [2005] performed a comparison study of toxic product yields obtained from a steady state tube furnace method (the purser furnace, IEC 60695-7-50), a static tube furnace, and a large scale test (ISO 9705 room). Excellent correlation between small and large scale experiments was reported for CO and CO_2 yield data of polypropylene as a function of equivalence ratio. Hull et al. [2000; 2002; 2005] extensively studied the Purser furnace and demonstrated the following

a. Purser furnace can create stable burning, even for poorly ventilated fire types.
b. The measured O_2 concentrations and CO_2/CO ratio show that the appropriate fire types are being created.
c. The product concentrations of CO and CO_2 and the fire toxicity show a marked dependence on the equivalence ratio [Pitts, 1995].

Though some systematic assessment on experimental parameters affecting the performance of the Purser furnace has been done, much more investigations need to be pursued [Carman et al., 2000]. Computational Fluid Dynamics (CFD) offers a convenient and affordable approach to do it. This work demonstrates the ability of the computational fire field modelling to simulate the test method. The simulation results were then validated with the experimental measurement.

5.3 Purser Furnace Toxicity Test Method

5.3.1 Experimental Setup

The tube furnace with a heating zone is equipped with an adjustable electric heating system capable of controlling the final temperature. The tube furnace is made of clear heat resistant quartz, resistant to the effects of fire effluent. Some of the photos on the Purser furnace setup taken at Fire Materials Laboratories, CMRI, University of Bolton is shown in Figures 5.2a to 5.2c. The decomposition conditions in the furnace are set using different combinations of temperature and primary air flow rate in separate test runs, to model the decomposition condition in a range of fire stages [ISO, 1989]. The characterisation of flaming combustion into fire types, showing the oxygen concentration, CO_2/CO ratio, and the temperature is given in Table 5.1.

5.3.2 Operating Procedure

As an operating procedure it is necessary to standardise the temperature to which the test specimen and the combustion products released from the test specimen are subjected as they pass through the quartz furnace tube. For the furnace to be acceptable the maximum temperature should be near the centre of the furnace under static conditions (i.e. with no air flow through the quartz furnace tube) and the maximum temperature should be around $(T_{controler} - 40)^0$ C where $T_{controller}$ is the temperature set in the furnace temperature controller. The inlet end of the quartz furnace tube has a closure with openings in it to allow the primary air inlet and the test specimen boat drive bar to pass through. Test specimen boat is also made from clear heat resistant quartz. The mixing or dilution chamber, consists of approximately a cubic box. Ports for sampling lines are provided in the chamber for taking samples from the test atmosphere. The fire effluent is expelled from the quartz furnace tube into the dilution or measuring chamber, where it is diluted with secondary air supply to a nominal total air flow rate of (50 ± 1) l/min through the chamber and then exhausted to waste. Secondary air supply tube passes through the wall of mixing and measurement chamber and ends approximately 70 mm above the end of the quartz

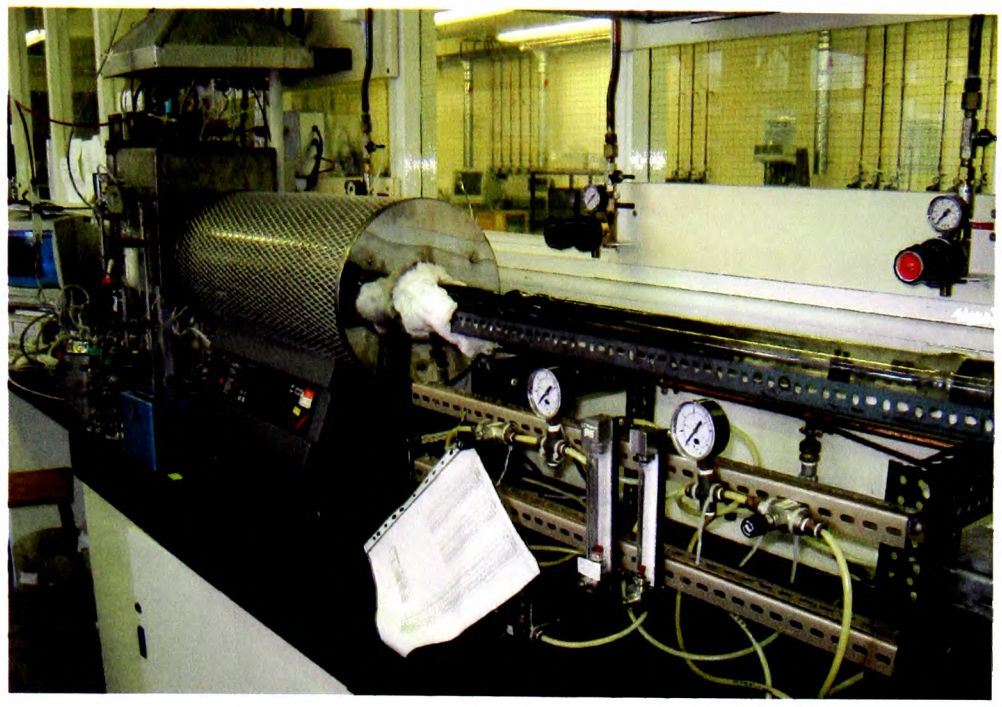

(a) Sample Drive Mechanism

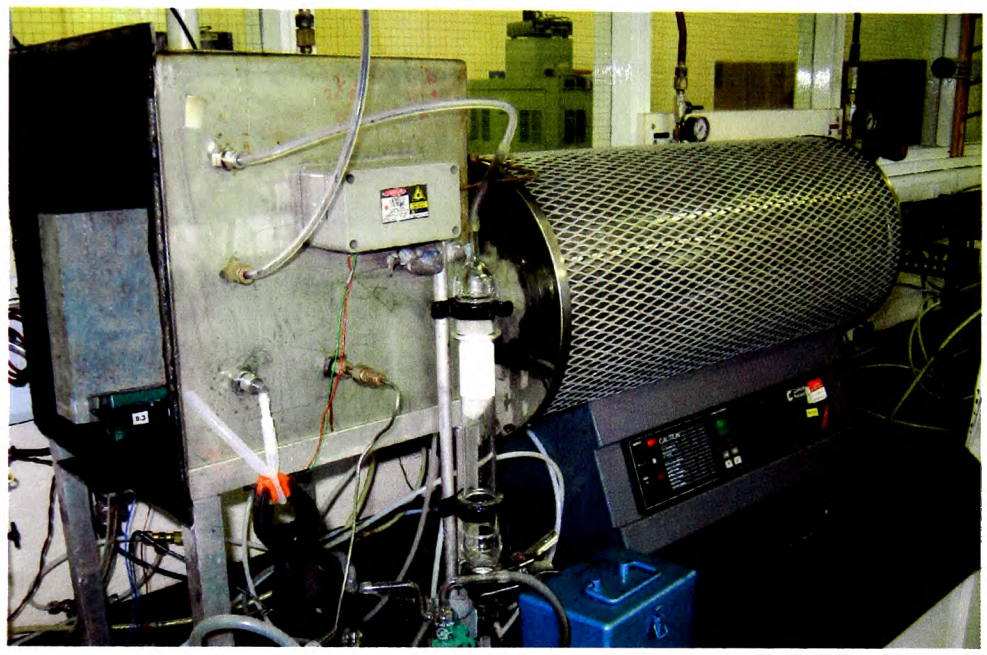

(b) Mixing Chamber ports and Furnace Controls

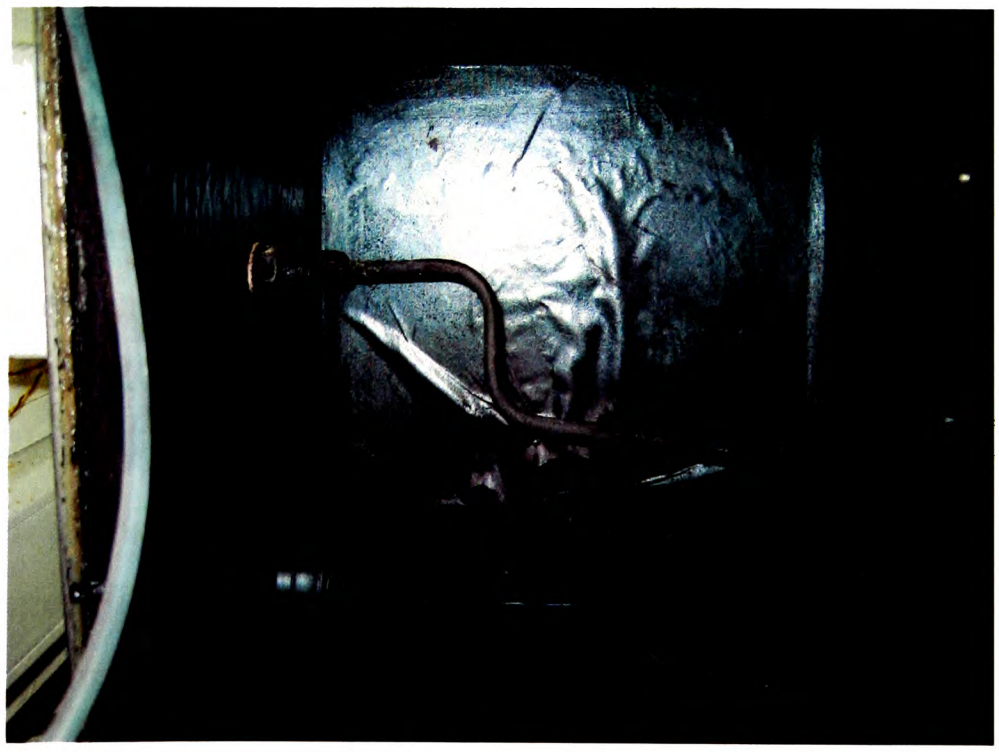

(c) Inside Mixing Chamber

Figure 5.2 Purser furnace photos

furnace tube so that the secondary air supply intercepts the rising plume to facilitate the efficient mixing of the test atmosphere.

IEC 60695-7-50 and BS 7990: 2003 standards describe the apparatus and procedure for this test method [2002; 2003]. ISO/DIS 19703 [2004] standard provides the definitions and formulae for the calculation of toxic product yields and the fire conditions under which they have been derived in terms of equivalence ratio and combustion efficiency.

The Purser tube furnace method was mainly developed for the generation of fire effluent for identification and measurement of its constituent combustion product yields. The data on combustion product constituents and yields obtained are used as part of the assessment of toxic potencies, toxic hazards from fires, health and safety assessments of combustion products etc. Operating parameters of the experiment like primary air flow rate, fuel mass feed rate, furnace temperature and geometry of the apparatus affect the stability of specimen burning inside the tube furnace. The test apparatus and the operating conditions should be set appropriately in order to obtain steady state conditions for all materials under all decomposition conditions. Several test runs are to be performed to set the apparatus for a particular decomposition condition in order to obtain stable, steady state condition for at least 5 min during which the concentrations of effluent gases can be measured.

5.3.3 Experimental Data

Experiments were carried out at Fire Materials Laboratories CMRI, University of Bolton. The CO and CO_2 yields versus equivalence ratio data obtained by burning NYM and NHMH type cables in purser furnace were shown in Figures 4.1 and 4.2. The correlation curves of product yields versus ϕ were obtained by fitting Tewarson's [1995] correlation function to the tube furnace data. The corresponding correlation functions with constants for the yields of CO and CO_2 were given by Equations 4.8 to 4.13

Fire type	Oxygen (%)	CO_2/CO ratio	Temperature (°C)	Upper layer temperature (°C)	Upper layer composition	Comments
Non flaming (oxidative) decomposition	5–21	N/A	<500	<425 °C	Exclusively from plume	Upper layer non reactive. Relative production rates of combustion products very similar for full range of ϕ.
Fully developed (flaming) (i) Relatively high ventilation	5–10	<100	600–1200	>625 °C	Fuel lean	Similar to fully ventilated fires. CO levels low (unless soot present to catalyse $CO_2 \rightarrow CO + O$).
Fully developed (flaming) (ii) relatively low ventilation	1–5	<10	600–900	>625 °C	exclusively from plume	Prediction of combustion products possible over the full range of ϕ. When $\phi > 1.5$ CO yields are relatively constant.
Developing fire (flaming)	10–15	100–200	400–600	425–625 °C	Exclusively from plume	Relative generation rates for combustion products dependent on upper layer temperature and upper layer residence time. Equivalence ratio needs to have a correction for temperature dependence.
Fully developed (flaming) with secondary air entering upperlayer. Not included in I. S. O. classification.				>625 °C	Direct entry of air to upper layer	This situation is commonly reported in real enclosure fires. The remaining fuel is oxidised to CO in preference to CO_2 in the upper layer. CO likely to be greater than predictions based on ϕ.

Table 5.1 Classification of fire types and correlation with parameters needed to predict CO yields [Richard et al., 2002].

5.4 Simulation of Purser (Tube) Furnace Test Method

This subsection investigates the Purser furnace using CFD fire modelling techniques. In section 5.4.1, the model approach is outlined and the rest of this chapter is dedicated to simulate two types of operating conditions i.e. one without the sample burning and the other with a burning sample. In section 5.4.3, we present the results for simulations in which there are no samples burning within the Purser Furnace. These simulations are intended to demonstrate that the temperature within the mixing chamber is uniform, a critical assumption of the Purser Furnace and operating procedure. The simulated temperature values inside the tube furnace and the mixing chamber are first validated with several thermocouple measurements from within the chamber. The model is then used to confirm that the temperature environment within the mixing chamber is indeed uniform. In section 5.4.4, we present model predictions of conditions within the mixing chamber when a sample is introduced into the Purser Furnace. These simulations are intended to demonstrate that the model is able to predict product yields inside the mixing chamber with reasonable accuracy. In addition, the model is used to demonstrate that product concentrations are uniform throughout the mixing chamber.

CFD fire field modelling software, SMARTFIRE [Galea et al., 1999; Ewer et al., 2004] is used to simulate the detailed thermal and fluid flow of cable fire inside the purser furnace. Three-dimensional transport equations based on conservation of mass, momentum, species and enthalpy are solved iteratively. The governing transport equations for all fluid variables can be expressed in the general form

$$\frac{\partial}{\partial t}(\rho\phi_i)+div(\rho u\phi_i)=div(\Gamma_i\, grad(\phi_i))+S_{\phi_i} \qquad (5.1)$$

where S_{ϕ_i} is the source term. The dependent variable ϕ_i may represent any of the following: three velocity components (u, v, w), pressure (p), enthalpy (h), turbulent kinetic energy (k), dissipation rate of turbulent kinetic energy (ε) or mass fraction of a species. The code uses the SIMPLE [Patankar, 1980] algorithm and models

turbulence using two-equation k-ε model with buoyancy modification [Rodi, 1985; Galea, 1989].

The tube furnace is represented by a circular surface (grey object in Figure 5.3) at a prescribed wall temperature and the cable burning by a fuel mass source (red object in Figure 5.4). Eddy dissipation model proposed by Magnussen and Hjertager [1977] is used to model gaseous phase combustion. Finally, radiation phenomena are taken care of by enhanced six-flux radiation model [Patankar and Spalding, 1973; Jia, 1997]. For more details see Chapter 3.

5.4.1 Toxicity Model

While using CFD technique to simulate the sample burning, the tube furnace domain is divided into thousands of control volumes. In each control volume, the fuel to air ratio is described by a conserved scalar, the mixture fraction,ξ, such that $\xi = 1$ for an unmixed fuel stream and $\xi = 0$ for an unmixed air stream. Under the assumption of equal diffusivity of species which is justified for most turbulent flames of practical interest, the source term for the mixture fraction disappears from the governing transport equation [Peters, 1984]. Mixture fraction can be defined in a simple way as

$\xi = \frac{\beta - \beta_2}{\beta_1 - \beta_2}$ where $\beta = Y_F - \frac{Y_O}{\nu}$ is also a conserved scalar and the indexes 1 and 2 refer to fuel and oxidant streams, Y_F and Y_O are mass fractions of fuel and oxygen, respectively. The simplest case of one-step irreversible combustion reaction is assumed for any hydrocarbon fuel

$$\text{Fuel} + \nu\ \text{Oxygen} \rightarrow (\nu + 1)\ \text{Products} \qquad (5.2)$$

where ν is the stoichiometric consumption of air as unit fuel is burned. The relation between the local equivalence ratio ϕ_l and the mixture fraction ξ in each control volume is [Tuovinen, 1995; Wang et al., 2001; Wang, 2007]

$$\phi_l = \frac{\xi \nu}{1-\xi} \tag{5.3}$$

It is also assumed that each control volume is like a miniature combustion apparatus and the mass fractions of combustion products are expressed with the mixture fraction by the following equations

$$Y_{CO} = y_{CO}(\phi_l)\,\xi \tag{5.4}$$

$$Y_{CO_2} = y_{CO_2}(\phi_l)\,\xi \tag{5.5}$$

where $y_{CO}(\phi_l)\,and\,y_{CO_2}(\phi_l)$ are yields of CO and CO_2 in g/g of fuel at local equivalence ratio ϕ_l.

In the present investigation the correlation of CO and CO_2 yields to the equivalence ratio, based on Purser furnace measurements, is used to predict the CO and CO_2 concentration distribution inside Purser furnace. Purser furnace experiments were carried out at Fire Materials Laboratories CMRI, University of Bolton. The CO and CO_2 yields versus equivalence ratio data obtained by burning NYM and NHMH type cables in Purser furnace are given in Figures 4.1 and 4.2. Thus the toxicity model based on the local equivalence ratio [Wang et al., 2007] is used to calculate the concentrations of CO and CO_2.

5.4.2 Numerical Details

Computational geometry used in the numerical investigation is shown in Figure 5.3. To incorporate the secondary inlet in the simulation, a body of dimension 24 x 5 x 17.5 mm was included in the geometry as shown in Figure 5.3(c). Computations were carried out using Grid I (23, 464 elements) and Grid II (38,504 elements). The change in the temperatures inside the mixing chamber by using Grid I and Grid II was less than 5%. Thus Grid I was chosen for computations in the present investigation. The computational grid used is shown in Figure 5.4. The red object represents the fuel source and the blue object represents the secondary air supply. According to the

standards, the length of hot zone of the furnace should not be more than 600 mm. The hot zone in the present experimental setup is 550 mm in length. In the present simulations, the furnace wall temperature profile is assumed to be uniform throughout the furnace hot zone (550 mm) and the average furnace wall surface temperature is calculated from the temperature measured inside the furnace tube (Figure 5.5 and Figure 5.6).

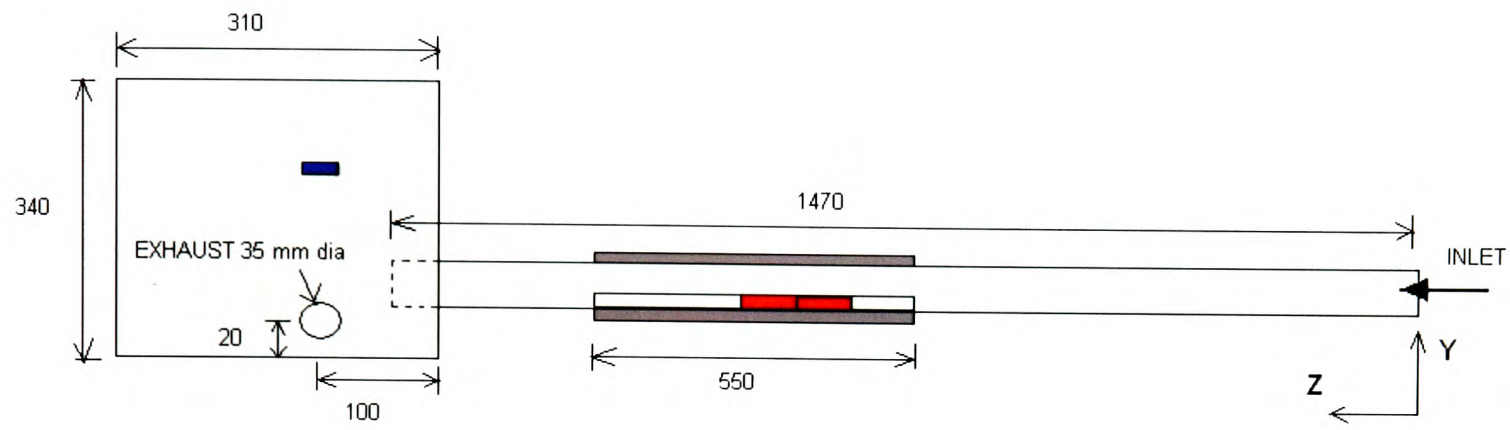

(a) Side view (Y-Z plane)

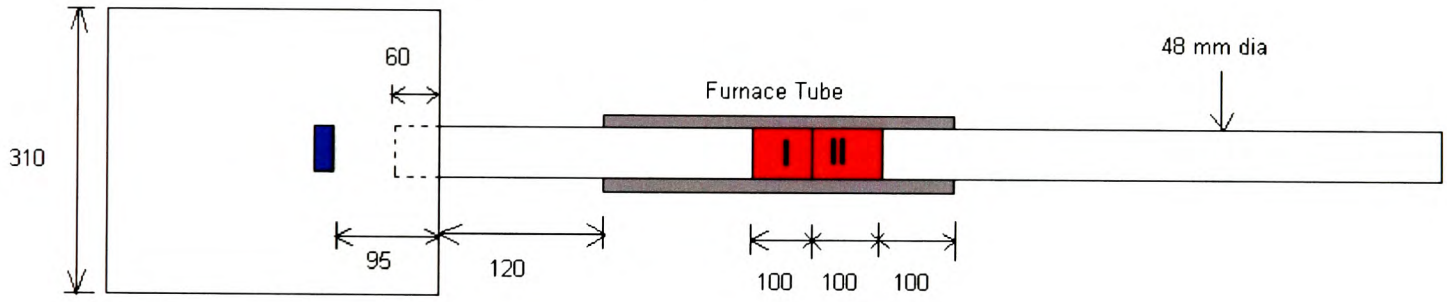

(b) Top view (X-Z plane)

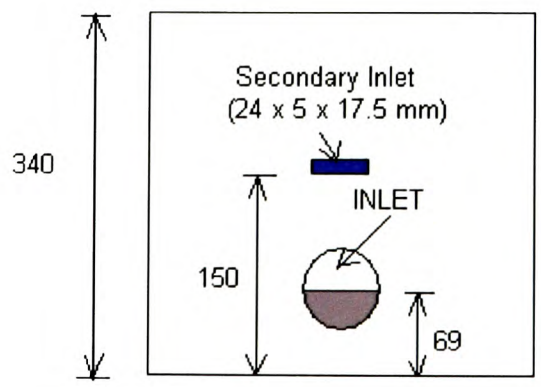

(c) Front view

Figure 5.3 Tube furnace geometry (X-Y plane).

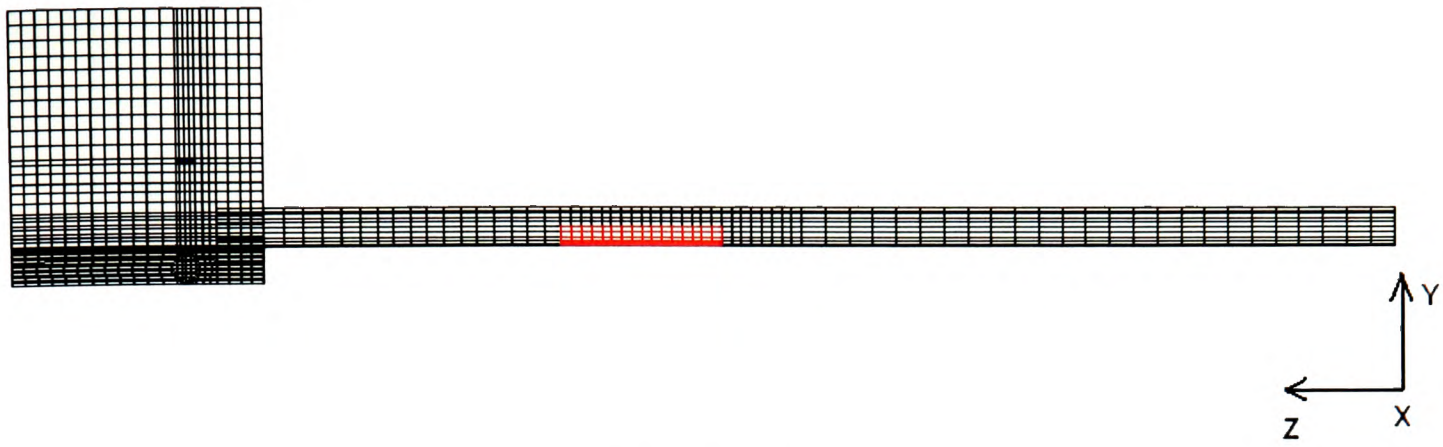

(a) Side view

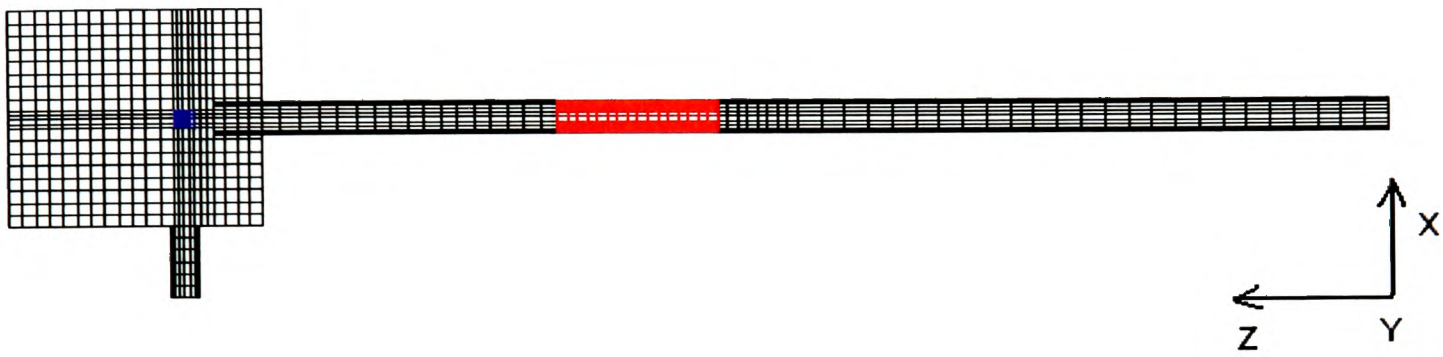

(b) Top view

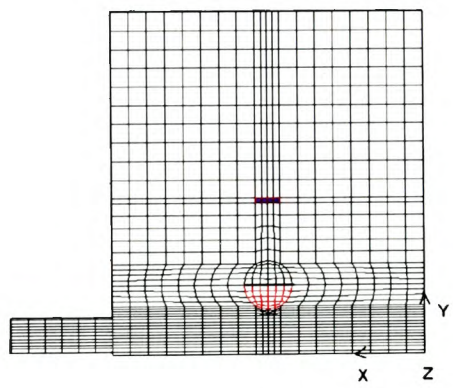

(c) Front view

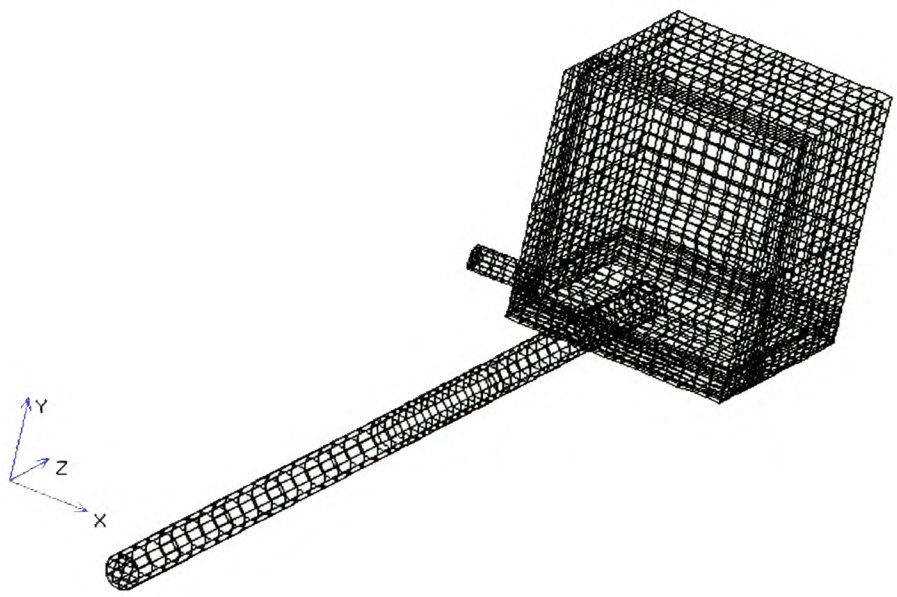

(d) Isometic view

Figure 5.4 Computational geometry and grid details

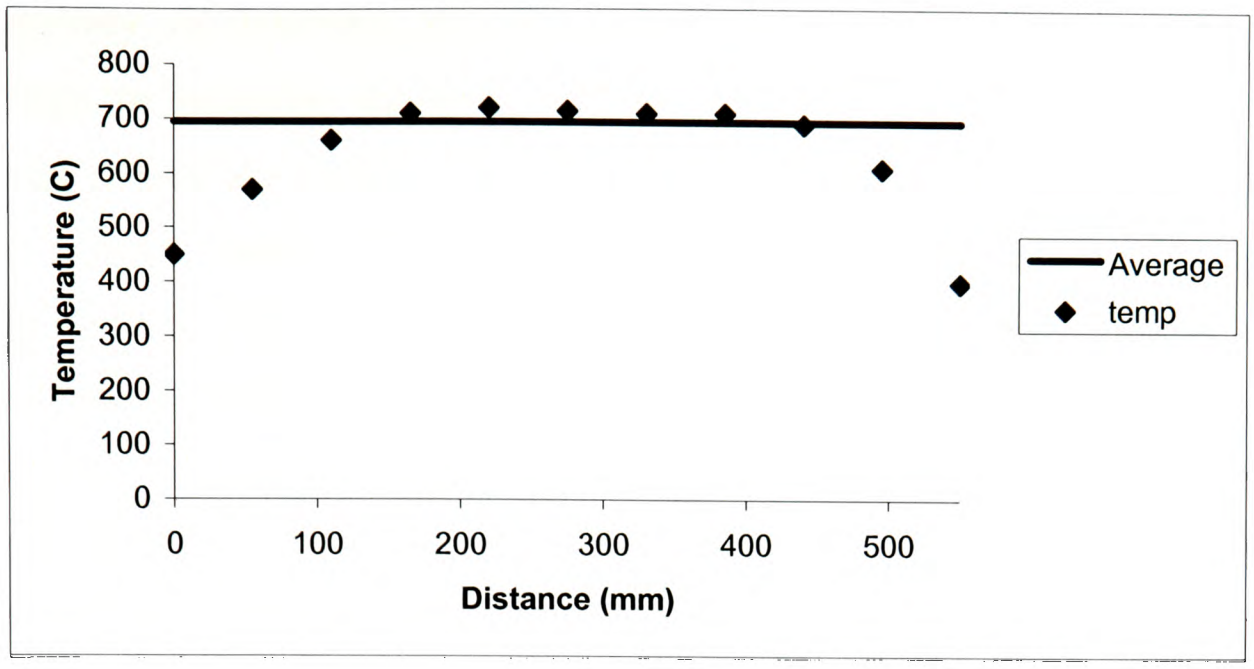

Figure 5.5 Wall temperature distribution of tube furnace hot zone (Primary air flow = 15 l/min).

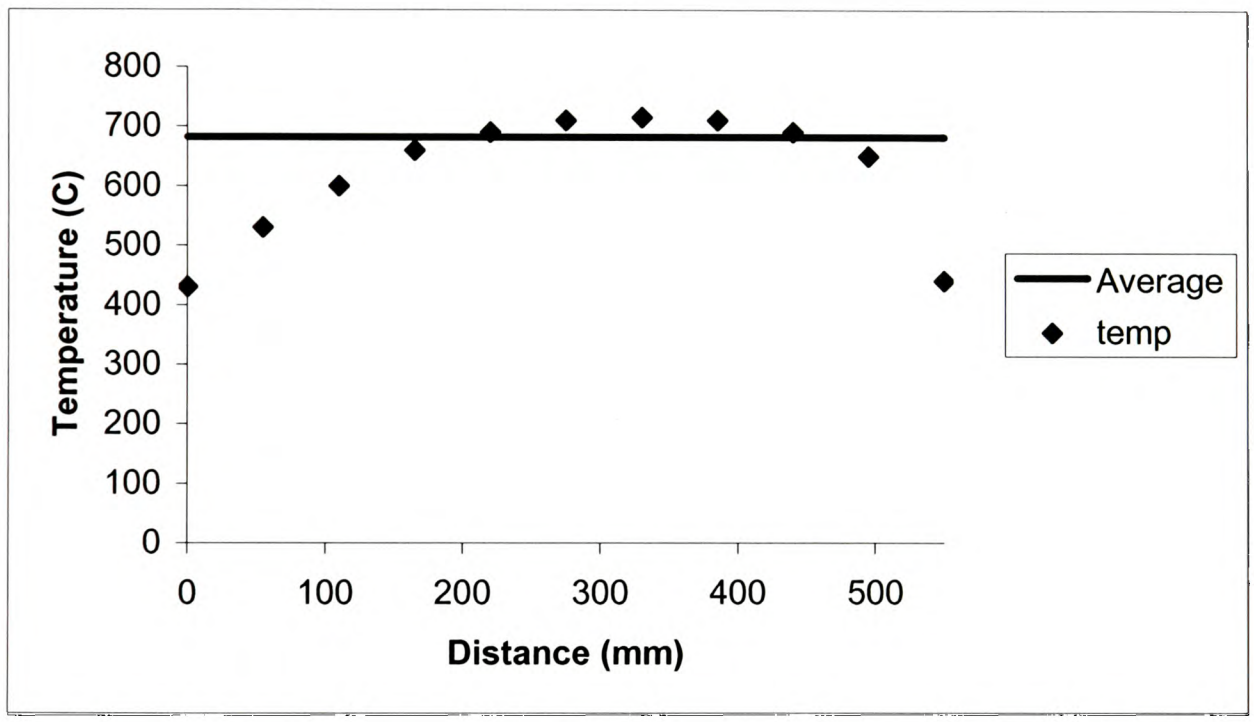

Figure 5.6 Wall temperature distribution of tube furnace hot zone (Primary air flow = 4 l/min).

5.4.3 Simulation of Purser Furnace without Cable Burning

For the fire safety engineering analysis to produce accurate results, the yield data must come from an apparatus that does not impose any significant influence on the results, i.e., the results should reflect the burning behaviour of the test specimen and not apparatus effects. For the effluent sampling from the dilution chamber to be accurate,

the secondary air flow must ensure proper mixing of fire effluent from the tube furnace and the secondary air supply. Therefore, the first step of this study is to assess the mixing process inside the dilution chamber by simulating the flow within the tube furnace without sample burning. Since temperature variation inside the dilution chamber reflects the uniformity of mixing, temperature measurements at various locations inside the mixing chamber (refer to Figure 5.7) were obtained from experiments without the burning of samples to evaluate the mixing process. Temperature values were observed to be similar in the upper and lower part of the dilution chamber which confirmed that the dimension of the mixing chamber and the location of secondary air inlet were sufficient to create proper mixing. A simulation of flow inside the tube furnace without the burning of samples was carried out and the temperature profile inside dilution chamber was utilised for validation purpose. The boundary conditions used in the two simulations are given in Table 5.2.

Table 5.2. Boundary conditions for simulations without sample burning

	Case 1	**Case 2**
Primary airflow	4 l/min	15 l/min
Secondary air flow	46 l/min	35 l/min
Inlet air velocity	0.0752 m/s	0.2763 m/s
Furnace temperature	700^0 C	700^0 C
Wall temperature	694 ^{0} C	682 ^{0} C

5.4.3.1 Results and Discussion

All five locations apart from location 3 (see Figure 5.7) where temperature was measured were in line with the end of the tube furnace (55 mm from the right wall of the dilution chamber). Geometrical details of the locations and the temperature comparison for 750^0C furnace temperature controller setting with empty boat (no fuel) for the two different primary air flow rates are given in Tables 5.3 and 5.4. For Case 1, at all locations except location 3 at which no measured temperature was provided, the predicted temperatures are in good agreement with measured values. At the highest and lowest temperature sampling points (location 5 and 1), both measured and predicted temperatures at the highest temperature sampling point are equal or nearly

equal to their counterparts at the lowest temperature sampling point, indicating a well mixed mixing chamber.

Temperature at location 3 in Case 2 was the highest both in the simulation and the experiment due to the fact that the location lies in the hot air plume emerging from the tube furnace. The difference between the computed and experimental temperatures at this location is the highest with 53% deviation from the experimental data. There are thought to be two reasons that explain this difference. First, location 3 lies inside the hot gas region where large temperature gradient exists. A small over prediction of velocity inside the tube might result in significant over prediction of the hot gas region. Secondly, there was considerable uncertainty involved with the temperature data at location 3. This was due to the thermocouple bending and some difficulty was experienced in positioning the thermocouple at the exact desired height at location 3. Hence the exact location of the thermocouple was not clear. The predicted temperature change trend at the five points is same as the measured one. The predicted temperatures at the two top points are close to the prediction at the lowest point, indicating the good mixing of the secondary air supply as observed in the experiment.

From the distribution of temperature observed during experiments, it is evident that temperatures were similar both in the upper and lower part of the dilution chamber. The simulations were able to capture this and the temperature distributions predicted inside the mixing chamber were in good agreement with the experiment. Figure 5.8 shows the temperature distribution across the Purser furnace when the primary air flow rate is 4 l/min. The peak temperature appears to be inside the tube furnace (967 K) which is similar to what was recorded during the experiment (~950 K). Uniform temperature distribution ($< 55^{o}$ C) was also observed inside the mixing chamber apart from the plume.

The velocity vector distribution across the Purser furnace is shown in Figure 5.9 The velocity vectors inside the tube (Figure 5.9a) shows a recirculation region before the tube furnace hot zone where the hot gas from the heating zone moves towards the inlet and gets entrained back into the incoming primary air flow. It is observed from

Figure 5.9b that the hot gas coming out of the tube rises up into the mixing chamber and gets intercepted appropriately by the secondary air supply thus enabling an efficient mixing process.

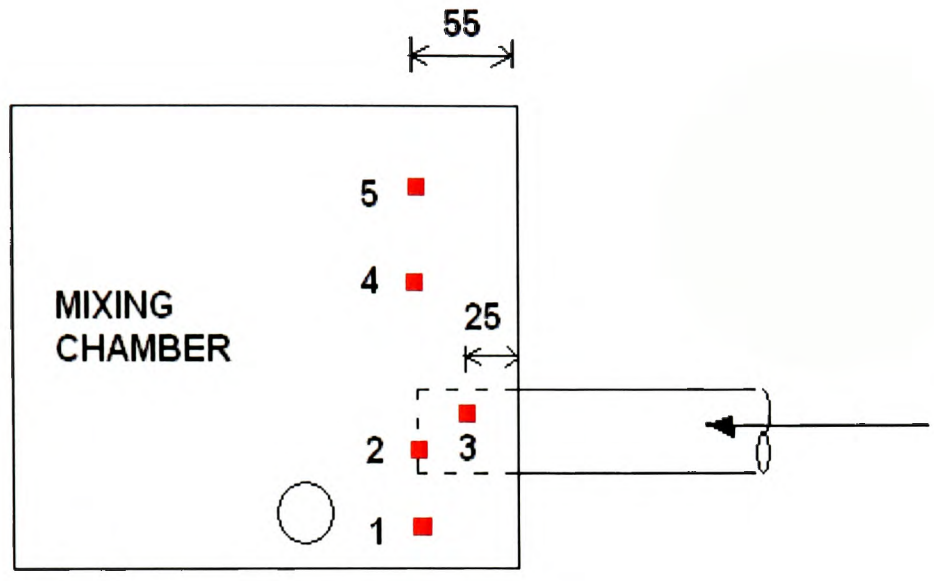

Figure 5.7 Thermocouple measuring locations (details given in Table 5.3)

Table 5.3 Case 1: Temperature inside mixing chamber (750 ^{0}C, 4 litres/min primary air flow with empty boat)

No	X (mm)	Y (mm)	Z (mm)	Experiment (^{0}C)	Computation (^{0}C)
1	155	25	1470	35	40
2	155	75	1470	135	138
3	155	85	1440	--	90
4	155	175	1470	47	50
5	155	275	1470	35	42

Table 5.4 Case 2: Temperature inside mixing chamber (750 ^{0}C, 15 litres/min primary air flow with empty boat)

No	X (mm)	Y (mm)	Z (mm)	Experiment (^{0}C)	Computation (^{0}C)
1	155	25	1470	70	94
2	155	75	1470	178	240
3	155	85	1440	250	383
4	155	175	1470	70	81
5	155	275	1470	75	99

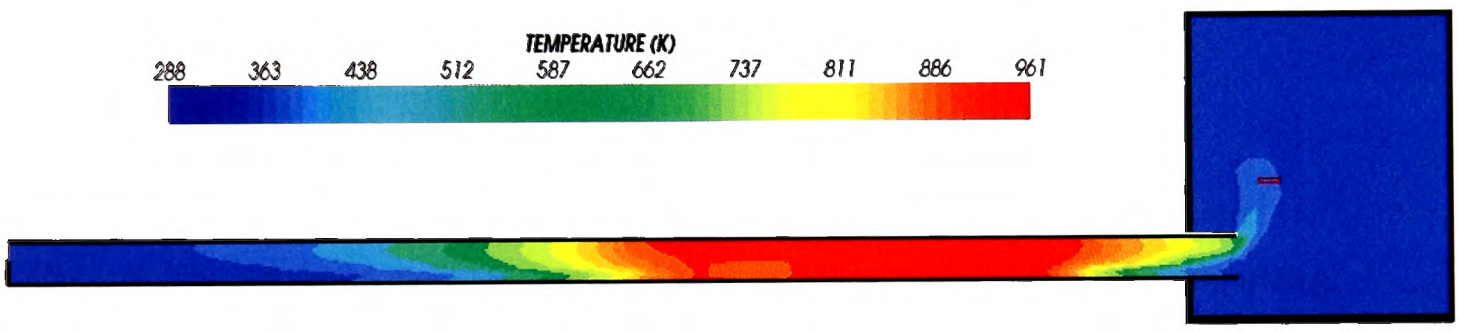

Figure 5.8 Temperature Distribution (K) for 750 ^{0}C, 4 litres/min primary air flow without sample burning.

5.4.4 Simulation of Purser furnace with NYM and NHMH Cable Burning

In this section, burning of NYM and NHMH cables inside the tube furnace at 800^0 C were simulated with the Bolton toxicity data and counter checked with the experimental yields. The sheath, bedding and insulation for NYM type power cables were all made of PVC material which contains PVC, plasticizer and chalk. The sheath, bedding and insulation of NHMH type power cables were made of chalk filled EBA, chalk filled polyolefin and Polypropylene respectively. The boundary conditions for 800^0 C furnace surface temperature case during NYM and NHMH cable burning and other model parameters are given in Table 5.5

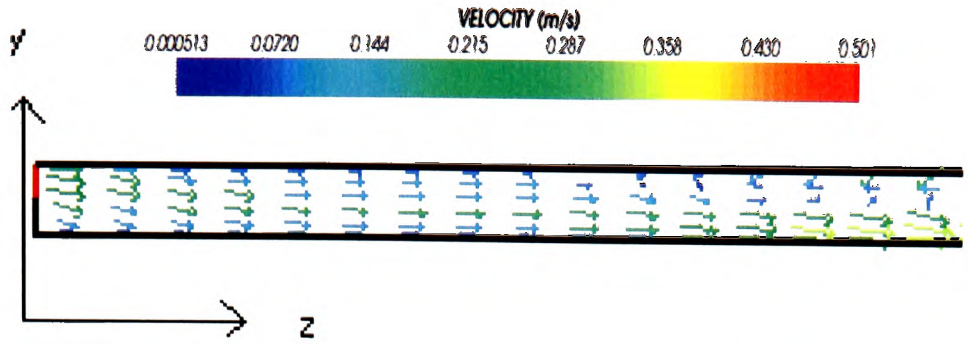

(a) Velocity vector distribution inside the tube from inlet (left) up to start of the tube furnace.

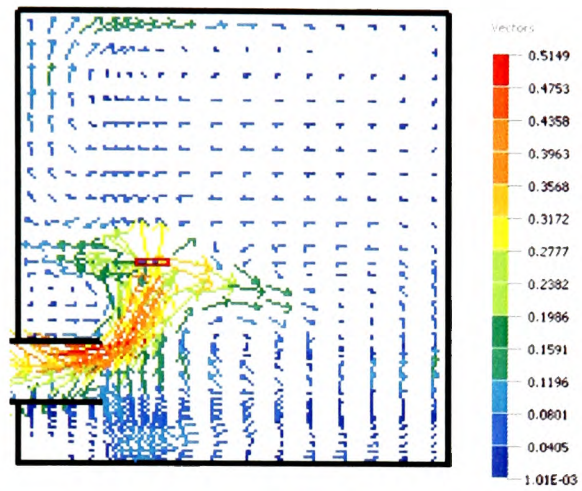

(b) Velocity vectors inside the dilution chamber

Figure 5.9 Velocity vectors across the Purser furnace

Table 5.5 Boundary conditions for simulations without sample burning

Primary airflow	4 l/min
Secondary air flow	46 l/min
Inlet air velocity	0.0752 m/s
Fuel mass loss rate	0.73 g/min
Furnace temperature setting	800^0 C
Heat of Combustion (NYM)	10.532×10^6 J/kg
Equivalence ratio (ϕ)-NYM	1.03
Heat of Combustion (NHMH)	20.526×10^6 J/kg
Equivalence ratio (ϕ)-NHMH	1.37

5.4.4.1 Results and Discussion

The computations were carried out for a primary air flow rate of 4 l/min under a furnace temperature setting of 800^0 C with NYM and NHMH cable samples burning. The corresponding equivalence ratios are 1.03 and 1.37 which were calculated based on the phi meter technique [Babrauskas, 1994]. Within the experiment, the effluent gases are sampled through individual ports for each product gas. A key operating assumption of the Purser furnace is that the fire effluent from the tube furnace is well

mixed by the secondary air supply within the mixing chamber and that the product concentrations are uniform throughout the mixing chamber.

The Reynolds number at the end of the tube furnace was ~2000 for 4 l/min case and the distributions of k, ε and turbulent viscosities for Case 1 are shown in Figure 5.10. The turbulent viscosities inside the tube furnace and the mixing chamber were 30-40 times that of the laminar viscosity for the lowest primary air-flow rate (4 l/m). Therefore the flow inside the tube is in a transition regime between laminar flow and turbulent one. The Reynolds number for the Case 2 (15l/min) is in turbulent regime (Re > 2000). Hence, for Case 1, turbulent flow results should be considered with caution.

The computed CO distributions inside the tube furnace in volume fraction are shown in Figures 5.11 and 5.12 for NYM and NHMH cable cases respectively. From the Figures 5.11 and 5.12 it is observed that the concentration is almost uniform through out the mixing chamber. This confirms that the secondary air flow works well in terms of generating a uniform mixture within the dilution chamber. More importantly it also confirms the assumption made in the experiments that the species concentrations within the chamber should be nearly uniform for the purpose of obtaining accurate and meaningful measurements of yields data.

The computed yields inside the mixing chamber are compared with the experimental yields and the comparison is given in Table 5.6. The yields of CO and CO_2 from the computation were calculated from the ratio of mass concentration of gases to the fuel mass loss concentration in the dilution chamber. The computational CO yield is under predicted and the CO_2 yield is in good agreement with the experimental yield for the NYM cable test. Under-prediction may be attributed to the fact that the CO yields obtained from the Purser furnace at higher equivalence ratios does not correlate well and the model heavily relies on the yield correlation. The computational CO yield is slightly over predicted and the CO_2 yield is slightly under predicted for the NHMH cable test case.

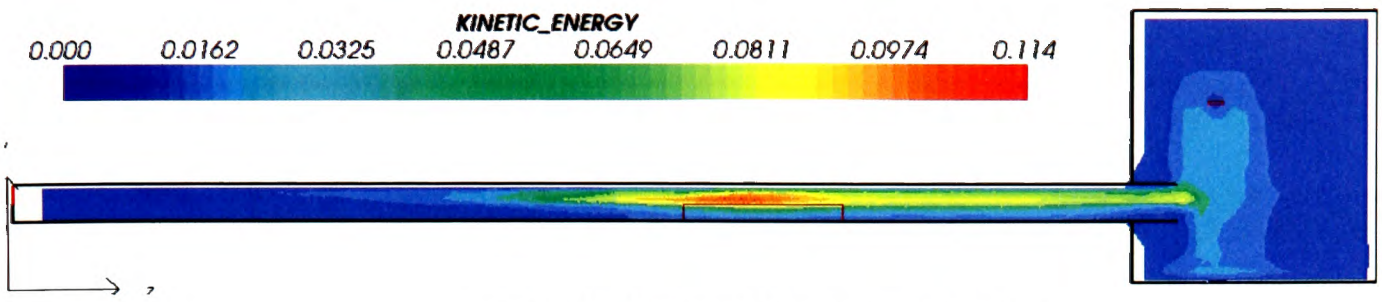

(a) Turbulent kinetic energy (k)

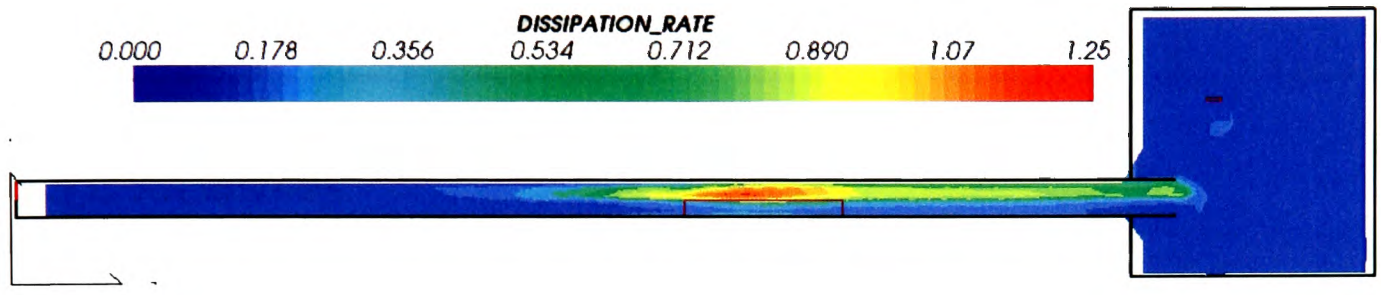

(b) Dissipation rate (ε)

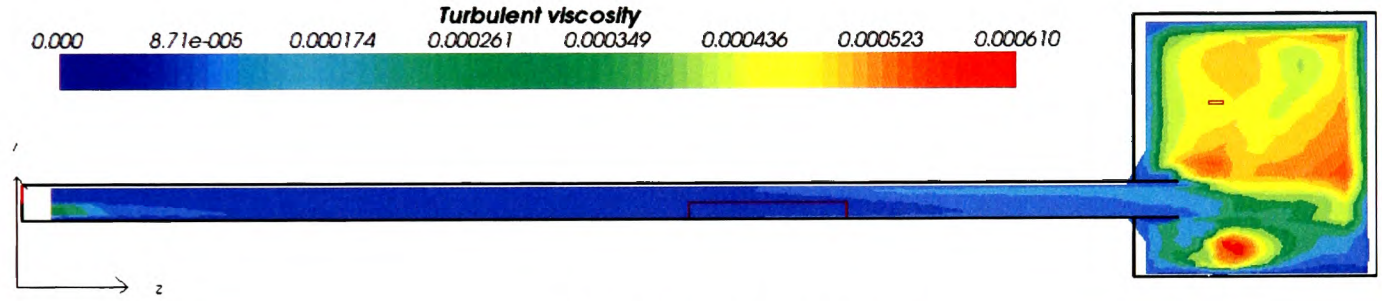

(c) Turbulent viscosity

Figure 5.10 Distribution of k,ε and turbulent viscosity inside the Purser furnace

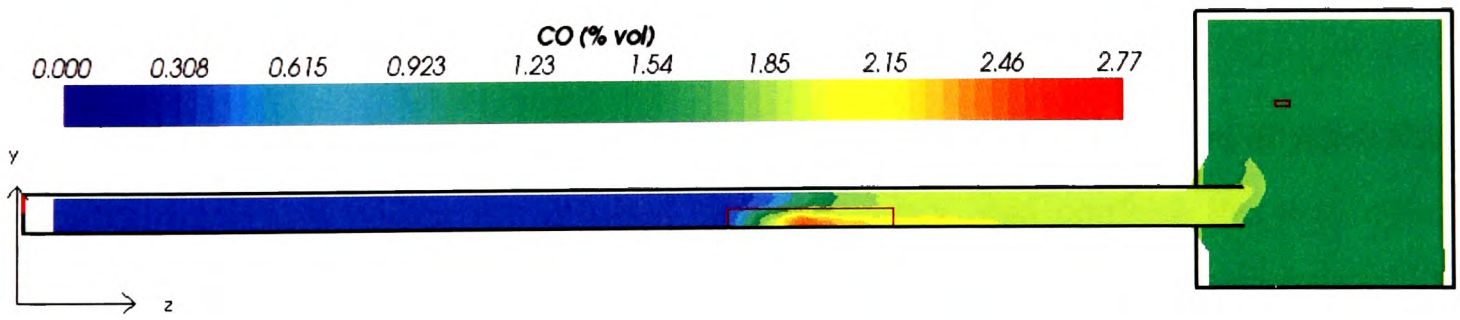

Figure 5.11 CO distribution inside tube furnace (NHMH)

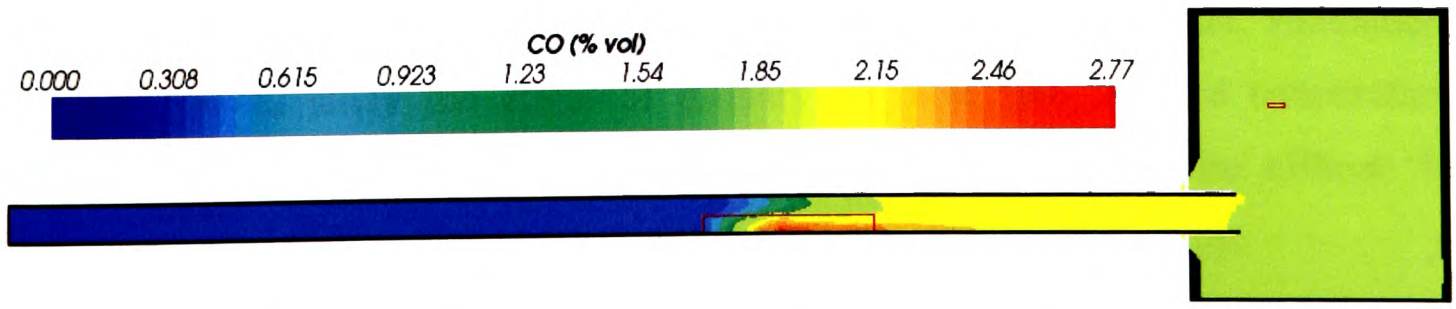

Figure 5.12 CO distribution inside tube furnace (NYM)

Table 5.6 Comparison of yields for NYM and NHMH

Cable	ϕ	CO yield (g/g)		CO_2 yield (g/g)	
		Experiment	Computation	Experiment	Computation
NYM	1.03	0.26	0.175	1.35	1.32
NHMH	1.37	0.17	0.186	1.25	1.147

5.5 Conclusions

The temperature values inside the mixing chamber were compared between the experiment and computation for 750^0 C furnace temperature case without sample burning. The comparison shows quantitative agreement between the experiment and computation.

Further, simulations for NYM and NHMH cables burning at 800^0 C furnace temperature were also carried out using the yield versus phi curve from the Purser furnace tests which were conducted at Bolton University. The computed CO and CO_2 yields were compared with the experimental yields. The comparison shows good agreement between experiment and the computational yields.

The simulations confirm that the secondary air flow works well in terms of generating a uniform mixture within the dilution chamber. They also confirm the assumption made in the experiments that the species concentrations within the chamber should be nearly uniform for the purpose of obtaining accurate and meaningful measurements of yields data. Hence, the ability of CFD to simulate fire environment inside the tube furnace is demonstrated in this study which is the first step towards using CFD as a design tool to improve the performance of the Purser furnace. Further, simulations may be used to study the effect of primary air flow rate, furnace temperature, geometry of the tube furnace, fire dynamics and quenching of fire effluent by secondary air on final yields which is difficult to quantify experimentally.

Chapter 6

Large-Scale Cable Fire Tests

6.1 Introduction

In order to validate the STEM-LER methodology, a series of fire tests involving various fire retarded cables were performed within a real-scale corridor. The experiments were conducted at the Department of Fire Technology at SP Swedish National Testing and research Institute during October 2005 [SP Report 2006] under the sponsorship of European Association of Producers of Flame Retardant Olefinic Cable Compounds (FROCC) and the PLUS-project. The PLUS-project is co-ordinated by Chalmers University of Technology, Sweden. Fire Safety Science (FSS) is an interesting challenge combining combustion, chemistry, fluid dynamics, toxicology and the human psychology. Thus the experiment team involved a cocktail of researchers such as fire safety engineering researchers from University of Greenwich, fire chemists from University of Bolton, fire researchers and technicians from SP and the fire researchers from cable industries like Borealis.

6.2 Objectives

Several experimental studies have been conducted to develop a better understanding of the species levels generated in the vicinity of fire and the gas levels being transported to remote locations [Gottuk, 1992; Ewens, 1994; Lönnermark et al., 1997; Lattimer et al., 1997]. Based on the review outlined in Chapter 2, the experimental

data from the reviewed studies lacked at least one of the following required criteria for the validation of STEM-LER methodology

- The geometry is too short or small to validate the species transported to distant location.
- Species generated per unit mass i.e., species yield correlation with respect to equivalence ratio was not available for the fuel used.
- The fuel is not a complex fire retarded combustible material.
- Measurements were available only at few locations.

Therefore, it was decided to conduct a series of full-scale fire tests involving fire retarded cable samples as a part of the project to obtain a detailed set of species concentration and temperature profiles along the full length of a long corridor.

Hence, the objectives set for this experimental campaign were

- To evaluate the correlation between the bench-scale tests and large-scale tests.
- To generate a comprehensive set of fire data to validate
    - ✓ Combustion models
    - ✓ Toxicity models
    - ✓ Species transport models

Three types of cables designated viz. NYM, NHMH and RZ1-K were used as the fire source under a variety of ventilation conditions.

6.3 Preliminary Simulations to Study the Layout for Large-scale Fire Tests

The tests were planned to be conducted indoors in the large fire test hall at SP, having an overall dimensions of 18 m x 22 m x 20 m (width x length x height (max)). Based on the available floor area at the large fire test hall at SP, a U-shaped corridor layout was selected having a corridor length of 40.6 m. The basic layout is shown in Figure

6.1. A room of dimension 3m x 4m is located at the inner corner between the first and the second corridor and is connected to the corridor through a 2 x 0.4 m ventilation opening at ceiling level. The room is placed for the purpose of performing preliminary assessment on the effect of fire environment on people evacuating. Prior to the experiments, fire simulations were carried out inside the U-shaped corridor to study the layout design. It was desired that the interior of the corridor geometry was able to generate a thicker upper layer facilitating in getting more species concentration data across the upper layer. Also to get a first hand experience on the typical upper layer, simulations were carried out inside the corridor layout for an hypothetical fire scenario having the fuel loss rate curve similar to that was measured in a ISO standard room test conducted by Borealis with PVC cables [Robinson et al., 2004]. The total duration of the test fire was 1500 seconds with a peak HRR of 300 kW occurring at around 600 seconds The temperature contours along the middle of the first corridor (19.1 m corridor housing the cable trays) is compared for the layout without the soffits and with the soffits and are shown in Figure 6.2. It is evident from the Figure 6.2 that the upper layer thickness is increased due to the presence of the soffits. Hence, Soffits of height 0.4 m were placed at four different locations along the corridor (see Figure 6.3). It was envisaged that the fire source being located at one end of the corridor will drive the fire gases through the corridor and exit at the other end of the corridor construction which will be collected under the hood system.

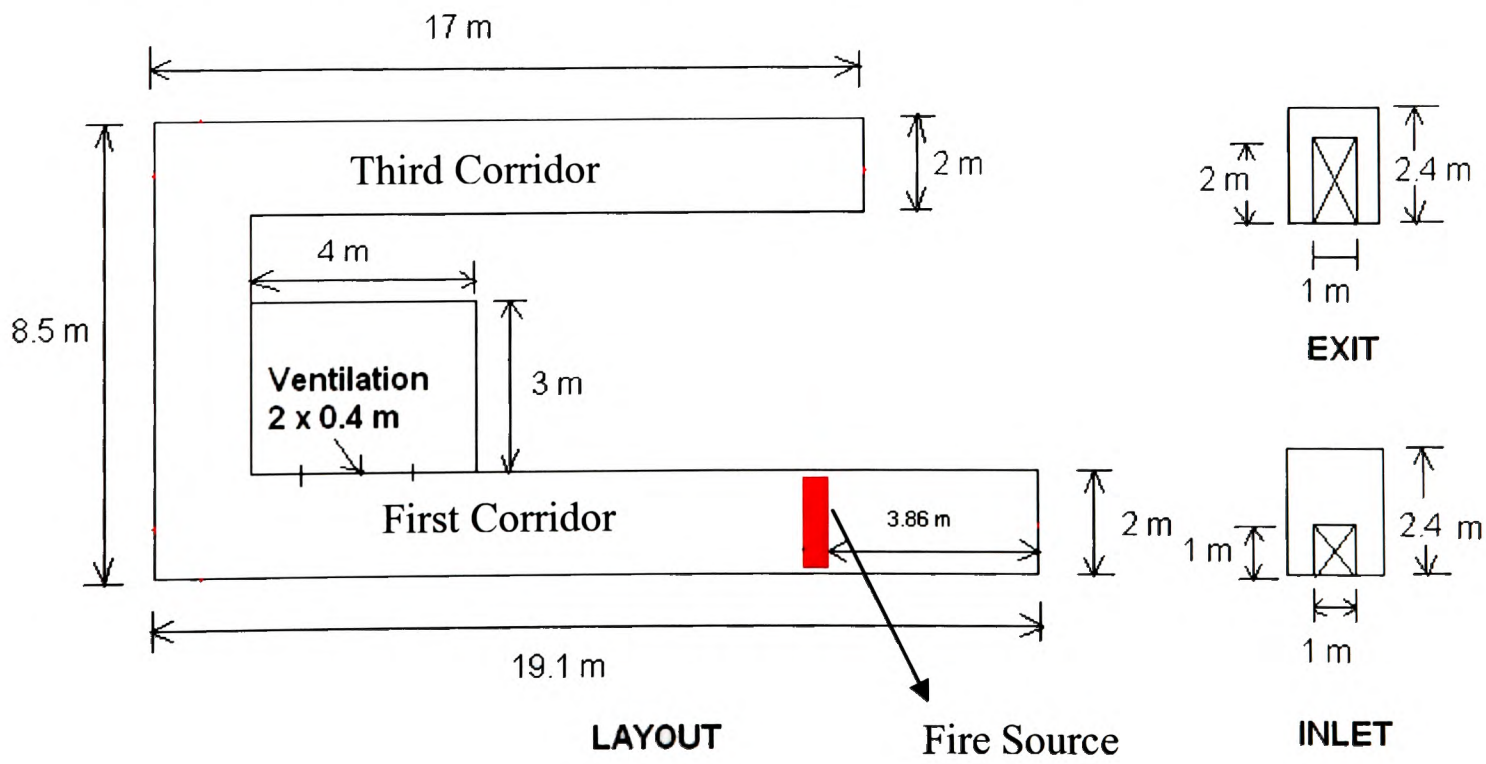

Figure 6.1 Basic Layout (without the soffits)

An inlet vent of 1m x 1m was placed at one end of the corridor at floor level near the fire source so that the fire plume will be able to draw fresh air through it. Further, two fire simulations were performed; one for over-ventilated condition and the other with under-ventilated condition using the same fuel source. The objective of these two simulations was to see if the under-ventilated conditions were created by reducing the inlet vent area. The comparison of the CO_2 concentration distribution in the fire corridor between 1m x 1m vent area (100 % Inlet area) and the 0.5m x 0.5m (25 % Inlet area) vent area case is shown in Figures 6.4(a) and 6.4(b). It is clear from the comparison that there is no significant change in the CO_2 concentration distribution between the two inlet vent cases. Since there was not much improvement observed in the upper layer CO_2 concentration by reducing the inlet vent area, simulation was performed with the inlet vent closed. The CO_2 concentration distribution along the first corridor for the scenario with the inlet closed is provided in Figure 6.4(c) and shows significant improvement in making the first corridor more under ventilated. The velocity vectors in the Figure 6.4(c) show fresh air being drawn into the fire plume from the second or middle corridor. Thus in order to prevent the fresh air reaching the base of the fire plume, a 1m weir was placed between the first corridor and the second corridor. Simulation was also carried out with the inlet closed and with 1m weir placed at the end of the first corridor. The CO_2 concentration distribution and the velocity vectors along the first corridor are outlined in the Figure 6.3(d). Despite the presence of the 1m weir the fresh air from the second corridor still managed to spill into the first corridor which is seen from the velocity vectors above the weir. However, the simulated scenario with the inlet vent closed and with a 1m weir placed in between the first and the second corridor was generating the most vitiated conditions.

Hence it was decided to go for the scenario with the inlet opening for well-ventilated experiments and with inlet vent closed and a weir placed in between the first and the second corridor for the under-ventilated experiments.

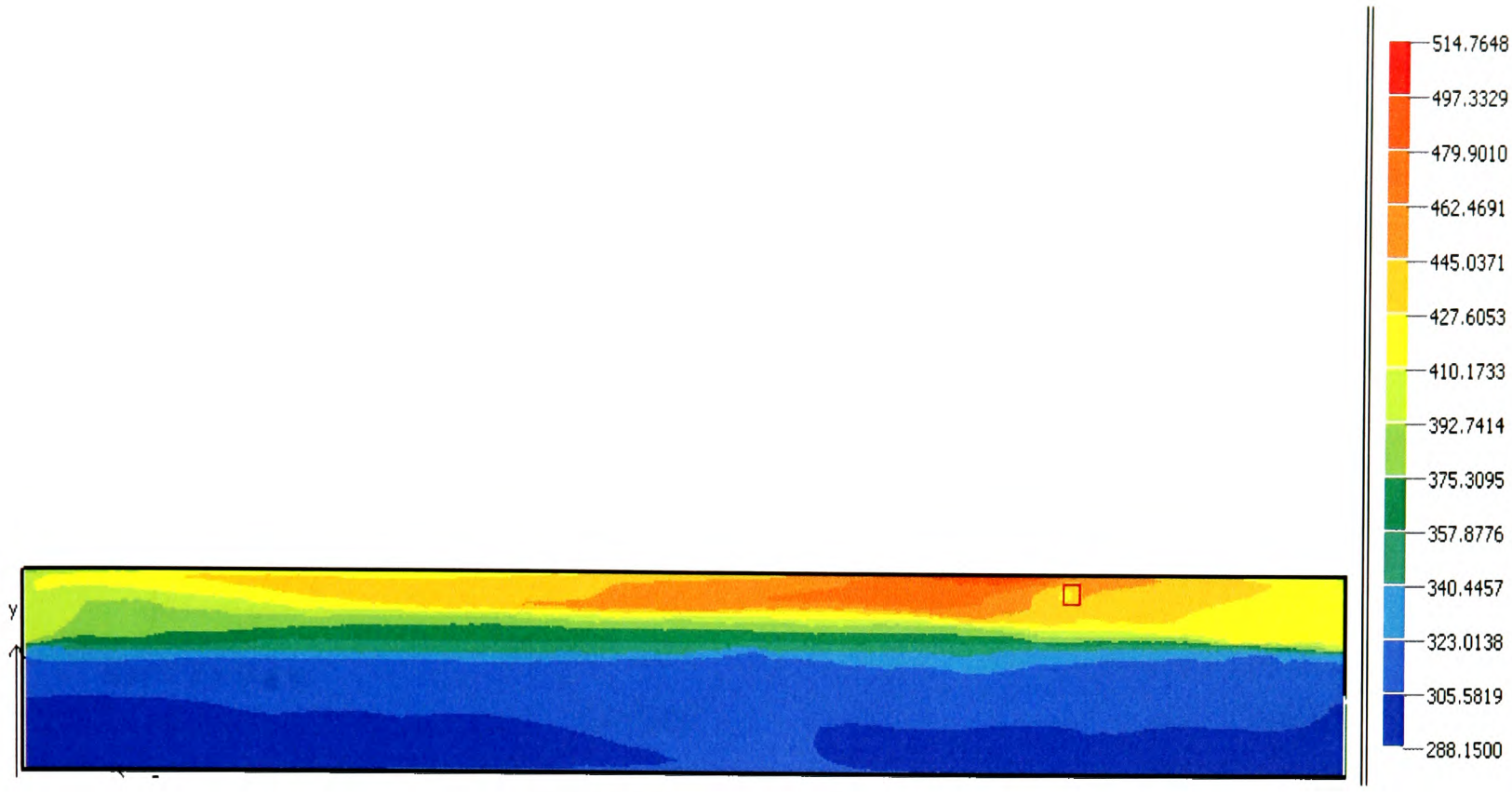

(a) With out soffits

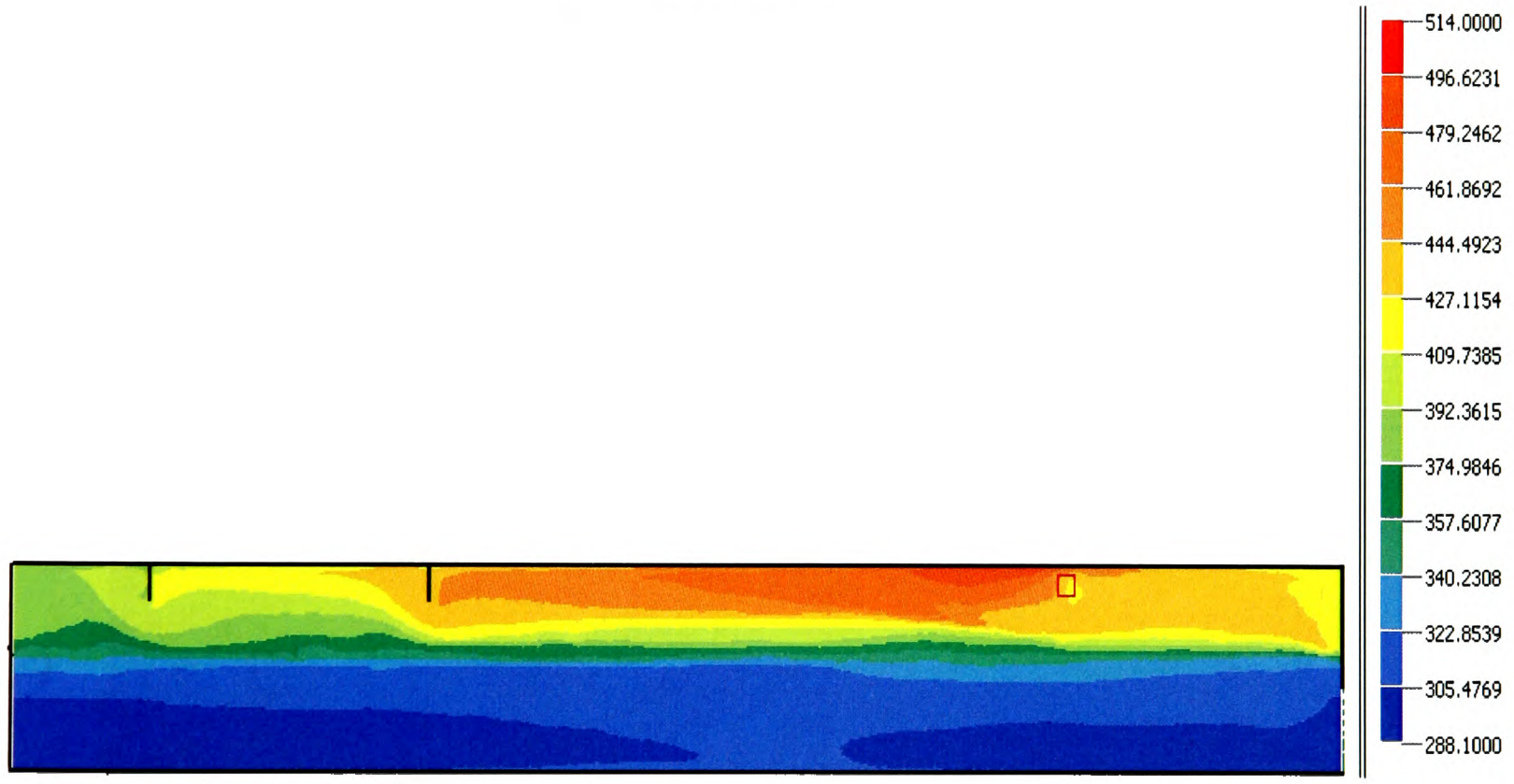

(b) With soffits

Figure 6.2 Temperature contours (^{o}K) along the fire corridor (Inlet vent is at the bottom right of the figures)

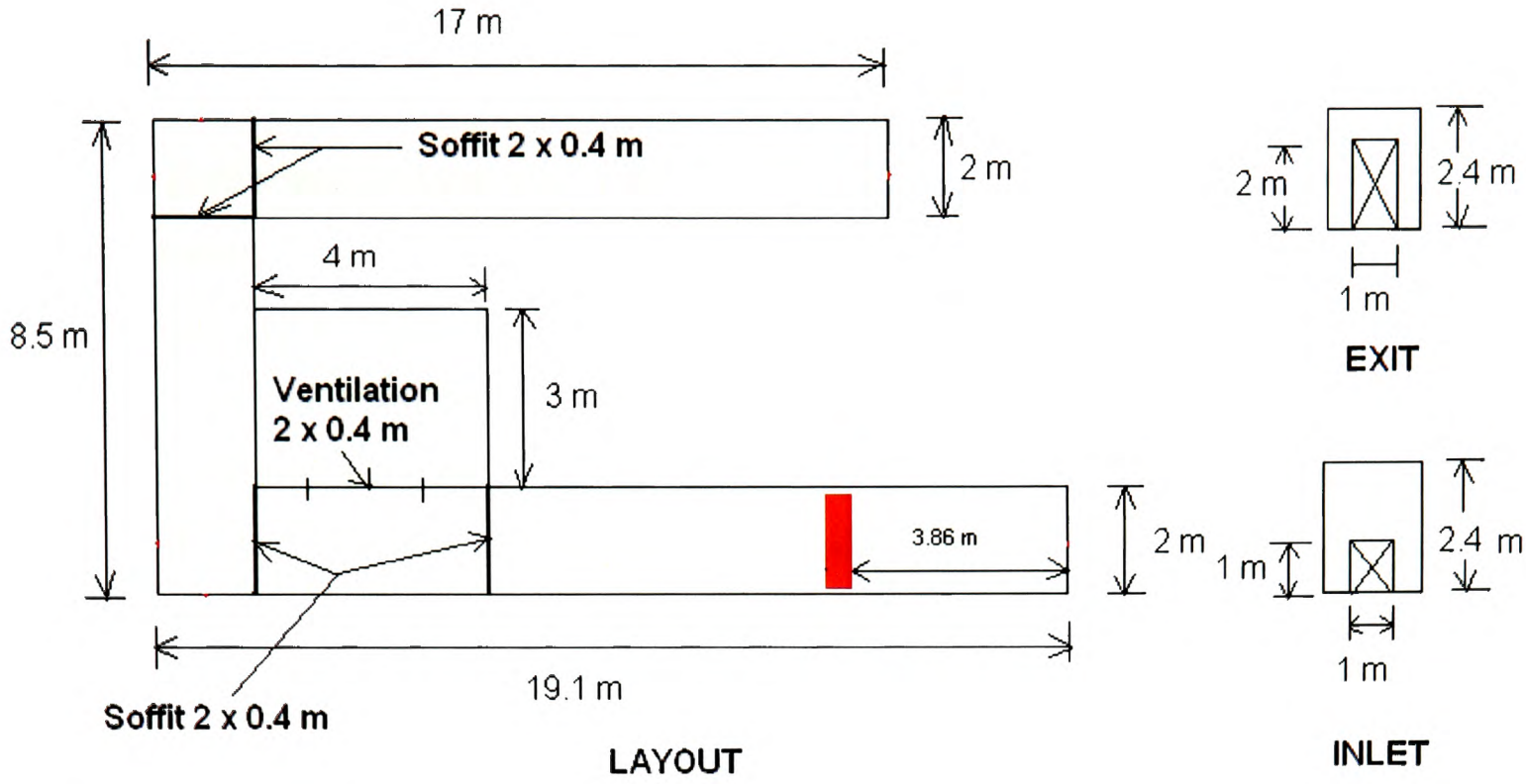

Figure 6.3 Layout with the soffits

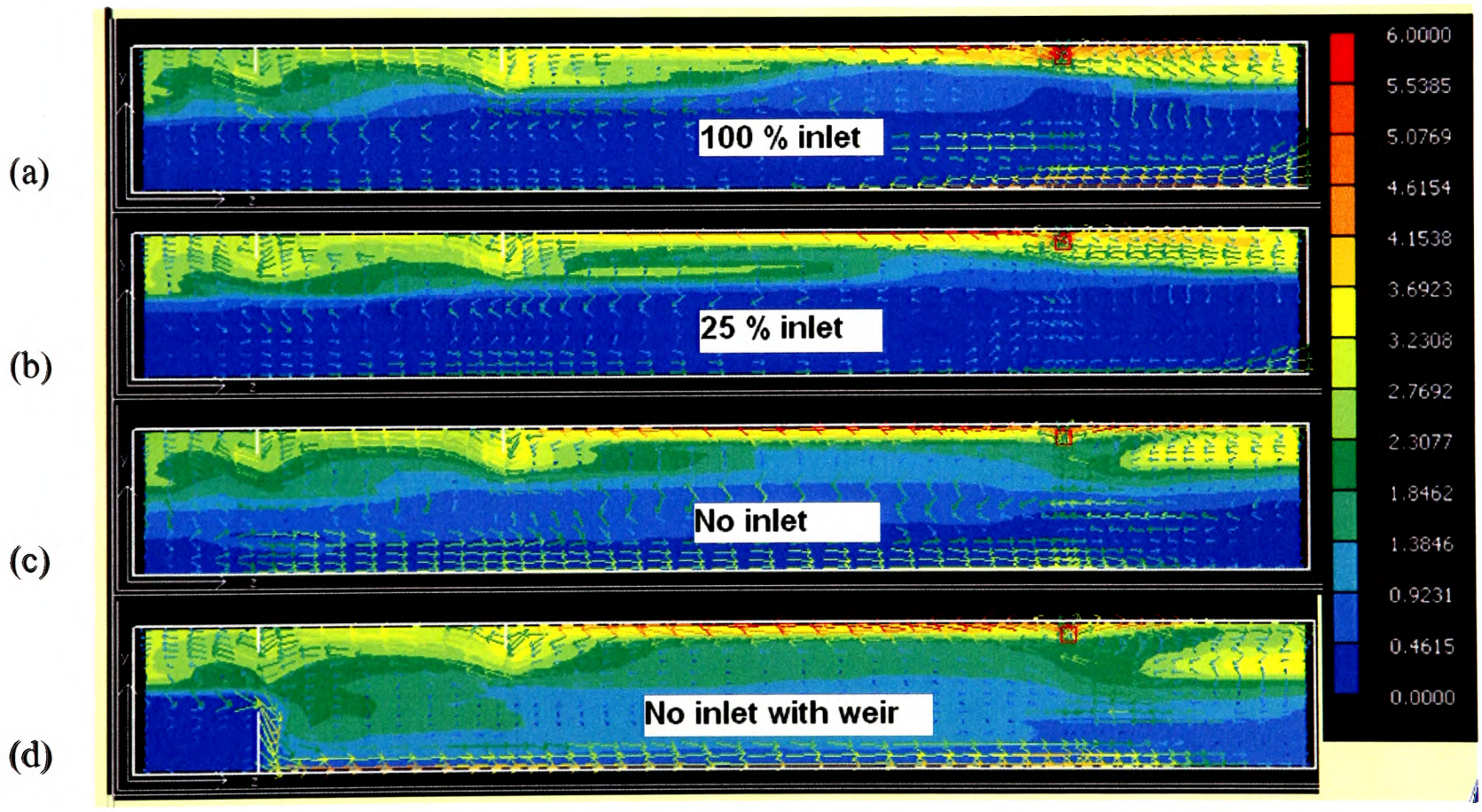

Figure 6.4 CO_2 (% volume) distribution and velocity vectors along the fire corridor (a) 100% inlet (b) 25% inlet (c) with inlet closed (d) with inlet closed and 1 m weir

6.4 Experiment Layout

After the preliminary assessment of the basic U-shaped corridor layout, the corridor layout geometry was finalised which is shown in Figure 6.5. The height of the corridor was 2.4 m. The ceiling and walls of the corridor were constructed using Promatect – H non-combustible boards. The inlet vent had a 1 m^2 opening situated at floor level. Some tests were performed with inlet closed and placing 1 m high weir at the end of first corridor to obtain more vitiated conditions. The corridor exit was positioned below a hood connected to a calorimeter system which measures the heat release rate using oxygen depletion calorimetry. The fire source was located at a distance of 3.9 m from the inlet and consisted of vertical and horizontal cable trays. A propane sand burner was used as ignition source which had a heat output of approximately 30 kW.

The summary on the specification and composition for the power cables (see Figure 2.8) used during the labyrinth tests are given in Table 6.1. In total, 10 fire tests were conducted and a summary of the test conditions are given in Table 6.2. Two sets of ventilation conditions were studied.

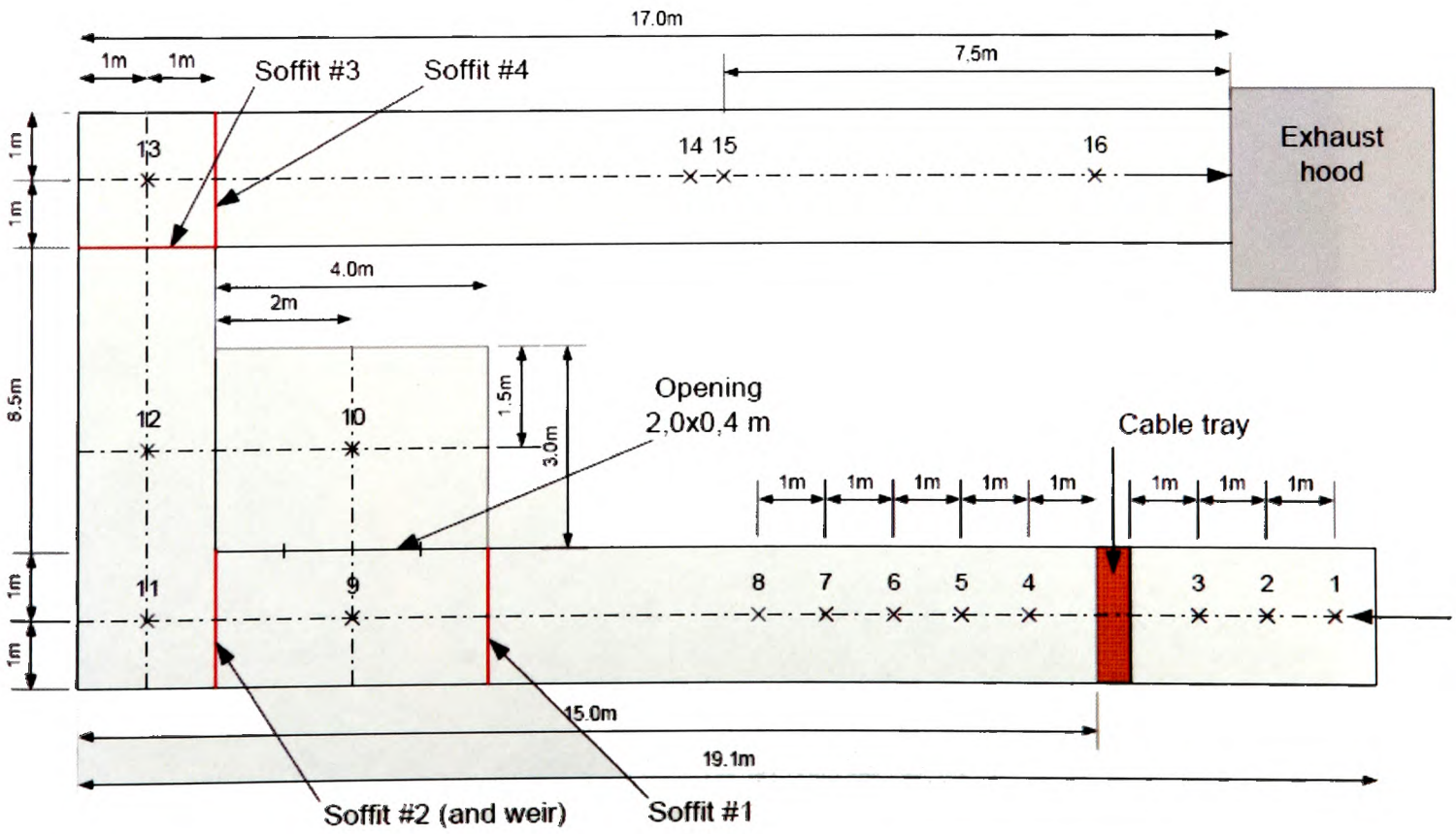

(a) Layout of Labyrinth

(b) Inlet (c) Exit

Figure 6.5 Details of the labyrinth

In one ventilation arrangement, an inlet opening of 1 m x 1m was kept open upstream of the fire. In the other ventilation arrangement, the inlet opening was completely closed and sealed and a 1 m high weir was installed at the end of the first corridor. Photographs of the labyrinth test setup are shown in Figures 6.6 and 6.7.

Figure 6.6 Overview of corridor construction with the first corridor to the right and the third corridor and the calorimeter hood to the left.

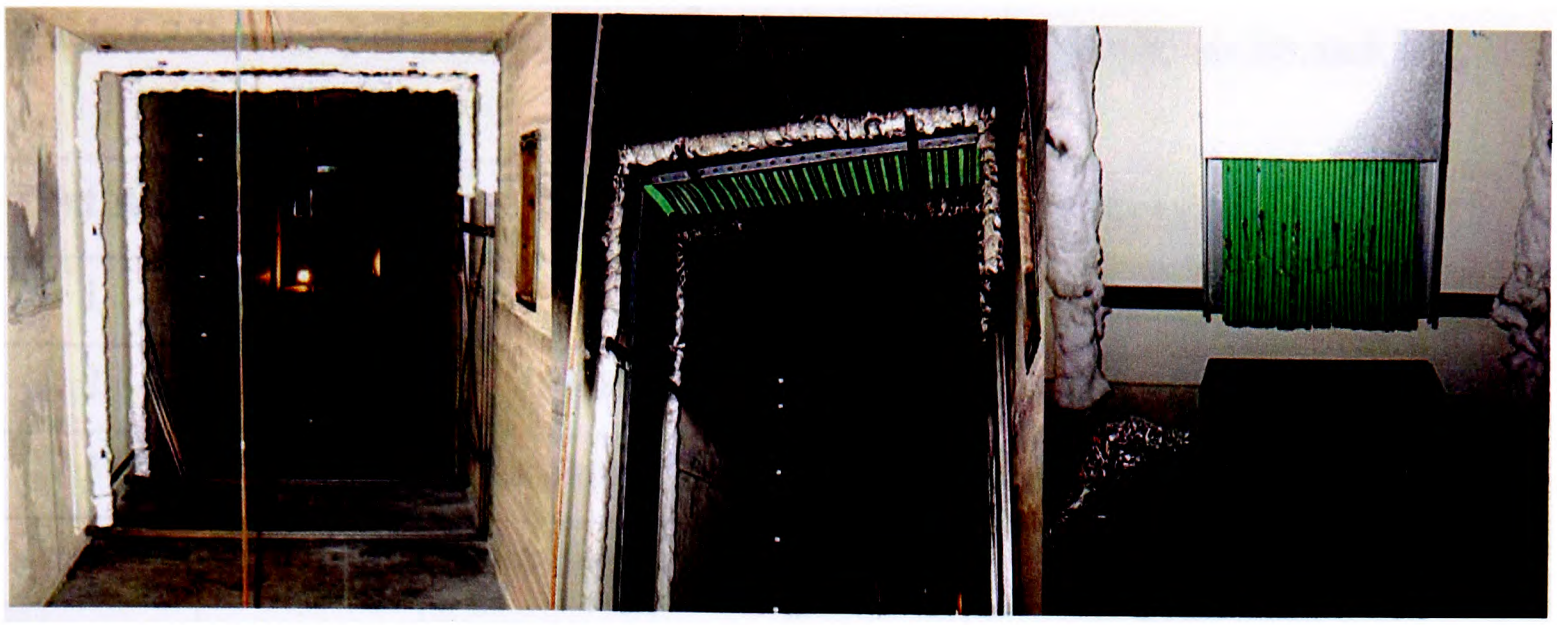

(a) View through the ventilation opening

(b) Cable tray mounted on the load cell

(c) Cable and Burner setup

Figure 6.7 Photographs of the large scale labyrinth construction

Table 6.1 Summary of data for the cables used during tests

Designation	**RZ1-K**	**NHMH**	**NYM**
Specification	UNE 21.123	VDE0250 Pt 215	VDE0250 Pt 204
Insulation	XLPE	PP	PVC
Bedding	None	Chalk filled polyolefin	PVC
Sheath	Hydrate filled EVA	Chalk filled EBA	PVC
No. of wire x area	3 x 1.21 mm^2	3 x 1.5 mm^2	3 x 1.5 mm^2
Weight of polymer (kg/m)	0.136	0.101	0.140
No. of cables	33	39	35
Length of each cable (m)	3.9	3.9	3.9
Total weight	17.5	15.4	19.1
Net weight of polymer (kg)	13.2	9.2	13.6

Table 6.2 Summary of the main test programme and the test conditions for each test.

Test no.	Cable	Ventilation	Remarks
1	RZ1	Inlet open	Error in load cell data
2	NHMH	Inlet open	Error in load cell data
3	NHMH	Inlet closed; 1 m Wier	Error in load cell data
4	RZ1	Inlet closed; 1 m Wier	
5	NYM	Inlet closed; 1 m Wier	
6	NYM	Inlet open; 1 m Wier	
7	RZ1	Inlet open; 1 m Wier	Repeat of Test 1
8	NHMH	Inlet open; 1 m Wier	Vertical cable cover tray removed
9	NYM	Inlet closed; 1 m Wier	Repeat of Test 5
10	NHMH	Inlet closed;1.5 m Wier	

6.5 Measurements and Recordings

In order to record the evolution of fire and the transportation of combustion products, extensive measurements were made along the corridor during each test. Concentrations of Carbon monoxide (CO), Carbon dioxide (CO_2), Hydrogen Chloride (HCl) and Oxygen (O_2) were measured at a number of locations. In addition, smoke obscuration and temperatures were also measured. The cable trays were mounted on a load cell platform which measured the mass loss of the cables during the fire. The Heat Release Rate (HRR) was measured by collecting the smoke gases at the corridor exit in a calorimeter system (based on measurements of mass flow, O_2, CO_2 and CO). Sample of photographs taken during one of the labyrinth cable fire tests is shown in Figure 6.8.

6.5.1 Gas analysis

Gas analyses were performed at 13 positions along the corridor as shown in Figure 6.9. A summary of sampling locations, and at various heights for measuring CO, CO_2,

O_2, HCl are also shown Figure 6.9. Due to a large number of sampling positions, most instruments were connected to two sampling probes at two different locations. A remote controlled valve was used to switch the gas sampling between the probes nominally every 30 seconds.

(a) Cables are ignited by propane burner

(b) Fully developed cable fire

(c) End of the cable fire

Figure 6.8. Photos taken during one of the fire test.

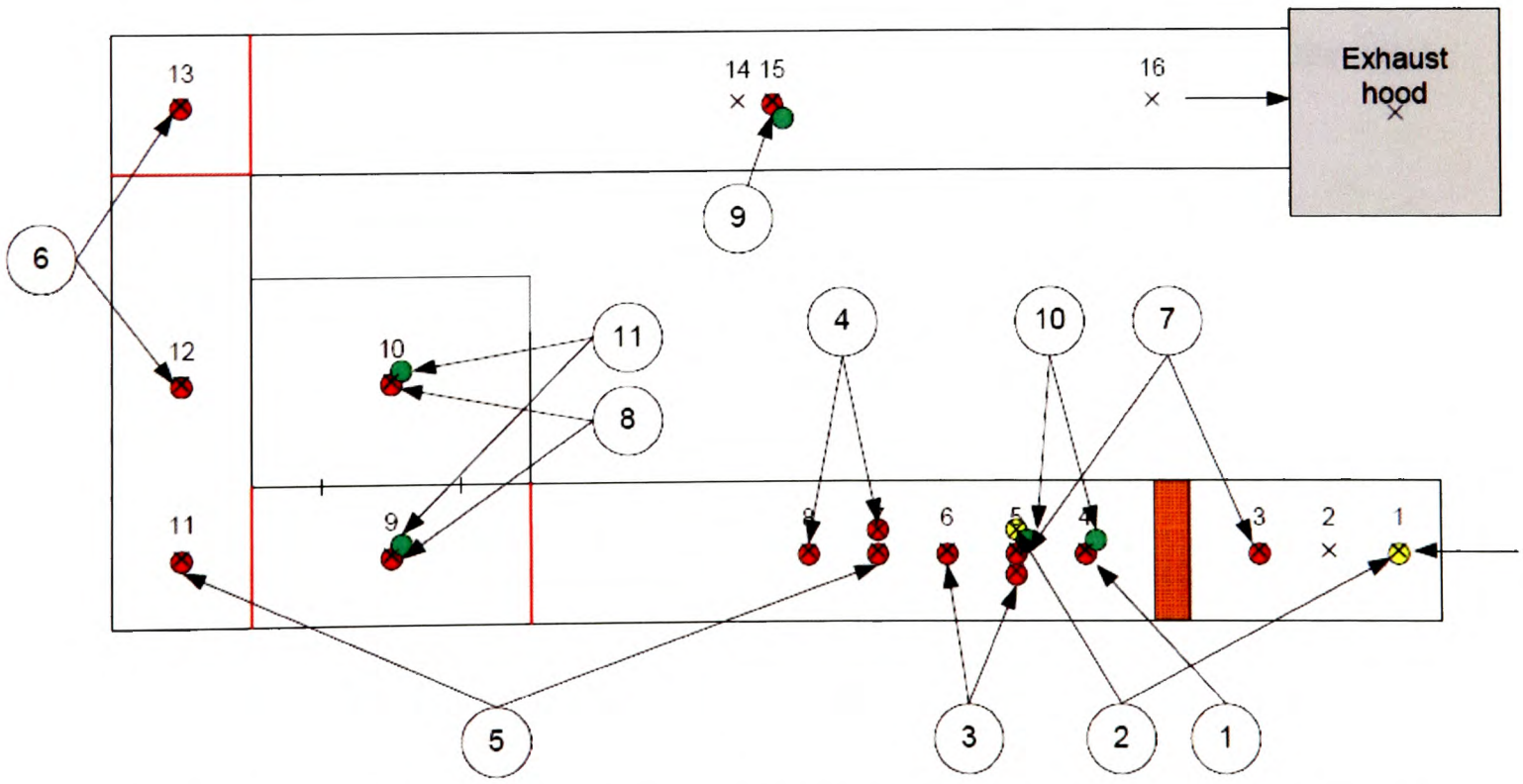

Figure 6.9 Summary of the arrangement of gas analysis instruments and position (×) for CO (yellow), CO_2 (red) and O_2 (green) measurements.

6.5.2 Temperature measurements

The temperatures inside the test setup were measured at 27 locations in total. In all cases where thermocouples were present (i.e., positions no. 2, 5, 7, 9, 10, 12, 15, 16), they were at 1.0 m and 2.2 m above the floor. For positions no. 2, 5 and 7, three additional thermocouples were located at 0.5 m, 1.5 m and 2.0 m above the floor. In order to record the temperatures at the fire source, one thermocouple was mounted approximately 100 mm from the corridor wall, just above the vertical section of the cable tray and one thermocouple was mounted at the centre of the corridor, above the horizontal cable tray. Both were located at 2.3 m above the floor (i.e., 0.1 m below the ceiling). The thermocouples above the fire source were 1.0 mm, shielded, type K thermocouples while the remaining thermocouples were made from 0.5 mm type K wire.

6.5.3 Heat release rate and mass loss

The mass loss of the burning cables was measured by positioning the entire cable tray arrangement on a load cell platform. The heat release rate was measured by collecting all the combustion gases at the corridor exit into an exhaust/calorimeter system. The total heat release rate could then be calculated by measurements of mass flow, oxygen consumption and generation of CO2 and CO. The calorimeter system and the heat release calculations are based on ISO 97054 [ISO 9705:1993(E), 1993].

6.6 Test Procedure

The following test procedure was followed in all the tests:

- 0:00 min:sec – start measurements (to obtain background conditions)
- 1:00 to 2:30 min:sec – start of video cameras
- 3:00 min:sec – ignition of propane burner
- The measurements were allowed to run for about 10 minutes after the fire was observed or judged to have self-extinguished, in most tests.

The cables mounted on the vertical cable tray were ignited at the bottom by a propane burner. The ignition times were different for the three cables. The NYM (PVC) cables had the lowest ignition time and RZ1-K type cables had the longest ignition time. This is in line with that observed during reaction-to-fire experiments [Sultan and Paul, 2002]. After the ignition of the cables, the flames then spread upwards due to buoyancy, heat conduction and radiation processes (similar to the 'trench effect'). As the flame reaches the top of the vertical cable tray the cables mounted on the horizontal cable tray gets ignited and proceeds until all the cables are completely burnt which is facilitated by the rising plume from the vertical cable tray. This seems to be the general fire behaviour for all the tests. The time to reach peak HRR and the duration of the fire were different for each test depending on the cable type and the ventilation condition.

In order to provide an overview of the fire behaviour during each test, the following data has been selected and plotted in the next section.

- Mass loss (load cell data)
- Total Heat Release Rate
- Temperature above the fire (both above the horizontal cable tray and vertical cable tray)

In addition, some comments based on the observation during the tests were also provided under each test sub-section. The calibration test with a propane burner (100 kW and 300kW) showed that the corridor construction was nominally air tight and had no significant influence on the HRR measurements. There was some loss of combustion gases from the corridor exit into the calorimeter hood system in the initial tests, but this was improved during the first tests by dropping down curtains around the hood base.

6.7 Results and Discussion

Out of the total 10 fire tests conducted, only four of them will be described in this section. The remaining six tests are provided in Appendix A. The following four tests will be then used to validate the STEM-LER methodology in the next chapter.

6.7.1. NYM Cable fire (Test 5) – Inlet closed and 1m Weir placed

During the fifth test, NYM type cables (see Table 6.1 for its physical and chemical properties) were involved. Total 35 cables were involved during the test which lasted up to 2000 seconds. The 1 m^2 vent was closed and a weir of 1m height was placed at the end of the first corridor (see Figure 6.5) during the test. The load cell data is shown in Figure 6.10 and the total mass lost during the test was around 7.37 kg. Figure 6.11 shows the temperature above the cable fire during the test. The peak temperature above the horizontal cable tray and the vertical cable tray were around 700^0C and 980^0C respectively. The time to reach peak temperature above the vertical cable tray was around 700 seconds. The total heat release rate (HRR) measured by the calorimeter system during test 5 is provided in Figure 6.12 and the peak HRR was 137 kW.

Intensive smoke generation was witnessed at the very beginning of the fire (at around 260 seconds). During the test, no dripping of plastics from the horizontal cable tray was observed.

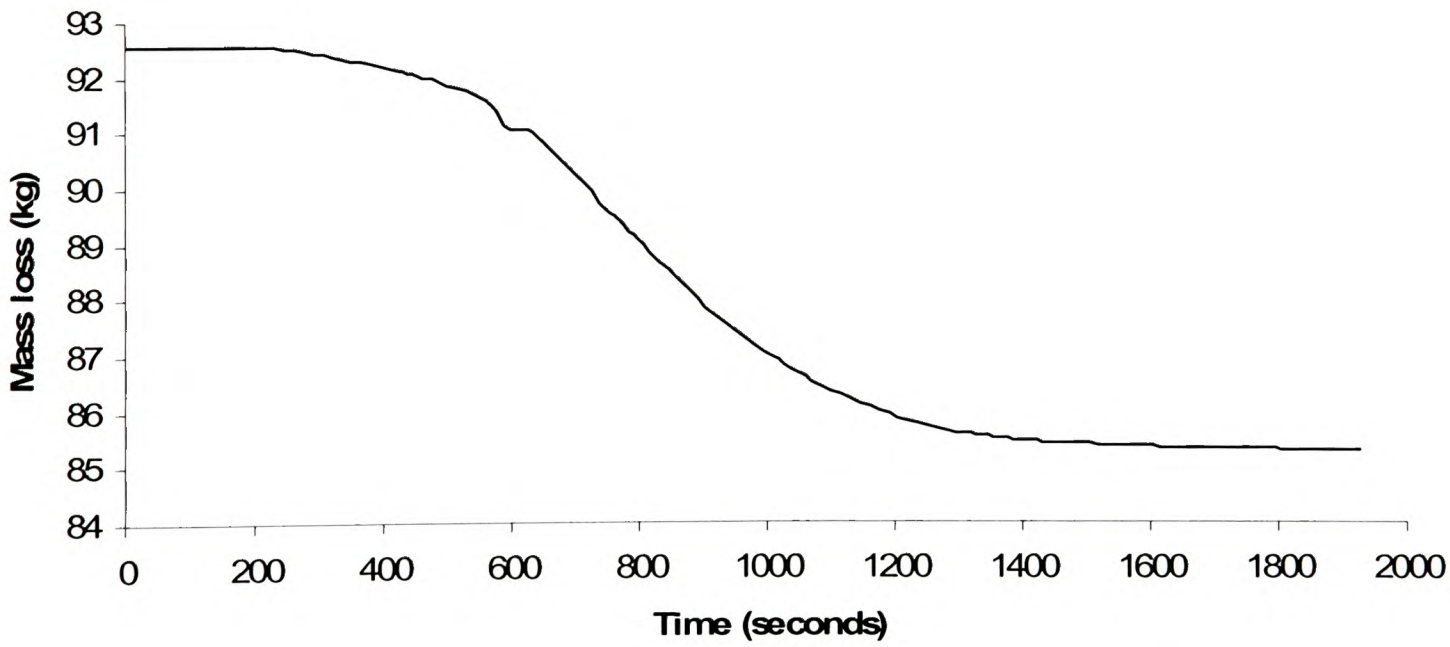

Figure 6.10 Load cell measurement of mass loss in kg (Test 5)

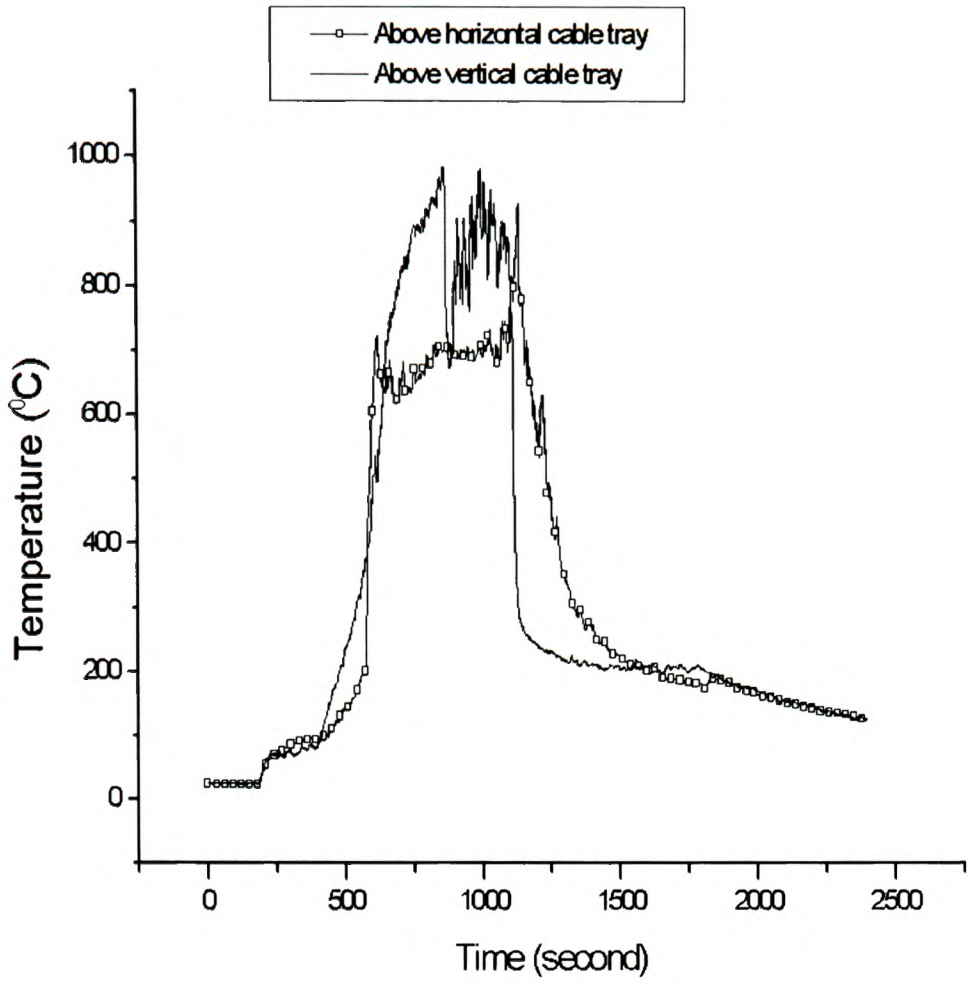

Figure 6.11 Temperature above horizontal tray and vertical tray (Test 5)

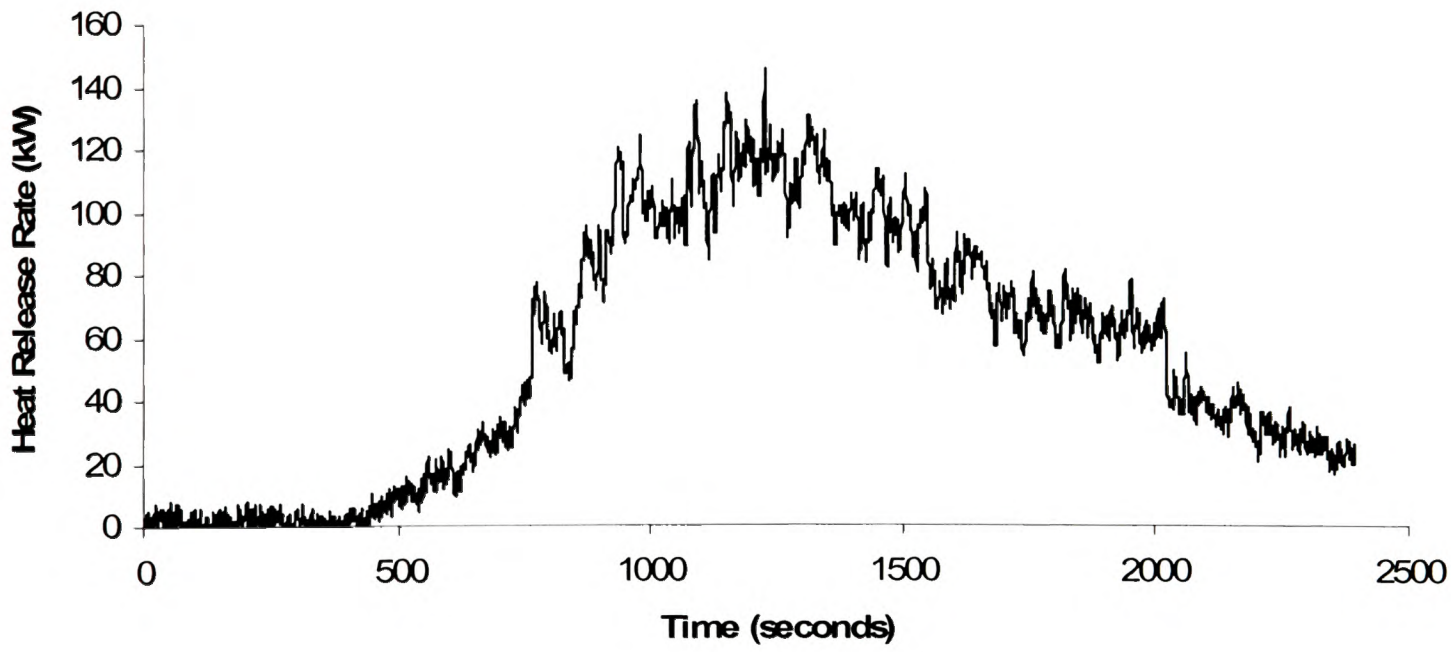

Figure 6.12 Total Heat Release Rate measured at exhaust hood by oxygen calorimetry (Test 5)

6.7.2. RZ1-K Cable fire (Test 7) – Inlet open and No weir placed

Test 7, a repeat of Test 1 was carried out in order to verify the repeatability and also to get proper weight loss measurements since the load cell arrangement was disturbed during Test 1. During this test, RZ1-K type cables were burnt. Total 33 cables were involved during the test which lasted up to 3500 seconds. The 1 m^2 vent was kept open during the test. The load cell data is shown in Figure 6.13 and the total mass lost during the test was around 8.23 kg. Figure 6.14 shows the temperature above the cable fire during the test. The peak temperature above the horizontal cable tray and the vertical cable tray was around 900^0C. The time to reach peak temperature above the vertical cable tray was around 1700 seconds. The total heat release rate (HRR) measured by the calorimeter system during test 7 is provided in Figure 6.15 and the peak HRR was 208 kW.

At around 1700 seconds both the vertical and the horizontal cable tray were involved in the fire. Dripping of plastics started around 1800 seconds and got intense around 2400 seconds.

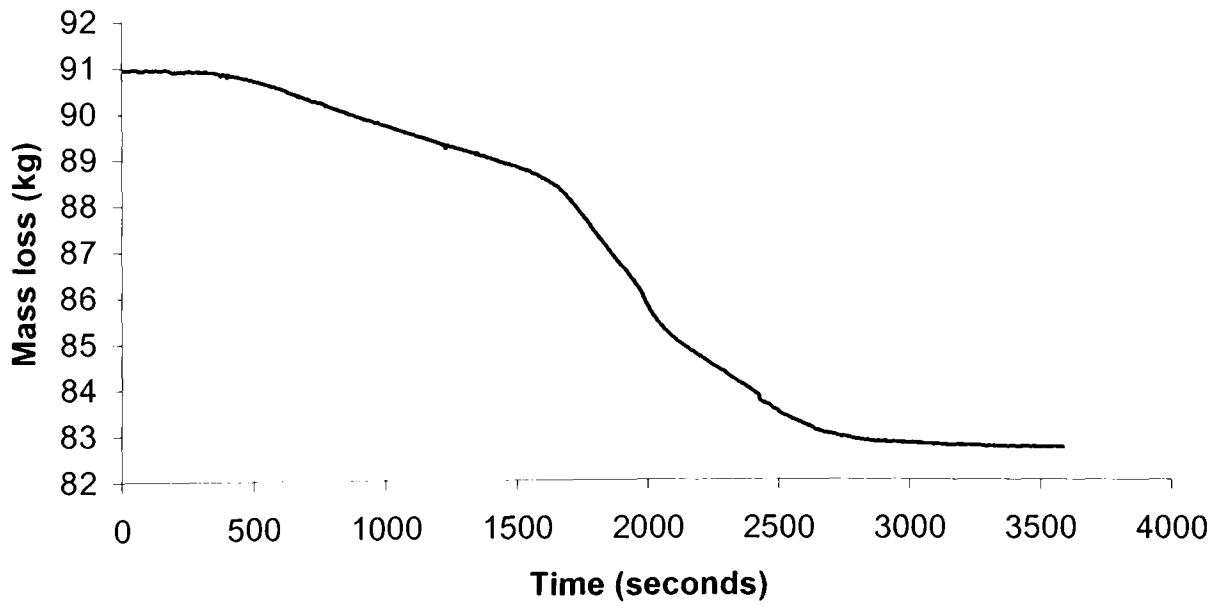

Figure 6.13 Load cell measurement of mass loss in kg (Test 7)

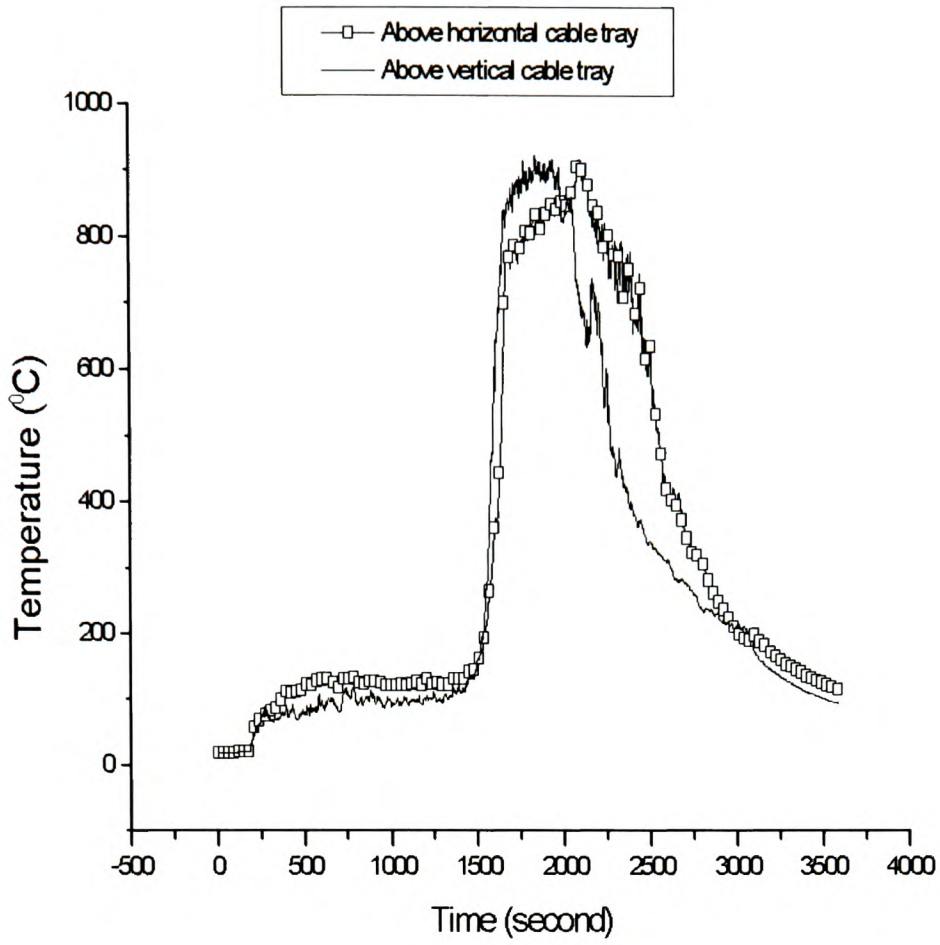

Figure 6.14 Temperature above horizontal tray and vertical tray (Test 7)

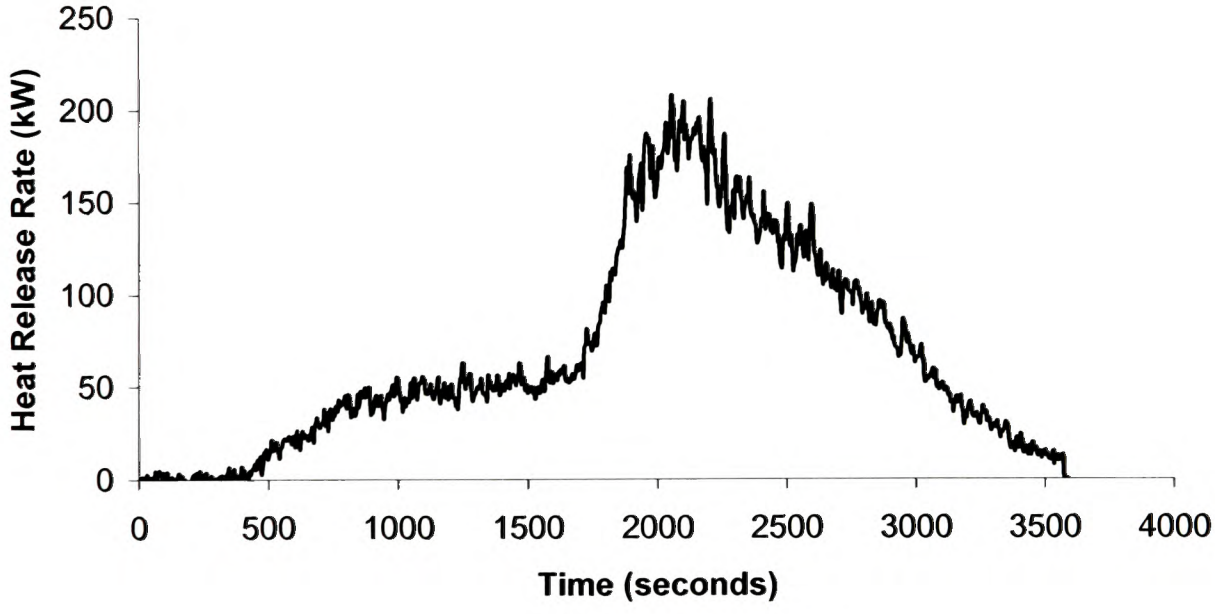

Figure 6.15 Total Heat Release Rate measured at exhaust hood by oxygen calorimetry (Test 7)

6.7.3. NHMH Cable fire (Test 8) – Inlet open and 1m Weir placed

During the eighth test, NHMH type cables were burnt. Total 39 cables were involved during the test which lasted up to 2000 seconds. Test 8 had a special ventilation arrangement. The 1 m^2 vent was kept open and a weir of 1 m height was placed at the end of the first corridor (see Figure 6.5) during the test. The cover on the vertical cable tray was removed during this test in order to get a glimpse of flame spread. The load cell data is shown in Figure 6.16 and the total mass lost during the test was around 6.77 kg. Figure 6.17 shows the temperature above the cable fire during the test. The peak temperature above the horizontal cable tray and the vertical cable tray was around 900^0C. The time to reach peak temperature above the vertical cable tray was around 800 seconds. The total heat release rate (HRR) measured by the calorimeter system during test 8 is provided in Figure 6.18 and the peak HRR was 608 kW.

Some dripping of plastics was noticed at around 790 seconds. At around 840 seconds, entire vertical and horizontal cable tray were involved in the fire and the dripping was found to increase. A small pool fire was observed on the floor at 1050 seconds. In order to measure the background conditions created by the propane burner, the measurements were continued even after the fire extinguished (at around 2000 seconds) for about 1400 seconds.

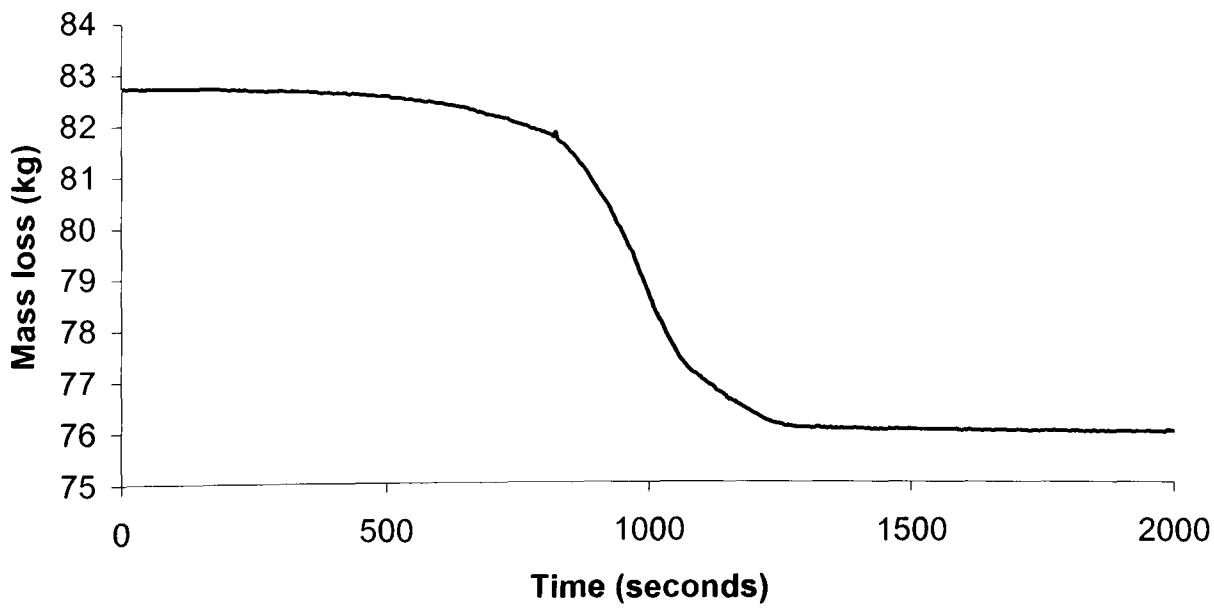

Figure 6.16 Load cell measurement of mass loss in kg (Test 8)

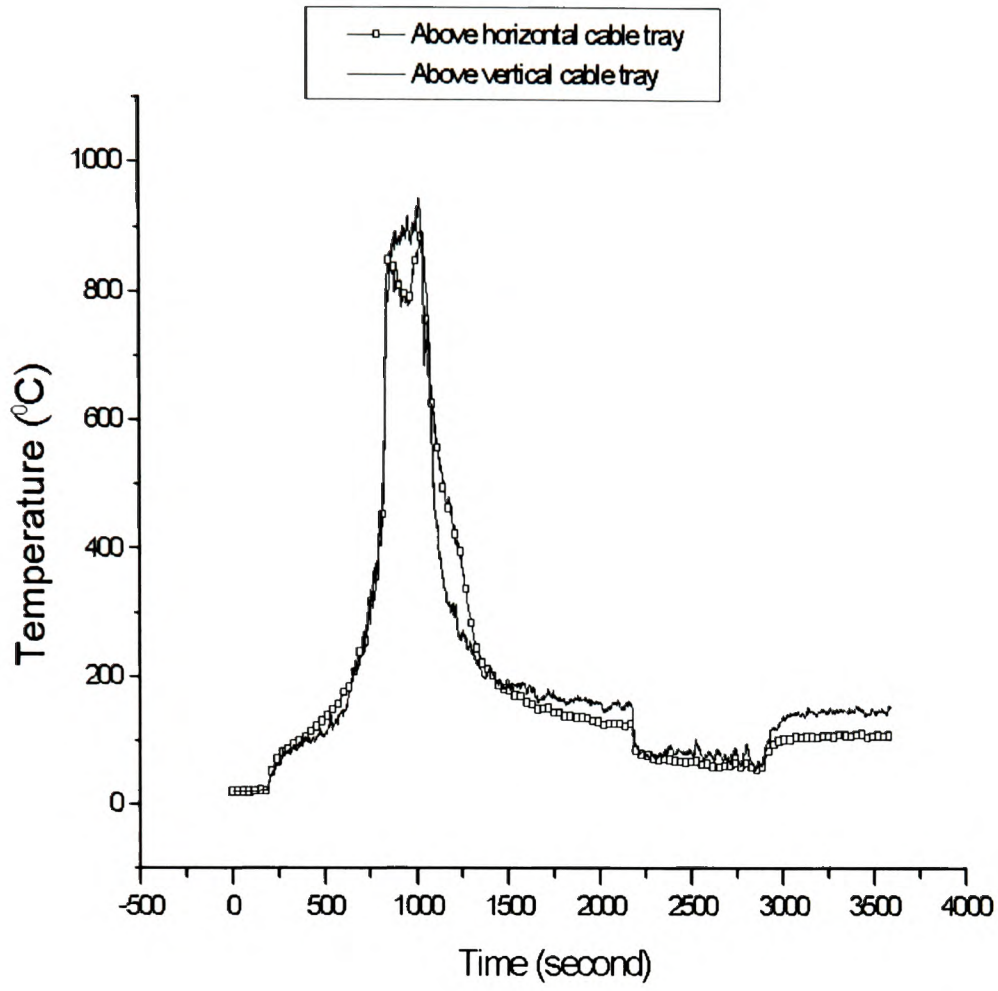

Figure 6.17 Temperature above horizontal tray and vertical tray (Test 8)

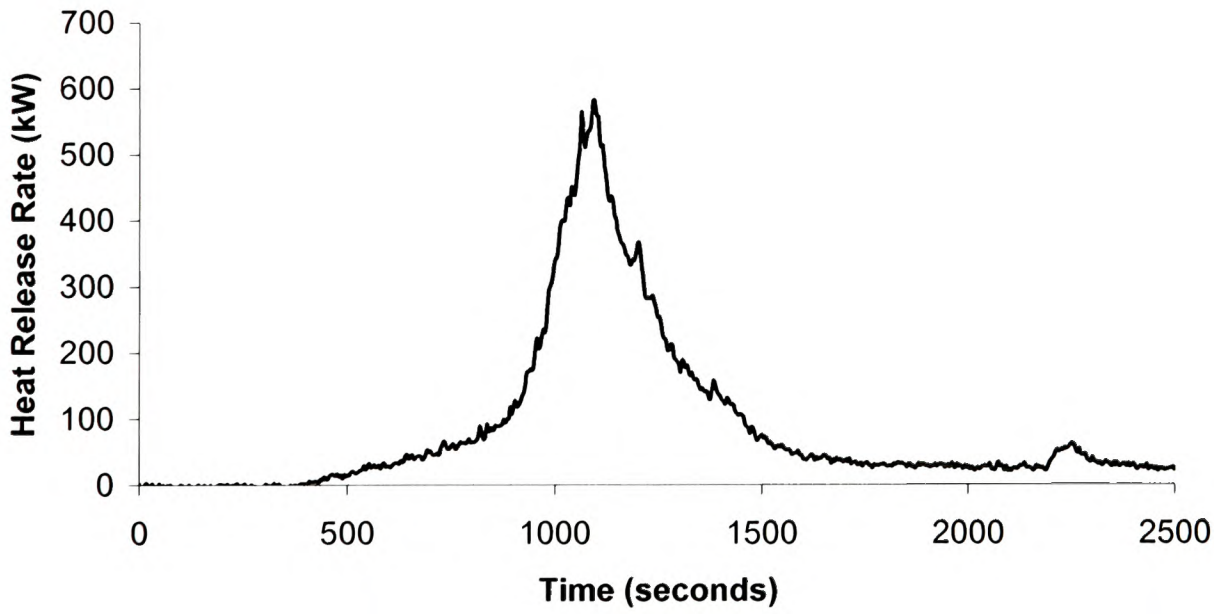

Figure 6.18 Total Heat Release Rate measured at exhaust hood by oxygen calorimetry (Test 8)

6.7.4. NHMH Cable fire (Test 10) – Inlet closed and 1.5m Weir placed

During the last test, NHMH type cables were burnt. Total 39 cables were involved during this test which lasted up to 1800 seconds. Test 10 too had a special ventilation arrangement. The 1 m^2 vent was closed and a weir of 1.5 m height was placed at the end of the first corridor (see Figure 6.5) during the test. The load cell data is shown in Figure 6.19 and the total mass lost during the test was around 6.29 kg. Figure 6.20 shows the temperature above the cable fire during the test. The peak temperature above the horizontal cable tray and the vertical cable tray were around 800^0C and 900^0C respectively. The time to reach peak temperature above the vertical cable tray was around 500 seconds. The total heat release rate (HRR) measured by the calorimeter system during test 10 is provided in Figure 6.21 and the peak HRR was 187 kW.

Some dripping of plastics was noticed at around 520 seconds. The visibility was very limited throughout the fire due to dense smoke.

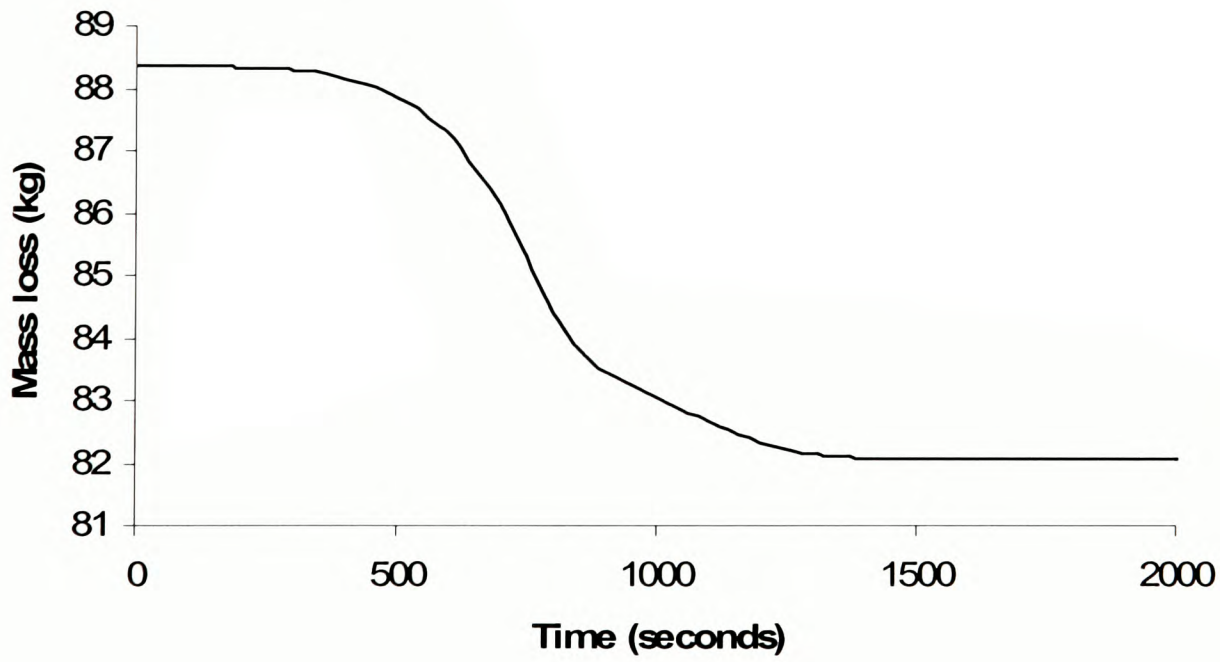

Figure 6.19 Load cell measurement of mass loss in kg (Test 10)

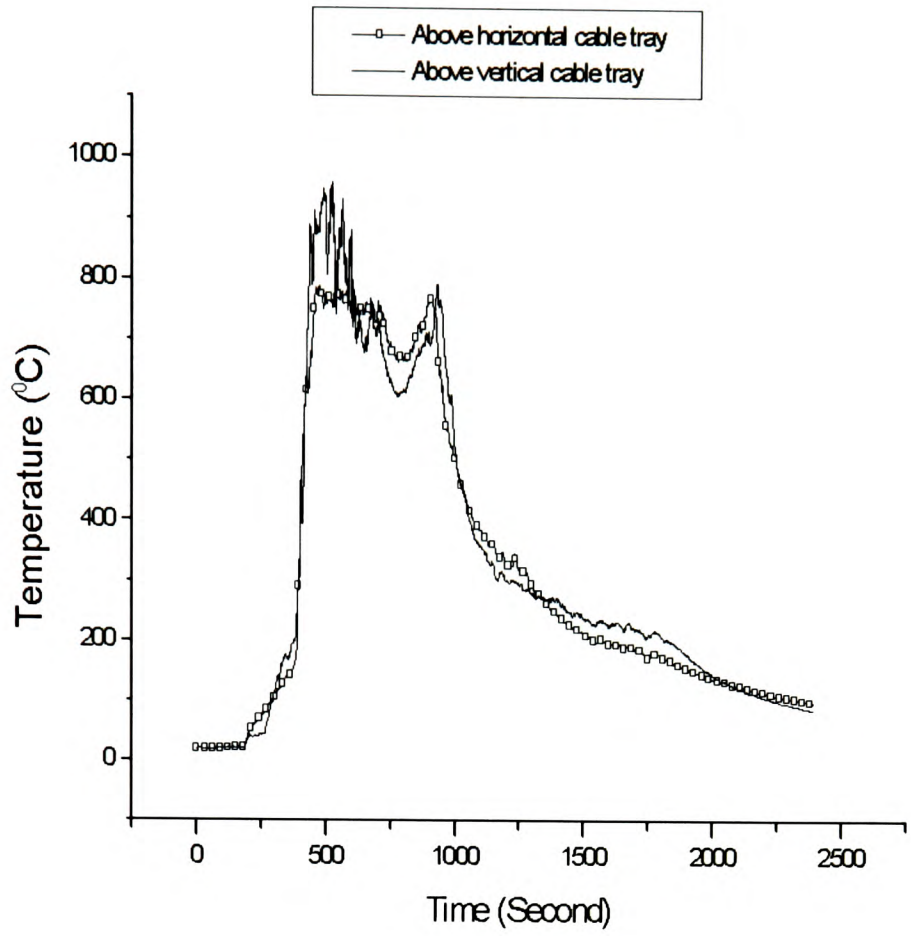

Figure 6.20 Temperature above horizontal tray and vertical tray (Test 10)

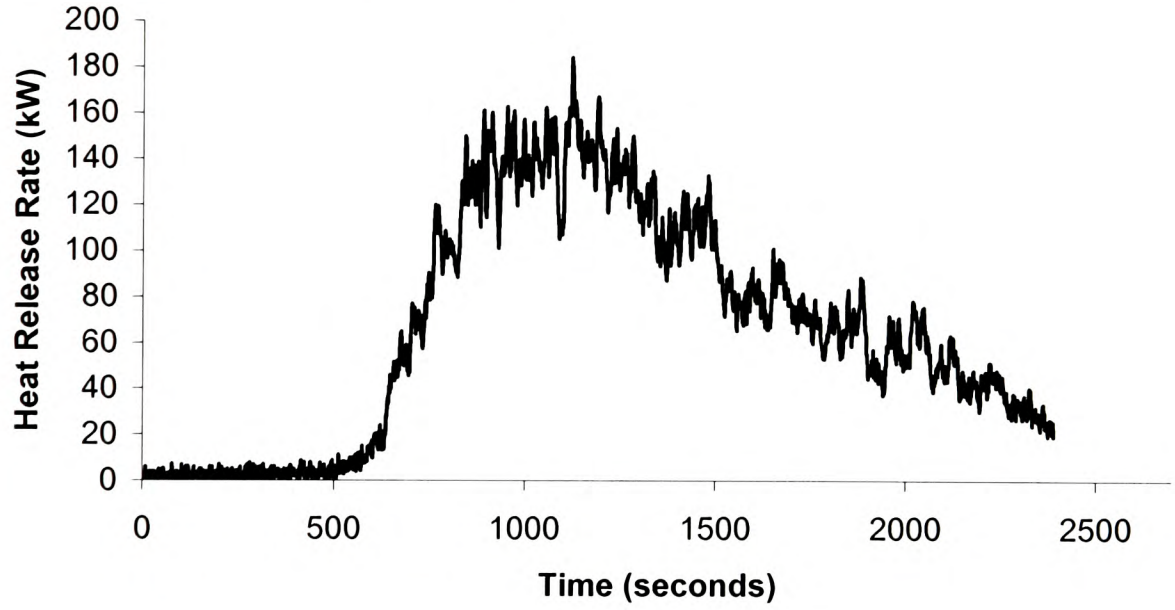

Figure 6.21 Total Heat Release Rate measured at exhaust hood by oxygen calorimetry (Test 10)

The results of the CO, CO_2 and temperature profiles at locations 5, 9, 15 along the corridor will be presented in Chapter 7 along with the modelling results.

6.8 Concluding Remarks

In summary, the measured fire data is sure to provide a unique collection of detailed test data, obtained under very controlled conditions. This makes the test data highly suitable for validation purpose to various fire sub models described in the section 6.2. From the author's point of view, the following set of experimental data would have culminated the above fire data into an ideal set of data.

- Measurement of smoke obscuration in the lower layer.
- Measurement of heat loss through walls and ceiling.
- Measurement of concentrations of CO, CO_2 and O_2 at some locations in the lower layer.

In the next chapter, the CO, CO_2 and temperatures measured at various locations along the corridor during the four cable fire tests described in this chapter is utilised to validate the STEM-LER methodology.

Chapter 7

Simulations of Large-Scale Cable Fire Tests

7.1 Introduction

Fire hazard calculations require modelling of generation of heat and toxic combustion products and its spread inside realistic building scenarios. In Chapter 4, a methodology has been presented which is based on solving transport equations for fuel, O_2, CO, CO_2 & H_2O and using the Local Equivalence Ratio (LER) concept to model the source terms to predict the CO and CO_2 generation and its transport during building fires. In this chapter, the STEM-LER methodology proposed in Chapter 4 is validated with the large scale cable fire tests described in Chapter 6. The CFD fire field modelling software SMARTFIRE is used as the computing platform to simulate the detailed thermal and fluid flow.

7.2 Numerical details

Using the STEM-LER model described in Chapter 4, simulations of four large-scale cable fire tests described in chapter 6 involving three different cable types was carried out. Figure 7.1 shows the computational domain and numerical grid used by the SMARTFIRE fire field model for the simulation of large-scale cable fire tests. Fine meshes were created near the walls, inlet vent, exit door, fire source, etc. A time step size of 2.0 s is adopted in the present simulations.

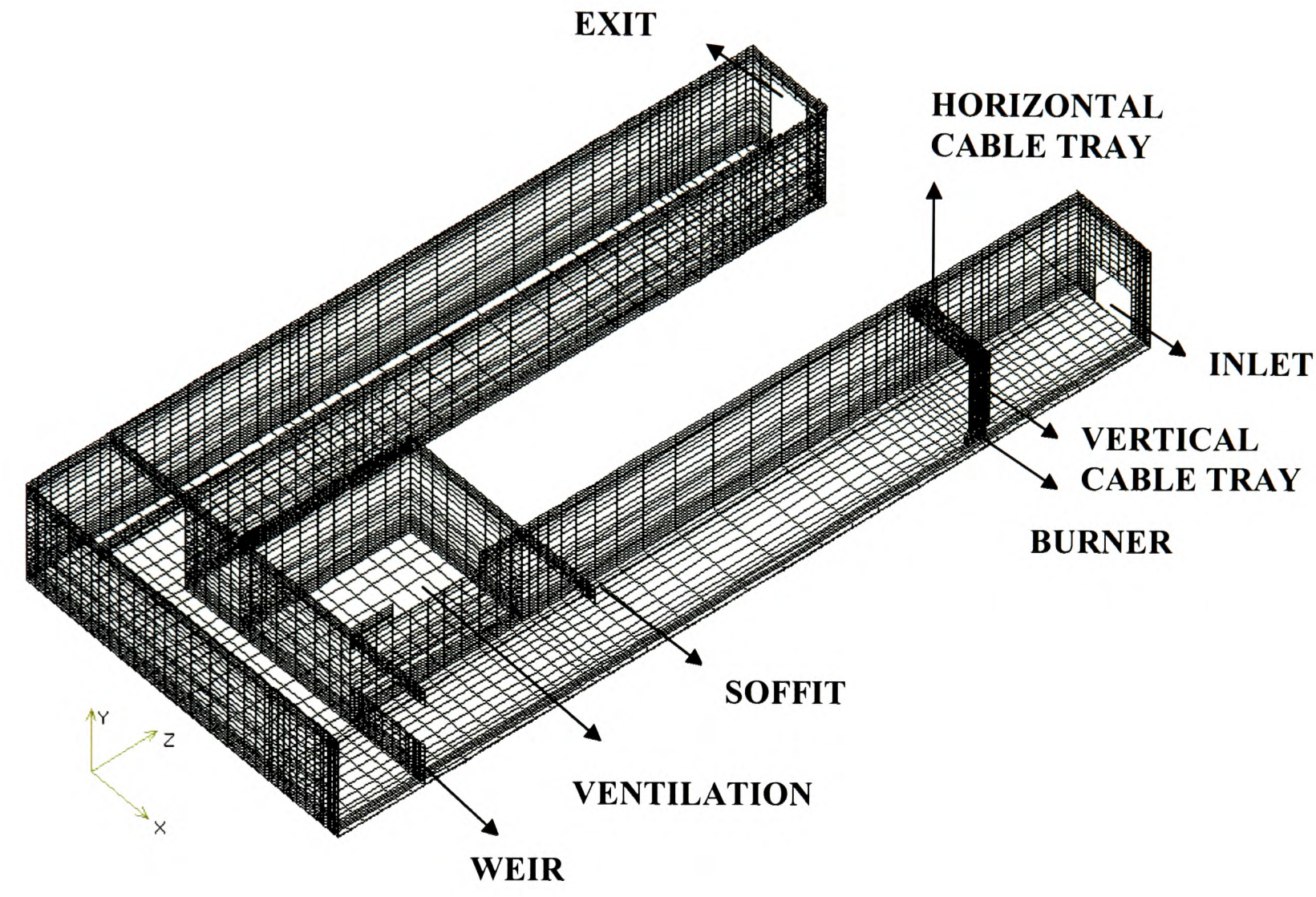

Figure 7.1 Computational domain and grid (Grid I)

The flow boundary conditions at the inlet vent and the exit door are treated using the 'Outlet' boundary condition. While using the 'Outlet' boundary condition, the pressure at the boundary cells is assumed to be the same as the external pressure which is the standard atmospheric pressure in the present simulations. All the other flow and turbulent variables on the boundary cells are assumed to be the same as in the calculated cells adjacent to the boundary cells. The walls are treated with 'no-slip' condition i.e., the fluid has zero velocity relative to the boundary. A logarithmic near wall profile is assumed for the near wall velocity profile where the turbulent kinetic energy (k) and dissipation rate (ε) in the near wall cells are calculated using the formulae:

$$k = \frac{sV^2}{\sqrt{C_\mu}} \tag{7.1}$$

$$\varepsilon = \frac{0.1643\, k^{3/2}}{\kappa \quad y} \tag{7.2}$$

where κ is the Karman constant, 0.435, C_μ is equal to 0.09, s is the wall skin friction factor, V is the fluid speed and y is the perpendicular distance from the near wall node to the wall. The six-flux radiation model described in Chapter 2 is used here to model the radiation phenomenon. The wall emissivity is assumed to be 0.8. Finally, the fire is treated as a volumetric fuel source and uses the fuel generation rate curve obtained from the load cell experimental curve.

7.3 Grid Sensitivity Analysis

Two grids namely GRID I and GRID II of grid size 40,848 and 75,992 cells respectively were selected to perform the grid sensitivity analysis. GRID I has 23 cells in the vertical direction (Y-Direction), 48 cells along the corridor (Z- Direction) and 37 cells across the layout (X-Direction). See Figure 7.1 for the co-ordinate axis. GRID II has 28 cells in the vertical direction (Y-Direction), 59 cells along the first corridor (Z- Direction) and 46 cells across the layout (X-Direction). Simulations were carried

out using both the grids for a test case where NHMH cables were burnt (cf. Chapter 6, section 6.6 under Test 8 for the test description). The peak CO and CO_2 volume fractions at locations 9 and 15 obtained using the two grids are given in Table 7.1. From the table it is shown that the maximum change in concentrations between the two simulations results was less than 7% for a grid refinement of around -100%. Hence, a non-uniform Cartesian mesh consisting of 48,600 cells (GRID I) was used in the present investigation with maximum grid points along x, y, z directions of 36, 25 and 54 respectively.

Table 7.1 Grid Sensitivity Analysis – Peak CO and CO_2 volume fractions at location 9 and 15 (Test 8).

	CO (% vol) Location 9 (h=2.2 m)	**CO_2 (% vol) Location 9 (h=2.2 m)**	**CO (% vol) Location 15 (h=2.2 m)**	**CO_2 (% vol) Location 15 (h=2.2 m)**
GRID I (40,848 cells) (37 x 23 x 48)	0.675	3.38	0.49	2.94
GRID II (75,992 cells) (46 x 28 x 59)	0.670	3.5	0.46	2.74

7.4 Simulations of Large-Scale Cable Fire Tests

In this section, simulations of large scale cable fire tests described in chapter 6 involving NYM, NHMH and RZ1-K type power cables were simulated and the results were compared with the experimental data. The sheath, bedding and insulation of NYM type power cables were all made of PVC material which contains pure PVC, plasticizer and chalk. For the simulation of fire tests involving NYM type power cables, the basic molecular structure of the fuel is assumed to be C_2H_3Cl (pure PVC). The sheath, bedding and insulation of NHMH type power cables were made of chalk

filled Ethylene Butyl Acrylate (EBA), chalk filled polyolefin and Polypropylene respectively. Finally, RZ1-K type power cable does not have bedding. The sheath and insulation of RZ1-K cables were made of cross-linked Polypropylene and a green coloured, non-toxic fire retarded Polyolephine respectively. For the simulation of fire tests involving NHMH and RZ1-K type power cables, the basic molecular structure of the fuel is assumed to be C_3H_6 (Polypropylene).

The mass loss rate curve for each fire test is derived from the load cell data and the net heat of combustion for each test is calculated from the total heat release rate curve measured by the calorimeter system positioned at the hood. Simulations were carried out for the whole of fire duration which ranges from 2000 seconds to 4000 seconds depending on the fire test. Analysis was made on the modelling of CO oxidation and the modified Eddy Break-Up combustion model in relation to one of the large scale cable fire tests before the validation of the STEM-LER model for four large scale cable fire tests.

7.4.1 Modelling of CO oxidation

The objective of this simulation is to study the effect of modelling the CO oxidation process on the prediction. Prediction of CO is very important to fire safety engineers since it is the most dominant toxic combustion product generated during fires. Due to computational limitations and the lack of chemical kinetic data for most fuels, combustion problems in two or three-dimensional geometries with turbulence-chemistry interactions are presently restricted to one to five–step global mechanisms to model the oxidation of the hydrocarbon fuel [Nicol et al., 1999]. Traditionally global reaction mechanisms involve only hydrocarbon oxidation which do not allow for the prediction of some important intermediate species like CO. Dryer and Glassman [1973] suggested a sequential two step approach to describe realistically the oxidation of a hydrocarbon; that is, in the first reaction, the fuel is oxidised to water and CO followed by the oxidation of CO to CO_2 as shown below:

$$CH_4 + \frac{3}{2}O_2 \Rightarrow CO + 2H_2O \qquad (7.3)$$

$$CO + \frac{1}{2}O_2 \Rightarrow CO_2 \tag{7.4}$$

Thus, the only species used in the above two-step global mechanism are the fuel, O_2, CO, CO_2, and H_2O. The rate expressions for the above two-step global mechanism given by DuPont et al. [1993] are as follows:

$$R1 = 10^{10.0} \exp\left(\frac{-12019}{T}\right)[CH_4]^{1.0}[O_2]^{1.0} \tag{7.5}$$

$$R2 = 10^{10.0} \exp\left(\frac{-12019}{T}\right)[CO]^{1.0}[O_2]^{1.0} \tag{7.6}$$

The units are kgmoles, cubic meters, seconds and Kelvin. The rate expression for the forward CO oxidation is utilised in the present investigation of real-scale cable fires to model the post-flame CO oxidation process.

Based on the chemical kinetics, the rate of CO oxidation is a strong function of temperature. The effect of change in temperature on upper-layer composition of a compartment fire according to Gottuk et al. [1995] is twofold:

1. Generation of intermediate species like CO in the fire plume depends upon the quenching of the fire plume by the upper layer. Quenching of the fire plume at various heights has significant effect on the final CO levels from the fire plume. Also as the compartment temperature increases, the fire plume temperature increases resulting in more complete oxidation of the fuel to CO_2 and H_2O within the plume thus reducing the final CO levels from the fire plume.
2. Oxidation of post-flame gases in the upper layer is also affected. Upper-layer temperatures > 900 K allow near complete oxidation of CO to CO_2 when $\phi_g <$ 1.1. However, for the upper-layer temperatures < 800 K, no CO oxidation is reported which indicates that the upper layer is fairly un-reactive.

Under the condition that no additional fuel introduced in the upper layer, the final levels of CO transported to remote locations depends upon the following mechanisms:

- Quenching of a turbulent fire plume upon entering a rich upper layer.
- Continued reaction within the upper layer for temperatures < 1100 K due to mixing of additional oxygen.
- Approach to equilibrium for high temperature combustion products in a fuel-rich upper layer for temperatures > 1300 K .

For the sample simulation considered in this section, a two step reaction mechanism is assumed in order to model the post-flame CO oxidation which is given by the following reactions:

$$C_3H_6 + a\,O_2 \rightarrow b\,CO + c\,CO_2 + d\,H_2O \tag{7.7}$$

$$CO + \frac{1}{2}O_2 \Rightarrow CO_2 \tag{7.8}$$

The total oxygen consumption rate is based on the production rates of CO, CO_2 and H_2O in the first reaction and the oxygen consumption in the second reaction. The first reaction given by Equation 7.7 is assumed to be infinitely fast and modelled by the STEM-LER model. The oxidation of fuel to CO, CO_2 and H_2O is based on 'fast chemistry' assumption and the generation of CO and CO_2 is calculated from their yields obtained from Purser furnace experiments. The CO oxidation reaction given by the Equation 7.8 is calculated by the kinetic rate expression, R2 (Equation 7.6). It is assumed that oxidation of CO does not take place if there is no oxygen available to oxidise the fuel present. The above assumption is based on the following observations

- The hydrocarbon oxidation to CO and H_2 is much faster than CO and H_2 oxidation to CO_2 and H_2O, respectively. This is due to the preferential combination of free radicals, such as OH, with hydrocarbons over CO. Carbon monoxide is oxidised almost exclusively by OH radical to CO_2 [Warnatz, 1984]. Therefore, it is not until the hydrocarbons are consumed that free radicals are able to oxidise CO to CO_2.

- Based on the chemical kinetics calculations for an isothermal plug-flow reactor, Pitts [1995] concludes that as long as fuel is present the oxidation of CO is strongly inhibited.

Two simulations were carried out for a NHMH cable burning test (Test 8); one with the secondary CO oxidation step included and the second without the CO oxidation step calculation. The upper layer CO volume fraction distribution at locations 5, 9 and 15 obtained from the two simulations are given in Figures 7.2 – 7.4. See Figure 7.6 for the positions of the locations. All the positions were at height 2.2 m above the floor. Figure 7.2 shows no change in CO volume fractions at location 5 between the two simulations which is understandable since near the fire, ϕ is greater than 1 and there is no oxygen available for the CO oxidation to take place. Also, the maximum temperature at this location was 550 ^{o}C (Figure 7.5) which is still lower than the temperature range 600-700 ^{o}C, above which the upper layer becomes reactive. Zukoski et al. [1989] and Gottuk et al. [1994] also have shown that the CO oxidation reaction almost 'freezes' below the temperature range 850-900 K. Figure 7.3 depicting the CO volume fraction at location 9, shows no change in CO concentrations. Finally, Figure 7.4 shows the CO volume fraction distribution at the location 15. At location I5, the comparison shows very small fraction of CO being oxidised during the peak HRR period. This may be attributed to significant time taken for the products to travel from location 5 to 15 which is 30 m (approximately 2 mins), where the temperatures varied from 250 ^{o}C to 70 ^{o}C between the two locations.

Also, given that the upper layer temperatures away from the fire plume in this cable fire tests were below 650-700^{o} C range, it can be deemed that the upper layers were non-reactive and hence no significant CO oxidation takes place away from the fire plume. Therefore, further simulations were carried out without the CO oxidation step since the post flame temperatures were lower than the temperatures required for the oxidation of CO.

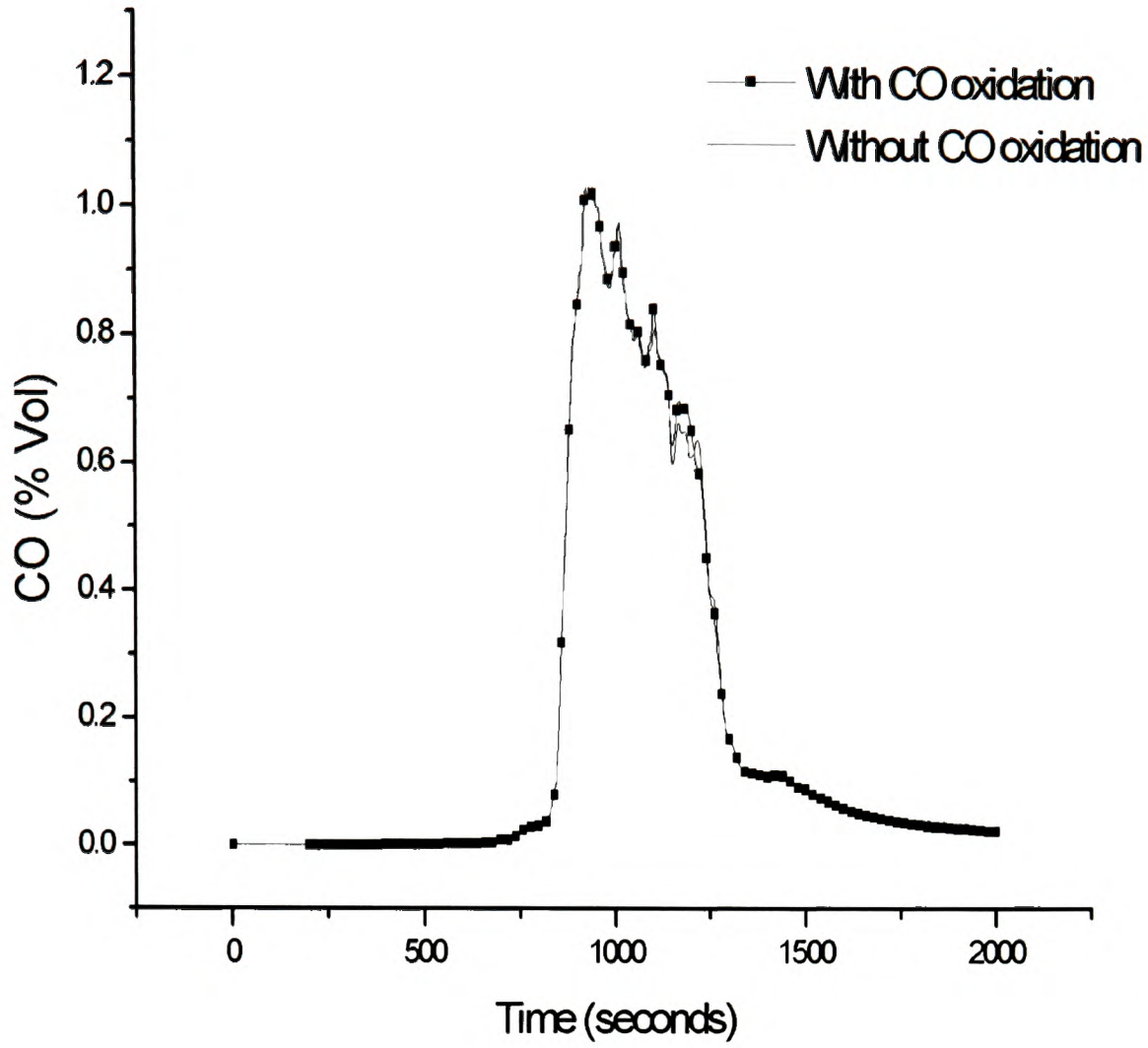

Figure 7.2 CO volume fraction at location 5

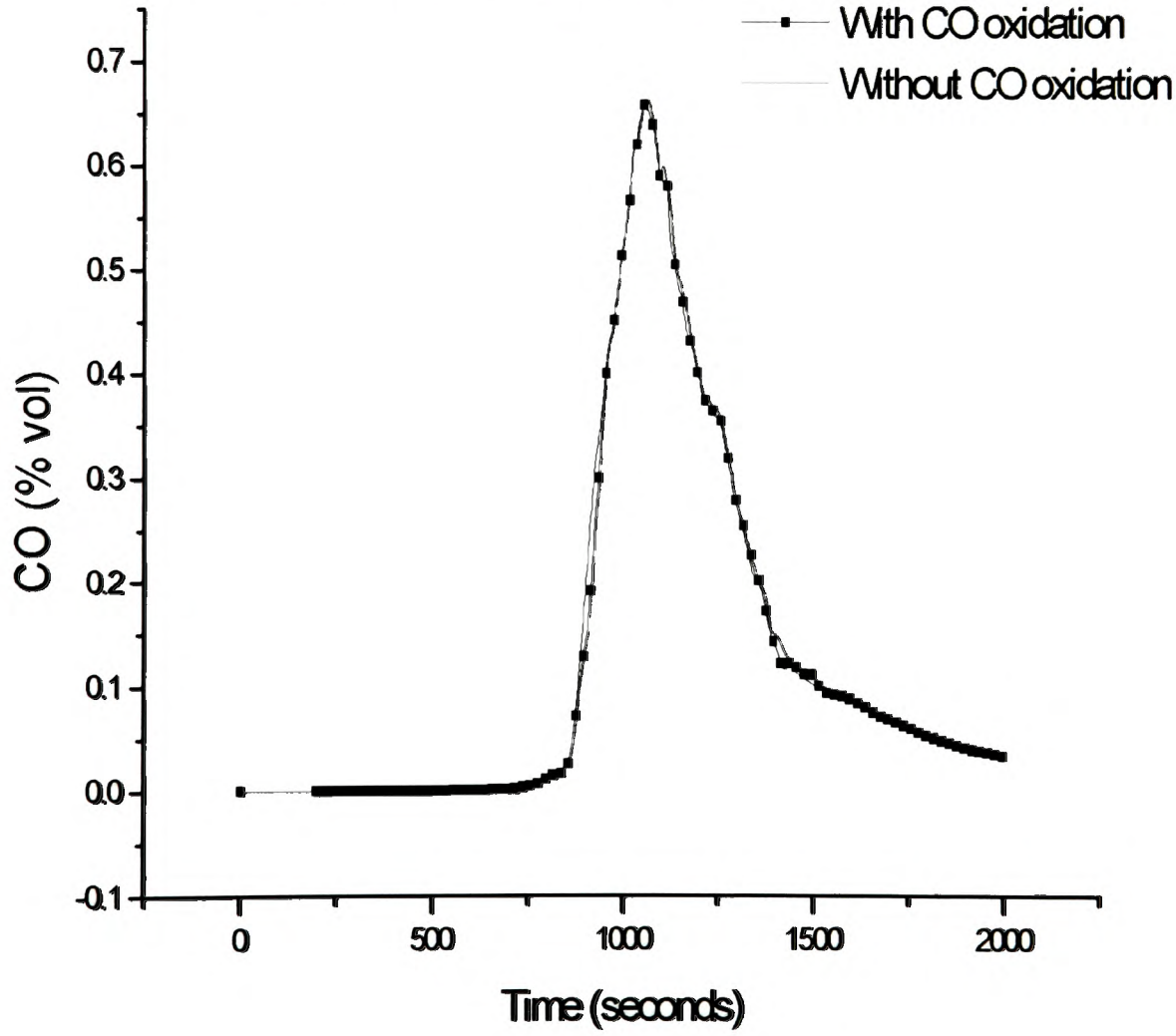

Figure 7.3 CO volume fraction at location 9

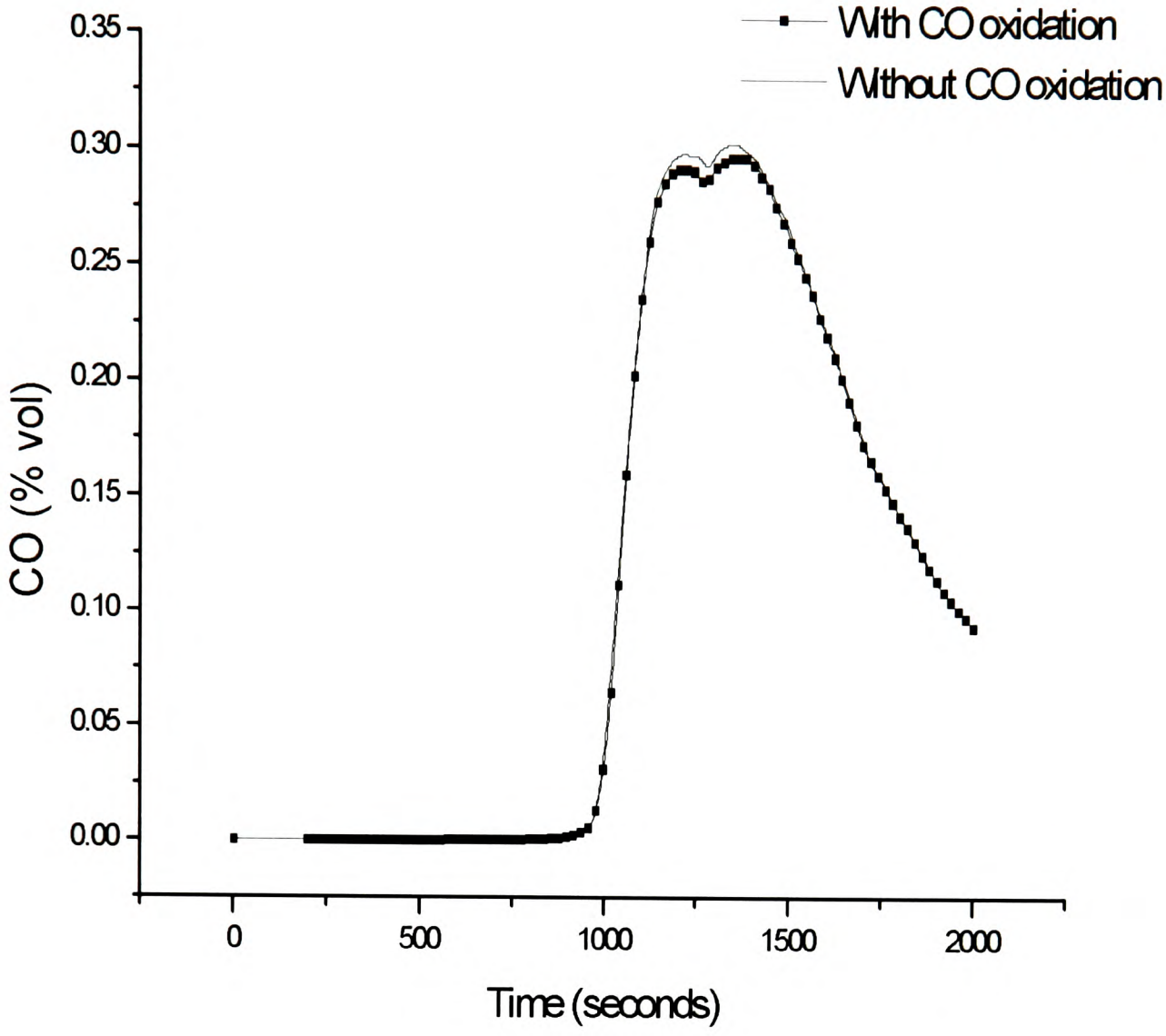

Figure 7.4 CO volume fraction at location 15

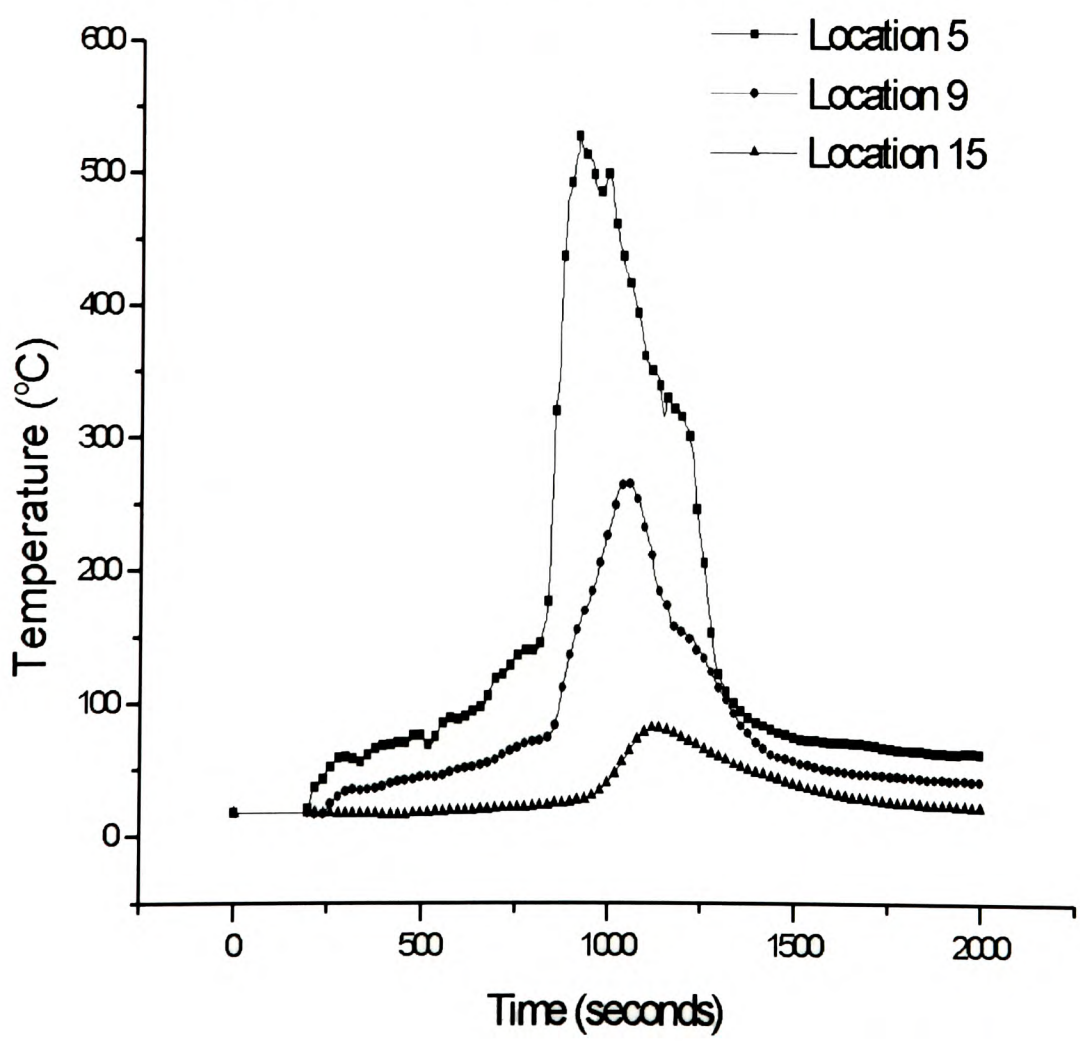

Figure 7.5 Computed temperature distributions along the corridor

7.4.2 Modified Eddy Break-Up Combustion model (EBU)

Eddy Break-Up (EBU) based combustion models are the most widely used combustion model with much success. The model originated from the works of Spalding [1971] and is based on the assumption that chemical time scales are fast compared to the turbulence scales. Spalding [1971] proposed that the reaction rate may be directly related to the time required for the reactants to mix at molecular level. In turbulent flows, this mixing time depends on the rate of break-up of the eddies by the action of turbulence, and therefore, the rate is proportional to a mixing time defined by the turbulent kinetic energy, k, and its dissipation rate, ε.

Magnussen and Hjertager [1977] have subsequently developed the EBU model and expressed the rate of reaction by mean concentration of a reacting species, turbulent kinetic energy and the rate of dissipation of this energy. According to Magnussen and Hjertager [1977], the fuel burning rate is given by

$$R_f = A\rho\frac{\varepsilon}{k}\min\left\{Y_f, \frac{Y_{Oxygen}}{r}\right\} \tag{7.9}$$

where the model constant A usually take the value of 4.0. Y_f, Y_{Oxygen} and Y_P are the mass fractions of fuel, oxygen and combustion products, and r is the stoichiometric ratio of oxygen to fuel.

In the fuel-rich regions of the flame, oxidant concentrations show strong intermittency hence the dissipation of the oxygen eddies will limit the combustion rate in fuel-rich regions. Fires under ventilation-controlled conditions inside enclosures are characterised by the production of some intermediate species like CO. Accurate predictions of such scenarios require suitable combustion models [Wen and Huang, 2000]. In the EBU combustion model, the fuel and oxygen are assumed to be consumed in their stoichiometric proportions with some stable intermediate species like CO being ignored. Hence, in fuel-rich areas, the model over-predicts the efficiency of the combustion process and the temperatures in the plume and hot layers are higher than the experimental values [Fletcher et al. 1994; Chow, 1995].

In the present version of EBU, the rate of fuel burning, R_f is modified as

$$R_f = A\rho\frac{\varepsilon}{k}\min\left\{Y_f, \frac{Y_{air}}{s(\phi_{local})}\right\} \tag{7.10}$$

where $(Y_{air}/s(\phi_{local}))$ is the amount of fuel that is consumed for the available air at vitiation condition, ϕ_{local}, taking into consideration the amount of CO generated. The ratio $s(\phi_{local})$ at various equivalence ratios can be calculated based on the yield vs equivalence ratio correlation obtained from the Purser furnace as described in Chapter 4 (Section 4.5.1). This modified EBU is denoted as MEBU hereafter. In this subsection, it will be shown that the EBU model when modified as given by Equation 7.10 is able to better predict the temperatures, CO, CO_2 concentrations and the CO_2/CO ratios near the fire and far away from the fire. Simulations of Test 8 case were performed using the two different combustion models: the EBU model (EBU) and the modified EBU model (MEBU) along with the STEM-LER model for the species. Positions of the locations 5, 9 and 15 along the corridor at which the species and temperature are compared are shown in Figure 7.6. Figures 7.7 and 7.8 compare the predicted CO and CO_2 concentrations using both the combustion models at location 9 (h = 2.2 m) with the experiments. The computed CO concentration profiles at this location using EBU and MEBU model were in good agreement with the experiment. On the other hand, MEBU based CO_2 profile was better than the EBU based prediction through out the fire. From the temperature profile comparison at the same location given in Figure 7.9, it is evident that the EBU based temperature profile has a delay in the profile and the peak temperature is over predicted outside of the combustion region while MEBU predicted correctly the time of the peak period and better values of temperature during the peak period. This can be explained from the way the fuel consumption is calculated in fuel-rich regions by the two combustion models. MEBU predicts more fuel consumption in fuel-rich regions than EBU. Hence the combustion region is smaller and intense which results in more CO being generated and higher temperature than EBU (Figure 7.14). This also explains the phase delay in the profiles predicted by EBU. Better the prediction of temperature

rise, less the time delay in the profiles and in order to get a better prediction of the temperature rise, the combustion region needs to be simulated with good accuracy.

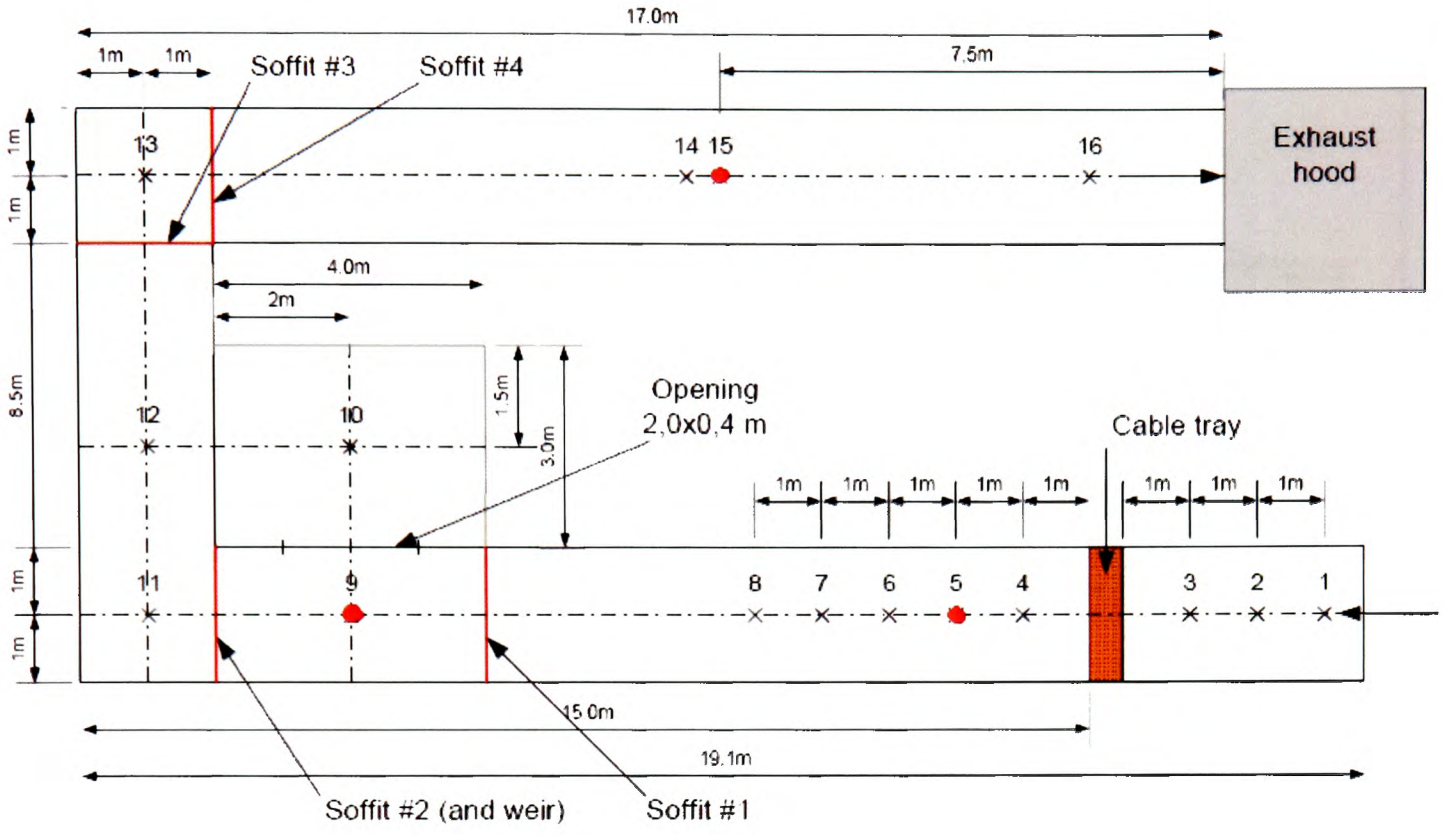

Figure 7.6 Positions of location 5, 9 and 15 highlighted by red dots

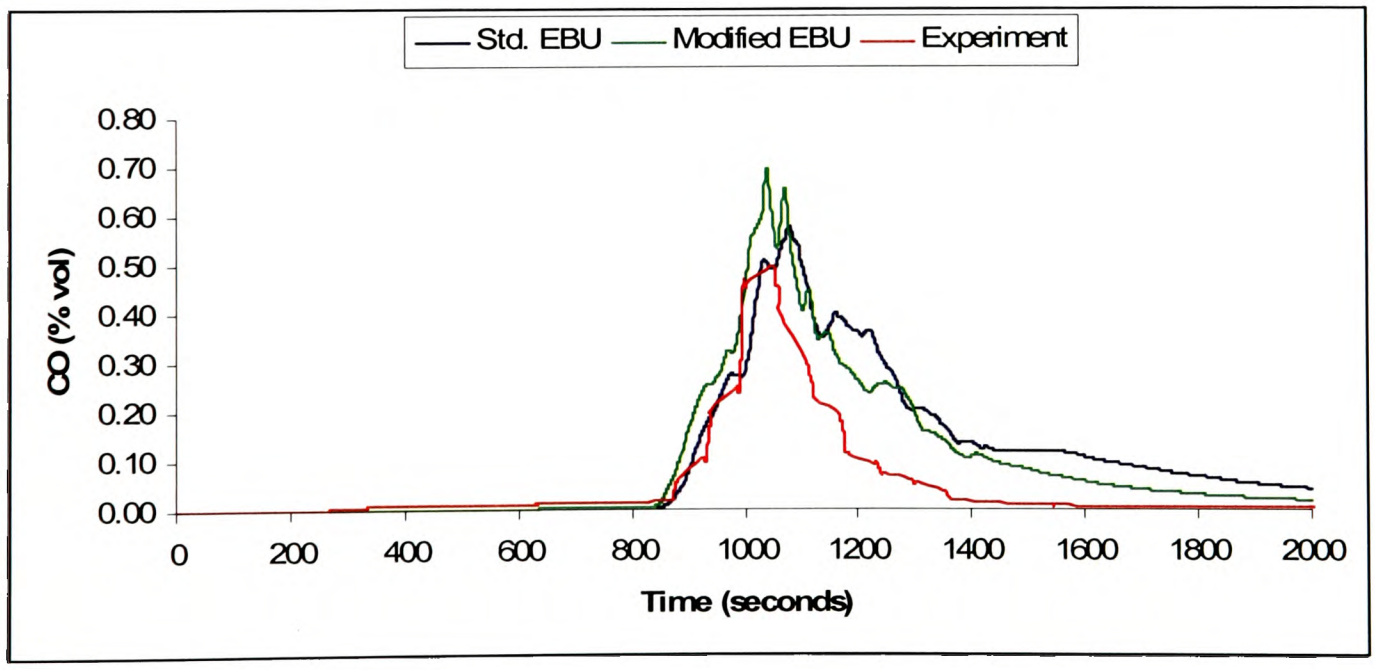

Figure 7.7 CO concentration at location 9 (Test 8)

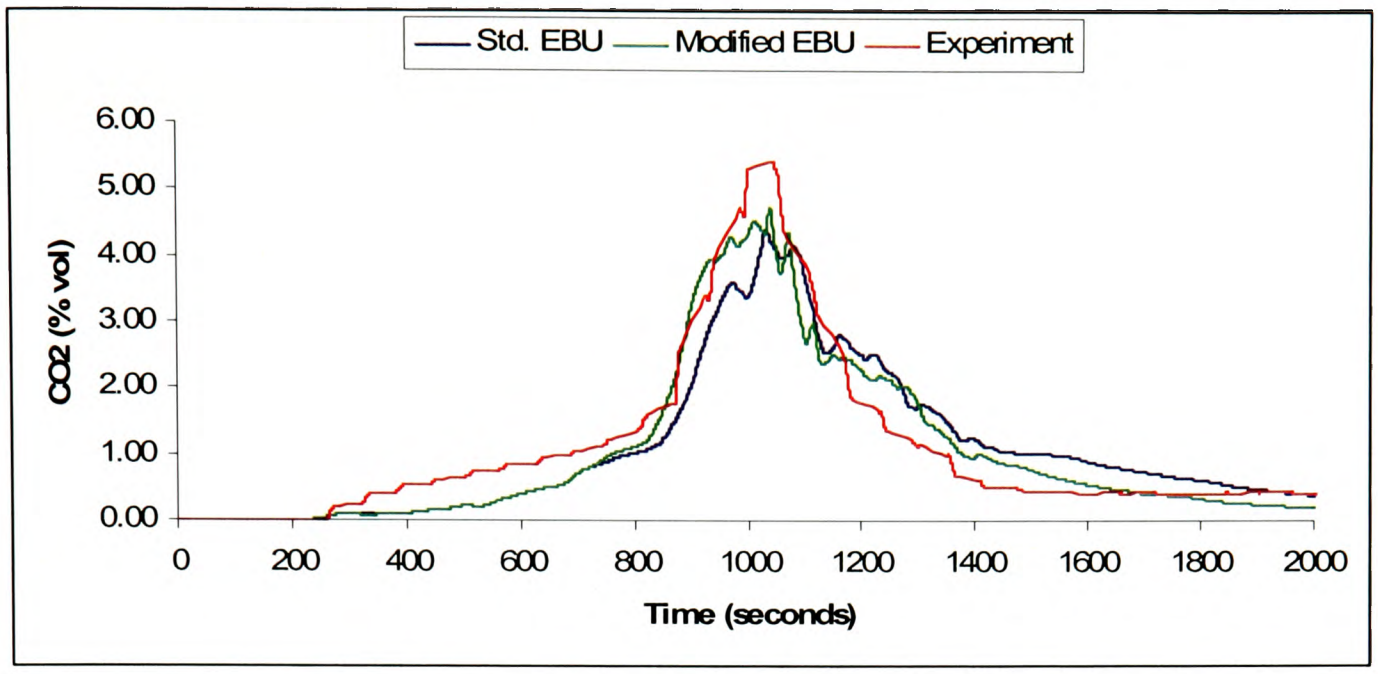

Figure 7.8 CO_2 concentration at location 9 (Test 8)

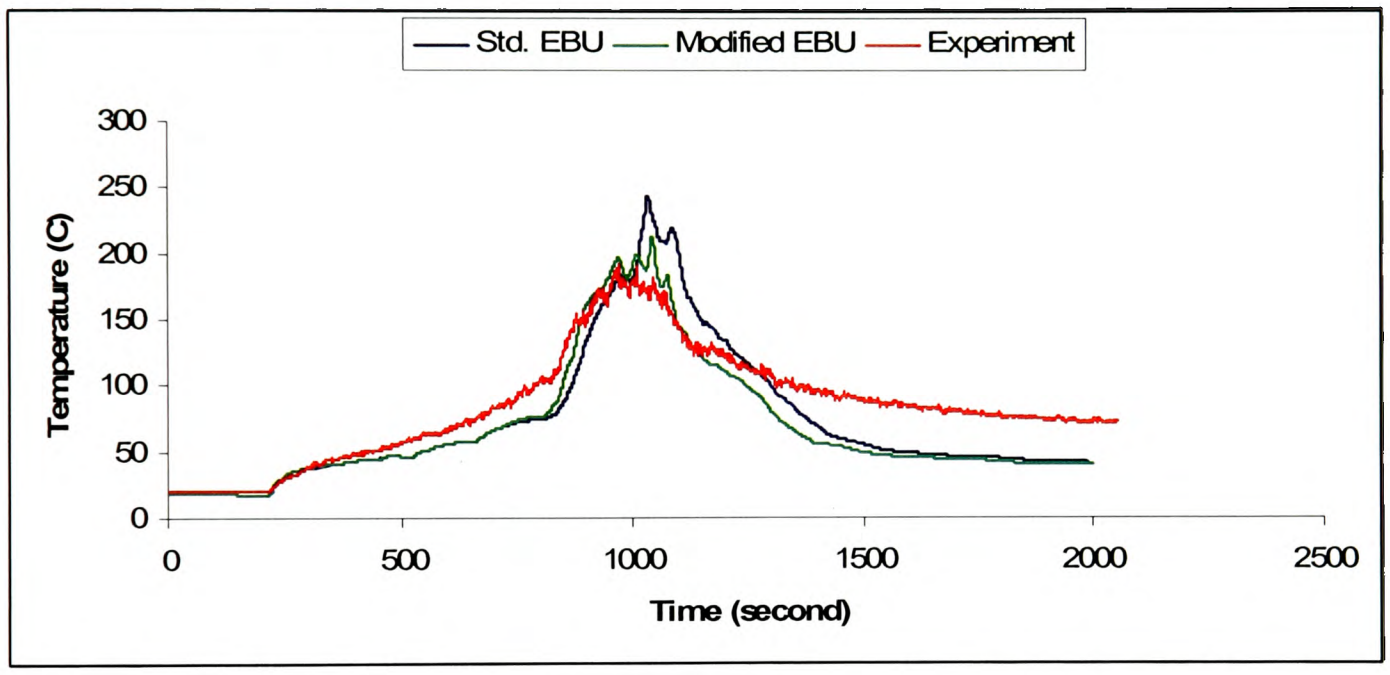

Figure 7.9 Temperature profile at location 9 (Test 8)

The EBU and MEBU based prediction of peak CO, CO_2 concentrations, CO_2/CO ratio and the peak temperature in the middle of the exit door corridor (location 15, h = 2.2 m) are compared with the experiment and given in Table 7.2 and depicted in Figures 7.10-7.11. The MEBU simulated peak CO and CO_2 concentrations, CO_2/CO ratio and the peak temperature are in better agreement with the experiments than the EBU based predictions. This emphasises the fact that it is important to model the combustion region accurately to get more accurate prediction of the concentration profiles near the fire and far away from the fire. The combustion region near the cable trays and the dynamics of the fire affects greatly the concentration profiles and peak concentrations both near the fire and far away from the fire.

Table 7.2 Comparison of peak CO, CO_2 concentrations and CO_2/CO at location 15

	CO (% vol)	CO_2 (% vol)	CO_2/CO	Temperature (C)
EBU	0.244	2.06	8.44	62.3
MEBU	0.3	2.68	8.93	59.2
Experiment	0.355	3.73	10.5	60

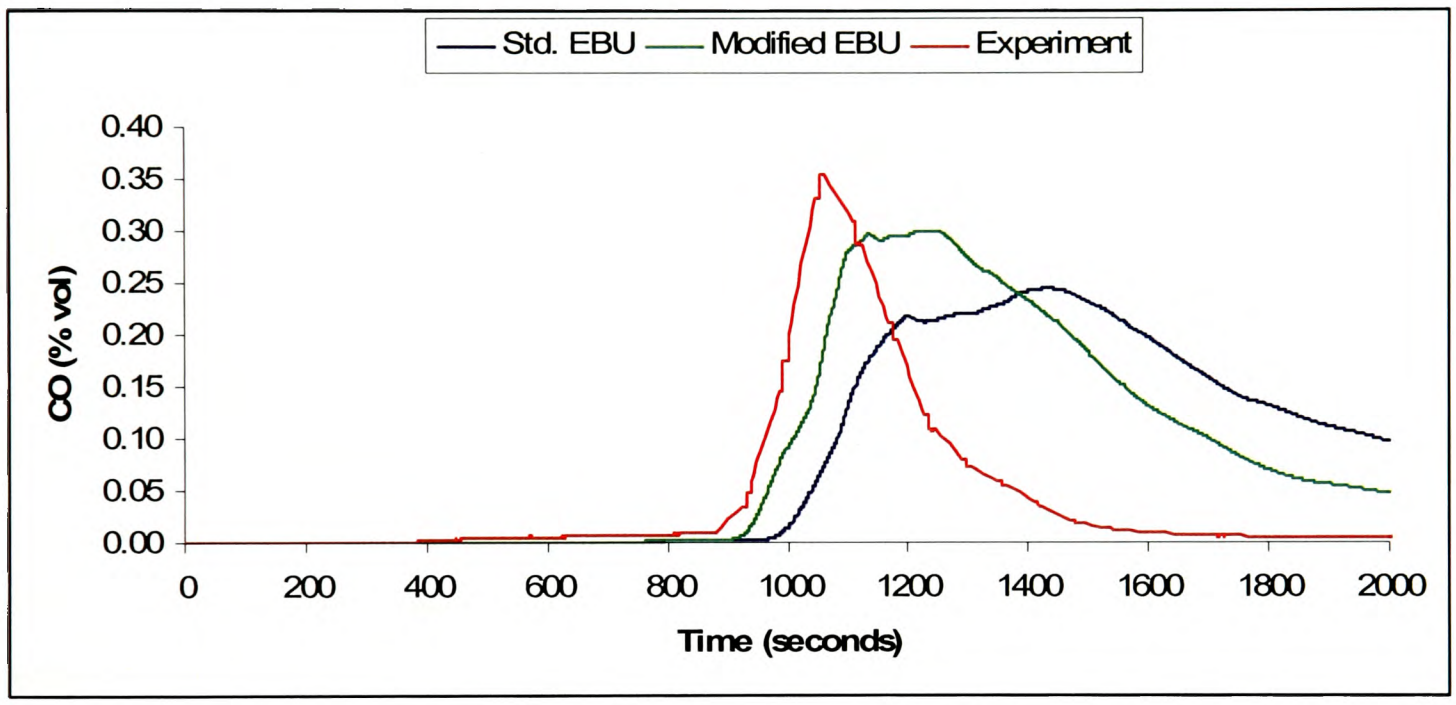

Figure 7.10 CO concentration at location 15 (Test 8)

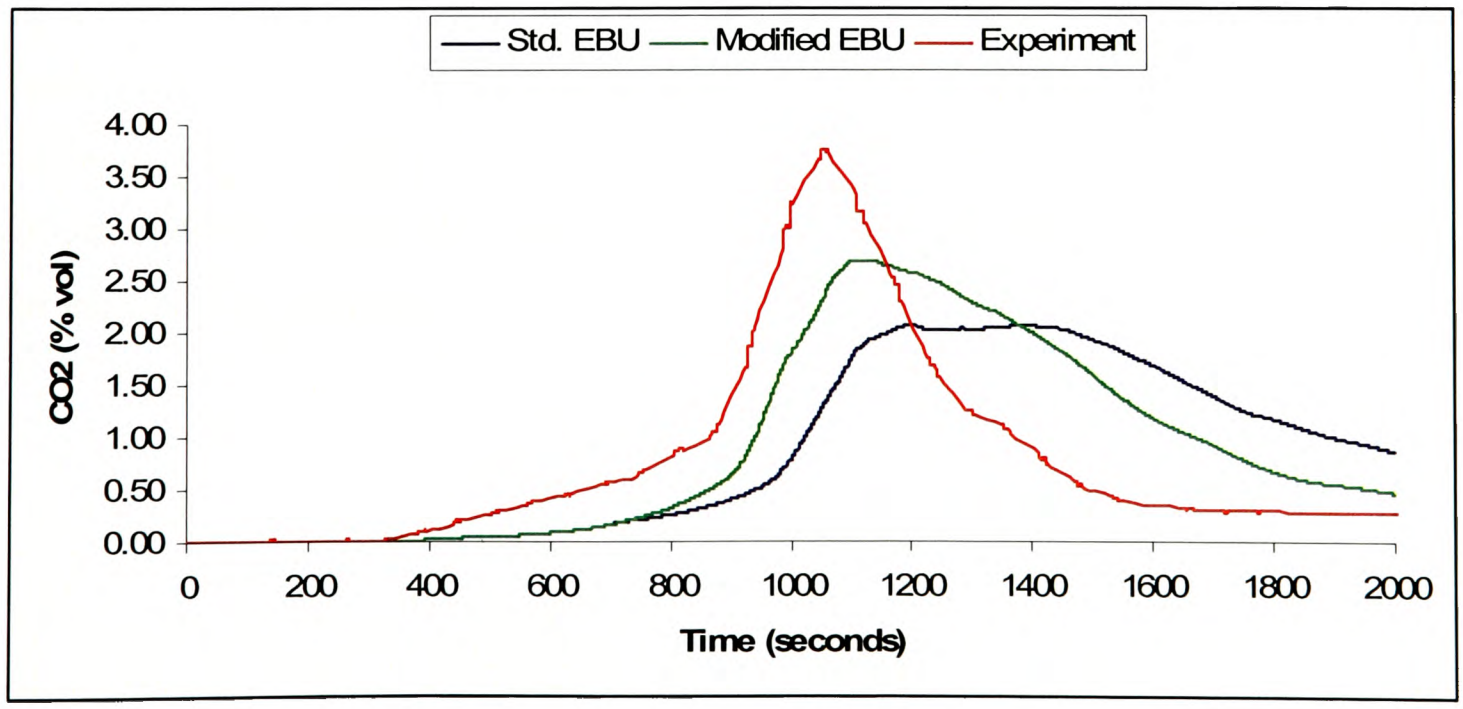

Figure 7.11 (a) CO_2 concentration at location 15 (Test 8)

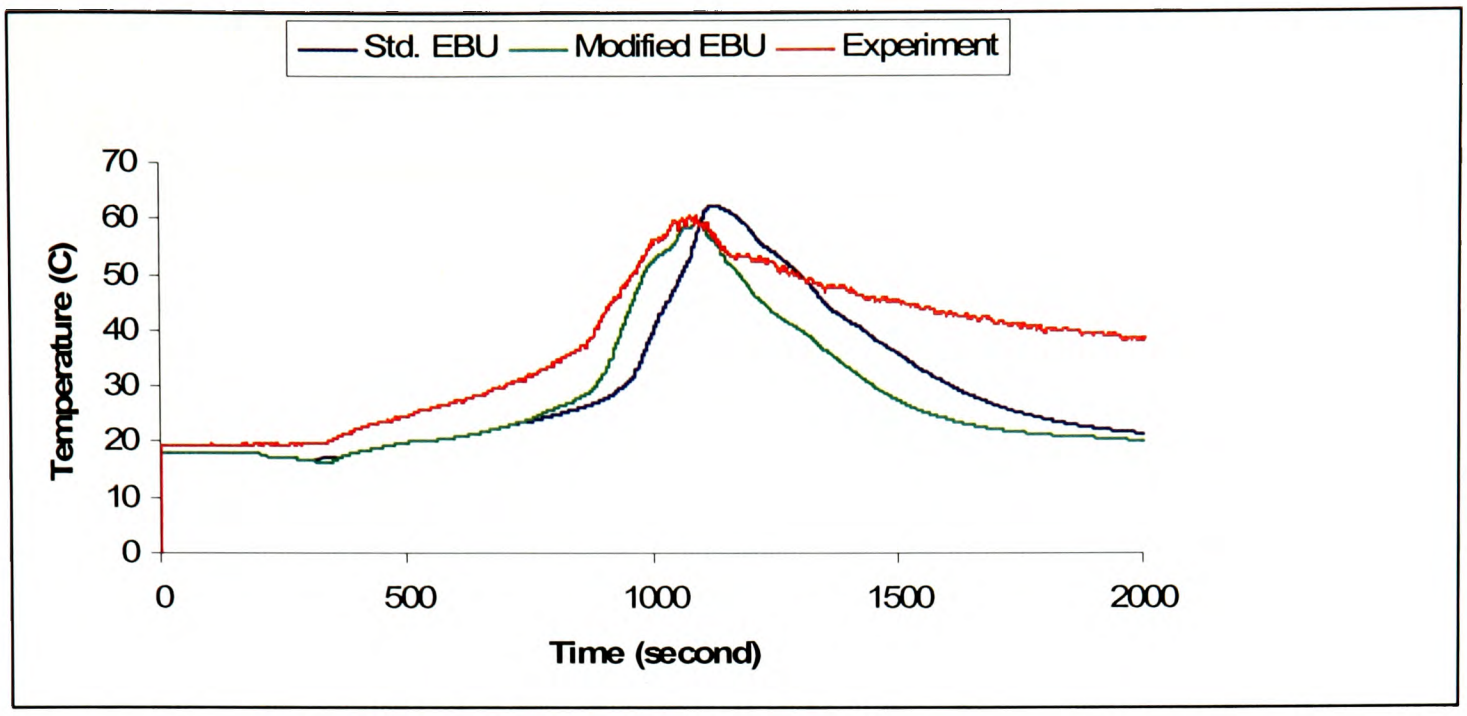

Figure 7.11 (b) Temperature profile at location 15 (Test 8)

Figure 7.12 (a) presents the comparison of the air-to-fuel consumption ratio, s(ϕ) with respect to the equivalence ratio (ϕ) between the standard EBU and the MEBU for NHMH cable sample. The standard EBU uses a constant air-to-fuel consumption ratio of 14.88 which is the stoichiometric air-to-fuel ratio for NHMH cable irrespective of the vitiation condition. MEBU on the other hand, calculates the air-to-fuel consumption ratio based on the LER and the corresponding yields of CO and CO_2. Since the MEBU predicts higher fuel consumption inside the combustion region, the temperature above the fire is higher than the temperature predicted by EBU (Figure 7.12 (b)). The air-to-fuel consumption ratio under well-ventilated conditions calculated by the MEBU is equal to the stoichiometric air-to-fuel ratio. This dynamic calculation of the air-to-fuel consumption ratio enables the MEBU to predict the combustion region and the temperatures better than standard EBU and as a consequence the concentrations of CO and CO_2 are predicted better. Henceforth in the simulations, the MEBU is used to model the source term in the transport equation for the fuel mass fraction.

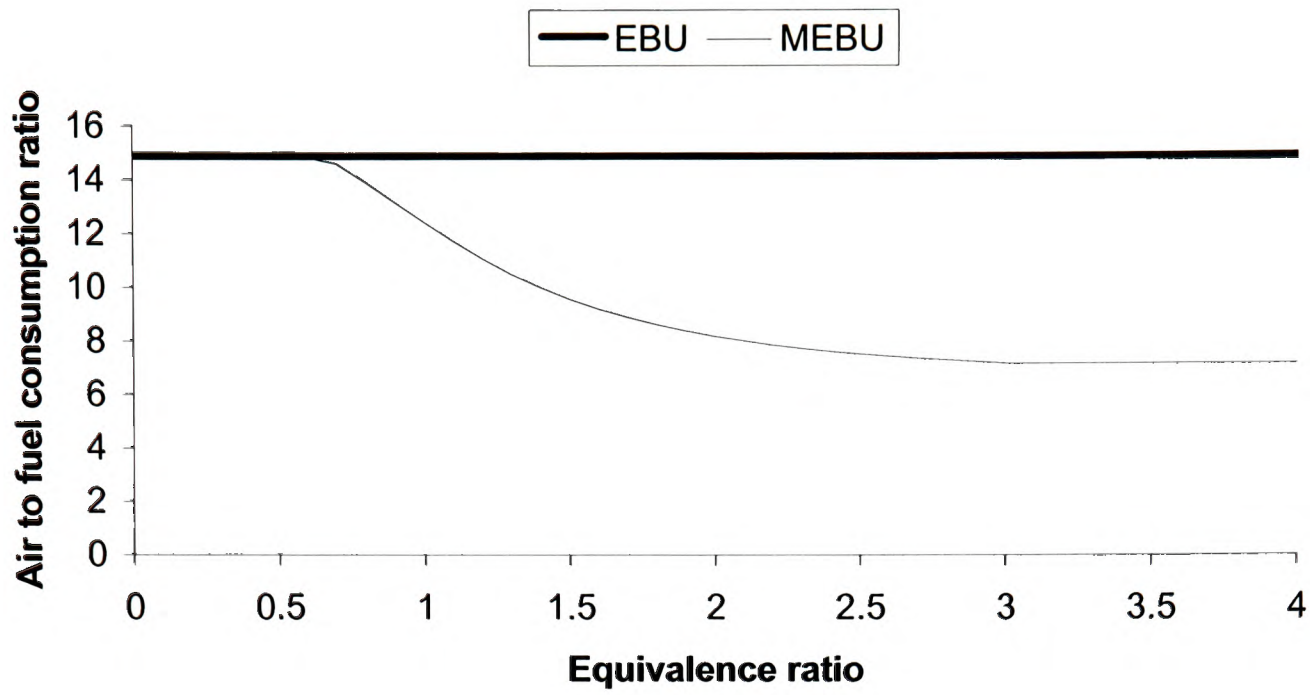

Figure 7.12 (a) Variation of s(ϕ) as a function of Equivalence ratio for NHMH cable

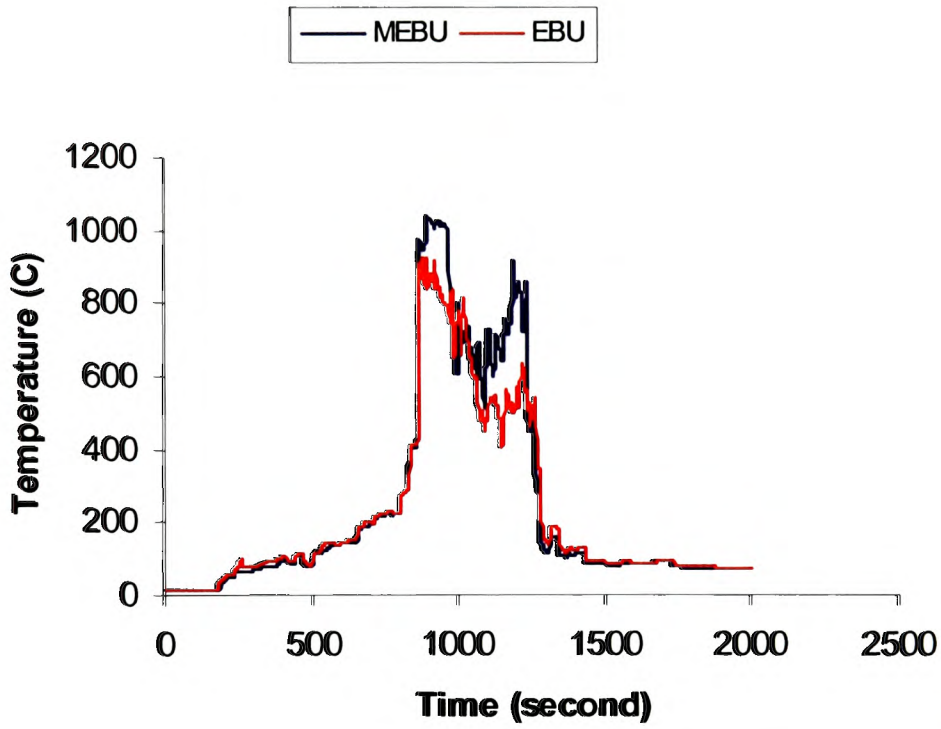

Figure 7.12 (b) Temperature above the fire (above horizontal tray)

In the following section, the STEM-LER model is validated with the experiments by simulating four of the large scale cable fire tests involving three different cable types, namely NHMH, NYM and RZ1 cables.

7.5 Validation of the STEM-LER model

In order to validate the STEM-LER methodology, a Borealis small room test and four large scale cable fire experiments described in the previous chapter were considered.

The selected test cases have different ventilation conditions and involve four different cable types. Hence the test cases considered in this section are diversified and complex enough to test the STEM-LER methodology.

7.5.1 Simulation of the Borealis small room cable fire test

7.5.1.1 Description of the experiment

In 1999 a series of single-compartment cable fire test were undertaken at the Borealis Antwerp fire research laboratory [Borealis Report, 2001; Robinson, 2004; Wang, 2007]. One of the investigation involved NYM power 220 volt cables. The compartment for the cable fire tests had the dimensions of 3x3x3 m and is shown in Figure 7.13(a). Two cable trays were used. One tray of cables ran vertically up the wall opposite the exit door wall while the second ran horizontally across the ceiling of the compartment. The opening door is of 0.8 m width and 2.0 m height. The tray was of 400 mm width and 50 mm depth. The cables were fastened to the trays by means of conventional polypropylene cable ties. A protective cover was placed on the vertical cable tray. An extraction system above the door opening collected the combustion exhaust gases and recorded the heat release rate by oxygen depletion calorimetry system. The heat release rates and the rates of generation of CO and CO_2 were measured at the hood.

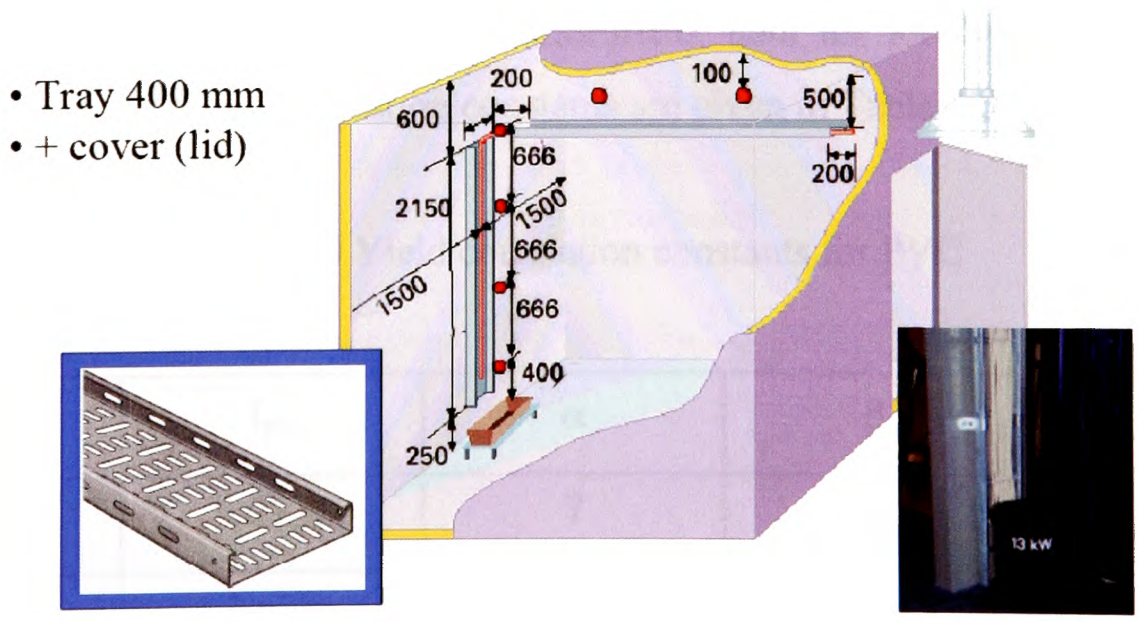

Figure 7.13 (a) Schematic of Borealis cable fire test compartment

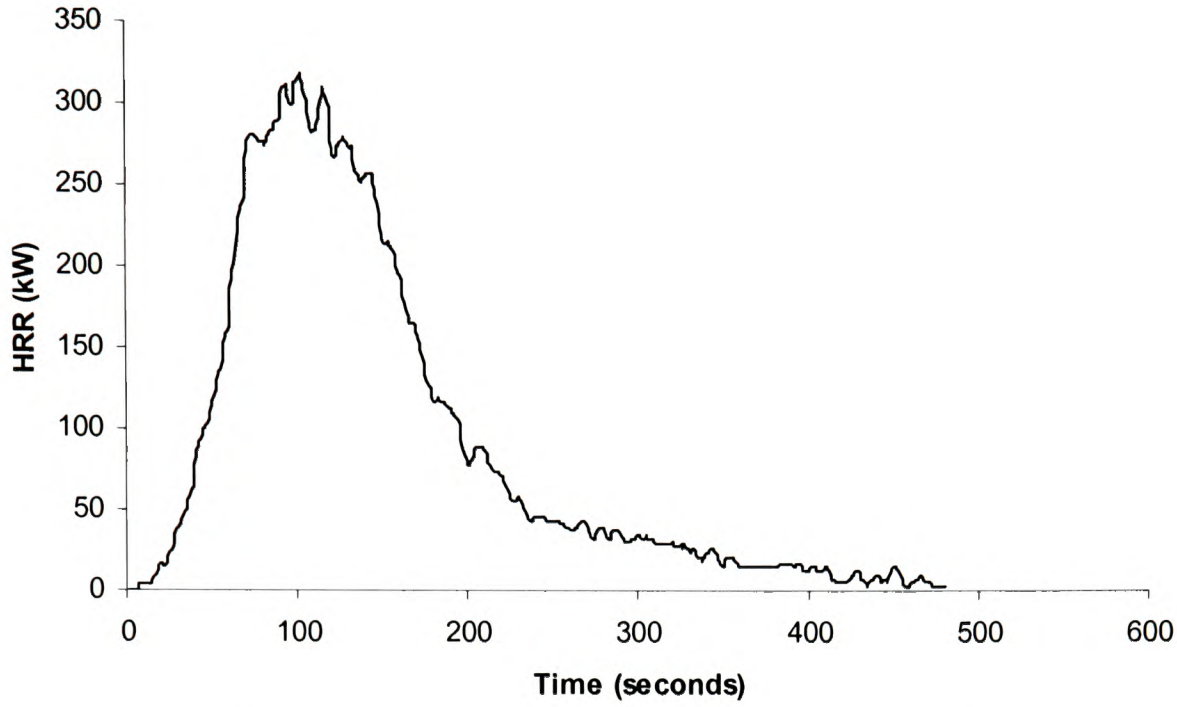

Figure 7.13 (b) Heat Release Rate during the NYM cable fire

7.5.1.2 Simulation

The SMARTFIRE V4.0 software is used to perform the calculations. In the simulations the fuel source is represented by two fire sources. The dimension of the vertical fire source is 0.2x0.2x2.4m and the horizontal one is 0.2x3.0x0.2m. The STEM-LER model is used to simulate the generation of CO, CO_2 and the fuel combustion rate. The fuel loss rate during the NYM cable fire test is obtained from the measured heat release rate (see Figure 7.13(b)) with a constant heat of combustion 9.0 MJ/kg. The yields of CO and CO_2 for this PVC cable have the form of Equation 4.7 and were derived from the cone calorimeter data for PVC cable in [Borealis report, 2001]. The other correlation constants are given in Table 7.3.

Table 7.3 Yield correlation constants for PVC

	$f_{p\infty}$	α	β	ζ
CO	0.0177	7	0.42	-8.0
CO_2	0.678	-0.4	0.53	-1.1

7.5.1.3 Results and Discussion

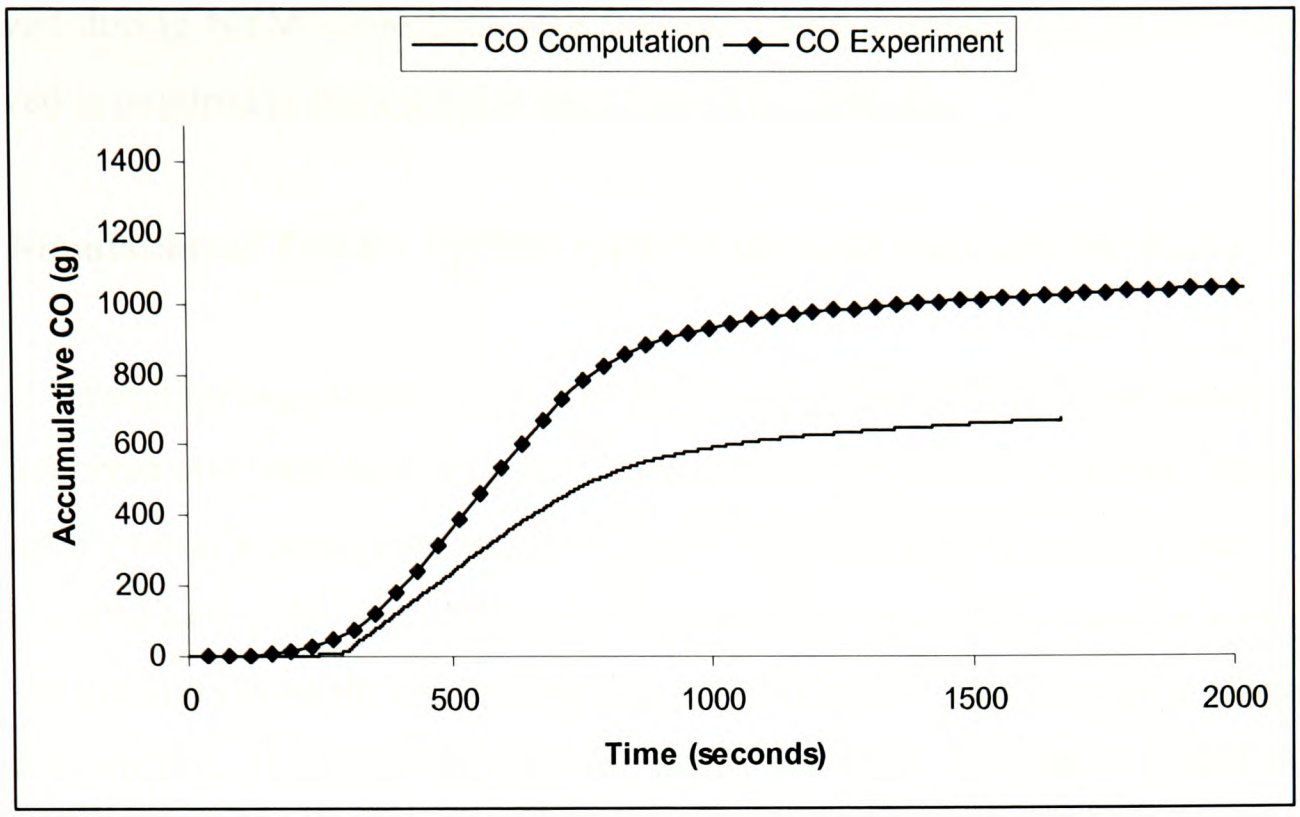

Figure 7.14 (a) Accumulative CO during the NYM cable fire

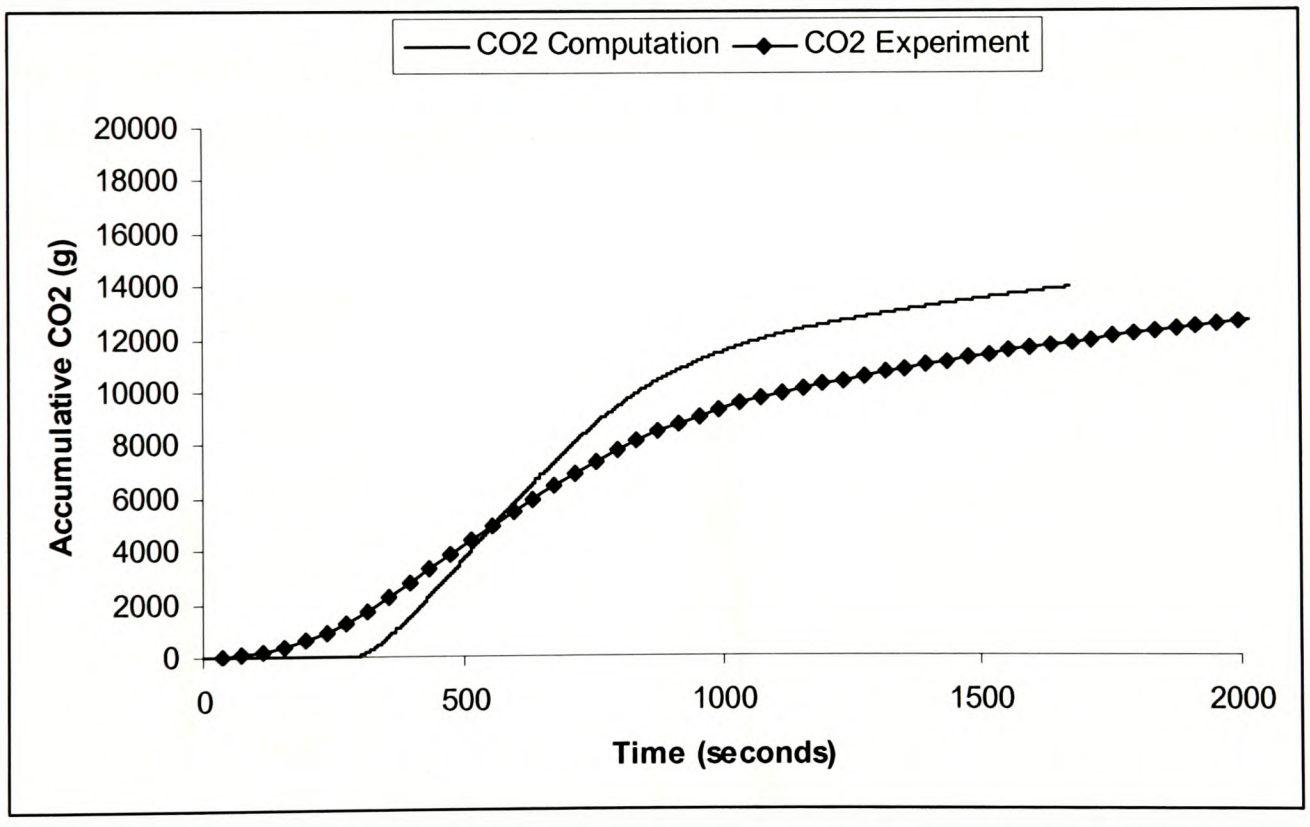

Figure 7.14 (b) Accumulative CO_2 during the NYM cable fire

The total predicted mass of CO and CO_2 passing through the hood (a horizontal monitoring plane outside the compartment at h = 2.28 m) and the measured accumulated products data for NYM cable fire are compared in Figures 7.14 (a) and (b). The simulated profiles of the accumulated CO and CO_2 collected at the hood are in qualitative agreement with the experiments. However, the predicted CO_2/CO ratios

are over-predicted throughout the fire which might be due to the complex chemistry involved during NYM cable fires (see Section 7.5.4). Further data on the chemistry involved is required to accurately predict the NYM cable fire.

7.5.2 Simulation of Test 8 – NHMH cables (Inlet vent open and 1m Weir)

In this subsection simulation results of Test 8 involving NHMH type power cables were reported and validated with the experimental data. The ventilation during this test was a special arrangement where the 1 m^2 vent was kept open and a weir of 1 m height was placed at the end of the first corridor (see Figure 6.5). There was no cover plate on the vertical cable tray during this test which was meant to get a glimpse of the flame spread. The mass loss rate curve derived from the load cell data (Figure 6.16) and the heat release rate (HRR) curve are given in Figures 7.15(a) and 7.15(b). The duration of the fire was approximately 2000 seconds and the simulation was carried out for 2000 seconds. The average heat of combustion during this fire test and used in the present simulation is 21 MJ/Kg which is calculated from the total heat released measured by the hood calorimeter and the total fuel lost measured using the load cell.

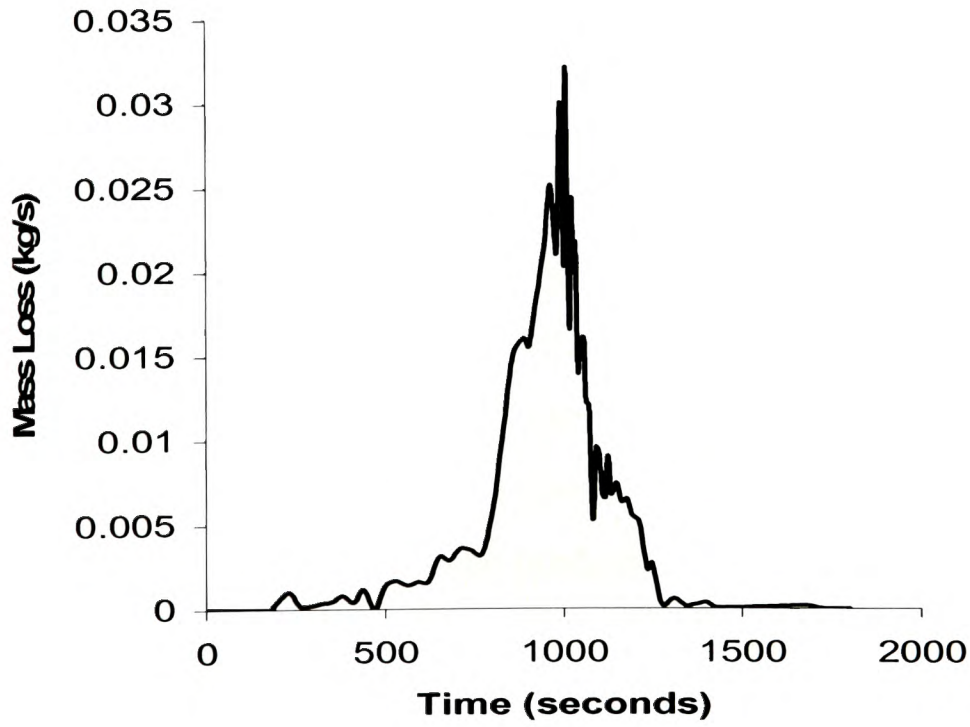

Figure 7.15(a) Mass loss rate curve (Test 8)

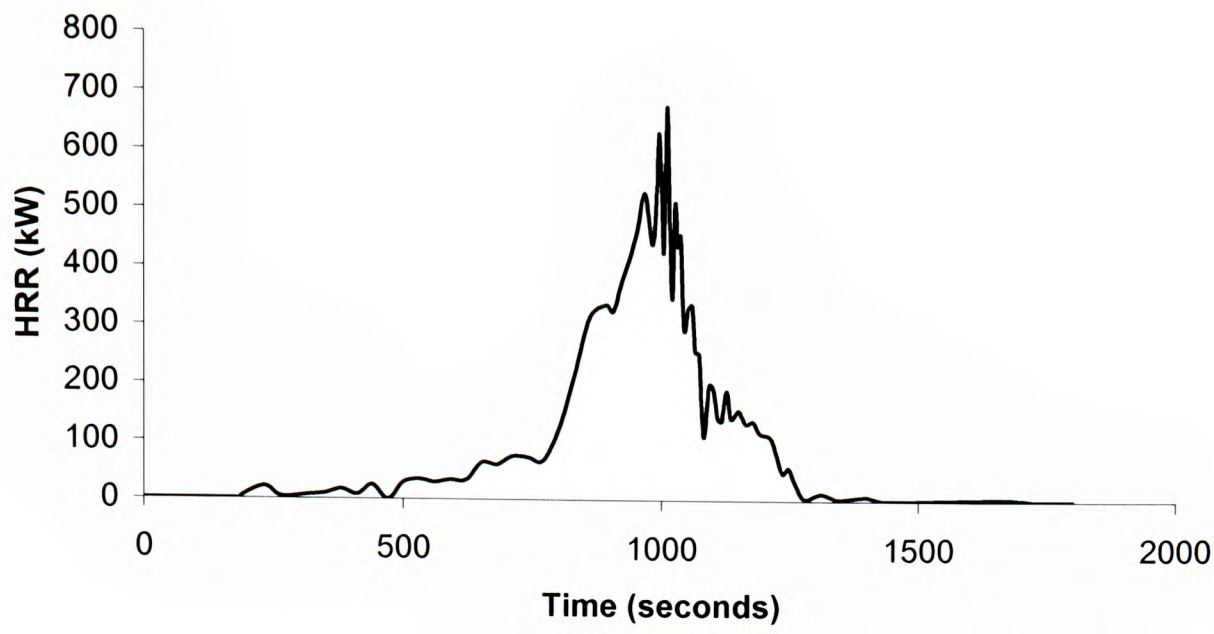

Figure 7.15 (b) Heat Release Rate curve (HRR) during Test 8

Figure 7.16 and Figure 7.17 describe the CO and CO_2 concentration evolution at location 5 (h = 2.2 m) during the fire. The measured peak CO, CO_2 concentration and the CO_2/CO ratio were 0.7 % volume, 7 % volume and 10 respectively. The STEM-LER model prediction of peak CO, CO_2 concentrations and CO_2/CO ratio were 0.9 %, 9% and 10 respectively.

Even though the peak CO and CO_2 concentrations at location 5 were over predicted by 28 %, the predicted CO_2/CO ratio is in good agreement with the experiments. Woolley and Fardel [1982] used the relationship between CO_2/CO ratio and the oxygen concentration in fires to describe complex processes occurring during fires [Tsuchiya, 1994]. The method was then adopted and expanded to classify various fires by ISO/TC92/SC3 (Table 5.1). Hence, CO_2/CO ratios are a important parameter defining the overall vitiation condition of a fire and is predicted well for this case by the STEM-LER model. The measured and simulated temperature profile at the same location is depicted in the Figure 7.18. The predicted temperature profile captured the rise in temperature up to 800 seconds and then the peak temperature is over predicted during the peak heat release rate period. Beyond 1200 seconds of the fire duration, the temperature is under predicted.

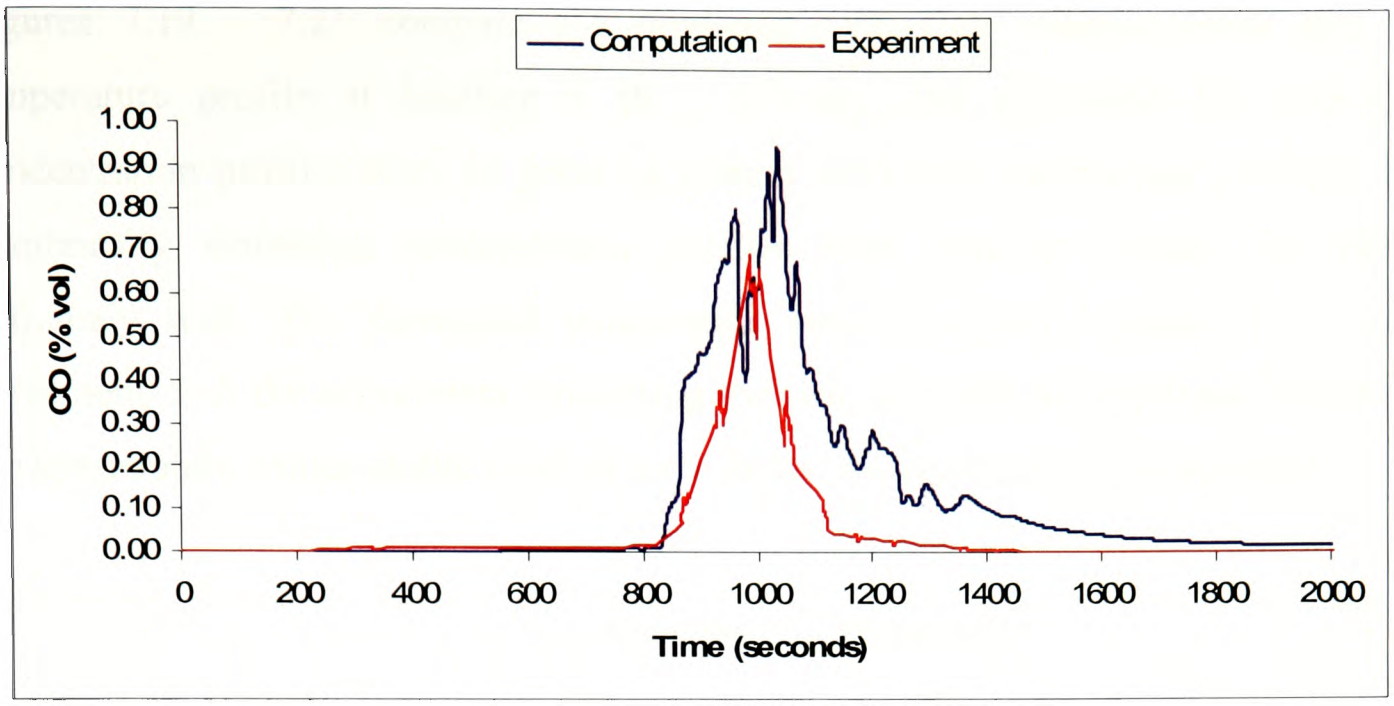

Figure 7.16 CO concentration at location 5 (Test 8)

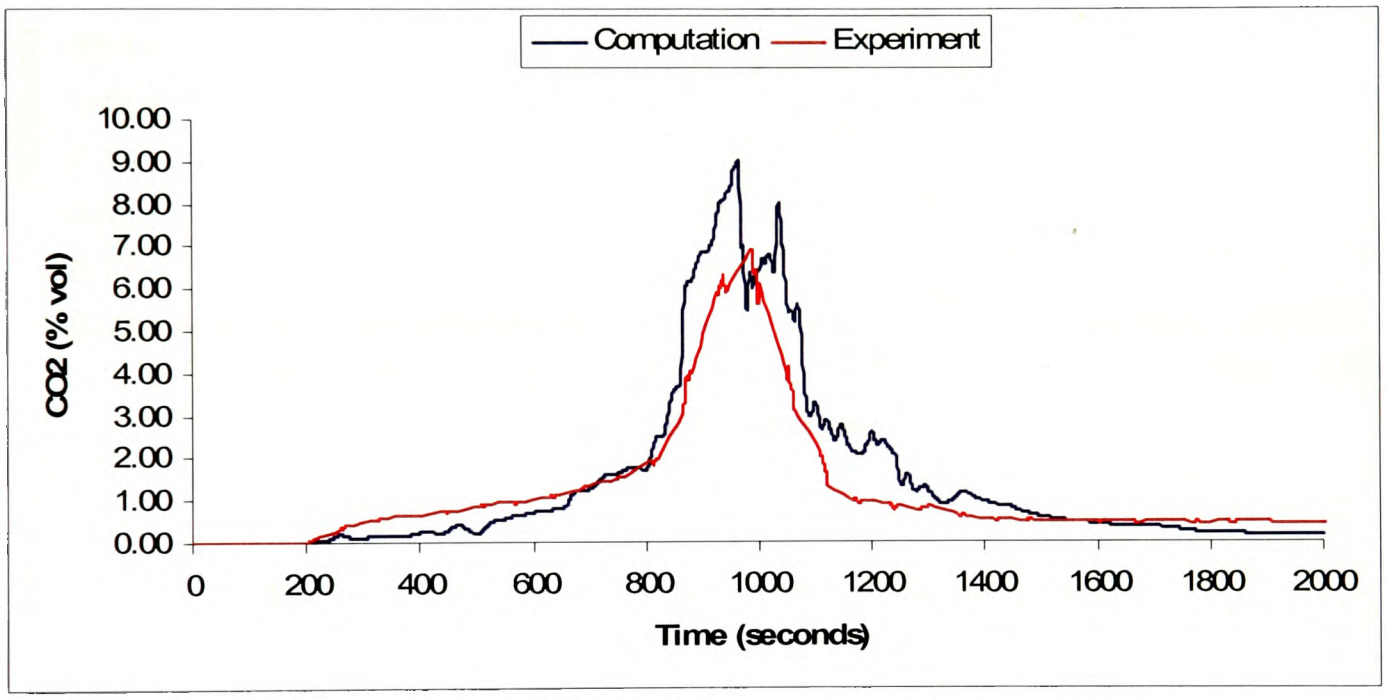

Figure 7.17 CO_2 concentration at location 5 (Test 8)

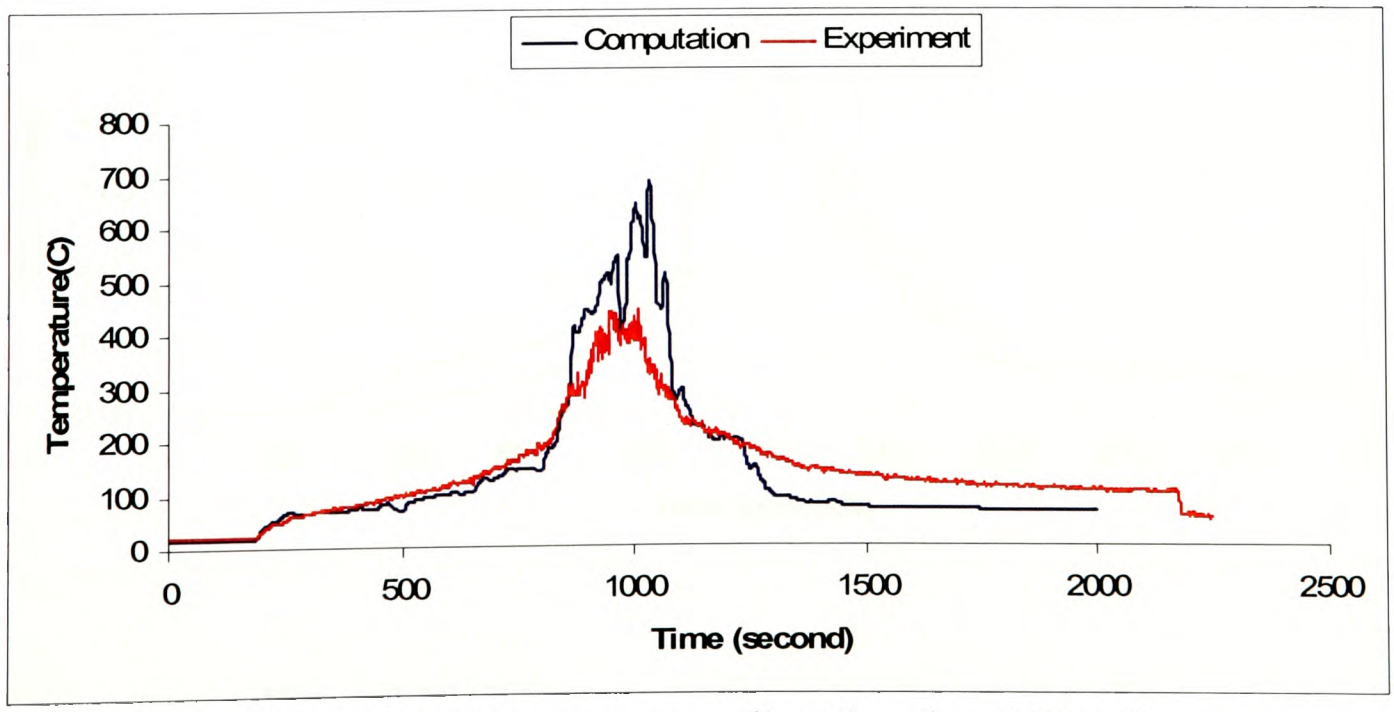

Figure 7.18 Temperature profile at location 5 (Test 8)

Figures 7.19 – 7.21 compare the predicted CO, CO_2 concentrations and the temperature profile at location 9 (h = 2.2 m). The simulated CO and CO_2 concentration profiles were in good agreement with the experimental profiles. The numerically simulated concentration profiles were able to capture the trends extremely well. The computed temperature profile at this location is in close agreement with the experiment simulating the rise and peak temperatures. However, the temperature values at this location were under predicted after 1200 seconds.

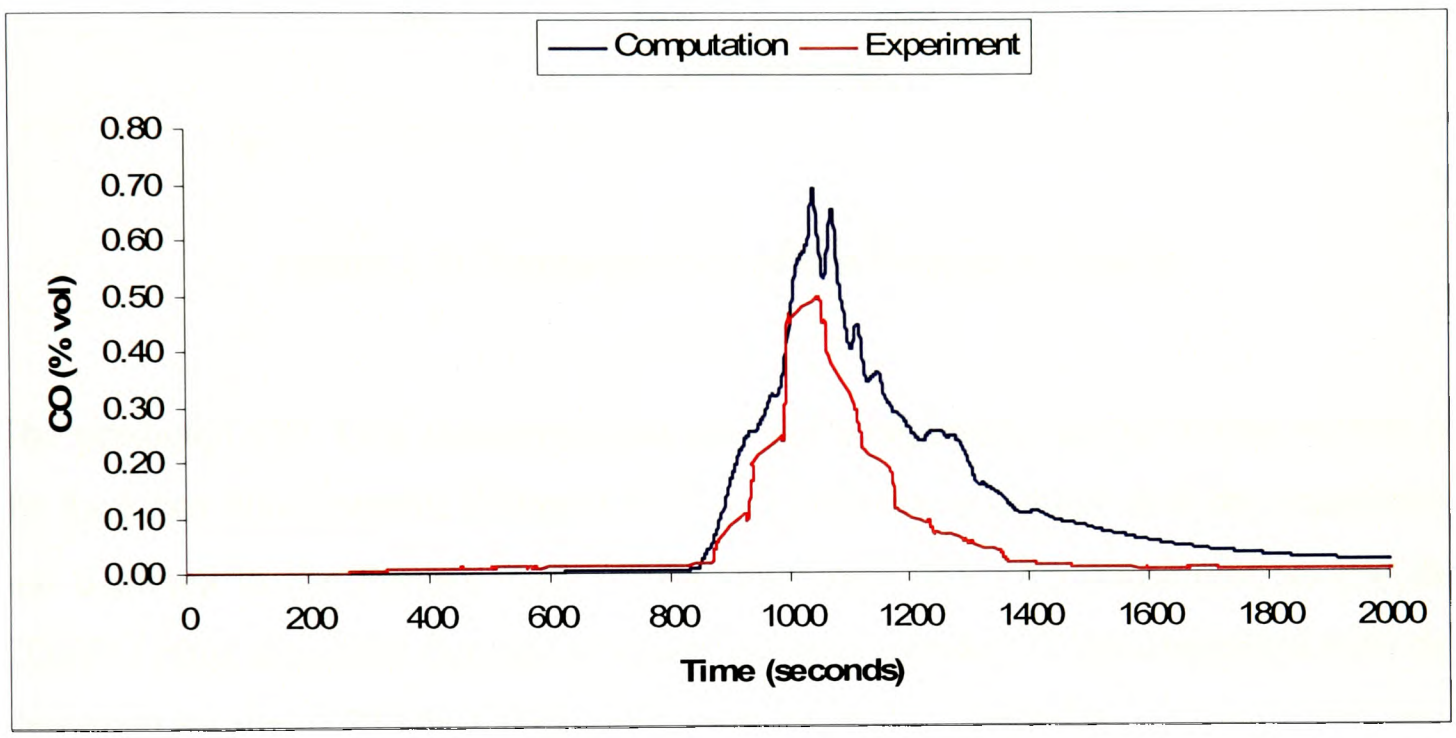

Figure 7.19 CO concentration at location 9 (Test 8)

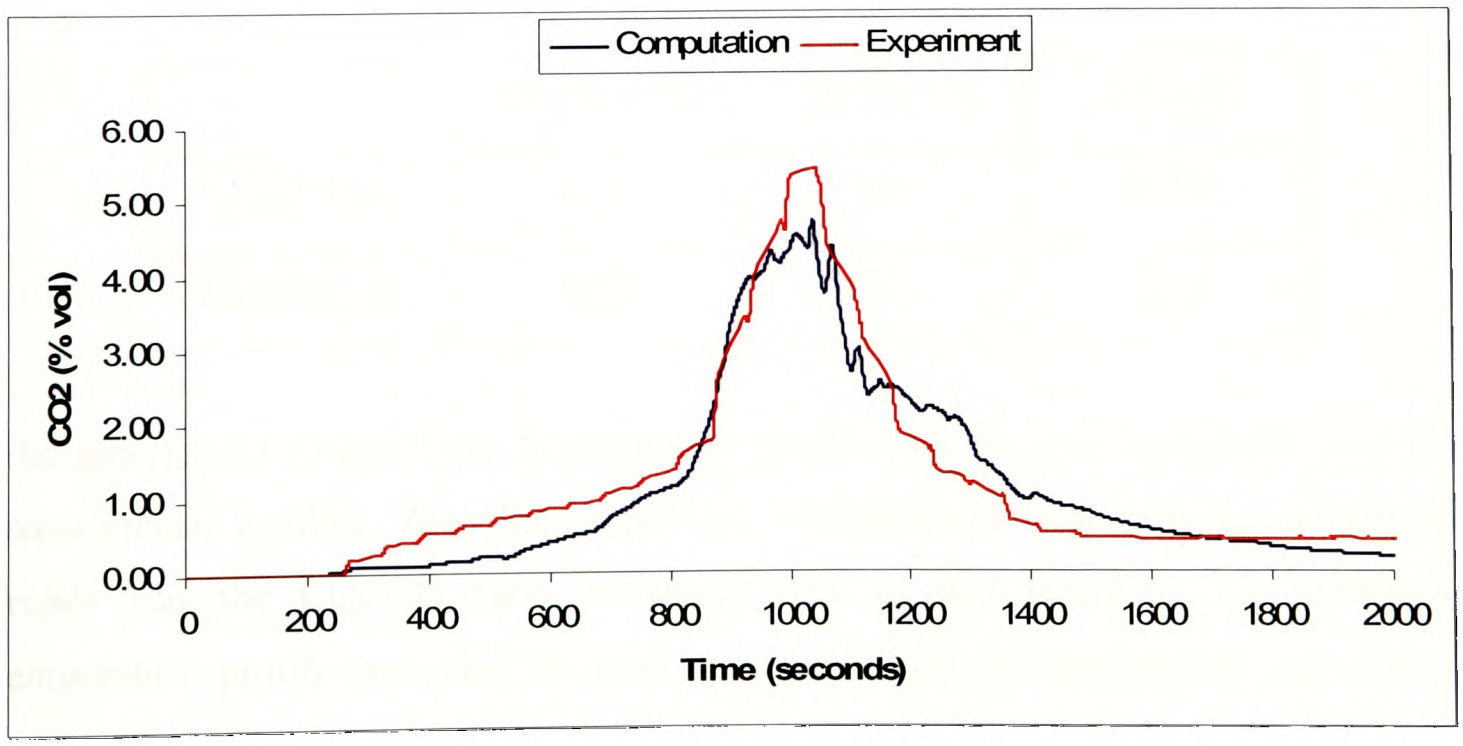

Figure 7.20 CO_2 concentration at location 9 (Test 8)

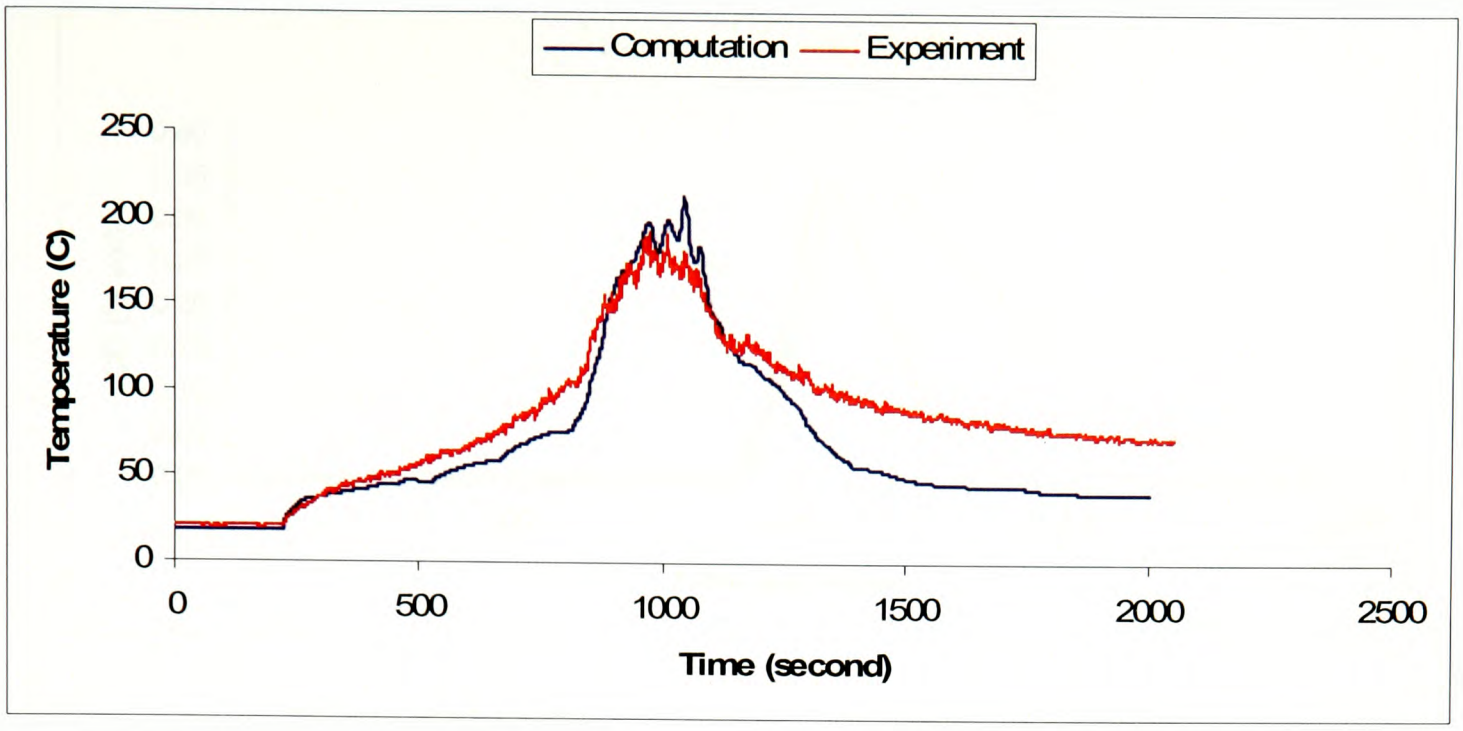

Figure 7.21 Temperature profile at location 9 (Test 8)

The predicted CO, CO_2 concentrations and the temperature profile in the middle of the long exit door corridor (location 15, h = 2.2 m) are compared with the experiment and depicted in the Figures 7.22 – 7.24. The peak CO, CO_2 concentration and the CO_2/CO ratio measured during the experiments at location 15 are compared with the simulated results of STEM-LER model and provided in Table 7.4.

Table 7.4 Comparison of peak CO, CO_2 concentrations and CO_2/CO at location 15

	CO (% vol)	CO_2 (% vol)	CO_2/CO
STEM-LER	0.3	2.8	9.34
Experiment	0.35	3.7	10.6

The simulated CO and CO_2 concentration profiles are in good agreement with the experimental profiles. Also the numerical concentrations were able to capture the trends and the CO_2/CO ratio extremely well at this location. The computed temperature profile was also in good agreement with the experiment and able to capture the peak temperature accurately.

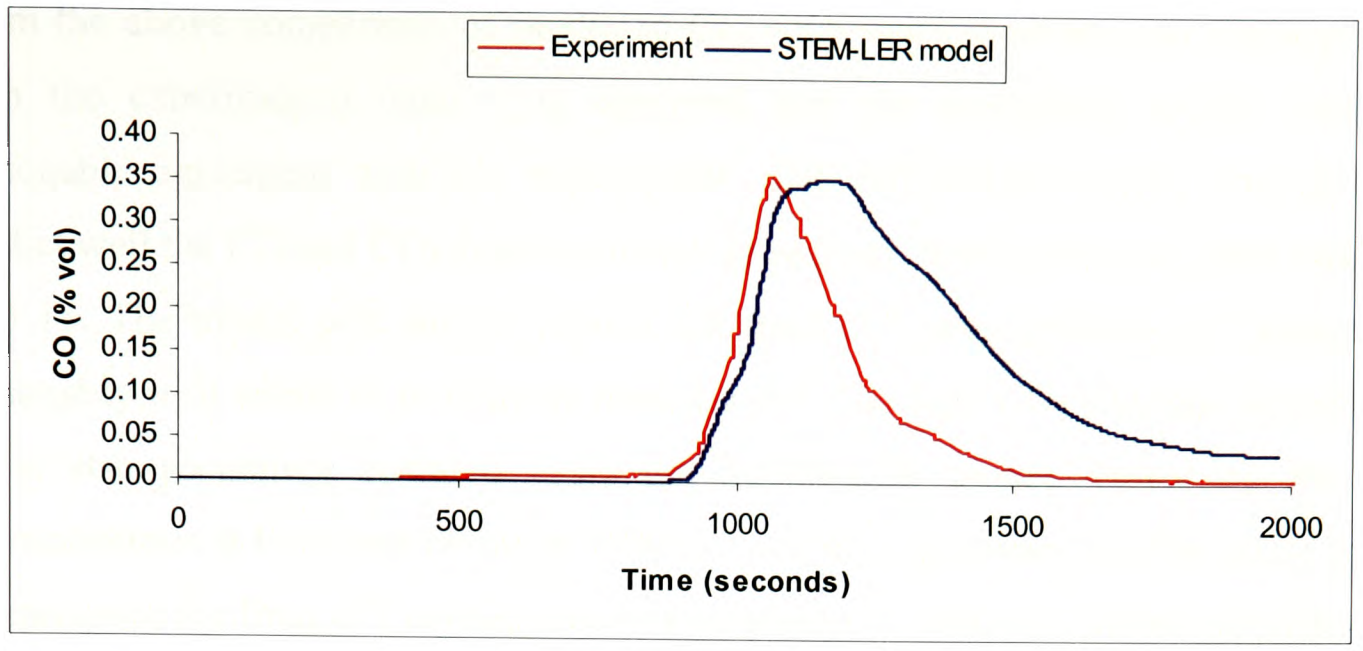

Figure 7.22 CO concentration at location 15 (Test 8)

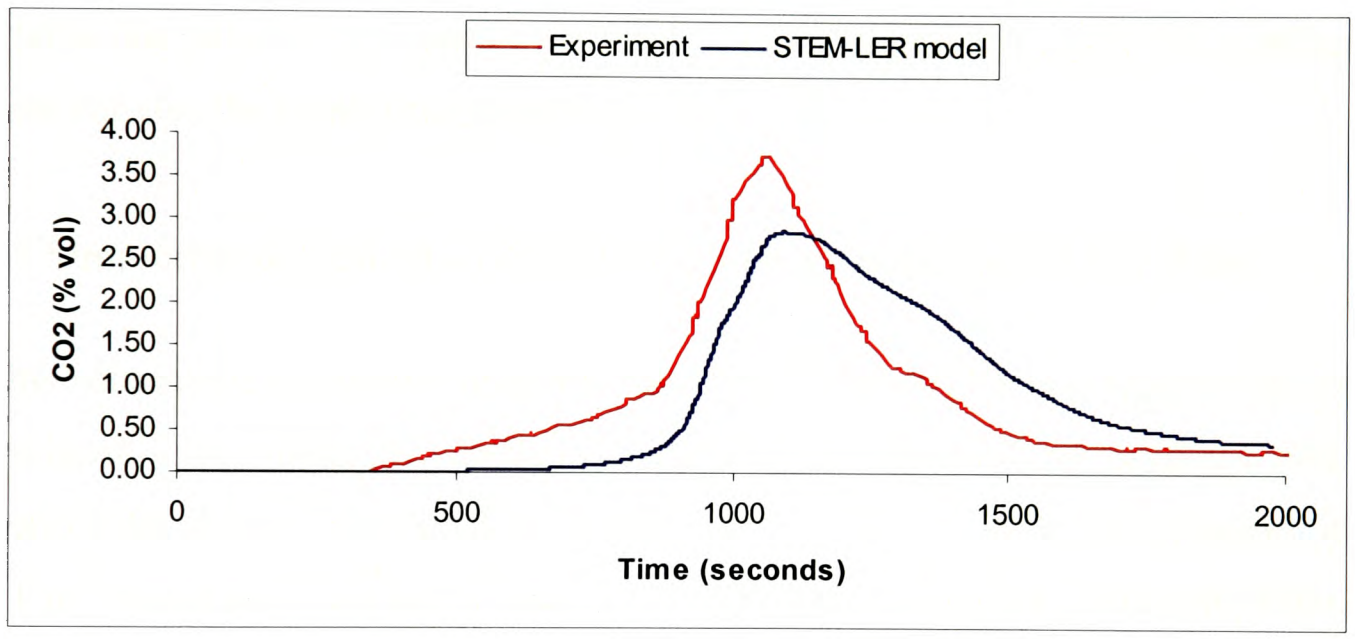

Figure 7.23 CO_2 concentration at location 15 (Test 8)

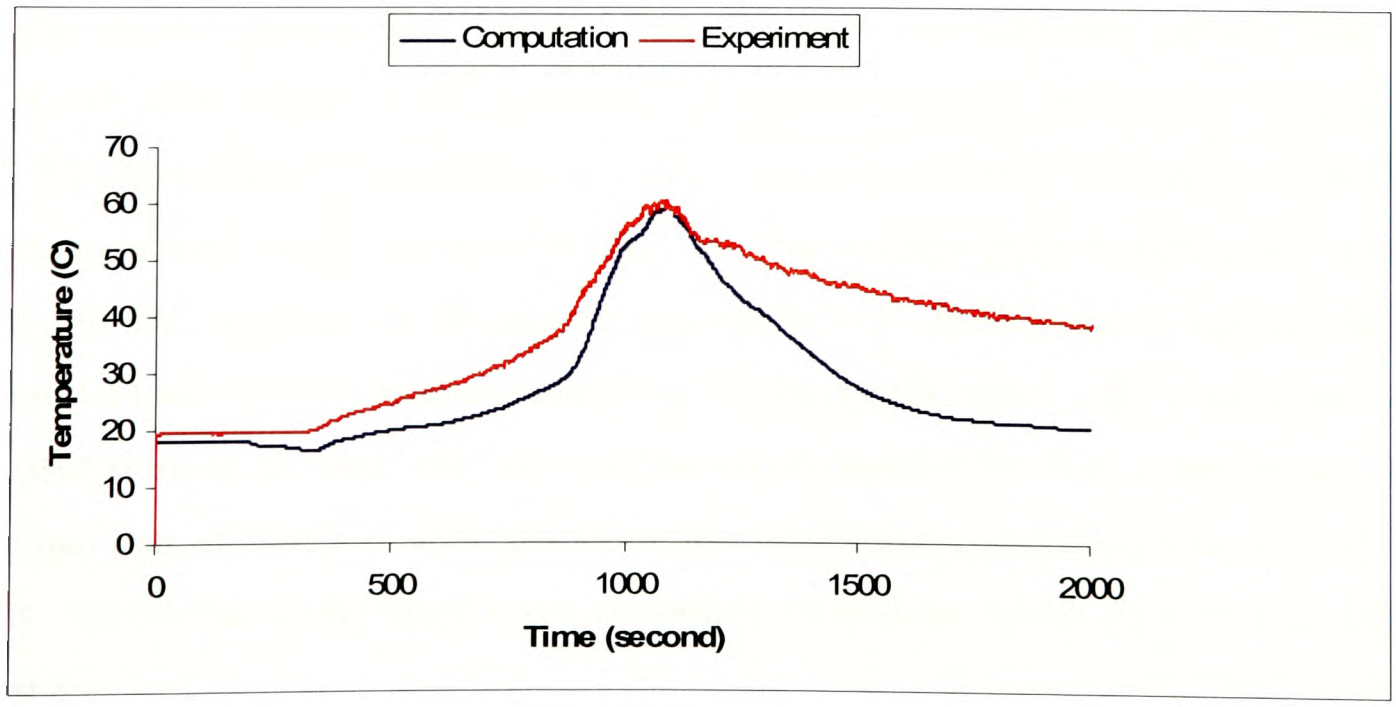

Figure 7.24 Temperature profile at location 15 (Test 8)

From the above comparison of predicted CO, CO_2 concentrations and temperatures with the experimental data, it is observed that the simulation results were in reasonable agreement with the experiments. The STEM-LER model was able to predict well the CO and CO_2 concentrations through out the corridor i.e. from location 5 to 15. The model was able to predict the final CO concentrations at location 15 reasonably well which is 30 m away from the fire. The final CO_2/CO ratio at location 15 is also accurately captured using the STEM-LER model. Predicting the CO concentrations at locations far away from fire origin is important for fire safety since it represents the final CO concentrations transported to remote locations far from the fire where people remaining within the fire building are exposed to the lethal gas. Accurate prediction of the final CO_2/CO at location 15 proves that the STEM-LER model is not only able to predict the local vitiation conditions inside the combustion region but also the combustion region per se.

7.5.3 Simulation of Test 10 – NHMH cables (Inlet closed and 1.5 m Weir)

In this subsection simulation results of the Test 10, where NHMH type power cables were burnt under different ventilation condition are reported and validated with the experimental data. The ventilation during this test was a special arrangement where the 1 m^2 vent was closed and a weir of 1.5 m height was placed at the end of the first corridor (see Figure 6.5). This ventilation arrangement was aimed to create more oxygen starved environment than the Test 8 condition by closing the inlet vent and raising the weir height from 1 m to 1.5 m. The mass loss rate curve derived from the load cell data (Figure 6.19) and the HRR curve are given in Figures 7.25(a) and 7.25(b) respectively. The duration of the fire was approximately 2000 seconds and the simulation was carried out for 2000 seconds. The average heat of combustion during this fire test and used in the present simulation is 14 MJ/Kg which was calculated from the total heat released measured by the hood calorimeter and the total fuel lost measured using the load cell. The net heat of combustion is 33 % lower during Test 10 than that of Test 8 in spite involving the same cable type and almost similar fuel loss. This is due to the much more controlled ventilation during Test 10 than during Test 8.

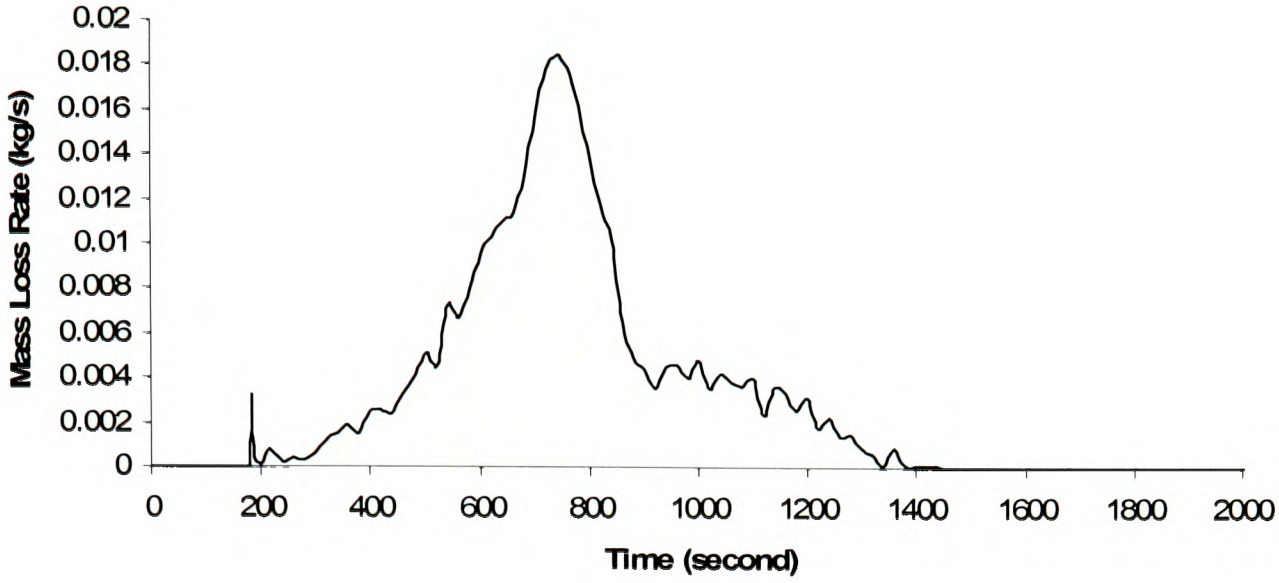

Figure 7.25 (a) Mass loss rate curve (Test 10)

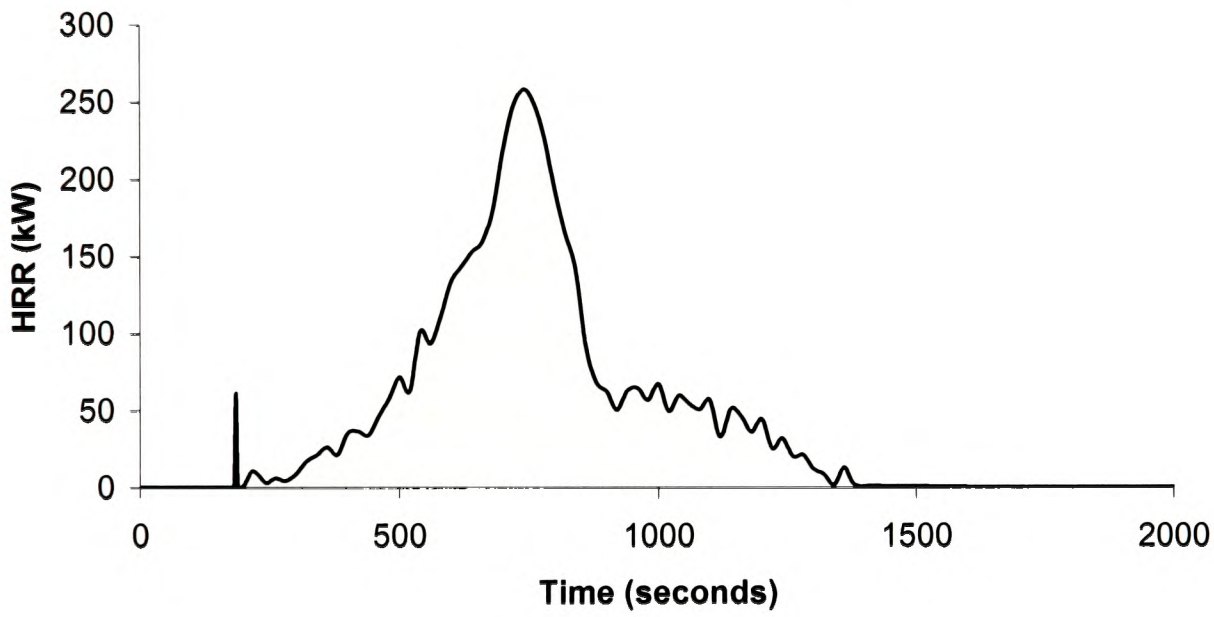

Figure 7.25 (b) Heat Release Rate curve (HRR) during Test 10

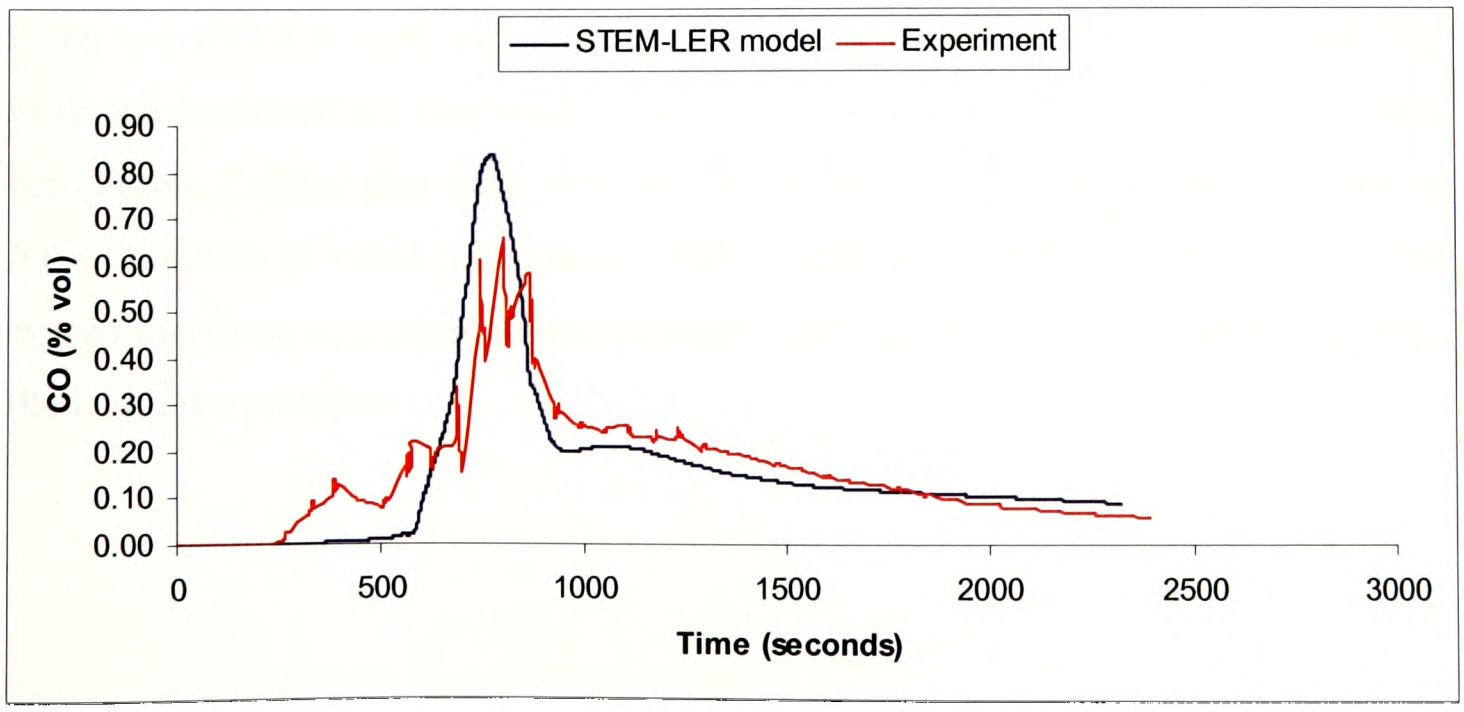

Figure 7.26 CO concentration at location 5 (Test 10)

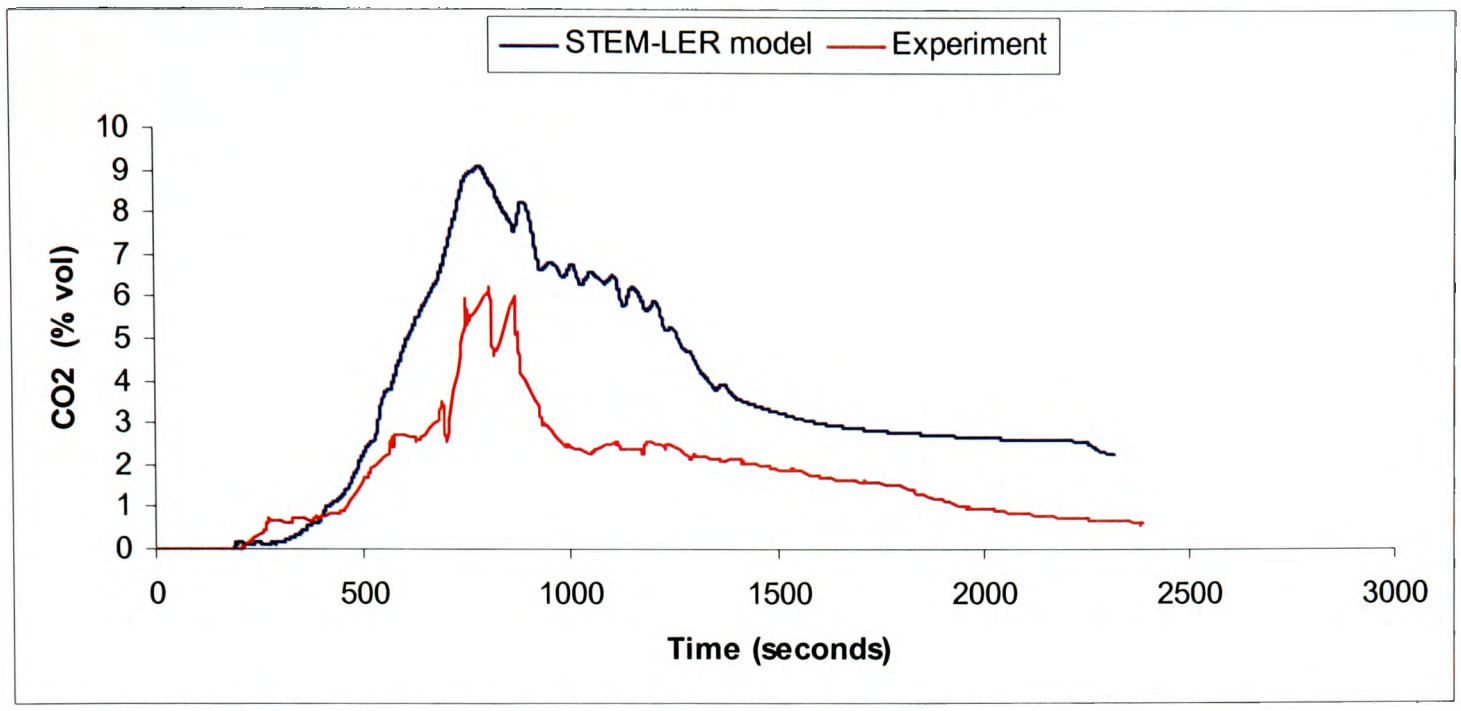

Figure 7.27 CO_2 concentration at location 5 (Test 10)

Figure 7.26 and Figure 7.27 describes the CO and CO_2 concentration evolution at location 5 (h = 2.2 m) during the fire. From the comparison of CO and CO_2 concentration profiles at this location, it is evident that the STEM-LER model simulations were in reasonable agreement with the experiments. While comparing the experimental profiles of test 10 with test 8 at location 5, both the test cases generated almost similar peak concentrations of CO and CO_2 which were approximately 0.7 % and 7% respectively, but the profile width for test 10 was much wider than test 8. Unlike test 8, the concentrations of CO and CO_2 during test 10 were significantly higher for most of the fire during the experiments. This is due to the recirculation of products within the first corridor caused by the more restricted ventilation system during test 10(1.5 m weir and inlet closed). Figure 7.28 show the CO_2 concentrations across the middle of the first corridor during test 8 and test 10. During test 8, it can be seen (Figure 7.28(a)) that fresh air is drawn into the fire through the inlet and that the CO_2 is confined to a thin upper layer. And, during the test 10 (Figure 7.28(b)), it can be seen that there is a recirculation inside the first corridor and the whole corridor is filled with the products.

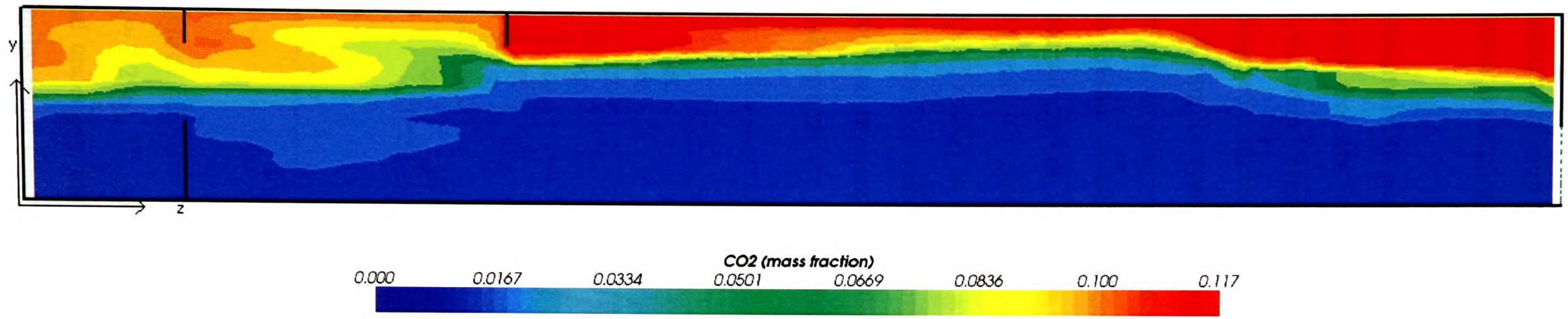

(a) Test 8

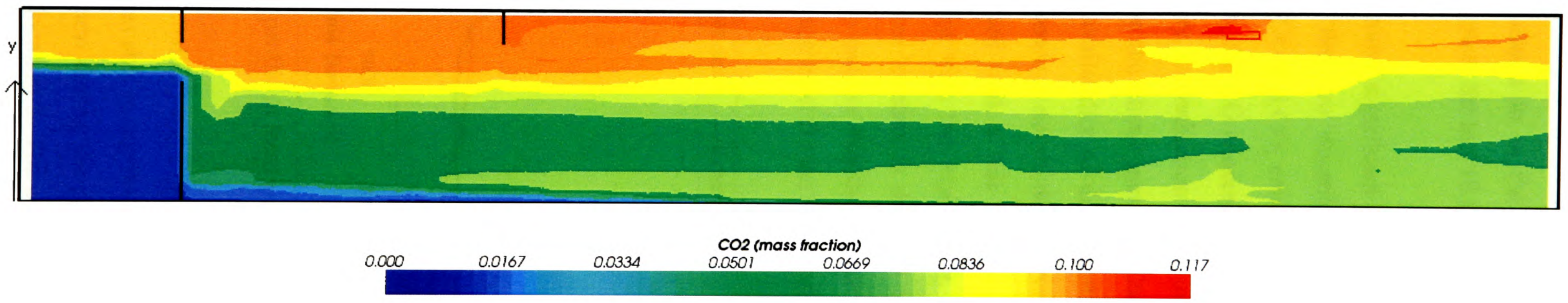

(b) Test 10

Figure 7.28 CO_2 concentration in the first corridor (X = 7.5 m)

The combustion efficiency is also lower during test 10 (33 % lower average heat of combustion) due to entrainment of products in to the fire plume and hence the measured temperature at this location is lower for test 10 than during test 8.

Simulated CO and CO_2 profiles show some significant concentration is maintained inside the first corridor for most of the fire duration as observed during the experiments. Even though the predicted CO and CO_2 concentration profiles are wider compared with the experimental profiles, the CO concentrations are under predicted excluding the peak HRR period. In reality, the reduction in the oxygen concentration and the entrainment of the products in to the plume increases the CO generation. In the present investigation due to the unavailability of data on the effect of oxygen concentration on the yields, this phenomenon is not modelled. Nevertheless, the peak CO and CO_2 concentrations are predicted well at this location, and the simulated CO_2/CO ratio is also in good agreement with the experiment. The measured and simulated temperature profile at the same location is depicted in Figure 7.29. The predicted temperature profile was able to capture exactly the rise in temperature, the peak temperature and the fall in temperature level for the full duration of the test.

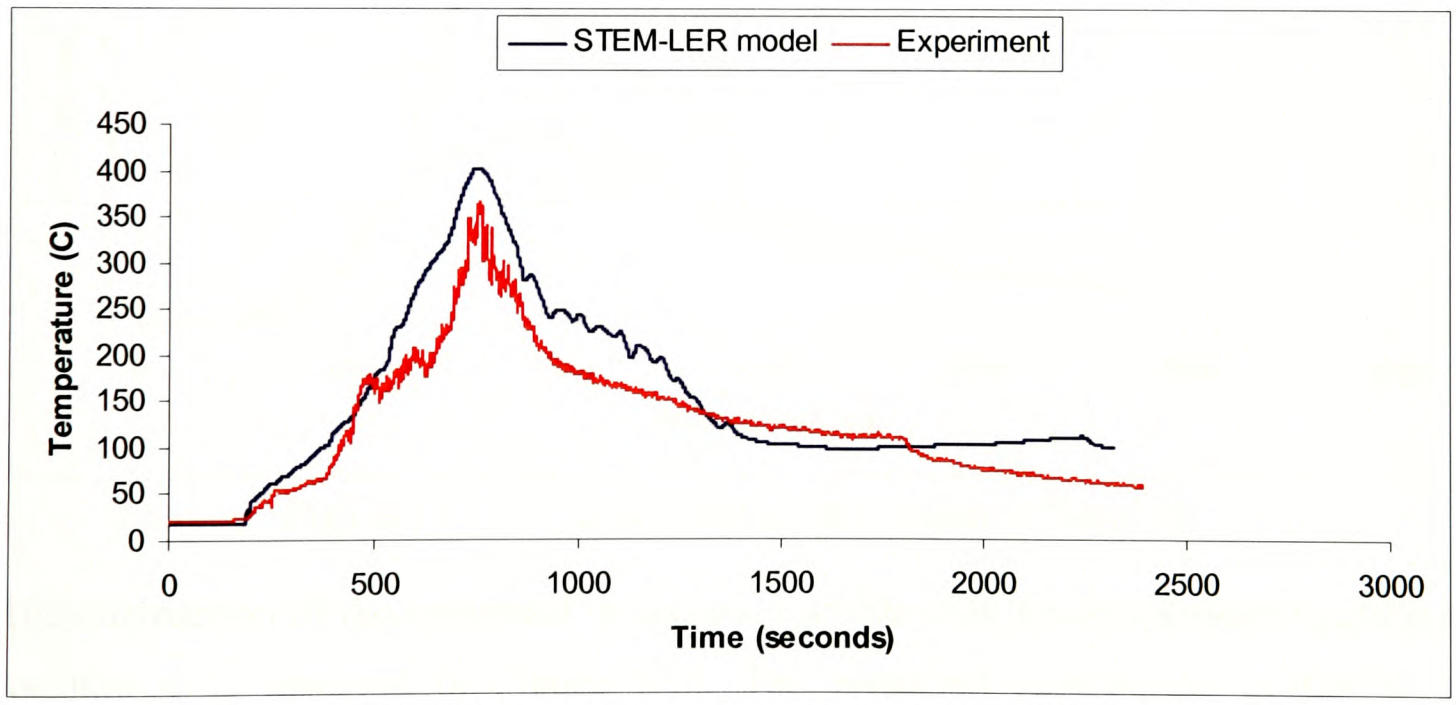

Figure 7.29 Temperature profile at location 5 (Test 10)

Figures 7.30 and 7.31 compare the predicted CO and CO_2 concentrations at location 9 (h = 2.2 m). The simulated CO profile was able to capture the peak concentration well and under predicted the CO concentration during the rest of period following the similar trend observed at the upstream location 5. The computed CO_2 concentration

profile on the other hand were able to follow the rise and fall fairly well and was over predicting after the peak HRR. Regarding the CO_2/CO ratio at this location the measured value was 10 and the computed CO_2/CO ratio is 11.7.

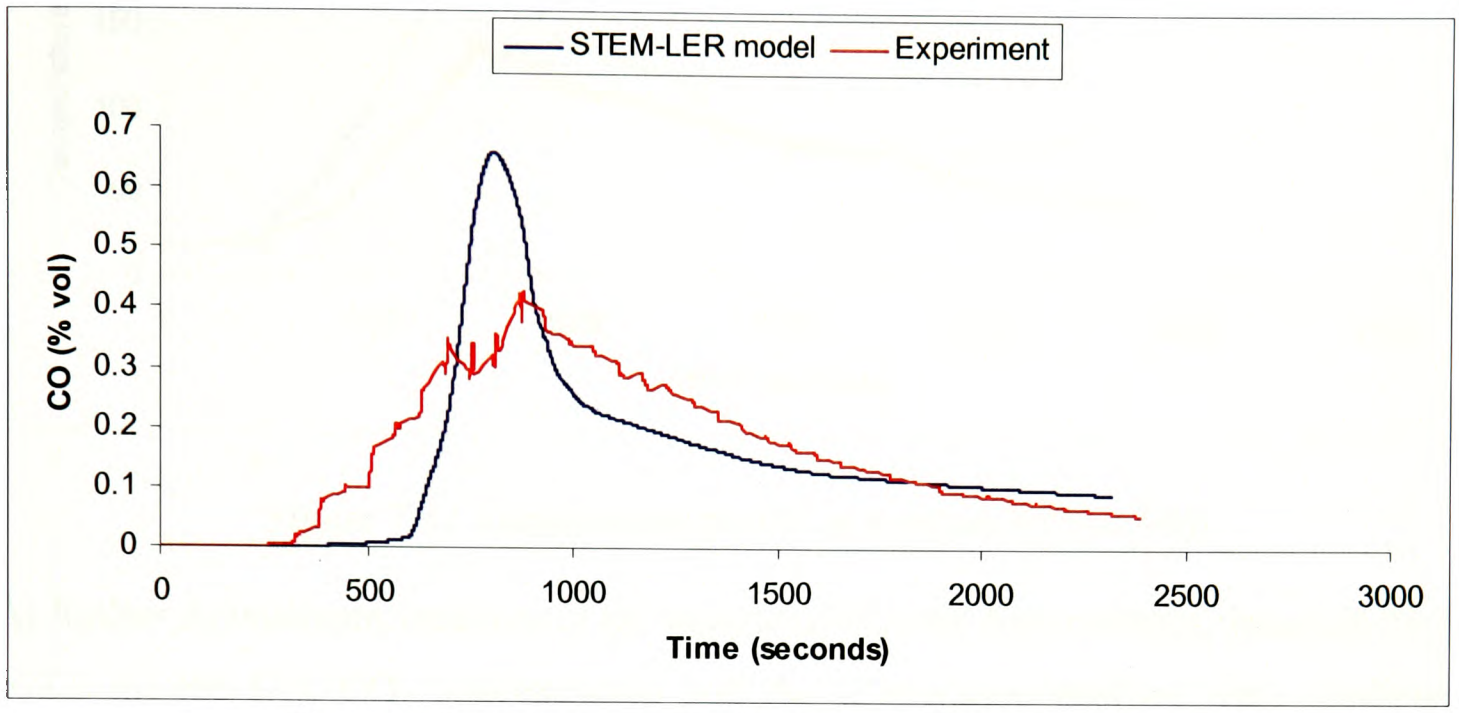

Figure 7.30 CO concentration at location 9 (Test 10)

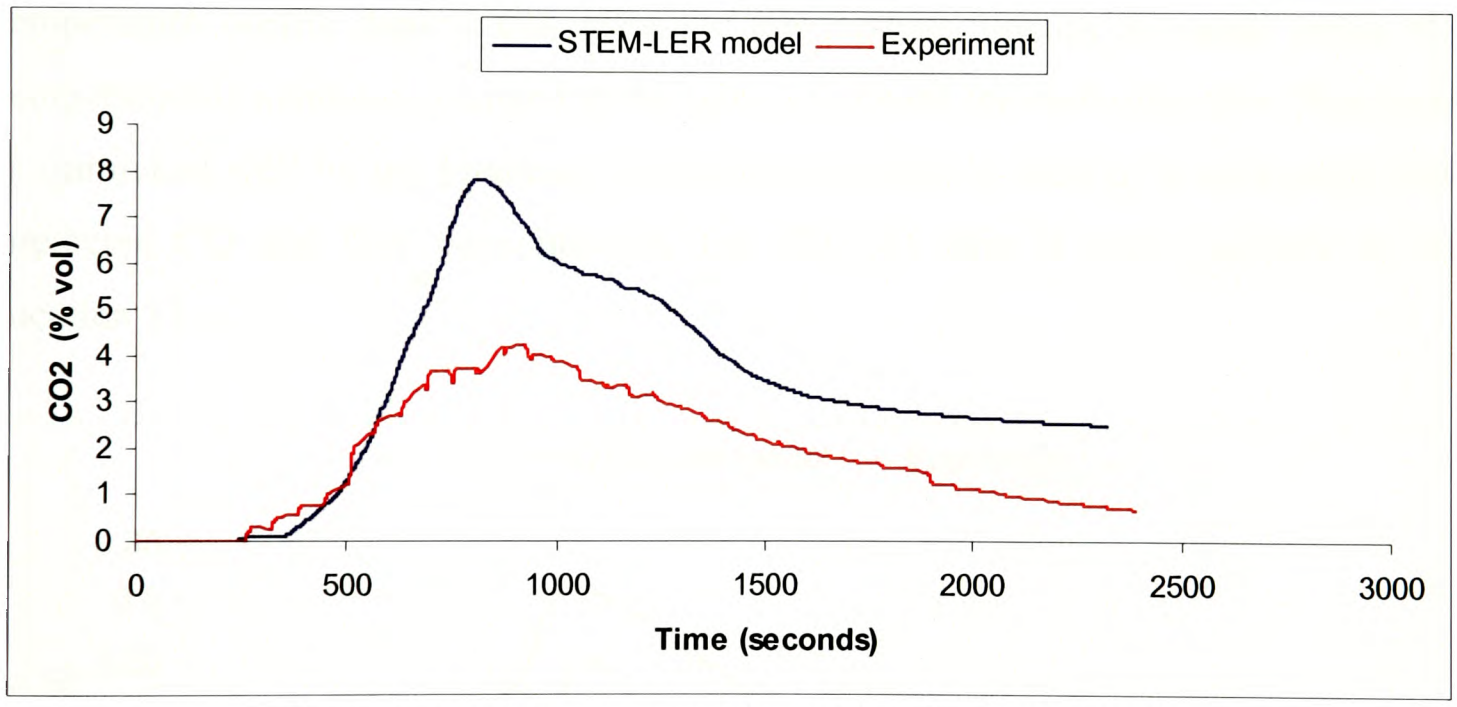

Figure 7.31 CO_2 concentration at location 9 (Test 10)

The comparison of the computed temperature profile with the experimental profile at location 9 is depicted in Figure 7.32. The predicted temperature profile is in qualitative agreement with the experiment and follows closely the rise and fall in the measured temperatures during the fire. However, the peak temperature value is over predicted by almost 50 %.

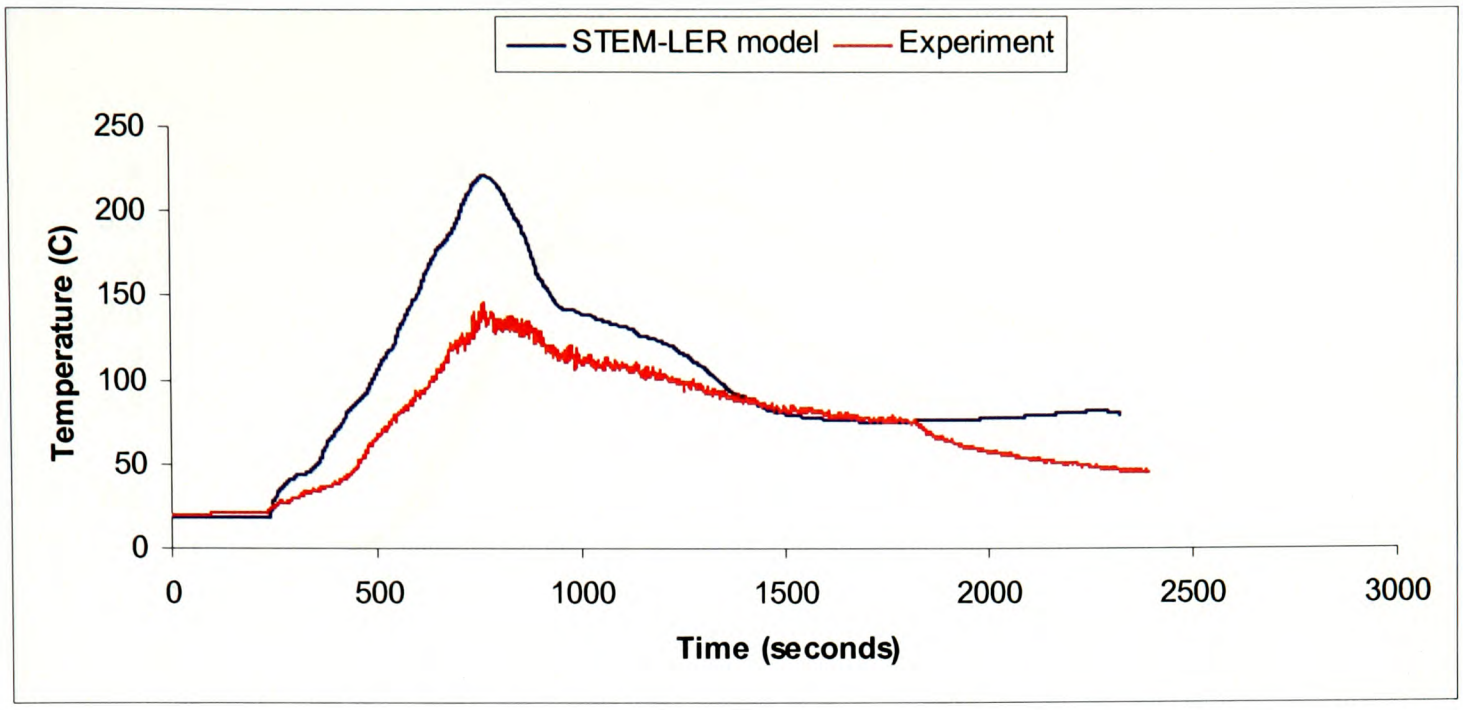

Figure 7.32 Temperature profile at location 9 (Test 10)

At further downstream location, in the middle of the exit door corridor (location 15, h = 2.2 m) the CO, CO_2 concentration and the temperature profiles were predicted reasonably well which are shown in the Figures 7.33 – 7.35. The experimental temperature profile depicts that after the temperature reaches the peak value; the temperature is maintained almost at the same level until the end of the fire. This trend is mimicked well by the predicted temperature profile. In spite of a reasonably well predicted CO and CO_2 concentration, the CO_2/CO ratio is over predicted at the location 15.

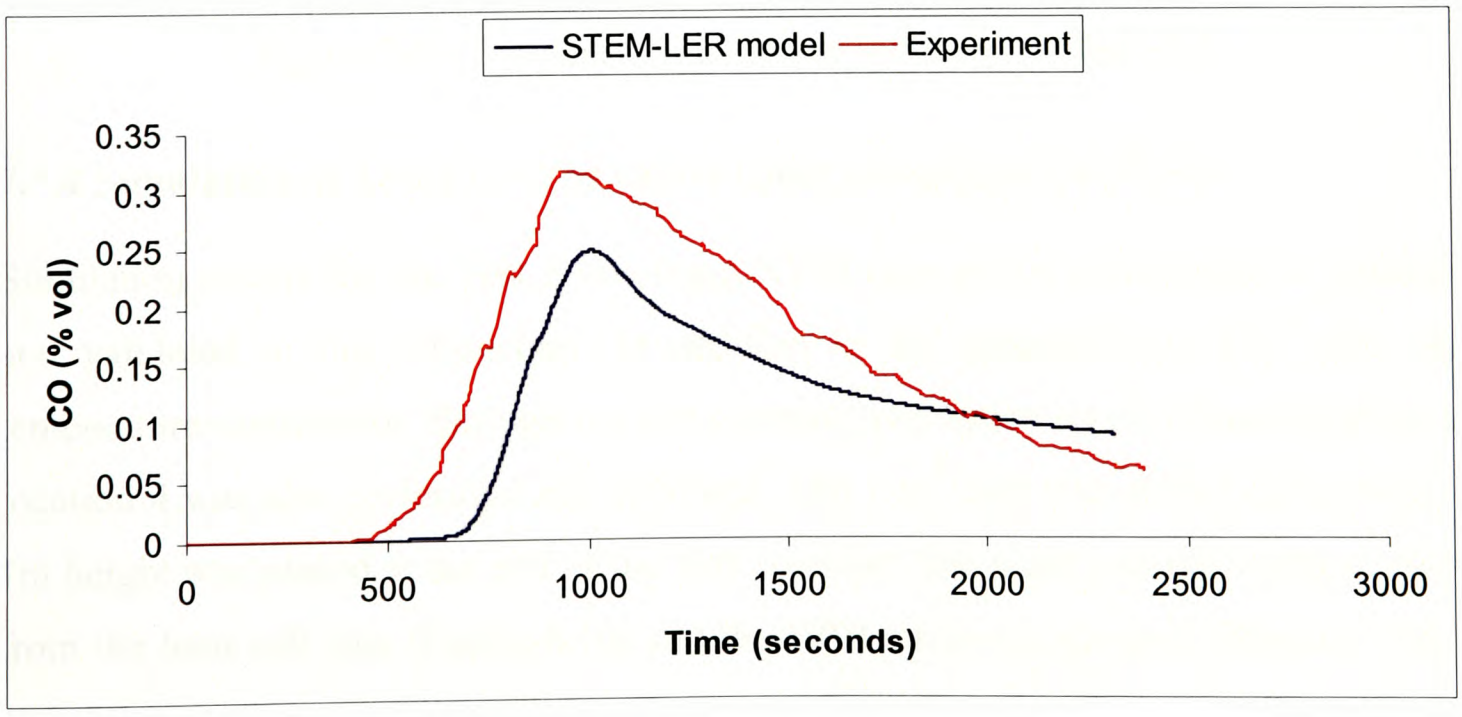

Figure 7.33 CO concentration at location 15 (Test 10)

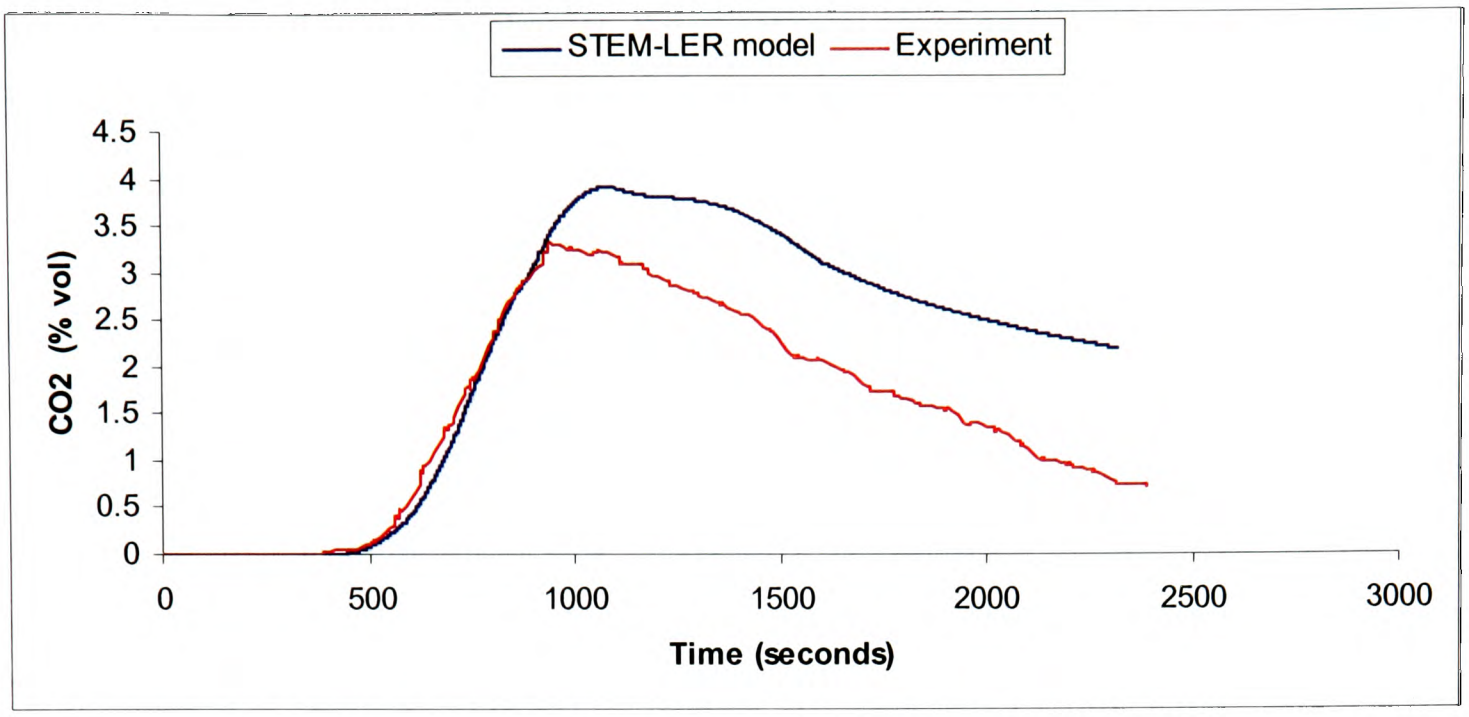

Figure 7.34 CO_2 concentration at location 15 (Test 10)

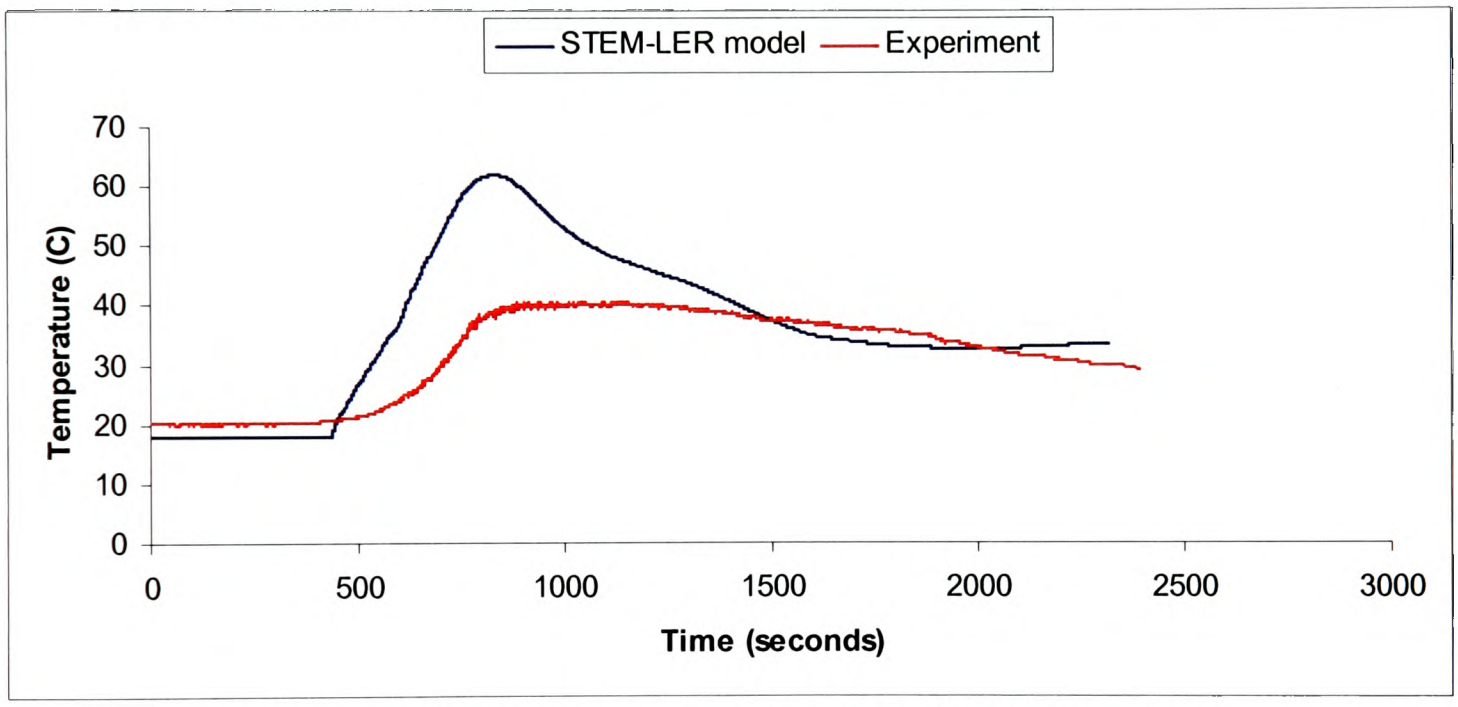

Figure 7.35 Temperature profile at location 15 (Test 10)

7.5.4 Simulation of Test 5 – NYM cables (Inlet closed and 1m Weir)

Simulation results for the Test 5 involving NYM type power cables will be reported and validated in this subsection. In addition to the simulation of CO, CO_2 and temperature distribution through out the corridor, prediction of HCl concentration at location 4 was also performed and validated. The 1 m^2 vent was closed and a weir of 1m height was placed at the end of the first corridor. The mass loss rate curve derived from the load cell data (Figure 6.10) and the HRR curve are given in Figures 7.36(a) and 7.36(b). The duration of the fire was approximately 2000 seconds and the simulation was carried out for 2000 seconds. The average heat of combustion during this fire test and used in the present simulation was 9.66 MJ/Kg.

As mentioned earlier in this chapter, the sheath, bedding and insulation for NYM type power cables were all made of PVC material which contains PVC, plasticizer and chalk. The basic molecular structure of the NYM cable material is assumed to be C_2H_3Cl (pure PVC) which contains the halogen atom Chlorine. Hence it also releases HCl gas as one of the combustion products. HCl gas is a highly irritant and toxic gas which hinders the evacuation process. The HCl yield for the NYM cables was also measured at University of Bolton along with the CO and CO_2 yields. The HCl yield used in the present simulation is 0.99 g/g of PVC polymer burnt. Based on the HCl yield and the mass loss rate, HCl release rate curve is obtained and shown in Figure 7.37. Mass loss rate curve (Figure 7.36(a)) shows sudden sharp peaks in the mass. This is due to the release of the HCl molecules. Thermal gravimetric experiments have shown that a complete and rapid dehydrochlorination reaction takes place for PVC compounds at about 300° C resulting in the loss of more than half of its weight [Sultan and Paul, 2002]. In the present simulation only the transport of HCL is modelled and the 'absorption by the wall' or 'decay' of HCL during the fires is not considered in the present investigation [Wang et al., 2007].

Figure 7.38 and Figure 7.39 describes the CO and CO_2 concentration evolution at the location 5 (h = 2.2 m) during the fire. The measured peak CO, CO_2 concentration and the CO_2/CO ratio were 0.3 % volume, 2.4 % volume and 8 respectively. The STEM-LER model predicted a peak CO, CO_2 concentrations and CO_2/CO ratio of 0.52 %, 6 % and 11.5 respectively. Even though the peak CO and CO_2 concentrations are over predicted at this location, the profile trends and the CO_2/CO ratio were captured reasonably well. Over prediction of the products and the temperature at location 5 may be mainly due the high combustion rate predicted in the fire plume. It should be noted that even in the well-ventilated cone calorimeter, the PVC compound produces high yields of incomplete combustion products, burning as if in an oxygen vitiated environment due to the vapour phase combustion inhibition resulting from the HCl acid gas released [Sultan and Paul, 2002]. Since the effect of the HCl concentration on the combustion rate is not modelled in the present investigation, the predicted combustion rate is higher resulting in more CO and CO_2.

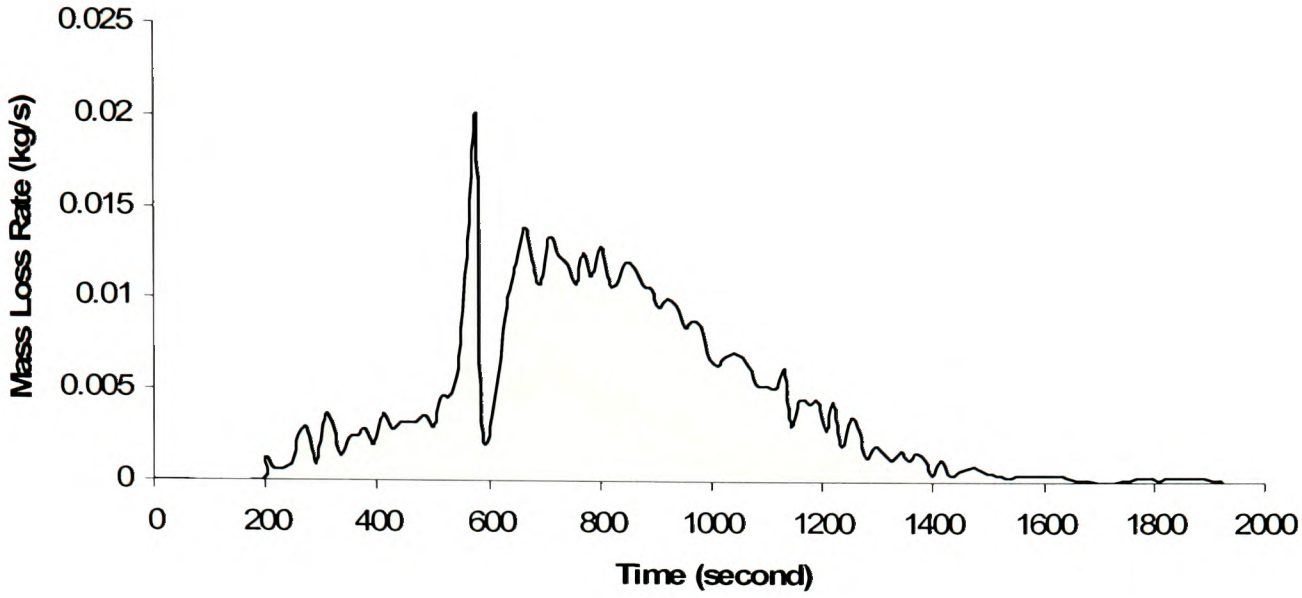

Figure 7.36 (a) Mass loss rate curve (Test 5)

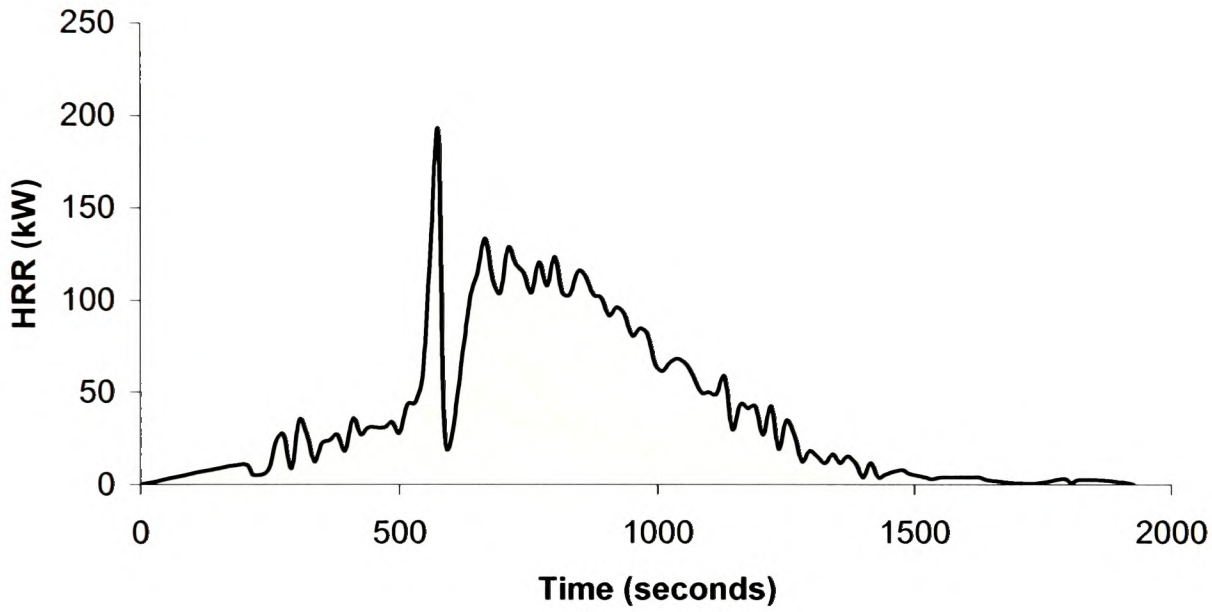

Figure 7.36 (b) Heat Release Rate curve (HRR) during Test 5

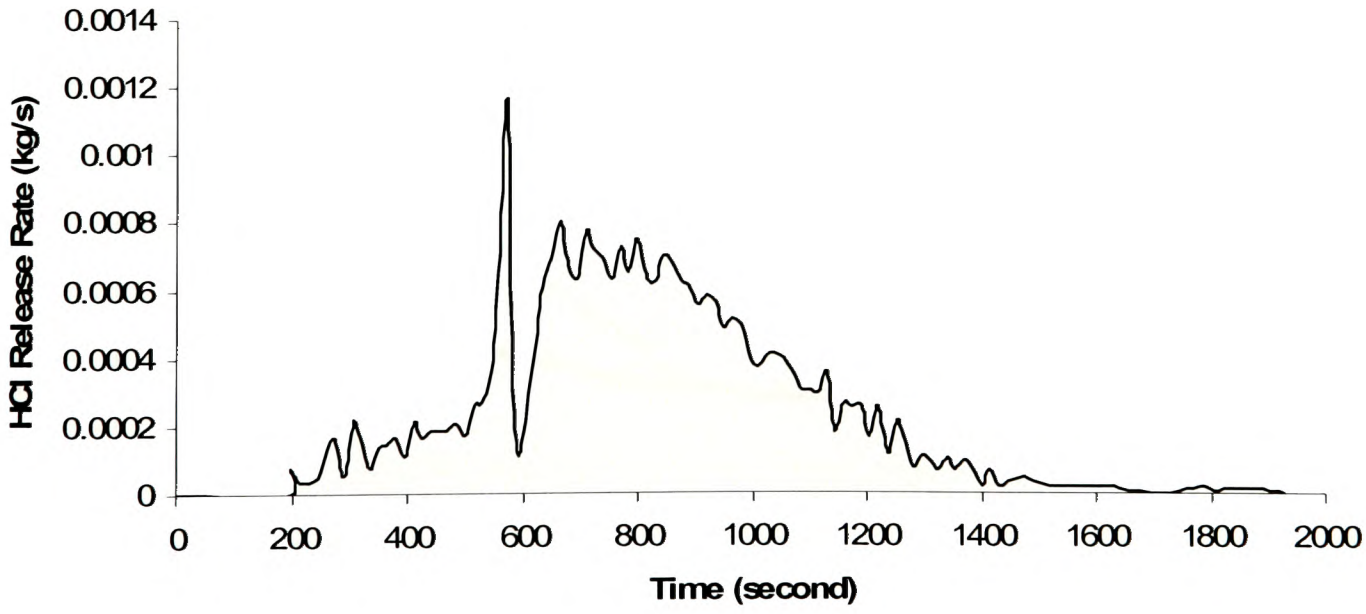

Figure 7.37 HCl release rate (Test 5)

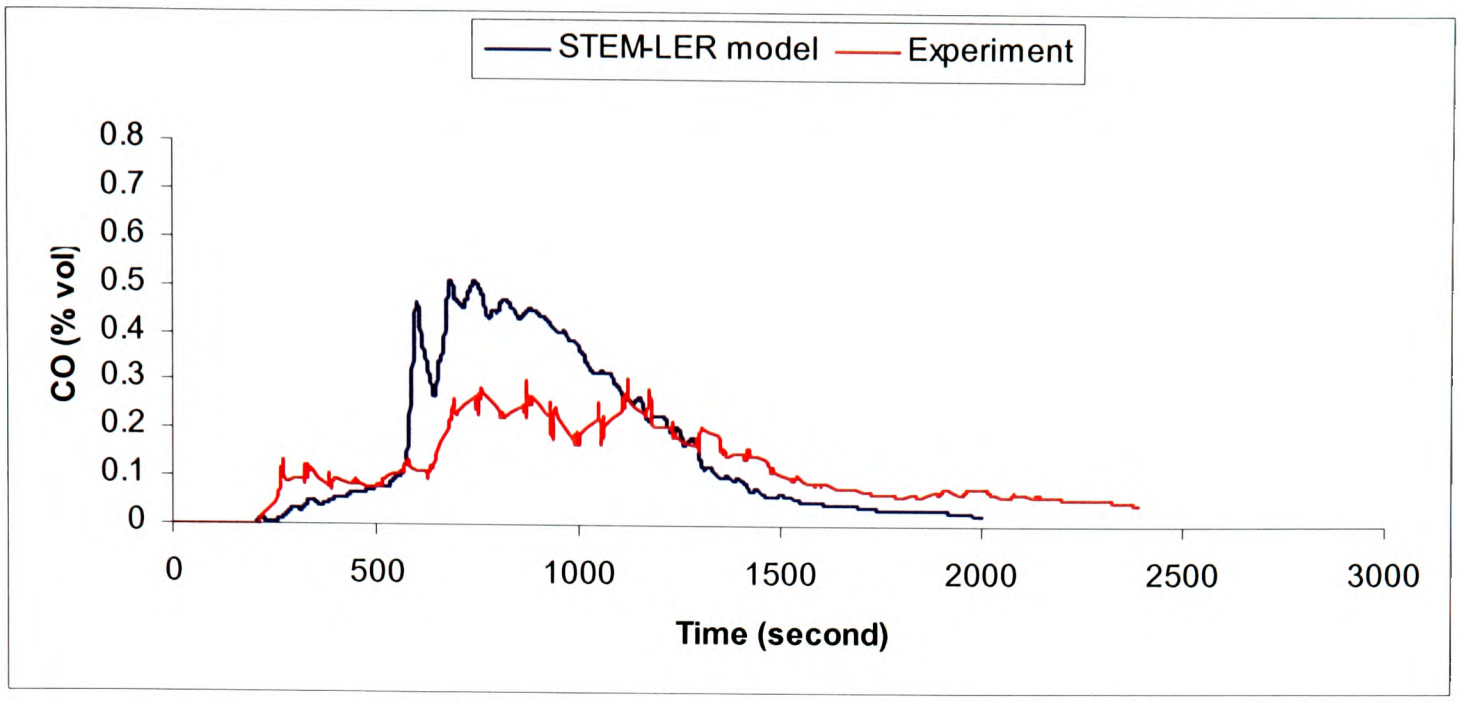

Figure 7.38 CO concentration at location 5 (Test 5)

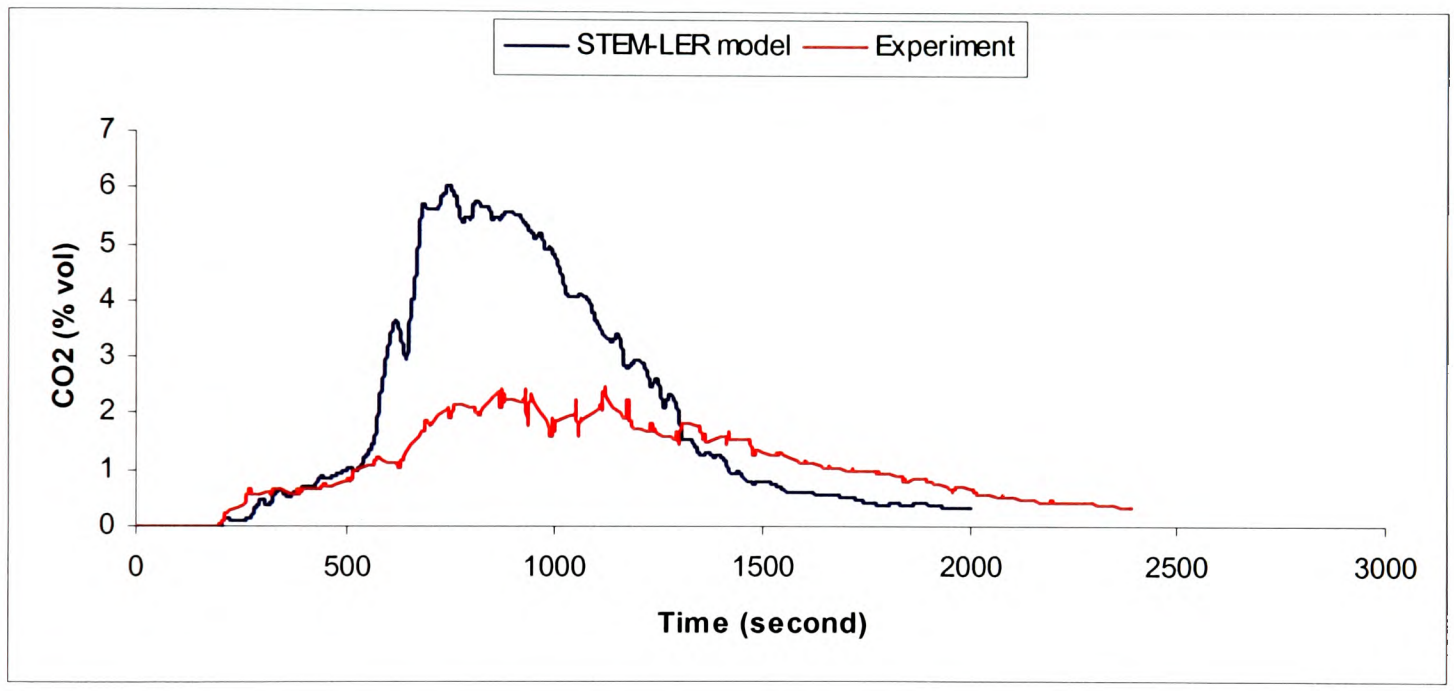

Figure 7.39 CO_2 concentration at location 5 (Test 5)

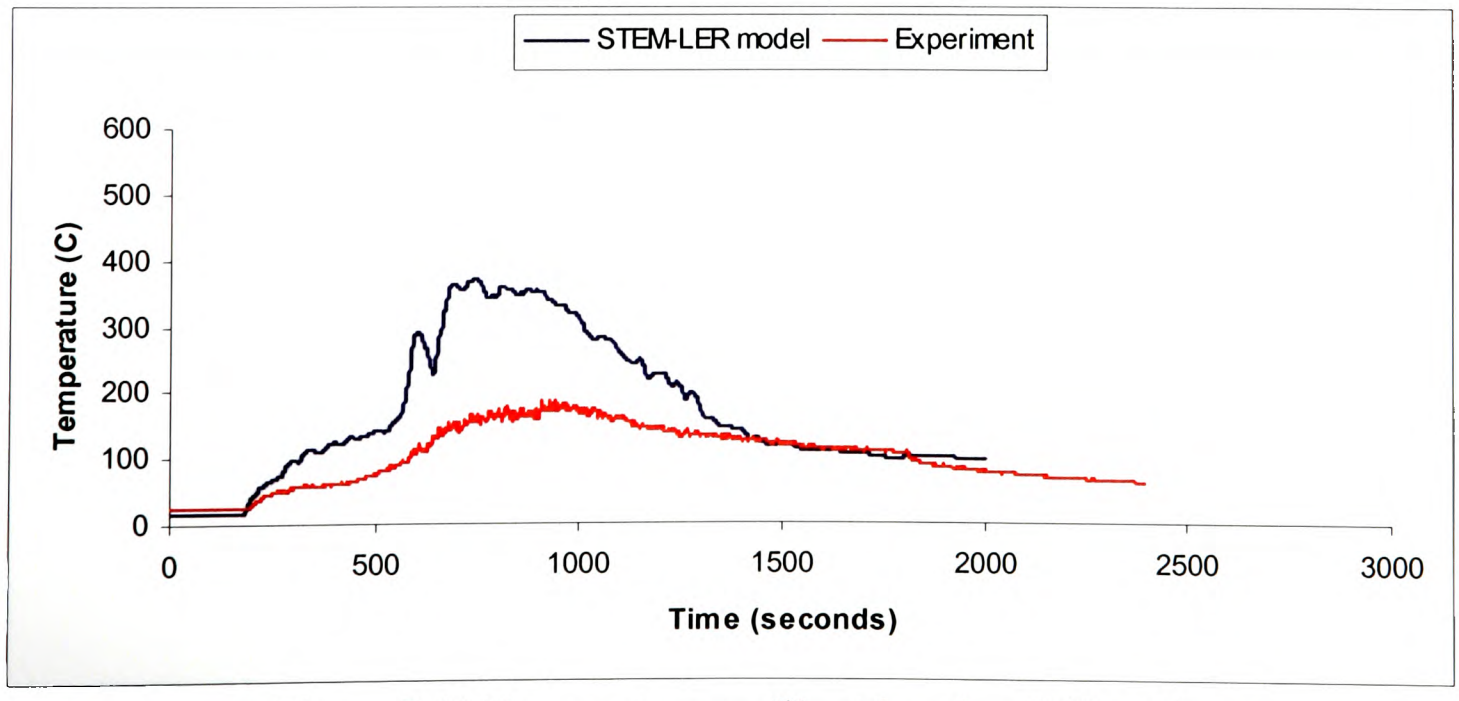

Figure 7.40 Temperature profile at location 5 (Test 5)

The HCl concentrations were measured continuously only at one location during the experiments i.e., at location 4 which is 1 m away from the fire and 1 m before the location 5 (h = 2.2 m). The measured and the computed HCl concentration at the location 4 during the fire are depicted and compared in the Figure 7.41 below. The concentration profile comparisons show that the predicted profile was able to capture the trend well. It should also be mentioned that in the present simulation of HCl transport, HCl absorption to the wall and the effect of temperature on the HCl yields were not taken in to account which might have contributed to the over prediction of the concentration during peak HRR period.

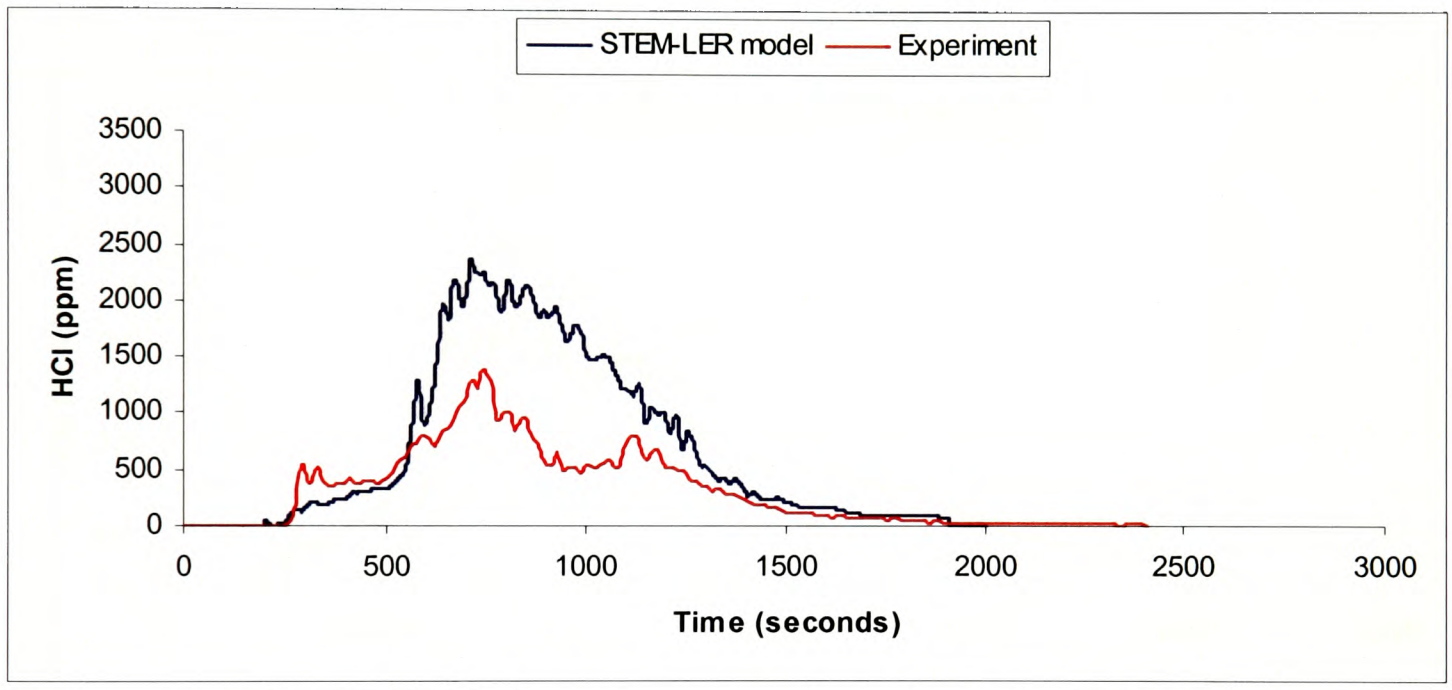

Figure 7.41 HCl concentration at location 4 (h = 2.2 m)

Figures 7.42 and 7.43 compare the predicted CO and CO_2 concentrations at location 9 (h = 2.2 m). The simulated CO concentration was in good agreement with the experimental values. The computed CO_2 concentrations on the other hand were able to follow the rise and fall well and over predicted only during the peak HRR duration. Temperature comparison at the same location is given in Figure 7.44. The simulated temperatures at location 9 were over predicted following the similar trends at the previous location 5.

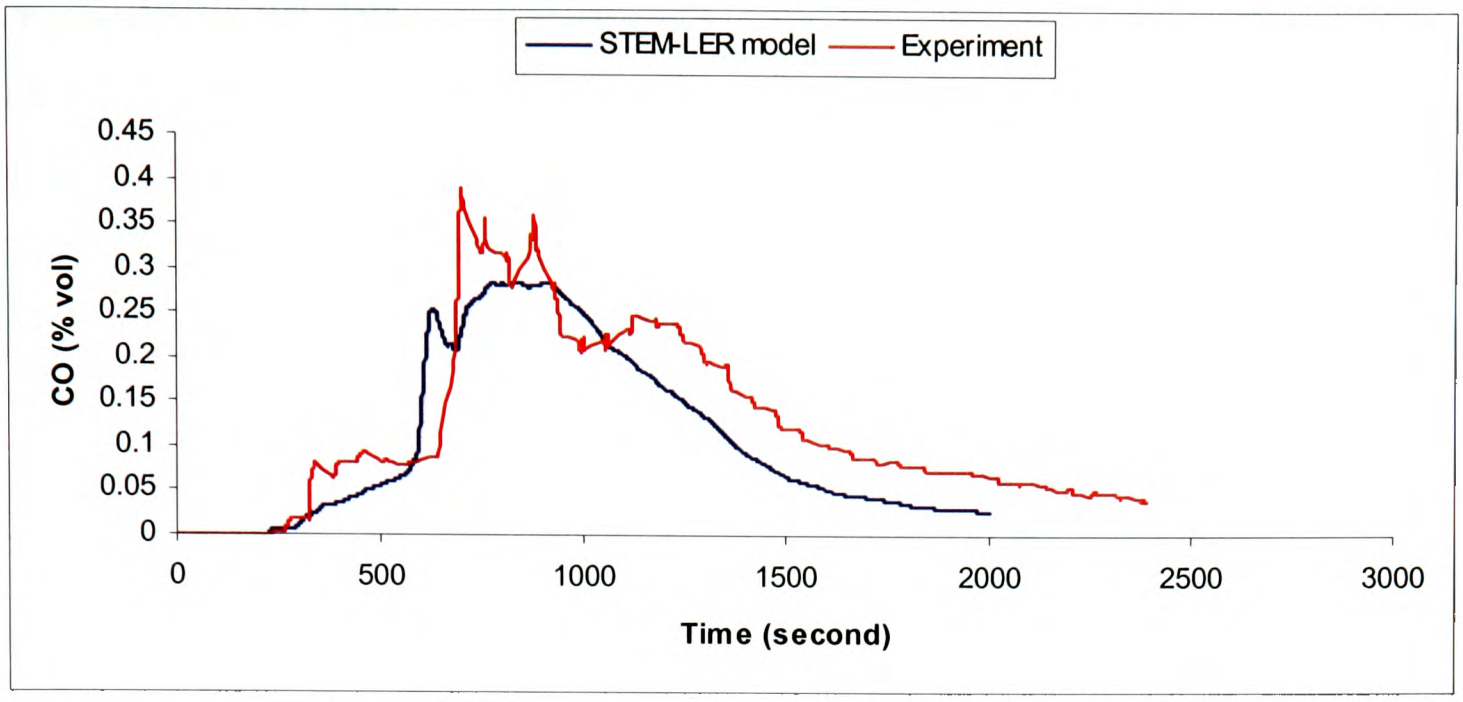

Figure 7.42 CO concentration at location 9 (Test 5)

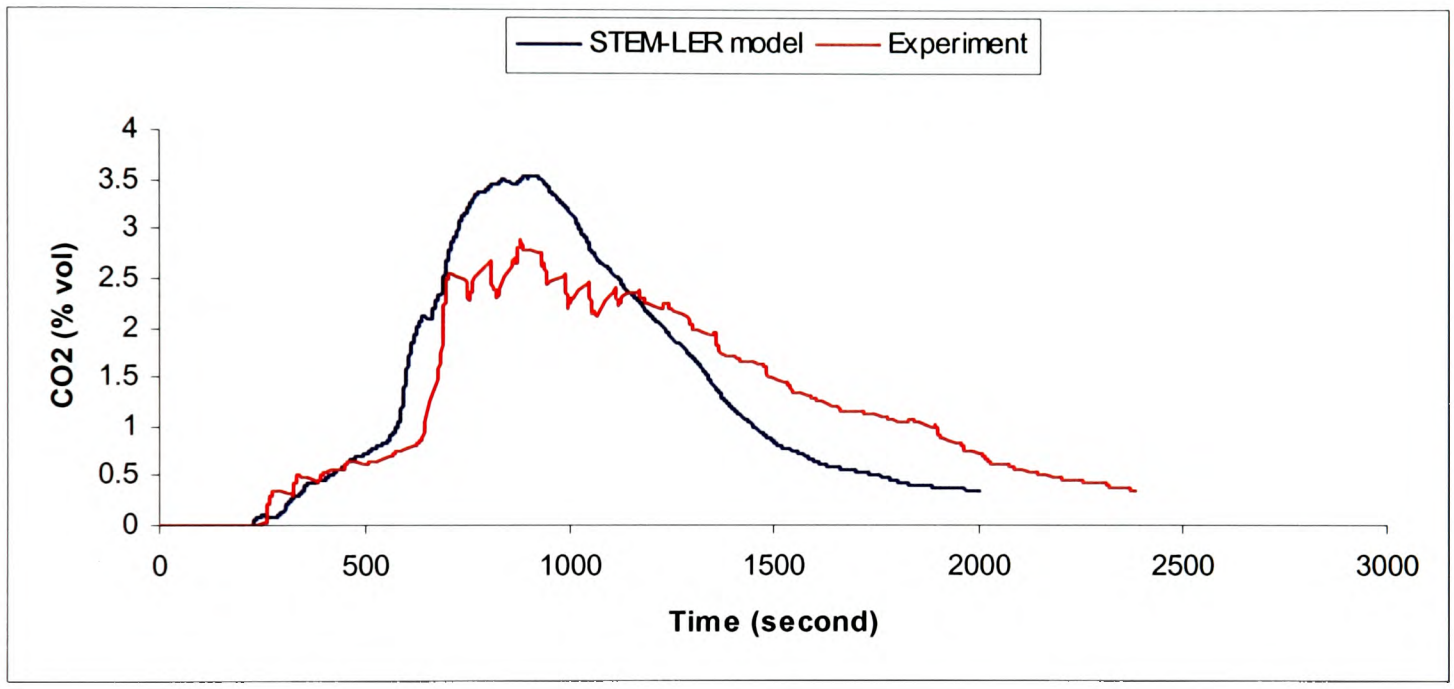

Figure 7.43 CO_2 concentration at location 9 (Test 5)

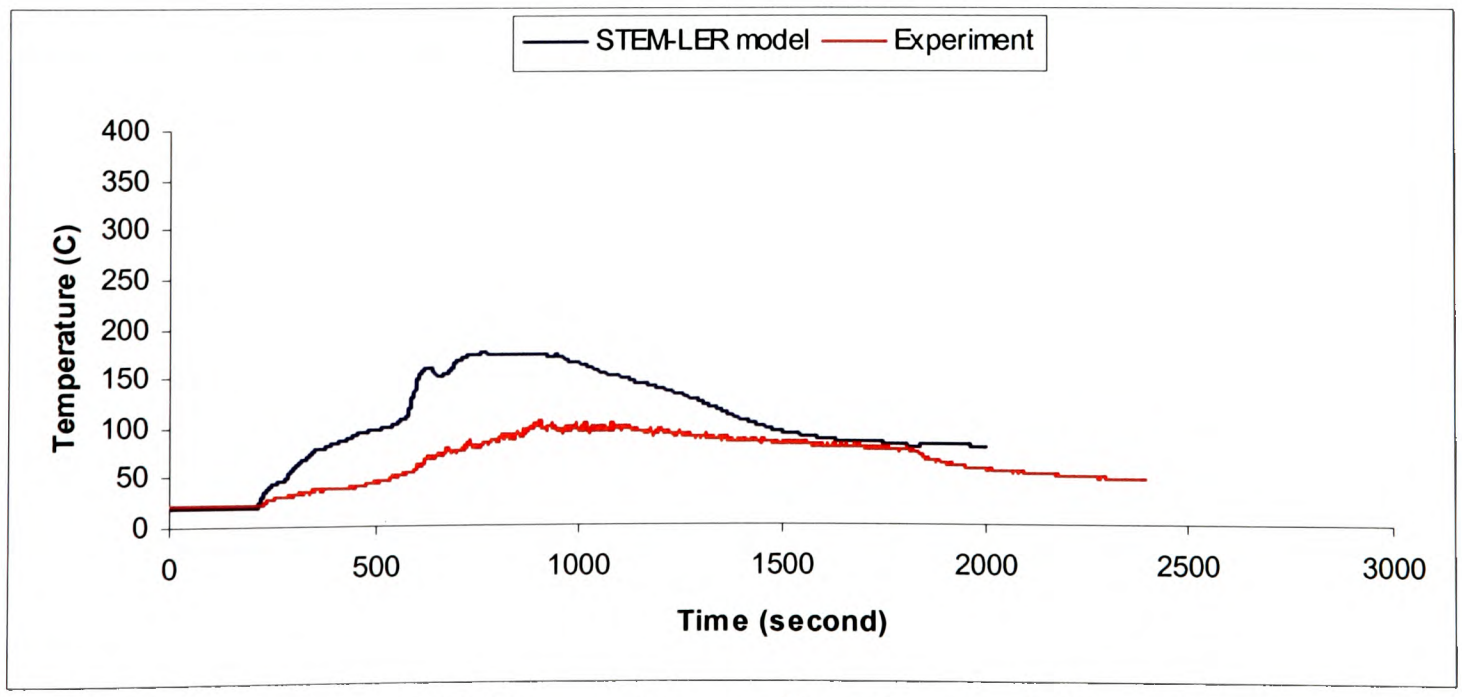

Figure 7.44 Temperature profile at location 9 (Test 5)

The predicted CO, CO_2 concentrations and the temperature profile in the middle of the exit door corridor (location 15, h = 2.2 m) were compared with the experiment and shown in the Figures 7.45 – 7.47. Simulated concentrations were able to follow the rise, peak and the fall in concentrations very closely. The CO_2/CO ratio describes the nature of the combustion. From the over prediction of the CO_2/CO ratio at this distant location, it is clear that the combustion is well-ventilated comparatively in the simulation case. This is due to the inhibition of the vapour phase combustion by the HCl gases during the experiment, which is not modelled in the simulation.

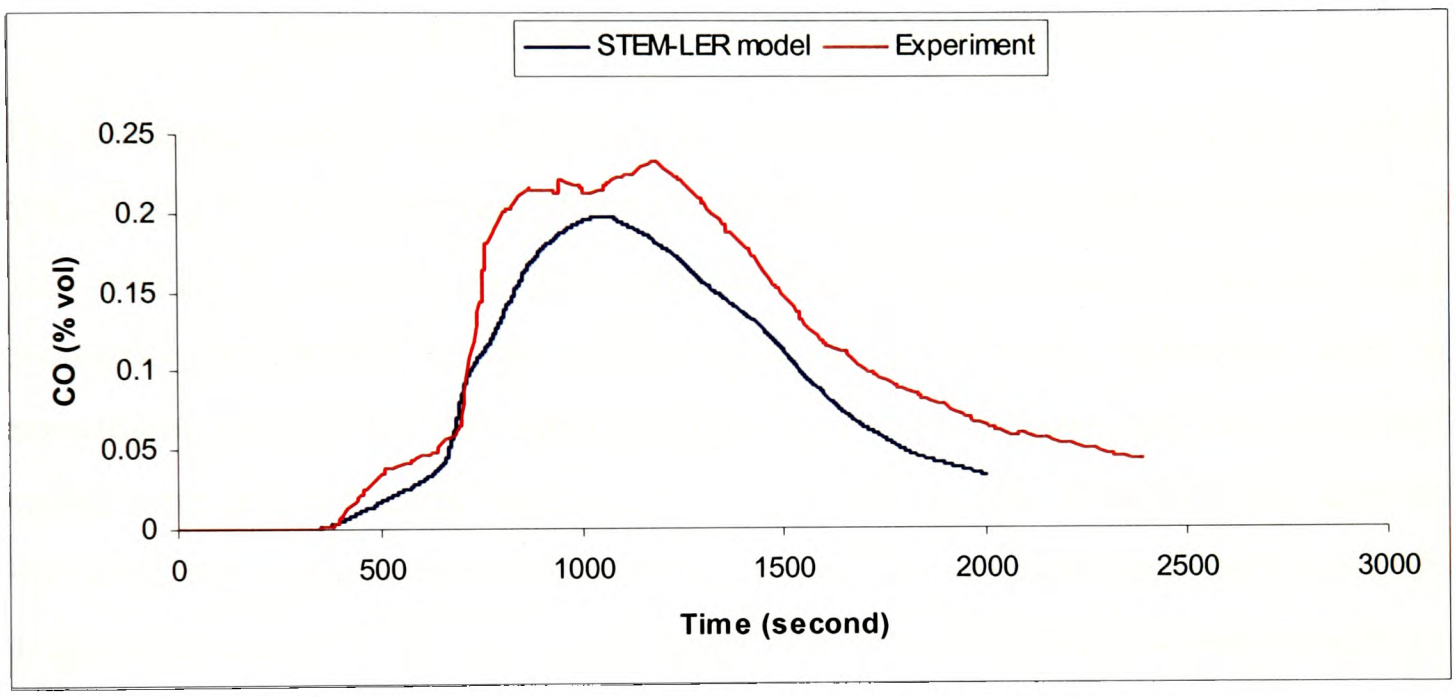

Figure 7.45 CO concentration at location 15 (Test 5)

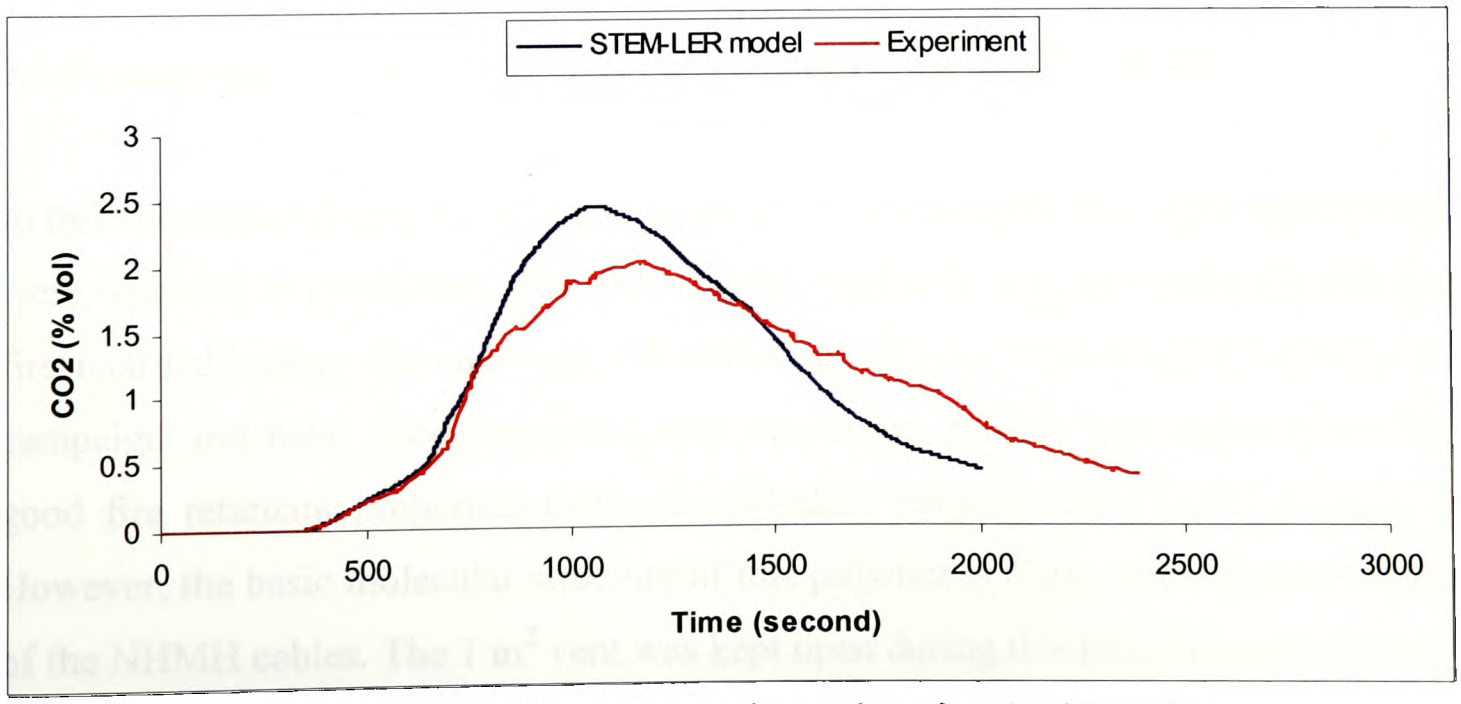

Figure 7.46 CO_2 concentration at location 15 (Test 5)

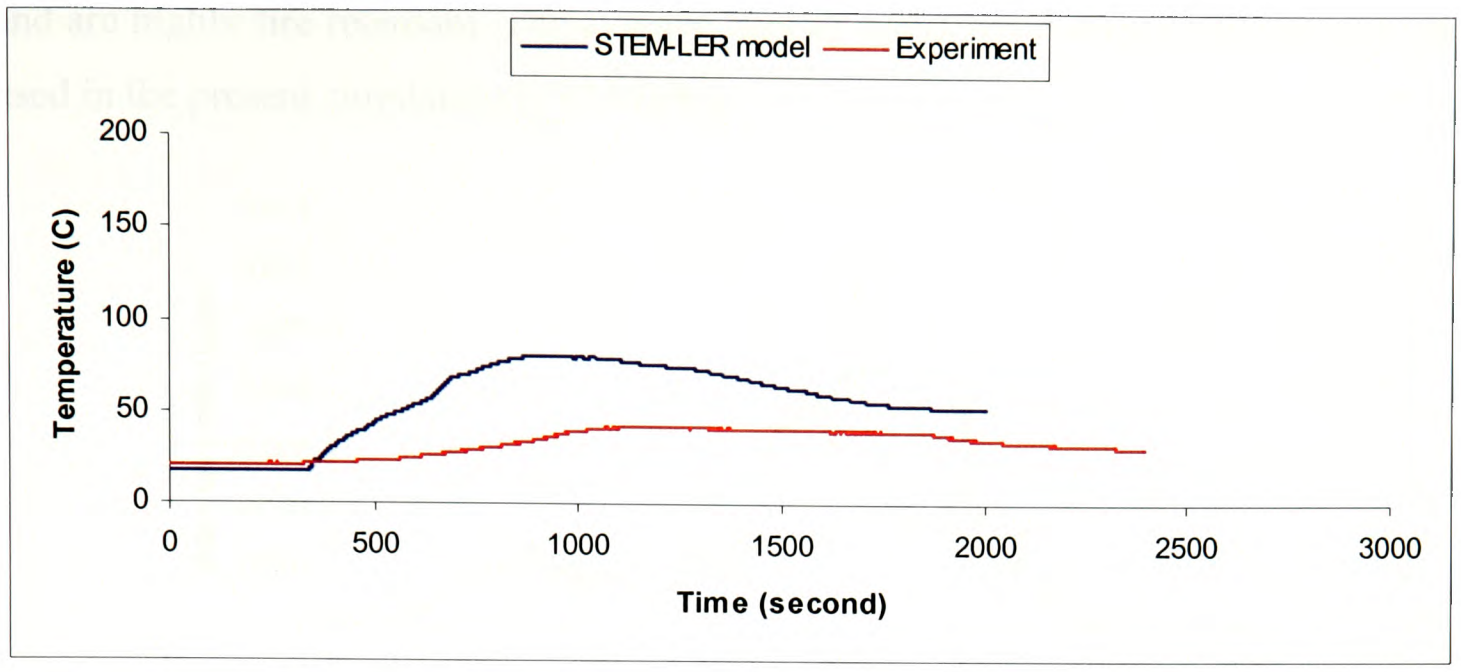

Figure 7.47 Temperature profile at location 15 (Test 5)

The measured peak CO and CO_2 concentrations at the location 15 are 0.235% and 2% respectively and the computed peak CO and CO_2 concentrations at the location 15 are 0.2% and 2.45% respectively. The simulated final CO peak concentration that will be eventually transported to the remote locations is in good agreement with the experiment. Overall, the simulated CO and CO_2 concentrations using the STEM-LER model were in good agreement with the experimental data throughout the corridor. However, the temperatures were consistently over predicted through out the corridor in this test case due to the over prediction of the combustion rate because the effect of HCL gases on the vapour phase combustion not modelled.

7.5.5 Simulation of Test 7 – RZ1-K cables (Inlet open and No Weir)

In this subsection simulation results for the Test 7 involving RZ1-K type power cables were reported and validated with the experimental data. RZ1-K cables are the most fire retarded among the three type of cables considered in the present experimental campaign and have good reaction-to-fire properties. RZ1-K type cable owes their good fire retardant properties to the cross-linked polyethylene (XLPE) compound. However, the basic molecular structure of this polymer is C_3H_6 which is same as that of the NHMH cables. The 1 m^2 vent was kept open during this test. The mass loss rate curve derived from the load cell data (Figure 6.26) and the HRR curve are given in Figures 7.46(a) and 7.46(b). The duration of the fire was approximately 3500 seconds and hence the simulation was carried out for 3500 seconds. The fire duration for this test case was the longest because RZ1-K type cables have the longest ignition time

and are highly fire retardant. The average heat of combustion during this fire test and used in the present simulation is 17 MJ/Kg.

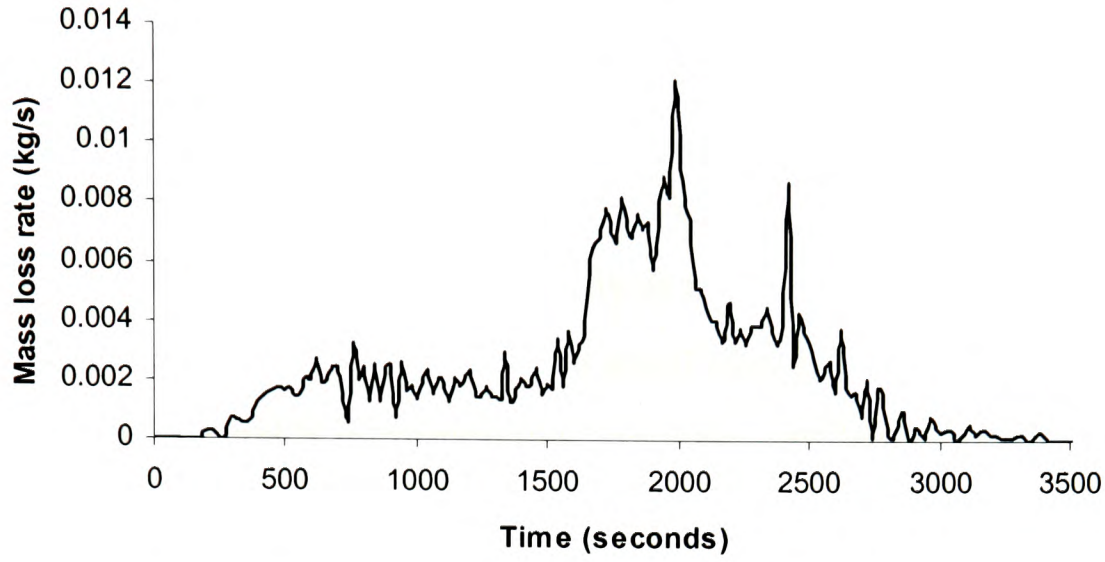

Figure 7.48 (a) Mass loss rate curve (Test 7)

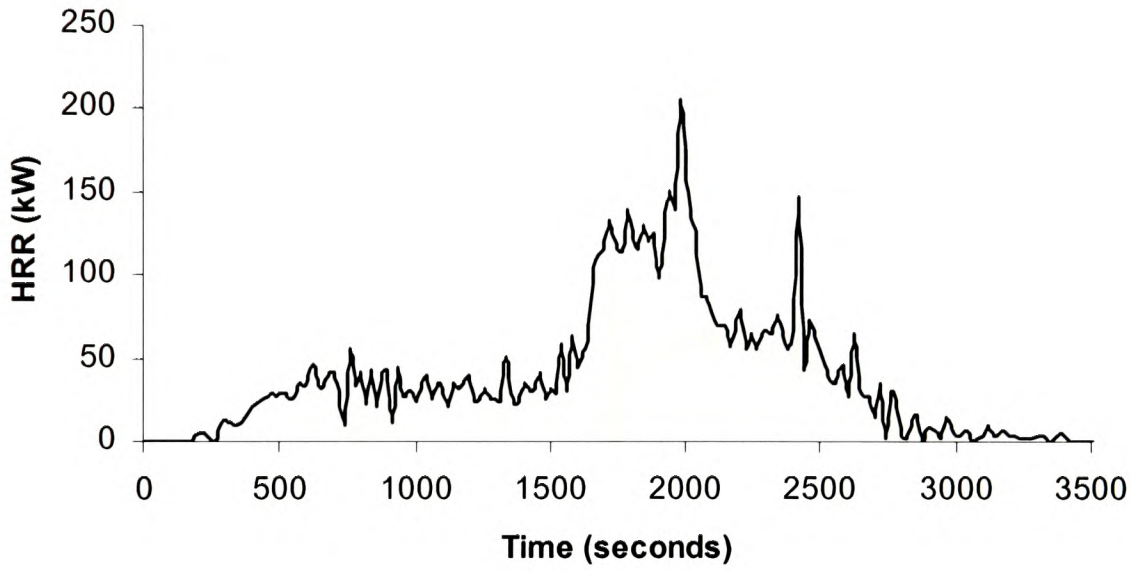

Figure 7.48 (b) Heat Release Rate curve (HRR) during Test 7

Figure 7.47 to 7.49 describes the CO and CO_2 concentration evolution and the temperatures during Test 7 cable fire test at the location 5 (h = 2.2 m). The predicted CO and CO_2 concentrations and temperature at this location were over predicted through out the fire duration also there were two spikes seen in the Figures 7.47 and 7.48. The spikes correspond to dripping of plastics on the floor at around 2000 and 2500 seconds (see Figure 6.13) which is a complex phenomenon to model [Butler et al., 2004]. Although 'Pool fire' was witnessed on the floor, the dripping of plastics was accounted as instant mass loss by the load cell. These spikes in the load cell measurement were responsible for the spikes in the calculated profiles. The first sharp spike in the CO and CO_2 concentrations at around 2000 seconds corresponds to the first sharp mass loss rate recorded by the load cell, occurring at 2000 seconds (Figure

7.46(a)). The second spike in the mass loss rate curve occurs around 2500 seconds and is responsible for the second small spike in the CO and CO_2 concentration profiles at around 2500 seconds. This is due a sharp rise in the fuel mass loss rate i.e. more fuel released which increases the LER and in turn the CO yields. For the RZ1-K type cable in particular the yields are very sensitive to the equivalence ratio (Figure 7.50) in the yield correlation. From the CO yield corresponding to the well-ventilated conditions ($\phi = 0.7$), the yield increases rapidly to reach the yield corresponding to the under-ventilated condition ($\phi = 1.1$). Hence a small over prediction of LER can end up in predicting high CO yields corresponding to under ventilated conditions instead of CO yields for well-ventilated conditions. The LERs at location 5 around the first peak are given in Table 7.5. From the table it can be deduced that the fuel/air ratio increases approximately 5 times during the first peak.

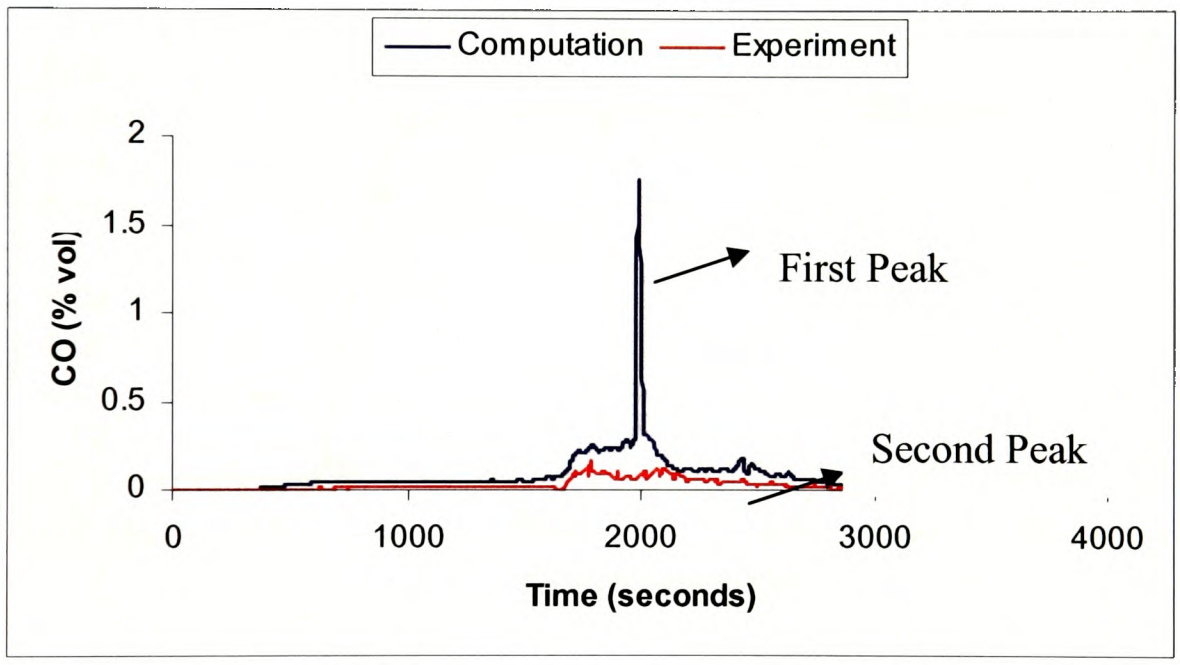

Figure 7.49 CO concentration at location 5 (Test 7)

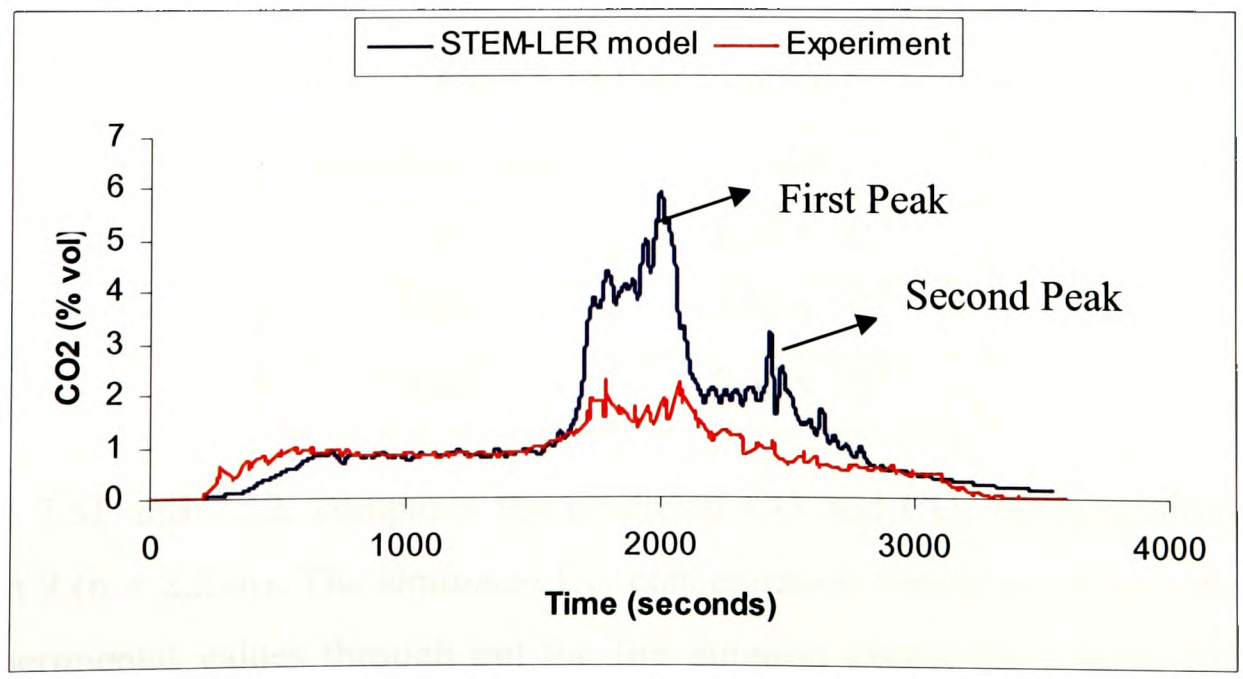

Figure 7.50 CO_2 concentration at location 5 (Test 7)

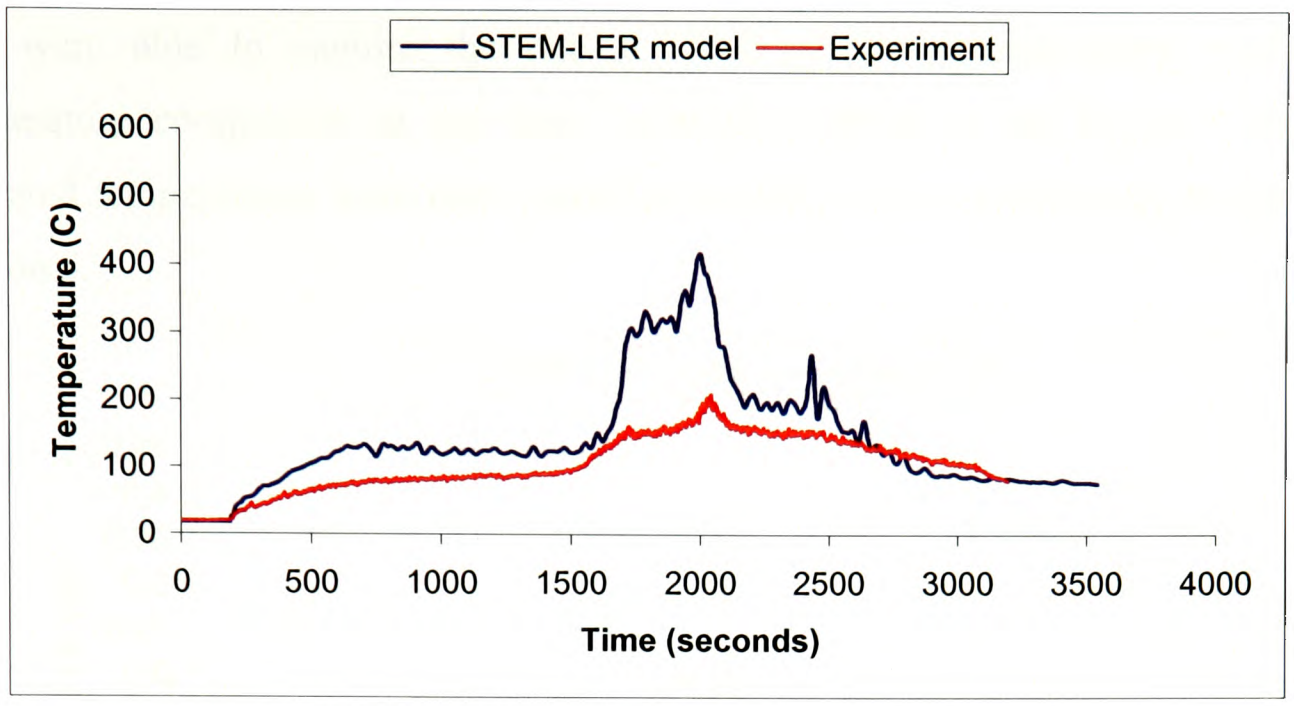

Figure 7.51 Temperature profile at location 5 (Test 7)

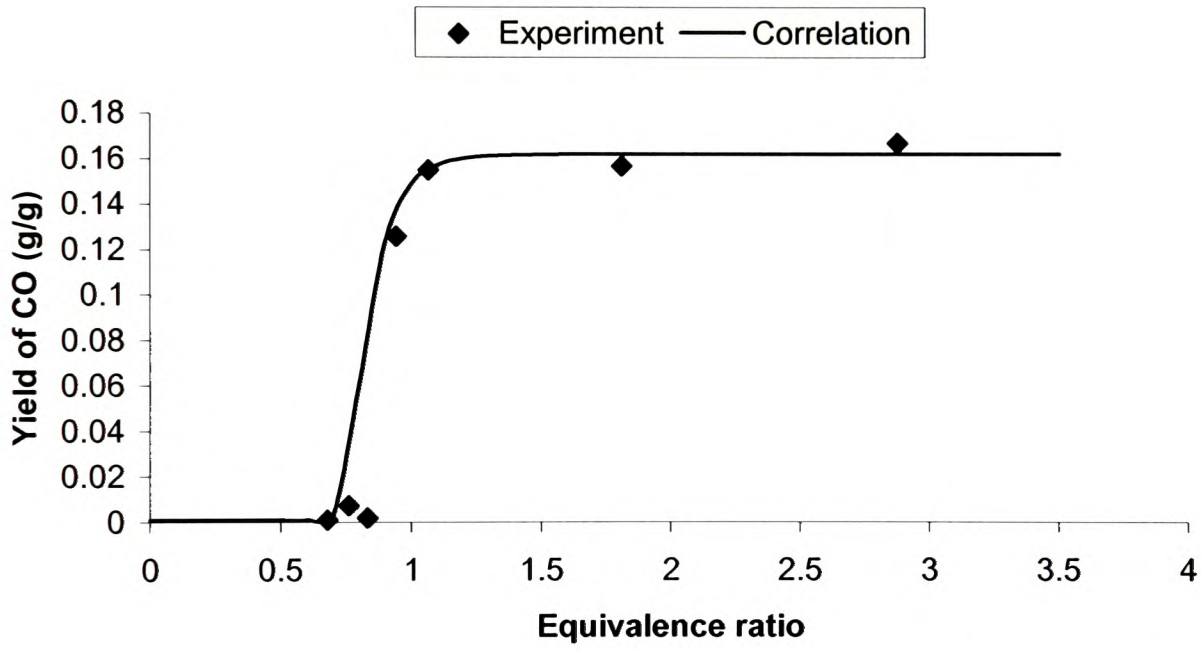

Figure 7.52 CO yields vs Equivalence ratio for RZ1-K cables

Table 7.5 LER at location 5

Time (seconds)	LER
1900	5.38×10^{-5}
1980	2.85×10^{-4}
2020	5.35×10^{-5}

Figures 7.51 and 7.52, compares the predicted CO and CO_2 concentrations at the location 9 (h = 2.2 m). The simulated CO concentration was in good agreement with the experimental values through out the fire duration except for a sharp rise in the

peak concentration at 2000 seconds. The computed CO_2 concentrations on the other hand were able to capture the rise and fall of the concentrations very well. Temperature comparison at the same location is given in the Figure 7.53. The simulated temperatures were over predicted similar to the prediction at the previous location 5.

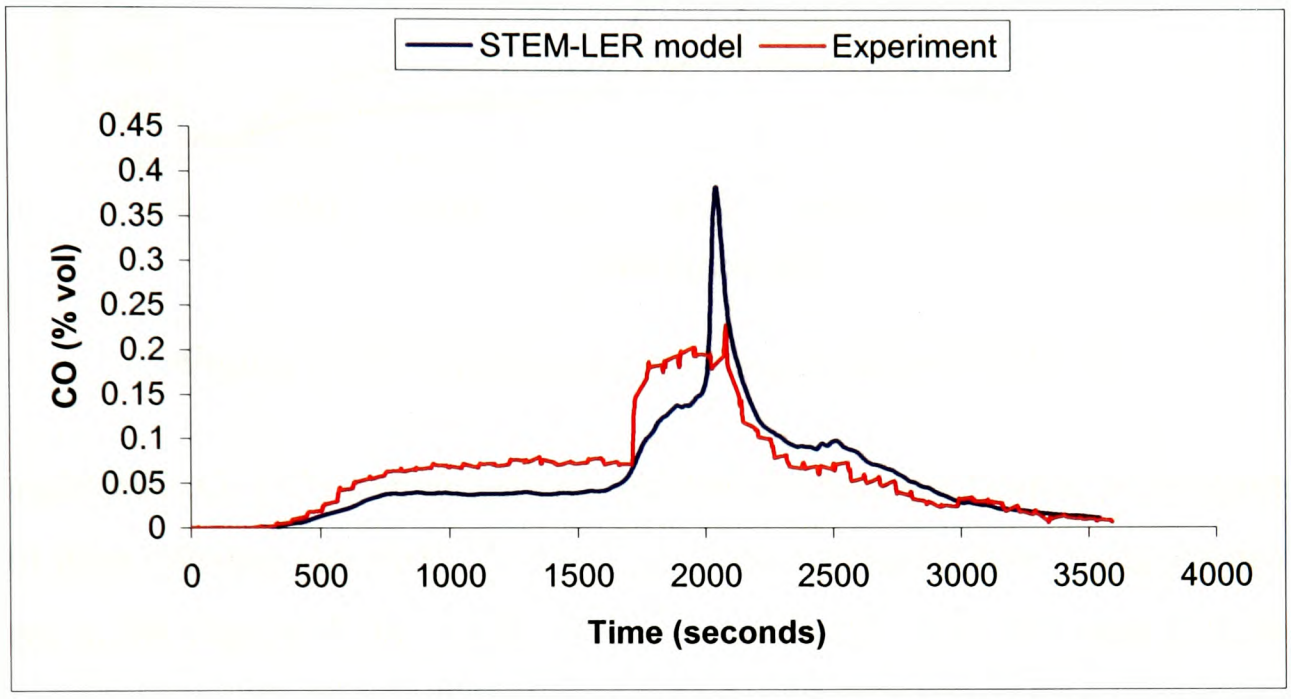

Figure 7.53 CO concentration at location 9 (Test 7)

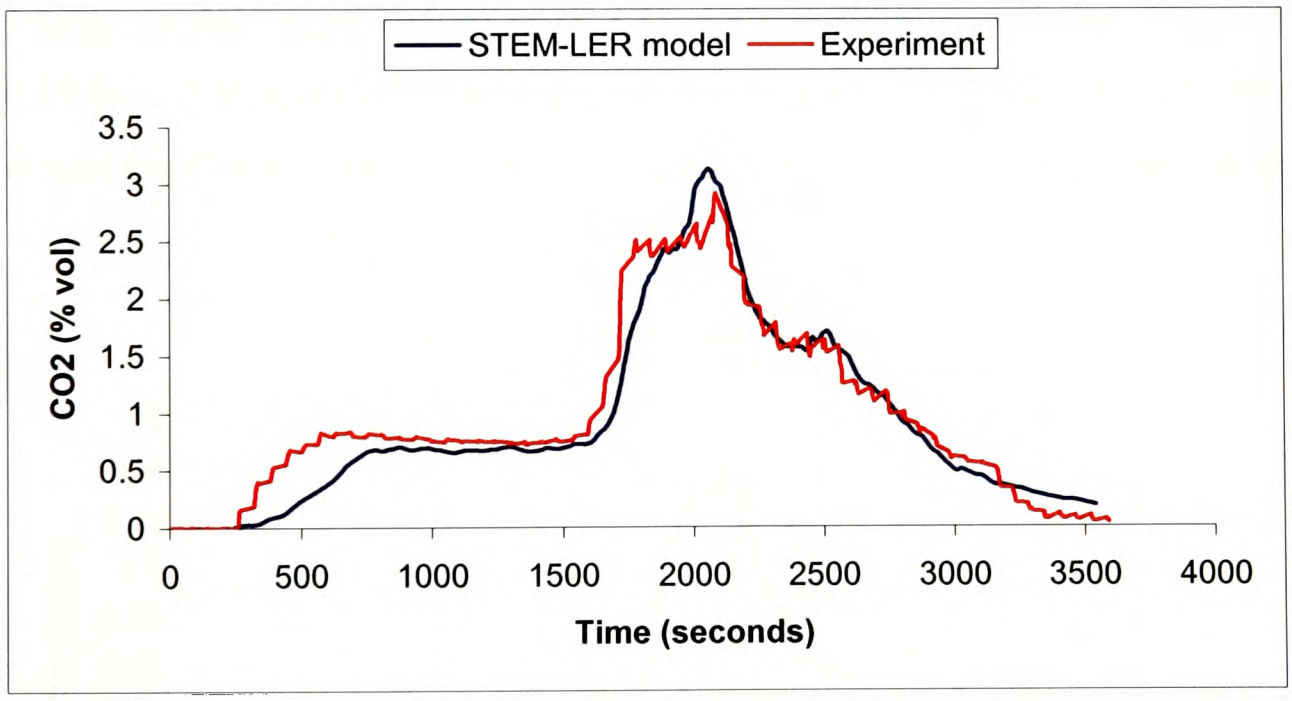

Figure 7.54 CO_2 concentration at location 9 (Test 7)

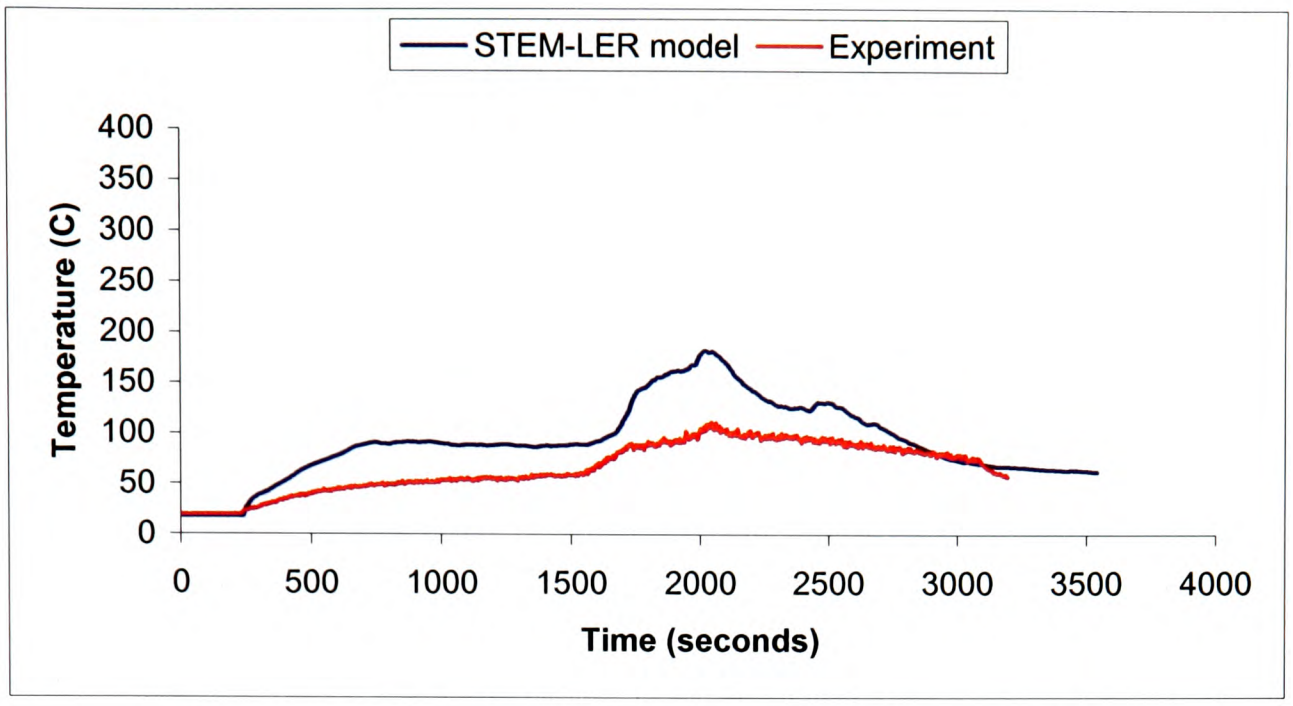

Figure 7.535 Temperature profile at location 9 (Test 7)

The predicted CO, CO_2 concentrations and the temperature profile in the middle of the exit door corridor (location 15, h = 2.2 m) are compared with the experiment and depicted in the Figures 7.54 – 7.56. The measured peak CO, CO_2 concentration and the CO_2/CO ratio were 0.138 % volume, 1.78 % volume and 12.89 respectively. The STEM-LER model prediction of peak CO, CO_2 concentrations and CO_2/CO ratio were 0.14 %, 1.7 % and 12.14 respectively. The simulated CO and CO_2 concentration profiles and the CO_2/CO ratio are in good agreement with the experimental profiles.

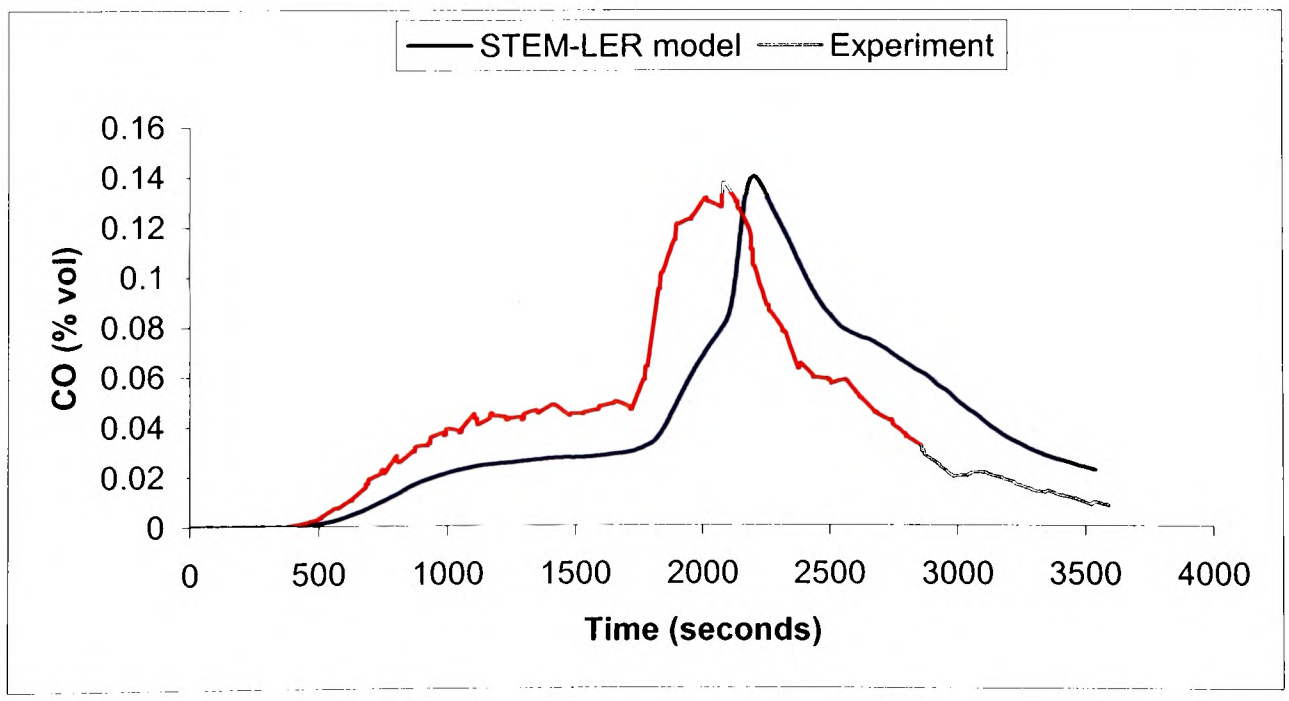

Figure 7.56 CO concentration at location 15 (Test 7)

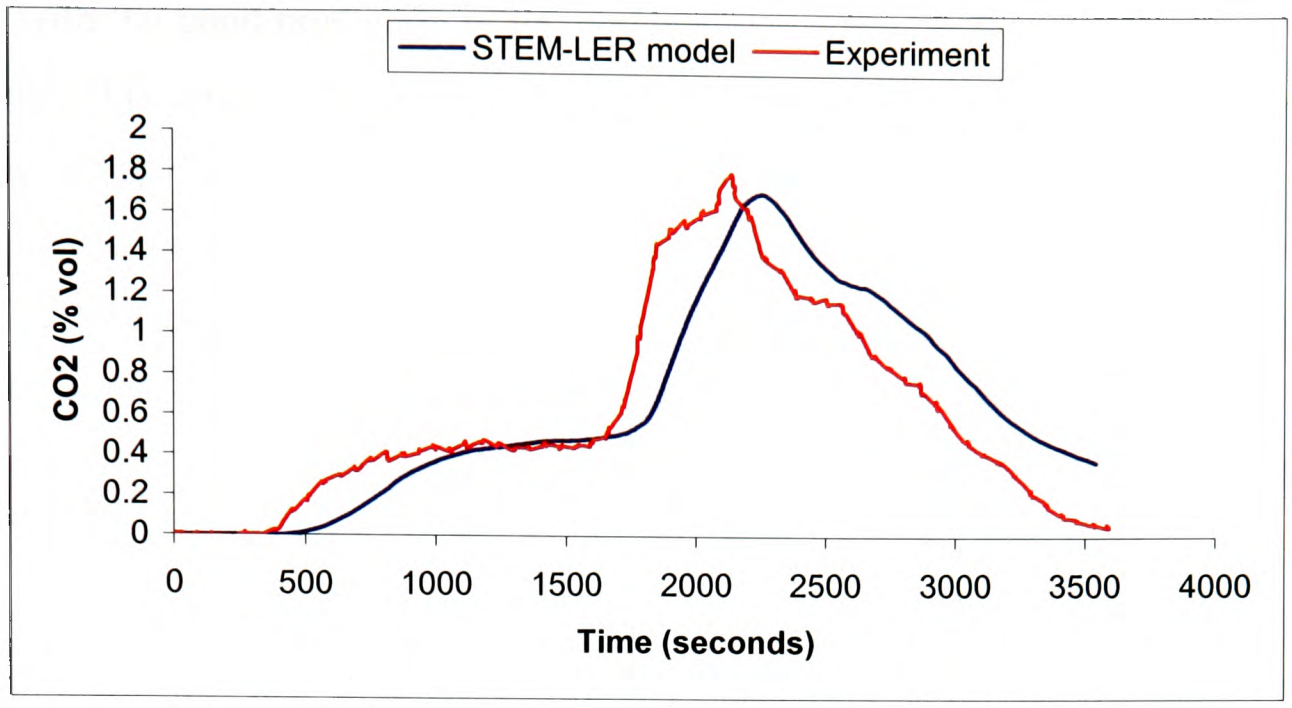

Figure 7.57 CO_2 concentration at location 15 (Test 7)

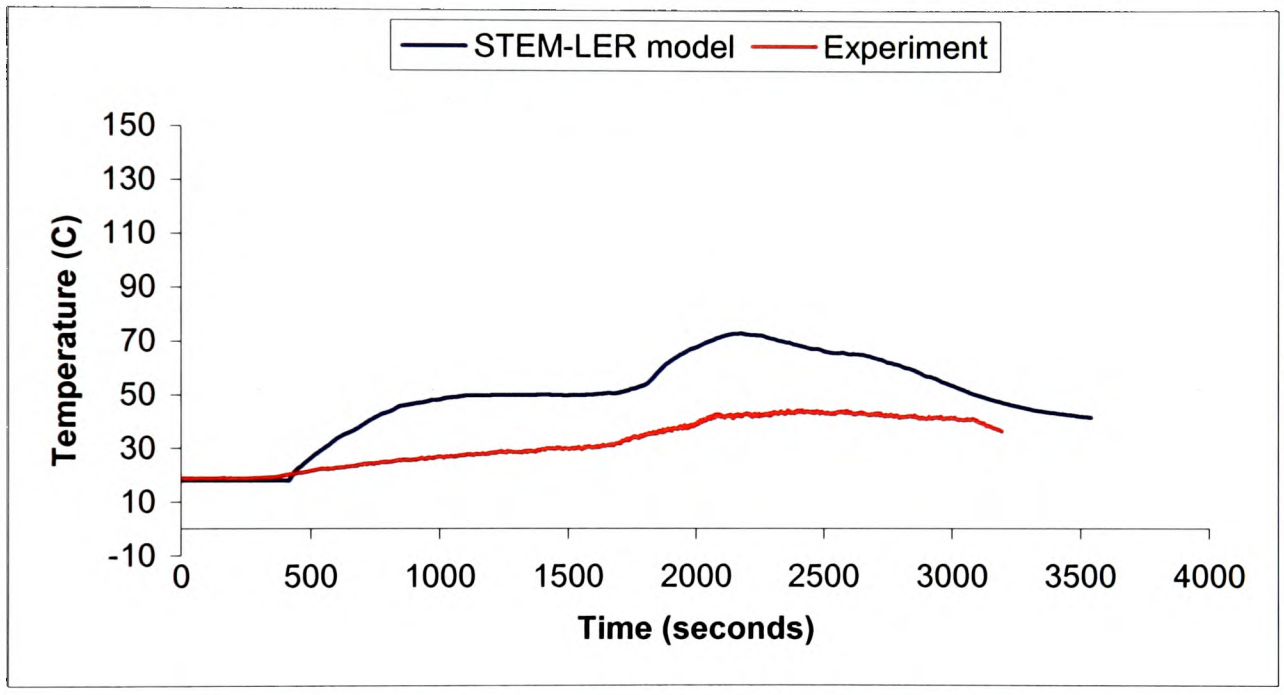

Figure 7.58 Temperature profile at location 15 (Test 7)

Overall, the STEM-LER model was able to predict reasonably well the final CO and CO_2 concentrations even at the distant location 15 which is 30 m away from the fire. The final CO_2/CO ratio at location 15 is also accurately captured using the STEM-LER model.

7.6 Concluding Remarks

The Scalar Transport Equation based Model (STEM-LER) described in Chapter 4 solves separate transport equations for the species and uses Local Equivalence Ratio concept to model the source terms. Prediction of toxic combustion products distributions in real-scale fires is dependant on the yield correlations of the materials

along with the good prediction of the combustion region. In this chapter, the STEM-LER model is used for the prediction of CO and CO_2 concentrations near the fire and final levels far from the fire and validated with the experimental data. In addition the STEM-LER model uses a modified EBU combustion model which takes in to effect the CO formation in calculating the fuel consumption rate in fuel-rich regions. Simulations were carried out for four large scale cable fire test involving three different cable types. The model was able to predict the CO, CO_2 concentrations, CO_2/CO ratios and the temperature reasonably well for all the four cases.

The simulations of four large-scale cable fire tests above involving NHMH, NYM and RZ1-K type cables testifies the following:

- The modified EBU model which takes into account the CO formation in modelling the fuel consumption performs better than the standard EBU combustion model in predicting the fuel consumption in fuel-rich areas and in turn predicts the combustion region better.
- The STEM-LER model is able to predict the CO, CO_2 concentrations, CO_2/CO ratios and the temperature reasonably well near the fire and far away from the fire origin in real fire scenarios.
- Yield correlations obtained from the bench-scale Purser furnace experiments were able to predict the CO and CO_2 concentrations in real fire scenarios which also validates that the Purser furnace toxicity method is able to reproduce the different stages of a real fire inside the tube furnace.

The simulated fire environment data of the four cable fires will be used in the next chapter to model an artificial evacuation scenario and also to analyse the sensitivity of the evacuation models on fire environment models.

Chapter 8

Preliminary Assessment on the Effect of Cable Fires on Building Evacuation

8.1 Introduction

Performance based fire safety engineering involves essentially the determination of two factors, the time available to the occupants for safe egress, sometimes referred to as the Available Safe Egress Time (ASET) and the time that is required by the occupants to evacuate from the structure generally referred to as the Required Safe Egress Time (RSET). For the building to be considered 'fire-safe', the RSET, plus some safety factor, should be less than the ASET. For the scenarios under consideration, fire simulation is typically used to determine at what time non-survivable conditions develop within the building, for example when the temperature or smoke concentration at head height reaches a critical value which is deemed detrimental to evacuation. The RSET is usually determined through evacuation simulation [Gwynne et al., 1999].

A more sophisticated approach is to incorporate the predicted fire atmosphere within the evacuation model and directly determine the impact of the fire on the ability of the simulated occupants to safely evacuate. This may be determined if the evacuation model incorporates Fractional Effective Dose (FED) models [Purser, 1999] and incorporates impact of smoke on reduced visibility and hence mobility [Jin, 1978; Jin

and Yamada, 1989]. Advanced egress models such as buildingEXODUS [Gwynne et al., 2001; Gwynne et al., 2006; Park et al., 2003] has this type of capability.

This chapter is dedicated to investigating the use of computed versus experimental fire hazard data for assessing survivability within buildings using evacuation models incorporating the Fractional Effective Dose (FED) models [Purser, 1999]. Also, a preliminary assessment on the effect of cable fires on the building evacuation has been carried out for the four cable fire test considered in the present study.

8.2 The buildingEXODUS evacuation software

'buildingEXODUS' [Galea et al., 2004; Gwynne et al., 2001; Gwynne et al., 2006; Park et al., 2003] is a software tool designed to simulate the evacuation and movement of large numbers of individuals within built environment. It is used to demonstrate compliance with building codes, evaluate the evacuation capabilities of all types of structures and investigate the effect of a design fire on population movement efficiencies within structures. The 'buildingEXODUS' software takes into consideration *people-people*, *people-fire* and *people-structure* interactions. The model tracks the trajectory of each individual as they make their way out of the enclosure, or are overcome by fire hazards such as heat, smoke and toxic gases. Thus, the behaviour and movement of each individual is determined by a set of rules. These rules have been categorised into five interacting sub-models, the OCCUPANT, MOVEMENT, BEHAVIOUR, TOXICITY and HAZARD sub-models. The evacuation simulation is performed using the 'buildingEXODUS' software [Galea et al., 2004] which makes use of the Purser FED toxicity model. This model considers the toxic and physical hazards associated with elevated temperatures (FIH), CO, CO_2 and low O_2 (FIN), and other toxic and irritant gases like HCN and HCl (FIC) and takes into account the visual obscuration effect caused by smoke into account using the Jin data [Jin, 1978; Jin and Yamada, 1989].

8.2.1 Hazard Effect Attributes

The hazard effect attributes used within the buildingEXODUS software that are relevant to the present assessment study are [Galea et al., 2004]:

FIH attribute

The FIH attribute measures the occupant's cumulative exposure to radiative and convective heat. The default value for FIH is zero. As the FIH increases the mobility attribute decreases and when FIH is equal to one, the occupant is incapacitated due to heat exposure. The heat hazard has two contributions, i.e. convective heat (elevated temperature) and radiative flux [Purser, 1999].

(a) Convected Heat:

$$FIH_c = 2.0 * 10^{-8} * T^{3.4} * t \qquad (8.1)$$

where t is the time in seconds and T is the temperature (^{o} C)

(b) Radiative Heat:

$$FIH_r = 60 * \frac{q^{1.33}}{D_r} * t \qquad (8.2)$$

where q is the radiative flux (kW/m^2) and D_r is the radiative denominator (dose required to cause effect).

FIN attribute

The FIN attribute measures the occupant's combined cumulative exposure to low O_2, HCN, HCL, CO and CO_2. The default value for FIN is zero. As the FIN increases the mobility decreases and when FIN is equal to one, the occupant is incapacitated due to the combined effect of these gases. The FED model [Purser, 1999] considers the combined effect in the following way,

$$FIN = FICO + (FICN + FLD)*VCO_2 + FIO \qquad (8.3)$$

where, $VCO_2 = e^{(CO_2/5.0)}$ is a multiplicative factor which measures the increased uptake of CO and HCN due to CO_2 induced hyperventilation.

FIC_{HCL} attribute

The toxicity model within the software also takes into account the impact of irritant fire gases on individuals. A Fractional Irritant Concentration (FIC) is determined which is a measure of the exposure concentration at any point in time to the concentration required to cause the effect. The irritant gases have a direct impact on the exposed individuals mobility or ability to move in a concerted manner towards the exit. As the irritant gas concentration (and hence FIC value) increases, the mobility of the exposed individual decreases. When the FIC is equal to 1.0, the person is considered to be incapacitated and hence unable to continue. Unless rescued, the person is likely to perish in the fire.

Each individual within the population is susceptible to differing levels of instantaneous exposures of the various irritant gases. The value depends on natural variations in the population such as age, gender, state of health, strength, etc. EXODUS uses a range of tolerance values suggested by Purser [Purser, 1999] intended to represent the distribution typically found in the population.

In the cases examined here, HCL is the only irritant gas considered and so only FIC_{HCL} is determined. To simplify the analysis all the occupants within the simulations presented here are given identical tolerance values to HCL equal to the median value for the population i.e. 900 ppm.

FLD_{HCL} attribute

As with the narcotic gases, the irritant gases can also cause death if sufficient quantities are inhaled. The accumulated dose of irritant gases received by an individual is measured by the FLD attribute. In the cases considered here only HCL is considered and so only FLD_{HCL} is determined in these simulations. As with the FIN

and FIH values, when FLD is equal to 1.0 the person is considered to have succumbed to the exposure.

Finally, in a similar manner to the narcotic and irritant gases, the presence of smoke directly affects the mobility of the individual. Smoke has the effect of obscuring vision and irritating the eyes thus impairing the ability of an individual to escape. The victim's movement rate decreases as the smoke concentration increases. This effect is related to the density of the smoke (measured by extinction coefficient) and does not increase with prolonged exposure. Within buildingEXODUS, the smoke density is linked to the occupant mobility attribute. The relationship between smoke extinction coefficient and occupant mobility is modelled using the Jin data [Jin, 1978; Jin and Yamada, 1989].

8.3 Comparison between the Effect of Computed and Experimental Fire Environment on Building Evacuation

8.3.1 Simulation of a NHMH cable fire scenario using computed and experimental fire hazard data

The purpose of this investigation is to assess for a given fire scenario, whether the fire hazard data generated using CFD based fire model is sufficiently accurate to provide a sound basis for engineering judgements of the suitability of the structure and its fitting for evacuation. The fire hazard data, either computed or experimentally measured, is used within the evacuation model to determine the FED received by the evacuating population. While the concept is widely used in fire risk assessment, little comparison with the thorough experimental data has been performed to test the sensitivity of the FED models and their overall impact on the unfolding evacuation.

A cable fire test involving NHMH cable (TEST 8) is considered in the present assessment where the CO, CO_2, O_2 and temperature distributions were measured during the experiment. The total duration of the fire was around 2000 seconds. In the

previous chapter it was shown that for the test 8, the computed results were in good agreement with the experiments.

In the 'buildingEXODUS' simulation, the labyrinth space is divided into 12 zones as shown in Figure 8.1.

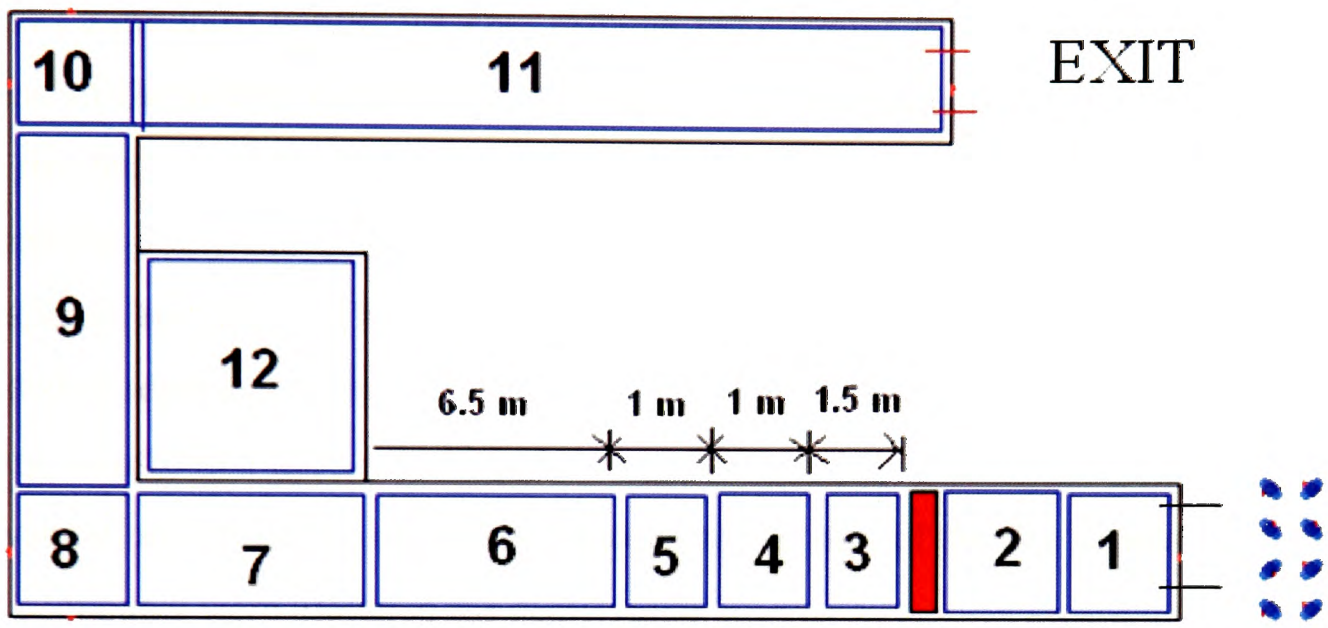

Figure 8.1 EXODUS zones and a hypothetical scenario

The lengths of zones were pre-determined based on the measurement locations where the concentrations of CO, CO_2 and O_2 were available. Each zone has an upper layer and a lower layer region. The upper layer spans from a height of 1.5 – 2.2 m and the lower layer region spans from 0.3 – 0.8 m. The experimental fire hazard data on each zone during the fire were determined from the values measured during the experiment at height 2.2m and in the middle of each zone. As mentioned in Chapter 6, the large-scale cable fire tests were, initially, intended to generate data for the validation of toxicity and combustion models only and hence the radiation fluxes were not measured during the experiments. Since the measured radiation was not available, the computed radiation fluxes at all zones were used in the experimental fire hazard. Also, thermocouple measurements at a height of 2.2m were not available at some zones near the fire and hence measured temperatures were shared between the zones as and where appropriate. On the other hand, the computed fire hazard data on each zone was determined from the average layer concentration that is calculated from the CFD simulation. Both the upper and lower layer regions are assumed to be uniform

with constant atmospheric values as measure/predicted at the given location. In 'buildingEXODUS' people are assumed to be exposed to upper layer concentrations when standing and lower layer concentrations when crawling. In the present study the 'crawling' option was disabled in order to expose them only to the upper layer concentrations.

The evacuation scenario considered in these simulations is somewhat artificial and involves a group of people walking through the corridor system from the hot side by the seat of the fire to the far exit (Figure 8.1). The occupants are initially protected from fire hazards until their response time expires. The response time is intended to sufficiently delay the occupants so as they can experience different levels of fire atmosphere severity. Therefore the response times used in the analysis are not intended to represent realistic values. The response times, measured from the start of the fire, considered here are, 500, 700, and 900 seconds (measured from the start of the evacuation simulation which corresponds to the start of the fire simulation) and all eight occupants were assigned the same value.

It should be noted that the start of the flashover event is determined to occur within the labyrinth at 723 seconds according to experimental observations and 776 seconds according to the simulations (Figure 8.2). In the context of this experiment, flashover is considered to be a local event, in the immediate vicinity of the burning cables and does not involve the entire corridor system. Hence, the response times of 500 and 900 seconds correspond to pre-flashover and post-flashover stages respectively.

The average hazard attributes values for the eight occupants for the three response times are given in Table 8.1-8.3. From the table it is observed that for all the response times (pre-flashover, during flashover and post-flashover), the FIN attribute and the evacuation times for both the computed and experimental fire hazard data are almost identical. However, the FIH attribute values differed more significantly.

This large difference in the FIH values between the two hazard data can be found in the $T^{3.4}$ dependence of the FIH_c with temperature (Equation 8.1). For example, the change in the incapacitation time with change in temperature is given in Table 8.4. It can be seen from the Table 8.4 that if the temperature is increased from 100^{o} C to 120^{o}

C (an increase of 20%) the incapacitation time is almost halved (decrease of 47%) and if the temperature is increased from 120° C to 140° C (an increase of 17%) the incapacitation time is again almost halved (decrease of 41%). Thus the time to incapacitation is sensitive to the air temperature. The temperatures in all the zones for both the measured and computed fire hazard during the evacuation process at three response times are given in Tables 8.5-8.7. The temperature difference between the experiment and the computation near the fire is ~30° C during pre-flashover regime (Response times of 500 and 700 seconds). Conversely, the difference in temperatures between the experiment and the computation near the fire is higher (~100° C) during the post-flashover regime (Response time of 900 seconds). At elevated temperatures, small changes in the temperature can have a large effect on the incapacitation time. Even though the predicted temperatures are considered to be good approximations to the measured temperatures, this can have a significant impact on the time to incapacitation. However, the overall outcome in terms of number of fatalities and evacuation times, does not appear to be significantly different.

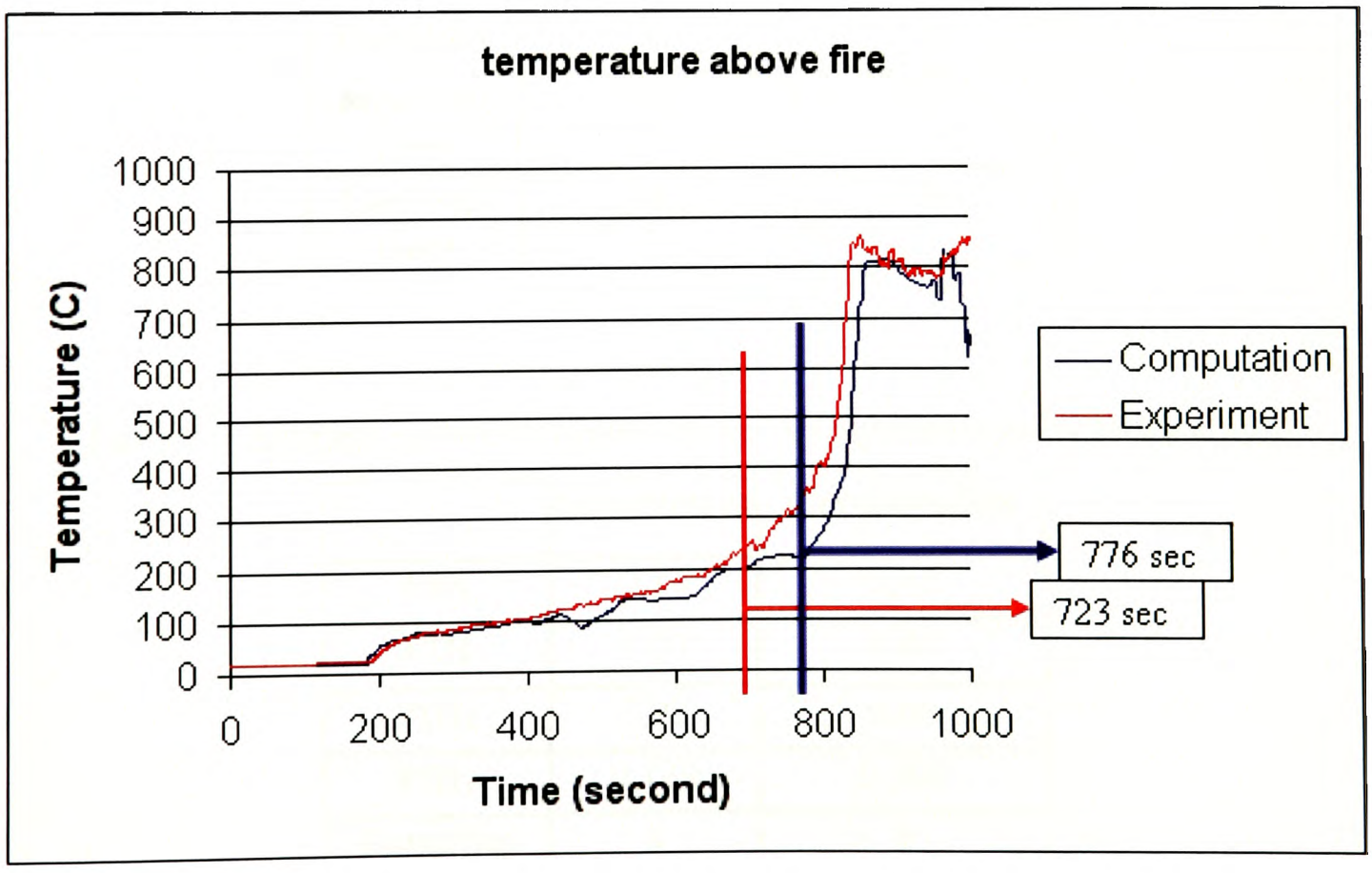

Figure 8.2 Onset of flashover during the NHMH cable fire (Test 8)

Table 8.1 Average hazard attribute values of response time of 500 seconds

	Experiment	Computation
FIN	0.05	0.05
FIH	0.06	0.02
FIHc	0.06	0.02
FIHr	0	0
Fatalities	0	0
First exit (sec)	571	572
Last exit (sec)	584	584

Table 8.2 Average hazard attribute values of response time of 700 seconds

	Experiment	Computation
FIN	0.07	0.08
FIH	0.2	0.09
FIHc	0.2	0.09
FIHr	0	0
Fatalities	0	0
First exit (sec)	771	772
Last exit (sec)	782	782

Table 8.3 Average hazard attribute values of response time of 900 seconds

	Experiment	Computation
FIN	0.14	0.17
FIH	1.07	1.01
FIHc	0.92	0.60
FIHr	0.139	0.408
Fatalities	8	8
First exit (sec)	-	-
Last exit (sec)	-	-

Table 8.4 Effect of variation in temperature on the Incapacitation times

Temp (C)	**Incapacitation time (min)**
100	8
120	4.26
140	2.52

Table 8.5 Zone temperatures for measured and computed fire hazard (pre-flashover)

Zone	500 seconds		540 seconds		580 seconds	
	Experiment (°C)	Computation (°C)	Experiment (°C)	Computation (°C)	Experiment (°C)	Computation (°C)
1	367	335	373	349	379	353
2	367	334	373	344	379	348
3	367	332	373	339	379	344
4	369	330	375	335	383	343
5	369	330	375	334	383	343
6	361	329	368	334	371	342
7	330	313	335	316	337	319
8	330	305	335	306	337	309
9	312	301	316	302	317	303
10	312	298	316	298	317	299
11	299	292	301	292	302	293
12	309	294	313	295	314	295

Table 8.6 Zone temperatures for measured and computed fire hazard (flashover)

Zone	700 seconds		740 seconds		780 seconds	
	Experiment (°C)	Computation (°C)	Experiment (°C)	Computation (°C)	Experiment (°C)	Computation (°C)
1	408	374	428	384	450	387
2	408	370	428	379	450	383
3	408	363	428	371	450	375
4	418	360	434	369	452	372
5	418	361	434	369	452	373
6	406	359	419	367	430	371
7	357	329	364	334	373	337
8	357	316	364	319	373	322
9	328	308	332	311	338	314
10	328	303	332	306	338	308
11	305	295	307	296	310	297
12	323	298	328	300	330	302

Table 8.7 Zone temperatures for measured and computed fire hazard (post-flashover)

Zone	900 seconds		940 seconds		980 seconds	
	Experiment (°C)	Computation (°C)	Experiment (°C)	Computation (°C)	Experiment (°C)	Computation (°C)
1	603	508	615	541	632	517
2	603	500	615	538	632	524
3	603	498	615	534	632	525
4	628	465	654	507	650	513
5	628	458	654	488	650	504
6	532	484	573	499	579	509
7	427	391	443	408	453	417
8	427	351	443	368	453	382
9	366	335	376	351	383	363
10	366	324	376	338	383	349
11	322	302	327	309	334	315
12	357	315	359	324	371	331

For the response time of 900 seconds, there were no survivors and Table 8.3 suggests that for this fire, the temperature was the critical component of the fire atmosphere driving survivability. The death locations for the 900 seconds based on computed and experimental fire environment are given in Figure 8.3. As the temperatures in the vicinity of the fire were higher in the experiment than those predicted by the fire simulation, the eight occupants passing through this region and exposed to these hazards have a shorter time to incapacitation than that found using the fire simulation hazard data. As a result, the eight occupants exposed to the experimental fire atmosphere are incapacitated and collapse before the occupants exposed to the fire model generated fire atmosphere. The bodies of the occupants exposed to the experimental fire atmosphere are therefore located closer to the fire than the bodies of the occupants exposed to the simulated fire. This is also likely to be the cause of the lower FIHc values and higher FIHr values for the victims of the computed fire compared to the experimental fire. However, it should be noted that the difference between the death locations for the computed and experimental hazard data is only a few metres but this is sufficient to place the victims within different hazard zones.

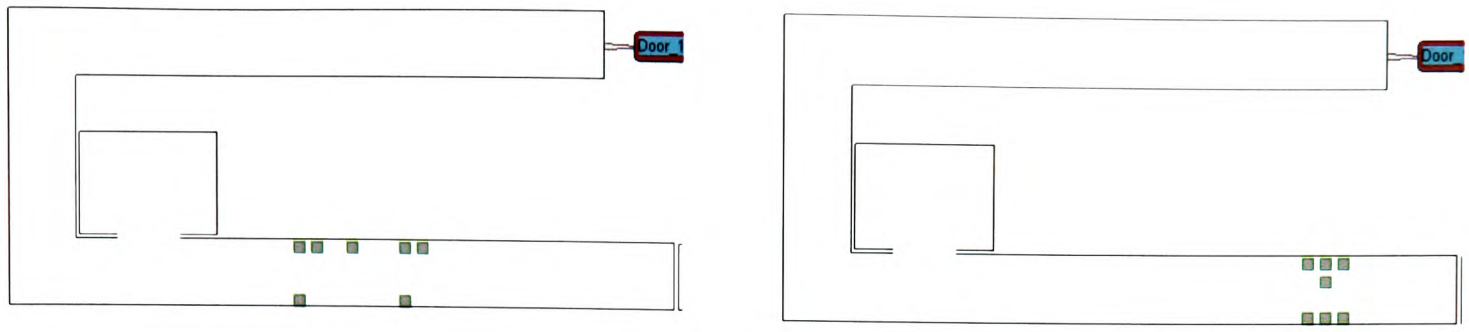

(a) Computed fire (b) Experimental fire

Figure 8.3 Death locations for response time of 900 seconds

In the present scenario, the times between 700 and 900 seconds were not considered for analysis because they were during the flashover period. During the flashover period there are likely to be large differences between predicted and experimental temperatures as during this period temperature change very rapidly. As there are likely to be great uncertainties in the precise value of the temperatures during the flashover period, there is also likely to be great uncertainty in the time to incapacitation. It is also worth noting that fire risk assessment associated with building design is usually concerned with pre-flashover evacuation analysis. It is therefore unlikely that life safety analysis will be undertaken during or post-flashover, at least as part of a fire engineered solution for a building design. Where this may be an issue is in post accident forensic investigation. In such applications it may be important to determine when a person died and/or where the body is likely to be found. Using computed data for the fire atmosphere may lead to uncertainties in the precise time of death, however, once again, it is probably that the overall conclusions as to the number of deaths will be reasonable. Overall, irrespective of the sensitivity of the FED values on temperature, the overall engineering conclusions regarding the survivability (overall evacuation time and likely number of fatalities) within the labyrinth evacuation system pre-flashover and post-flashover are identical regardless of whether the predicted or measured fire atmosphere is used.

8.3 Preliminary Assessment of Cable Fires on Building Evacuation

As mentioned in Chapter 6, the room at the corner of the first corridor was utilised in this sub-section to perform preliminary evacuation modelling on the effect of the cable fire environment simulated using STEM-LER model on the unfolding

population. To assess the effect of the fire environment on people evacuating, a hypothetical scenario is considered where eight people are located inside the room as shown in Figure 8.4.

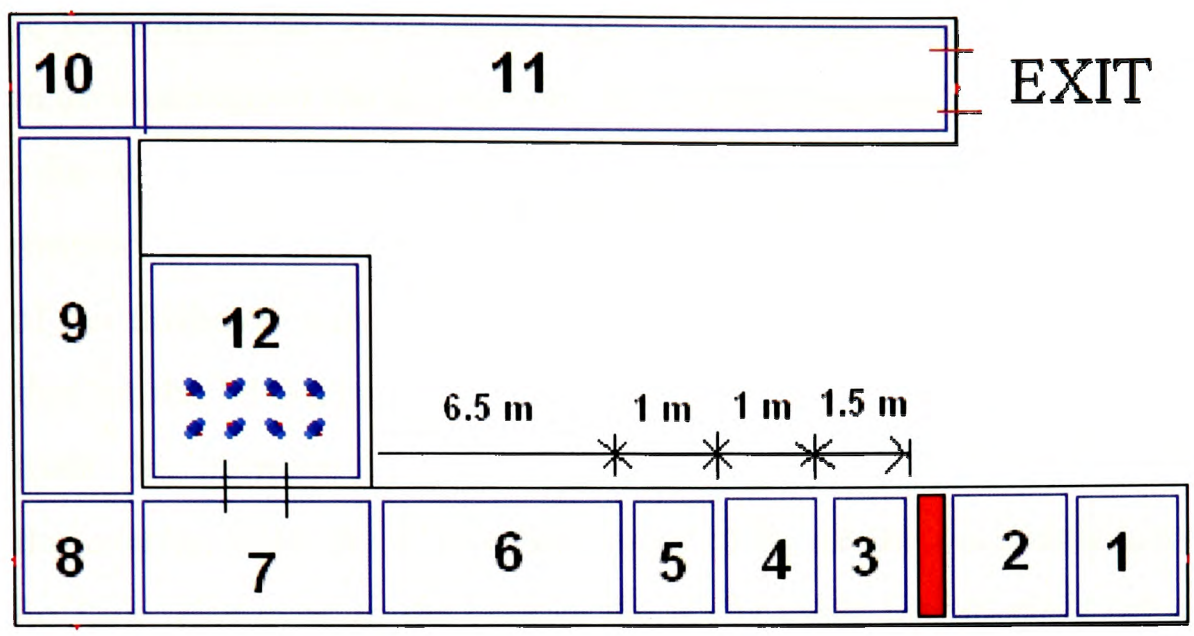

Figure 8.4 EXODUS zones and a hypothetical scenario

Simulations were carried out to obtain the suitability of the three power cable types for the given labyrinth corridor structure. The response time for each test is selected depending on the time at which the localised flashover starts. Based on the computed fire, the times at which localised flashover begins are given in Table 7.5. The time at which localised flashover starts, in the present investigation, is the time at which the temperature above the horizontal cable tray begins to rise rapidly to reach the peak value. In this analysis only computed fire atmospheres are used. It should also be noted that for the NYM cable fire test, HCL values were not measured in the experiment. Only predicted HCL values are available for analysis.

Table 8.8 Various times at which flashover starts

	NHMH- Test 8 Inlet open and 1m Weir	NHMH-Test 10 Inlet closed and 1.5m Weir	NYM-Test 5 Inlet closed and 1m Weir	RZ1-K-Test 7 Inlet open and no Weir
Experiment (seconds)	720	540	570	1540
Computation (seconds)	800	540	540	1600

The average FIH, FIN, FLD_{HCL}, FIC_{HCL} attribute values for all the eight occupants and the fatalities during the four cable fire test cases are given in Table 7.6 for a response time of 540 seconds (minimum flashover start time among the four tests). While the occupants start to evacuate after 540 seconds, they are initially located some 10m downstream of the fire source. So while 540 seconds is close to the time to flashover for two of the cables, as described earlier, this flashover event is a localised event restricted to the immediate vicinity of the cables. Thus the occupants are outside of the flashover zone. With a response time of 540 seconds (pre-flashover) we find that for the NHMH and RZ1-K cables it is possible for the eight occupants to escape from the corridor system well before no-survivable conditions develop. Indeed, the average FIH and FIN values incurred by all the occupants are very low (see Table 7.6). However, in the case of the NYM cable fire all eight occupants are predicted to succumb to the fire atmosphere.

Table 8.9 Average values of hazard effect attributes for a response time of 540 second

Average values	NHMH- Test 8 Inlet open and 1m Weir	NHMH-Test 10 Inlet closed and 1.5m Weir	NYM-Test 5 Inlet closed and 1m Weir	RZ1-K-Test 7 Inlet open and no Weir
FIN	0.05	0.05	0.22	0.05
FIH	0.01	0.0	0.31	0.0
FLD_{HCL}	0	0	0.024	0
FIC_{HCL}	0	0	2.09	0
Incapacitated	0	0	8	0

In the NYM fire scenario, atmospheric values of HCL to which the population are exposed reach critical values causing the incapacitation of all eight occupants. Just as the occupants start their evacuation, (shortly after 540 seconds), the predicted atmospheric concentration of HCl was approximately 1000 ppm in zone 7. It should be noted that had a HCL tolerance value of greater than 1000 ppm been implemented it is possible that the occupants would have travelled further through the corridor system or even exited before dangerous levels of HCL were attained. However, since

the FIC attribute is linked to the occupant's mobility, as FIC increases, the occupant travel speed decreases thus prolonging exposure to other dangerous fire hazards. As can be seen in this case, average FIH and FIN values for these occupants at the point of incapacitation are large. This suggests that if they are not removed from the fire environment, they are likely to perish due to heat exposure or inhalation of narcotic gases.

Hence, the case involving NYM cable fire case was the worst scenario and the sole cause for the incapacitations was the HCL gas released during the fire. The incapacitation locations of all the eight occupants during the NYM cable fire scenario is shown in Figure 8.5. It can be seen from the figure that all the incapacitation locations were just outside the room.

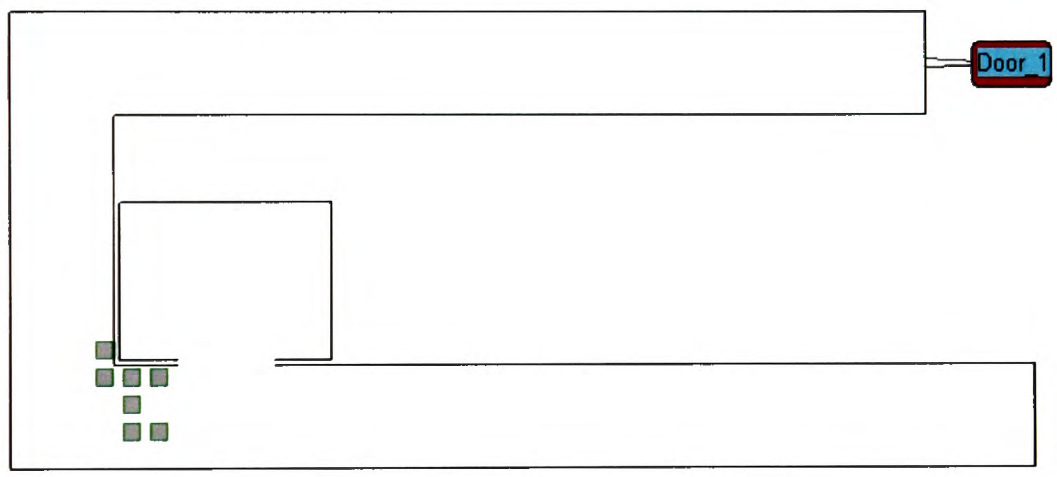

Figure 8.5 Incapacitation location during NYM cable fire (Response time = 540 sec)

8.4 Concluding Remarks

This chapter dealt with two aspects of evacuation modelling. The first aspect was to investigate the use of computed versus experimental fire hazard data for assessing survivability within buildings using evacuation models incorporating the Fractional Effective Dose (FED) model. While the concept is widely used in fire risk assessment, little comparison with the thorough experimental data has been performed to test the sensitivity of the FED models and their overall impact on the unfolding evacuation. A cable fire test involving NHMH cable (TEST 8) was considered for a hypothetical evacuation scenario involving a group of people walking through the

corridor system at three different times during the fire, i.e. 500, 700 and 900 seconds corresponding to three different stages of fire development. Only for a starting time of 900 seconds (post-flashover environment) were there no survivors. The FED model was found to be very sensitive to the precise nature of the temperature distribution within the fire atmposhere. Relatively small differences between computed and measured temperatures produced rather large differences in computed FIH values. However, irrespective of the sensitivity of the FED values on temperature, the overall engineering conclusions regarding the survivability (overall evacuation time, likely number of fatalities and death locations) within the labyrinth evacuation system for pre-flashover and post-flashover, were identical regardless of whether the predicted or measured fire atmosphere was used.

In the second part, a preliminary assessment of the impact of fires produced by four different types of cables on building evacuation has been carried out. To assess the effect of the fire environment on evacuation, a hypothetical scenario was considered where eight people located inside compartment were required to evacuate through the corridor system during the pre-flashover period. For each cable this was some 540 seconds after the fire had started. It was found that for the NHMH and RZ1-K cables it was possible for the eight occupants to escape from the corridor system well before non-survivable conditions developed. Indeed, the average FIH and FIN values incurred by all the occupants were very low. However, in the case of the NYM cable fire all eight occupants are predicted to succumb to the fire atmosphere and the sole cause for the incapacitations was the HCL gas released during the fire.

To sum up, the conclusions that can be drawn from the above simulations were as follows:

- The FED attribute is sensitive to temperature which can be found in the $T^{3.4}$ dependence of the FIH with temperature.
- Irrespective of the sensitivity of the FED values on temperature, the overall engineering conclusions regarding the survivability within the labyrinth evacuation system for pre-flashover and post-flashover, are identical regardless of whether the predicted or measured fire atmosphere is used.

- Evacuation simulation results for the four cable fire tests for a pre-flashover scenario revealed that all the occupants in the NYM cable fire test are likely to be incapacitated prior to exiting. The sole cause for the incapacitation was the high level of HCL concentration generated during the NYM cable fire.

Chapter 9

Conclusions

9.1 Summary

Real fire incidents involve complex fuels such as combustible plastics. Almost all of the investigators modelling the cable fires have targeted their research on predicting the mass loss rate, flame spread or heat release. Also, the majority of investigations modelling the CO and CO_2 during fires deals with liquid or gaseous fuels which have simpler molecular structure and are often easy to conduct combustion experiments. Hence, it is imperative to model the real fires involving realistic fuels to improve the available toxic gas hazard modelling. The objectives set for the present research were as follows:

1. Literature review on the available toxicity models for the simulation of toxic combustion products formation in fires involving complex solid fuels.
2. Development of a methodology to predict levels of CO and other toxic products generated and transported to distant locations from the fire origin.
3. Identification of appropriate and corresponding toxicity data required for the materials to be considered in the present study as inputs to the model from the bench scale experiments.
4. To conduct large scale fire test and obtain a comprehensive set of fire data in order to validate the above toxicity model.

5. Validation of the methodology developed in the present study to predict the final levels of CO and other toxic products generated and transported to distant location from the fire origin.
6. Validation of the experimental data (yield correlations) obtained from the bench-scale tests (Purser furnace) in predicting the large-scale fires.

In Chapter 2, a detailed literature survey was carried out with the focus on the following

- To gain the present understanding on the formation mechanisms of CO and other toxic combustion products and their transport in fires via hood experiments, compartment fire experiments and full-scale experiments. Emphasis was given on combustible polymers like wood, plastics etc.
- Review on the state-of-the-art combustion and toxicity models in modelling of the complex solid fuels in real-scale fires.
- Review on the available large-scale experimental data for combustible polymers to validate the combustion, toxicity and the transport model.

Chapter 3 described the theoretical basis for the field modelling approach. In addition, turbulence model, radiation model and combustion model used in the present investigation were also discussed.

In Chapter 4, a **S**calar **T**rasport **E**quation based **M**odel using the **L**ocal **E**quivalence **R**atio (**STEM-LER** Model) to close the source terms was proposed to model accurately the generation of combustion products and the transport of products to remote locations. Separate species transport equations for fuel, CO, CO_2, O_2 and H_2O are solved using the yield correlations obtained from a bench-scale toxicity method which in the present work was the Purser furnace. This chapter was also devoted to give a brief account on the various fire simulation works which were based on the equivalence ratio concept.

In Chapter 5, CFD simulations of the fire environment inside the Purser furnace were carried out to understand the working of IEC 60695-7-50 standard toxicity test

method (Purser furnace). The temperature values inside the mixing chamber were compared between the experiment and computation for 750^0 C furnace temperature case without sample burning. Further, simulations for the NYM and NHMH cables burning at 800^0 C furnace temperature were also carried out using the yield versus phi curve obtained from the Purser furnace tests which were conducted at University of Bolton. The computed CO and CO_2 yields were then compared with the experimental yields.

For the reasons stated in the beginning of Chapter 6, full-scale fire experiments involving cables were performed and conducted a detailed measurement of the toxic combustion gases. The series of cable fire tests were performed within a real-scale corridor at the Department of Fire Technology at SP Swedish National Testing and research Institute during October 2005. The comprehensive set of experimental data thus obtained is utilized to validate the STEM-LER model proposed to simulate the generation and transport of combustion species in real-scale fires involving combustible plastics. Chapter 6 gave a brief description about the experimental setup, instruments used, test procedures, and some important results for four cable fire tests.

Using the STEM-LER model described in Chapter 4, simulations of four test cases involving three different cable types were carried out and discussed in Chapter 7. The predicted temperatures and volume fractions of CO and CO_2 in the upper layer (h = 2.2 m) at locations 5, 9 and 15 were validated with the experiments. Along with the validation of the model, analyses were made on the modelling of CO oxidation and the benefit of the modified Eddy Break-Up combustion model using the simulation of one of the large scale cable fire test.

9.2 Conclusions

Precise modelling of the generation of combustion products requires a detailed knowledge of their chemistry. Burning behaviour of most fuels are complex in nature, and the kinetic mechnisms are not well defined if not least understood. Real fire incidents involve complex fuels such as combustible polymers. Three types of cable materials having different fire retardant mechanisms were selected for this study. To allow an estimation of the fire hazard, the amount of each toxic product produced per

unit fuel burned must be assessed, i.e., the species yield must be estimated. The species yields were obtained from the bench-scale experiments. Purser furnace experiement is an IEC 60695-7-50 and ISO/CD 19700 standard test method to measure the yields of combustion products at various controlled equivalence ratios. The main focus of the present study was to develop a CFD based methodology to predict the real-scale fires involving complex building materials by using the combustion product yield data obtained from the Purser furnace.

From the comparison of predicted CO, CO_2 concentrations and temperatures with the experimental data, it was evident that the simulation results were in reasonable agreement with the experiments. The STEM-LER model was able to predict well the CO and CO_2 concentrations through out the corridor i.e from location 5 to 15. The model was able to predict the final CO concentrations at location 15 reasonably well which was 30 m away from the fire. The final CO_2/CO ratio at location 15 was also accurately captured using the STEM-LER model demonstrating its ability to calculate the local vitiation conditions inside the fire plume and simulate the generation of species in the combustion region.

Finally, a preliminary assessment on the effect of cable fires on building evacuation was performed for an artificial evacuation scenario at two different response times. Evacuation simulation results revealed that there were no survivors during the NYM cable fire test. The sole cause for the fatalities was the high level of HCL concentration generated during the NYM cable fire.

Apart from the development of STEM-LER methodology, the present study has addressed the research questions raised in Chapter 1 which were as follows:

- ✓ *How can the species generation and transport in real-scale fires be predicted using the yield data obtained from the Purser furnace bench-scale tests (IEC 60695-7-50 and ISO/CD 19700 standard test method)?*

Production rates of CO and CO_2 in g/g of polymer consumed under various vitiation conditions (GER) were obtained using a tube furnace called Purser furnace. It is assumed that each control volume is similar to a miniature Purser furnace. The

combustion conditions within a control volume and the associated LER is assumed approximately equivalent to that in the Purser furnace with the same value of GER. In the present study, the LER is calculated from the fuel to air ratio as

$$LER = \frac{\left(\frac{Fuel}{Air}\right)}{\left(\frac{Fuel}{Air}\right)} \quad \begin{matrix} \text{control volume} \\ \\ \text{stoichiometric} \end{matrix}$$

The correlation between yields of CO & CO_2 and GER obtained from the Purser furnace tests is then used in this study to model source terms in the transport equation for CO and CO_2. Thus by equating GER in the correlation with the LER in each control volume, generation rates of species are estimated. With these generation rates, the transport of species in fires and through out the enclosure was modelled by the corresponding transport equations.

The simulation results in Chapter 7 also proved that the yield correlations obtained from the Purser furnace experiments can be used to predict the local generation of combustion products in real-scale fires. This also testifies that the fire environment created inside the Purser furnace correlates well with the real-scale fires.

✓ *Can CFD simulate the thermal and flow conditions inside bench-scale experiments like Purser furnace? How CFD can be used as a design tool to improve the performance of the Purser furnace?*

Purser furnace, a bench-scale toxicity test method is an IEC and ISO standard test method designed to reproduce the decomposition conditions similar to the different stages of a real fire. It was identified that the species yields as a function of equivalence ratio for the three cable materials were the required toxicity data to pursue the present investigation. Simulations of flow and fire condition inside the Purser furnace were carried out to understand the modus operandi of the Purser furnace toxicity test method and to demonstrate the ability of CFD in simulating the fire conditions inside small-scale experiments like the Purser furnace

The temperature comparison inside the mixing chamber showed a good quantitative agreement between the experiment and computation. The simulations confirmed that the secondary air flow works well in terms of generating a uniform mixture within the dilution chamber.

Burning of NYM and NHMH cables inside the tube furnace at 800^0 C were also simulated using the toxicity data measured at the University of Bolton and validated with the experimental yields. The comparison shows good agreement between experiment and the computational yields. They also confirm the assumption made in the experiments that the species concentrations within the chamber should be nearly uniform for the purpose of obtaining accurate and meaningful measurements of yields data.

Hence, the ability of CFD to simulate fire environment inside the tube furnace was demonstrated in these simulations which is a first step towards using CFD as a design tool to improve the performance of the Purser furnace.

Further, simulations may be used to study the effect of primary air flow rate, furnace temperature, geometry of the tube furnace, fire dynamics and quenching of fire effluent by secondary air on final yields which is difficult to quantify experimentally.

- ✓ *How are the combustion models important in predicting the species concentrations at distant locations? Eddy Break-Up model [Magnussen and Hjertager, 1977] under predicts the combustion rate in fuel-rich regions, how this model can be modified to improve the prediction?*

The combustion rate and quenching of the fire plume have a significant impact on the concentration of products at distant locations from the fire origin. The EBU model is the most widely and successfully used combustion model in fire simulations up to date. However, it is also well-known that EBU model still under-predicts the combustion rate in fuel-rich regions i.e. significant CO is generated in the fire plume, for a given oxygen concentration and the actual fuel consumed is more than that is predicted by the EBU. In the present investigation, the EBU model is modified to calculate the actual fuel involved in the fuel-rich combustion region. In Chapter 7

(section 7.4.2), the EBU model is compared against the modified EBU proposed in the present study. From the comparison it is evident that the modified EBU is able to predict the species concentration and temperatures better at far locations.

Therefore, the combination of the modified EBU and the set of transport equations for species which makes use of the yield correlation obtained from the Purser furnace to model the source term were able to predict the toxic combustion products generation and its transport in real fires involving complex fuels.

- ✓ *How does the fire environment affect the movement of people during evacuation? Can the computed fire environment in real-scale building scenarios be used to provide good engineering judgements such as the 'survivability' and 'suitability of materials'?*

Performance based fire safety engineering involves essentially the determination of two factors, the time available to the occupants for safe egress, sometimes referred to as the Available Safe Egress Time (ASET) and the time that is required by the occupants to evacuate from the structure generally referred to as the Required Safe Egress Time (RSET). For the building to be considered 'fire-safe', the RSET, plus some safety factor, should be less than the ASET. The RSET is usually determined through evacuation simulation. A more sophisticated approach is to incorporate the predicted fire atmosphere within the evacuation model and directly determine the impact of the fire on the ability of the simulated occupants to safely evacuate. This may be determined if the evacuation model incorporates Fractional Effective Dose (FED) models and incorporates impact of smoke on reduced visibility and hence mobility. Advanced egress models such as 'buildingEXODUS' has this type of capability.

The FED model considers the toxic and physical hazards associated with elevated temperatures (FIH), CO, CO_2 and low O_2 (FIN), and other toxic and irritant gases like HCN and HCl (FIC) and takes into account the visual obscuration effect caused by smoke into account using the Jin data.

In Chapter 8, a cable fire test involving NHMH cable (TEST 8) was considered for a hypothetical evacuation scenario involving a group of people walking through the corridor system at three different times during the fire, i.e. 500, 700 and 900 seconds corresponding to three different stages of fire development. Only for a starting time of 900 seconds (post-flashover environment) were there no survivors. The FED model was found to be very sensitive to the precise nature of the temperature distribution within the fire atmosphere. Relatively small difference between computed and measured temperatures produces rather large differences in computed FIH values. However, irrespective of the sensitivity of the FED values on temperature, the overall engineering conclusions regarding the survivability (overall evacuation time, likely number of fatalities and death locations) within the labyrinth evacuation system for pre-flashover and post-flashover, were identical regardless of whether the predicted or measured fire atmosphere was used.

Chapter 10

Future Work

CFD as 'Design-tool' to improve bench-scale toxicity experiments

The accuracy of prediction of combustion products generation depends mainly on the accuracy of toxicity and combustion data obtained from the small-scale experiments. Hence, the Purser furnace toxicity test method needs to be further investigated in analysing the performance and accuracy of the yield data. For example, simulations may be used to study the effect of primary air flow rate, furnace temperature, geometry of the tube furnace, fire dynamics and quenching of fire effluent by secondary air flow on final yields which is difficult to quantify experimentally at present.

Modelling the effect of temperature on species yields

For the more detailed prediction of the generation and transport of combustion products in real-scale fires, some more additional toxicity data are needed. For example, the data on the effect of temperature on yield vs equivalence ratio correlations is required to incorporate the effect of temperature on species production rates. Data on the effect of residence times on the yields might help in including the non-equilibrium chemistry effects affecting the species generation rates.

Modelling the effect of oxygen concentrations on species yields

It is a fact that the species yields are affected by the oxygen concentrations. Some researchers claim that the species yields can vary up to 200% by reducing the oxygen concentration by 50%. Hence, adding this to the previous suggestion, the yield correlations should be a function of equivalence ratio, temperature and the oxygen concentration.

Integrating various fire sub-models to model 'external burning' and 'back-draft'

It is evident that the STEM-LER model framework has been built on a strong foundation i.e. using scalar transport equations. The source terms of the individual species transport equation provides ample scope for the inclusion of various physical processes affecting the generation rates of species. By incorporating additional features like flame spread model, flammability data, kinetics, and advanced yield data correlations (i.e yields as a function of temperature and oxygen concentration), the STEM-LER model will be able to predict more accurately the real fires involving complex combustible fuels.

Improving the heat transfer and turbulence model to predict the flow field better

Various factors that might have significant impact on the species concentrations and temperatures at distant locations are convective heat transfer, radiative heat transfer, turbulence models and multi-component diffusion process etc. [Wen et al., 2001; Lui et al., 2002; Woodburn and Britter, 1996]. Hence, to predict the combustion product concentrations and temperature accurately at distant locations far from the origin of fire, the above processes need to be modelled accurately.

Use of CFD and Evacuation models in Euro-Classification

In 1988, the European Commission released the 'Construction Product Directive (CPD)'. The main objective of this directive is to 'remove technical barriers to trade arising from national laws and regulations in Member States of the EU, thus enabling the single European market in construction products'. Hence, the purpose of the CPD

is trade liberalisation. In the same year it was decided that fixed cables within buildings should be regarded as one of the construction products. Euro-classification rates the cables in terms of a number of parameters viz., fire growth, heat release, flame spread, dripping and smoke. These parameters for any cable products is normally assessed by prescriptive standards such as single and bunched vertical burning. Essentially these tests concern fire propagation on a pass/fail basis.

Cable producing companies are working on a mission to change the CPD regulations towards performance based Euro-classification. In order to change the regulations such as CPD, real and quantifiable benefits needs to be brought out. Also a detailed quantitative risk assessment corresponding to different building materials can be performed for any building scenario to decide upon the safest material. Carrying out real-time CFD fire simulations can be time consuming and hence an array of CFD simulation can be done in advance for various materials. This 'CFD library' can then be linked to the EXODUS in real-time which can be used as a tool-kit by the construction technicians to conduct a quick quantitative risk assessment to decide upon the suitability of any material.

Appendix A

A.1 Measurements and Recordings during Experiments

A.1.1 Gas Analysis

Each gas analysis consisted of a sampling probe and sampling line of 8 mm copper tubing. A schematic diagram of the sampling set-up is shown in Figure A.1. Each pair of sampling lines had approximately the same length to obtain similar response times. On the analyser side of the sampling line, a short piece of Teflon tubing was connected to the sampling line and to a small filter unit. After the filter, the gas passed a membrane pump which was connected to the switch valve.

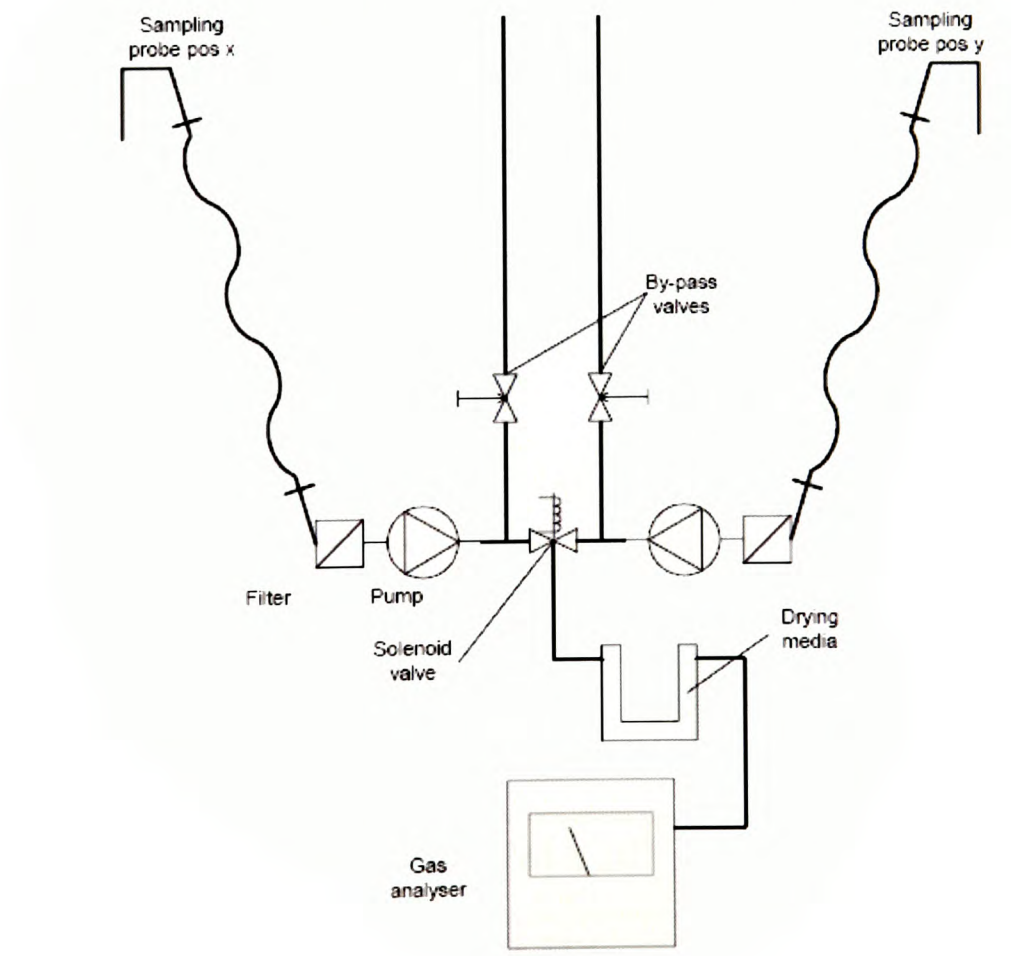

Figure A.1 Gas analyses arrangement

After this valve, the gas passes through a U-tube with drying media (Drierite) before entering the gas analyser. In order to ensure a gas flow through the sampling line, even when the switch valve was in the closed position, there was a T-connection between the pump and the valve providing a by-pass flow.

The gas analysers used were selected for various measuring positions depending on their measurement range. The instrument having the highest range for CO was located closest to the fire source while others were used further away. A list of the instruments used and their ranges is presented in Table A.1. Measurements of CO_2, CO and HCl were made using an on-line FTIR technique at sampling position 4. A BOMEM MB 100 FTIR spectrometer with a heated gas cell (150° C) was used for the measurements.

Table A.1 List of analysers and their ranges

Instrument no.	**Type of Instrument**	**Range**
1	BOMEM MB-100 FTIR	CO 0-8%, CO_2 0-20%, HCl 0-0.5%
2	Maihak 'UNOR 6N'	CO 0-10%
3	LH 'Binos 100'	CO 0-3%, CO_2 0-20%
4	Siemens 'Ultramat 22P'	CO 0-1%, CO_2 0-10%
5	Siemens 'Ultramat 22P'	CO 0-3%, CO_2 0-10%
6	LH 'Binos 100'	CO 0-3000 ppm, CO_2 0-20%
7	Rosemount 'Binos 100'	CO 0-10%, CO_2 0-30%
8	Leybold-Heraeus 'Binos'	CO 0-1%, CO_2 0-10%
9	Maihak 'multor 610'	CO 0-5000 ppm, CO_2 0-10% O_2 0-21%
10	M&C 'O_2 analyser PMA 10'	O_2 0-30%
11	Siemens 'Oxymat 5E'	O_2 15-21%
Phi- meter	M&C 'O_2 analyser PMA 10'	O_2 0-100%

A.1.2 Calibration tests

Each instrument was calibrated according to instrument specific instructions. The zero was set using nitrogen as the calibration gas (or 16 % O_2 for some oxygen analysers) and three different calibration gases was used for the span calibration. The calibration gases had the following composition, 0.25 % CO + 6 % CO_2, 0.6 % CO + 6 % CO_2, 2.5 % CO + 6 % CO_2. Ambient air was used for the oxygen analysers. The gas was flushed around the sampling probe inside the corridor which also allowed a check of the entire sampling system. After calibration of each instrument using the displayed value at the instrument, the output signal in mV was logged and a conversion factor calculated to achieve a direct reading on the data logging computer. The sampling lines, instruments and conversion factors were checked daily by using the procedure described above and any necessary corrections were made.

In order to determine the total response time for each instrument (sample transport time and instrument response), a calibration test was performed before the main test series. This was performed using the normal calibration routine but allowing the calibration gas (0.25% CO and 6% CO_2) to flush around each sampling probe for a couple of minutes in order to see the instrument response during a number of switch sequences. The time delay between the operation of the switch and the first response from the instrument varied slightly depending on the instrument (gas flow, instrument response, gas concentration, etc.) but was of the order 5-15 seconds. When splitting the signal from each instrument during the data evaluation process, only a part of the 30 seconds sampling sequence was used in order to avoid the signal when the instrument was changing from the different concentrations in the sampled locations (see example in Figure A.2).

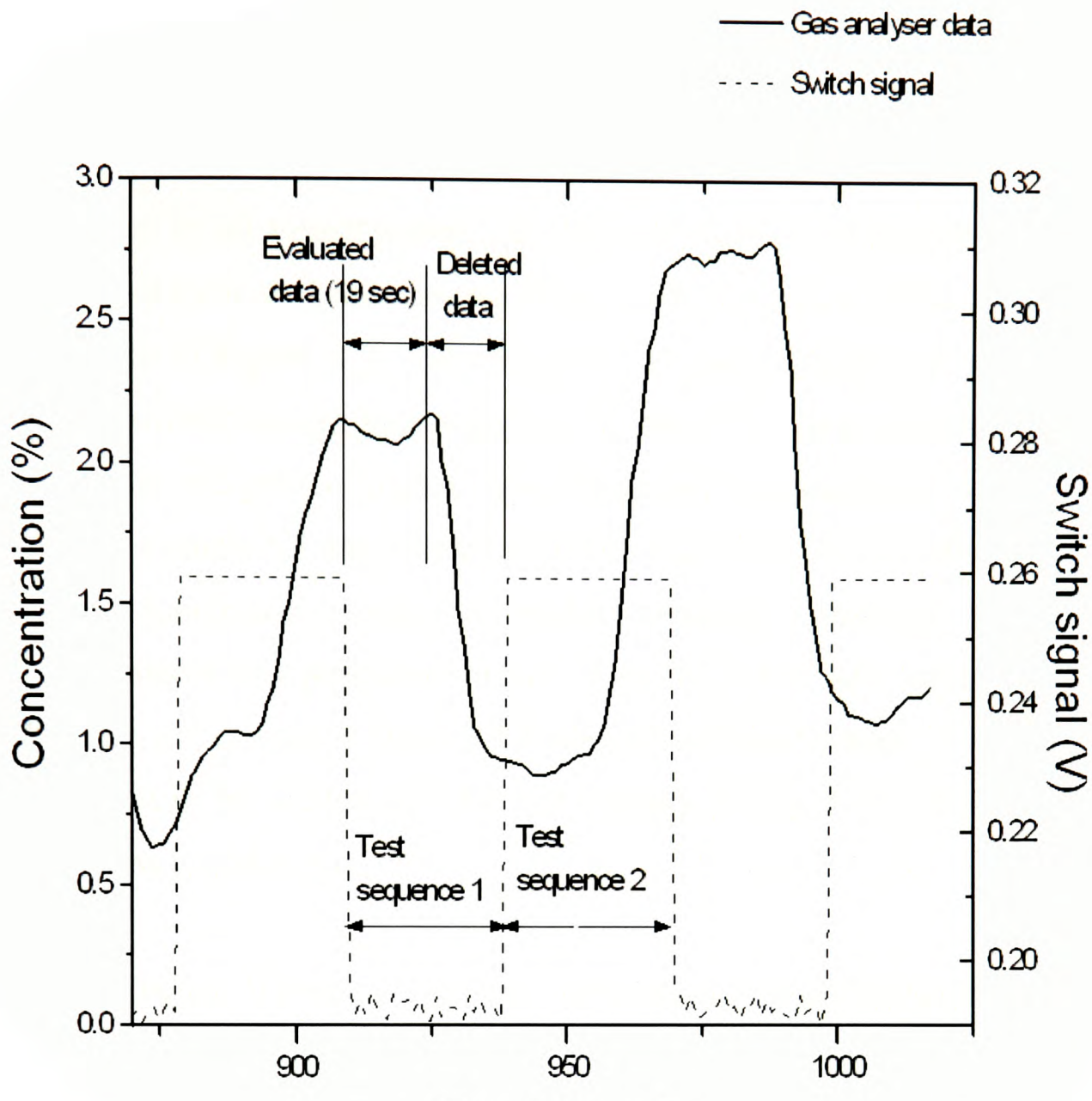

Figure A.2 Example of signal from gas analyzer during a number of switch sequences and the selected time sequences during data evaluation (Results from Test 8, CO instrument at position 10 and also position 9)

A.1.3 Smoke obscuration

The smoke obscuration across the corridor was measured at a total of six positions, five in the corridor and one in the adjacent room, as seen in Figure A.3. The measurements were made at 2.2 m above the floor for positions no. 6, 9 and 10 (inside room), and at 2.0 m above the floor for positions no. 12, 13 and 15. A 5 mW laser with 650 nm wavelength was mounted on one side of the corridor and a GaAsP detector with a large detection area on the opposite, giving a beam length of 2.0 m. Inside the room (position 10) the laser and detector were mounted on a rig along the centre of the ceiling to provide a beam length of 2.0 m.

A.1.4 Video recordings and visual observations

As a complement to all measurements, the fire development and smoke generation was also recorded by four video cameras. These were designated V1 to V4 and their location is shown in Figure A.3. The cameras were placed outside the corridor and faced into the corridor through glass windows. Camera V1 was positioned at the inlet end of the corridor and gave a detailed view of the cable tray and the fire development during the tests. Camera V3 was located in the far end of the first corridor and aimed towards the fire source and recorded the smoke movement at soffit #2. When a weir was used, the camera was positioned about 1.3 m above the floor while in the tests without the weir, it was located about 0.5 m above the floor. Camera V2 recorded the smoke movement in the second corridor and Camera V4 the third corridor and was aimed towards the corridor exit.

In order to have points of reference for the video cameras, luminous EXIT-signs were mounted on each side of soffit #1 and at the end of the second corridor (visible for V2). At position 6, 9, 12, 13 and 15 (corresponding to the location of the lasers), reflective markings were also mounted on a pole along the corridor wall. The markings were positioned at every 0.5 m above the floor. The visual observations made during the tests and recorded in the protocol were mainly made from the inlet end of the corridor, either through the 1.0 m^2 opening or through the adjacent observation window. There was also a window in the wall at position 3, making it possible to study the fire spread along the cable tray during the tests. In addition, there were a number of windows making it possible to look into the room and the corridors (including those for the video cameras).

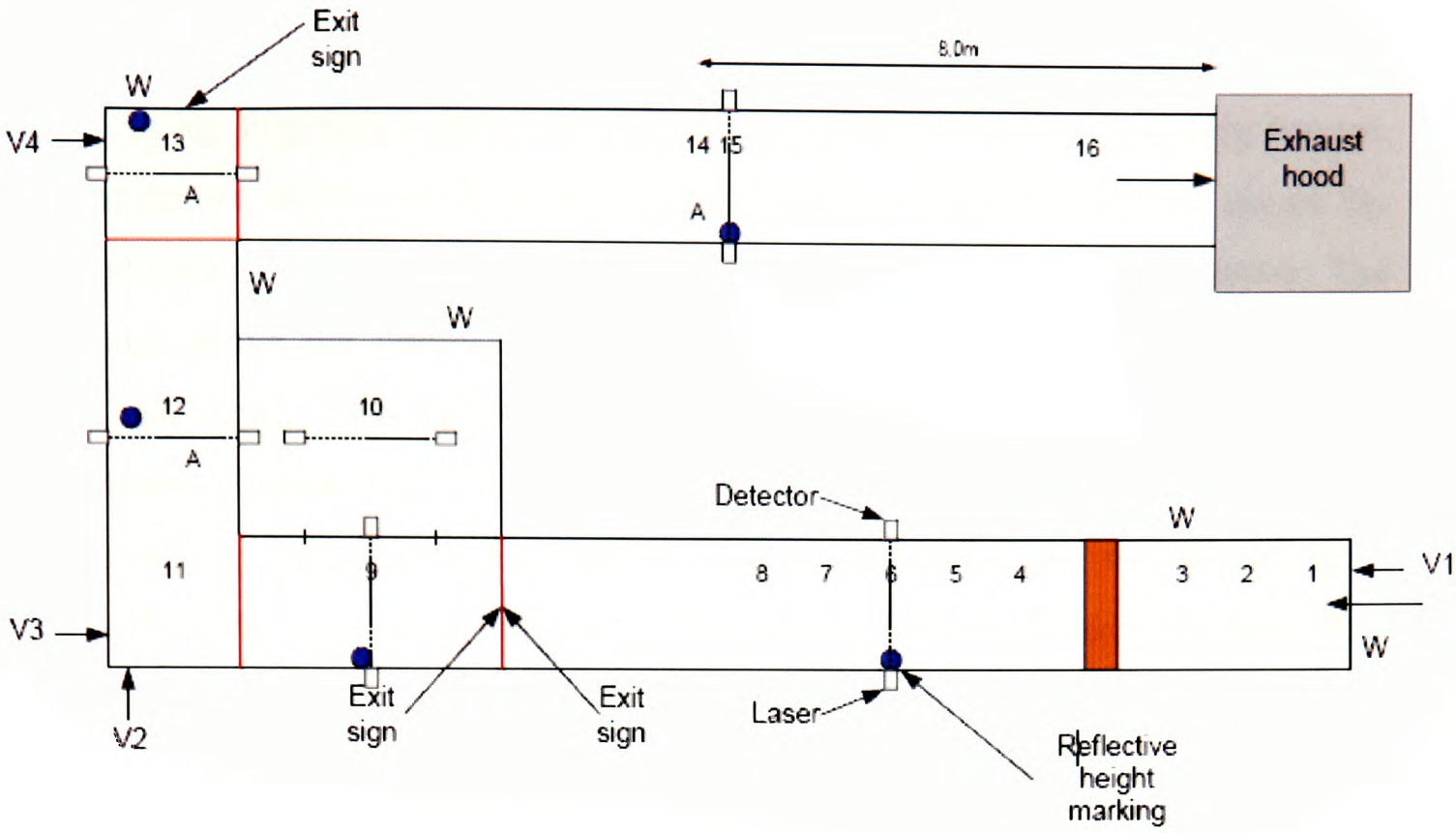

Figure A.3 Location of smoke measurements, video cameras (V1-V4), exit signs, reflective height markings and additional windows (W) for observations during the tests.

A.1.5 Data acquisition system and presentation of the results

The various instruments and sensors, including the HRR system, were connected to five Solartron IMP 5000KE data loggers, all controlled by a PC computer using LabView software [Wells, 1995]. The data was recorded at a rate of one scan per second.

A.2 Results and Discussion

In total, 10 fire tests were conducted and a summary of the test conditions is given in Table 6.2. Six test cases other than the four described in Chapter 6 is outlined in this section.

A.2.1 RZ1-K Cable fire (Test 1) – Inlet open and No weir placed

During the first test, RZ1 type cables (see Table 6.1 for its physical and chemical properties) were involved. Total 33 cables were burnt during the fire test which lasted

upto 4500 seconds. The 1 m^2 vent in the floor level was kept opened during this test. The load cell data is shown in Figure A.4 and the total mass lost during the test was around 8.11 kg. Figure A.5 shows the temperature above the cable fire during the test. The temperature above the horizontal cable tray was measured 10 cm above the horizontal cable tray and 6 cm below the ceiling and at the middle of the corridor. The temperature above the vertical cable tray was measured 10 cm above the top of vertical cable tray. Two temperature peaks were observed from the temperature measurements (Figure A.5). The first temperature peak corresponds to the peak mass loss rate of the cables mounted on the vertical cable tray and the second peak corresponds to the peak mass loss rate of the cables mounted on the horizontal cable tray. The peak temperature above the horizontal cable tray and the vertical cable tray were around 800^0 C and 820^0C respectively. The time to reach peak temperature above the vertical cable tray was around 2400 seconds. The total heat release rate (HRR) measured by the calorimeter system during Test 1 is provided in Figure A.6 and the peak HRR was around 220 kW.

Since the vertical cable tray cover was fixed to the frame with only two screws at the lower end, a part of the cover opened up during the test. This opening up of the cover might have resulted in additional air supply and a more intensive fire. During the test, the weight loss measurement was disturbed, probably due to thermal expansion of the cable tray and the supporting system (see Figure A.4).

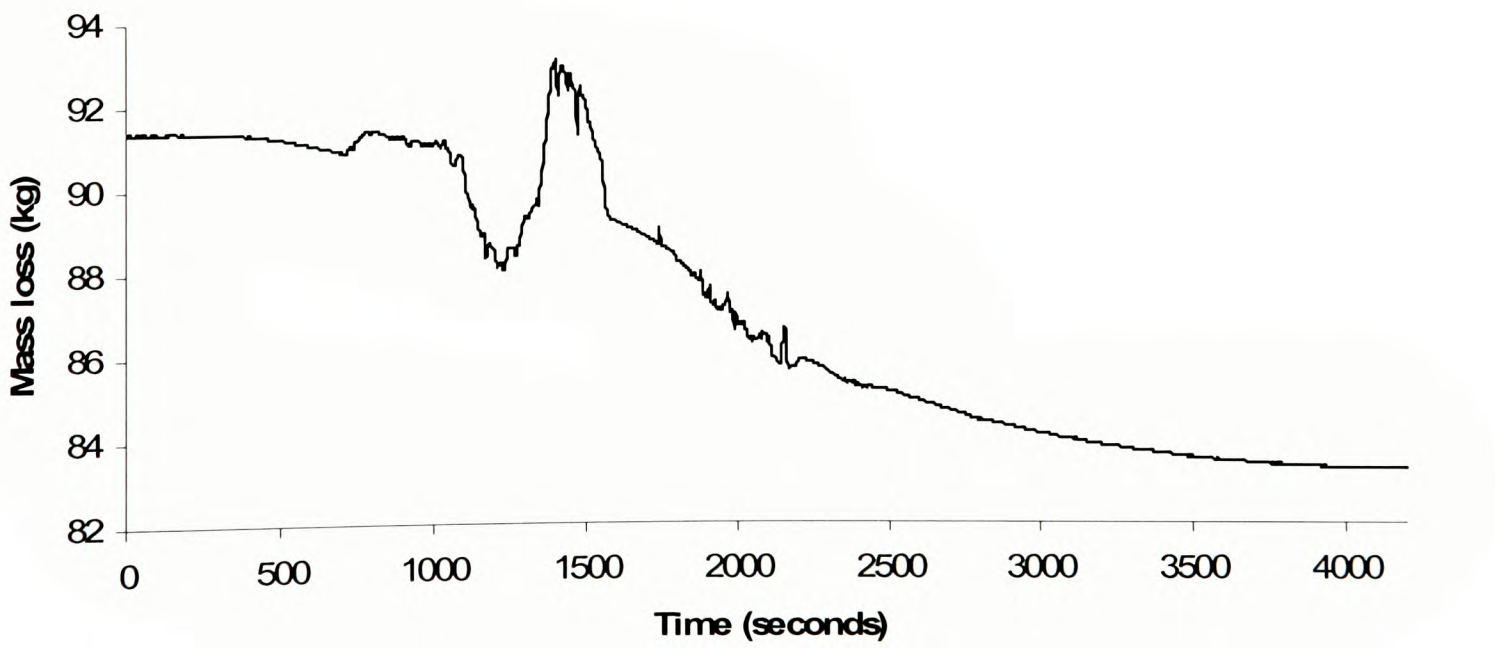

Figure A.4 Load cell measurement of mass loss in kg (Test 1)

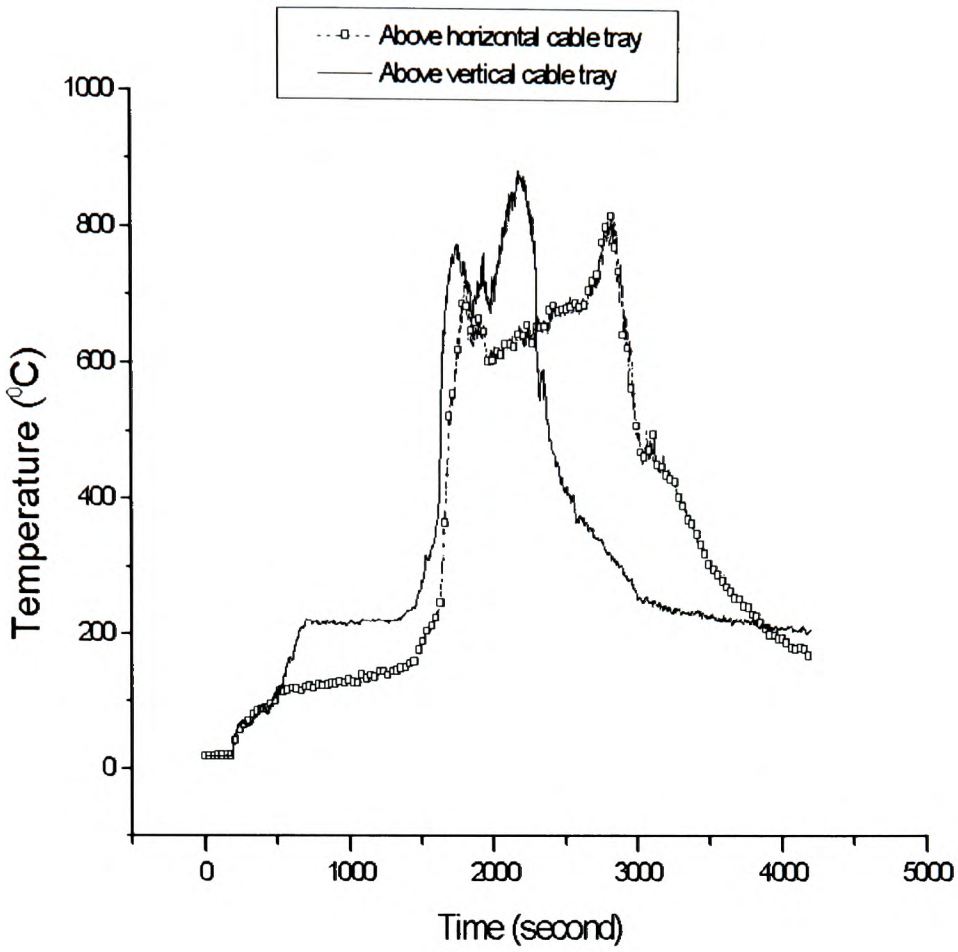

Figure A.5 Temperature above horizontal tray and vertical tray (Test 1)

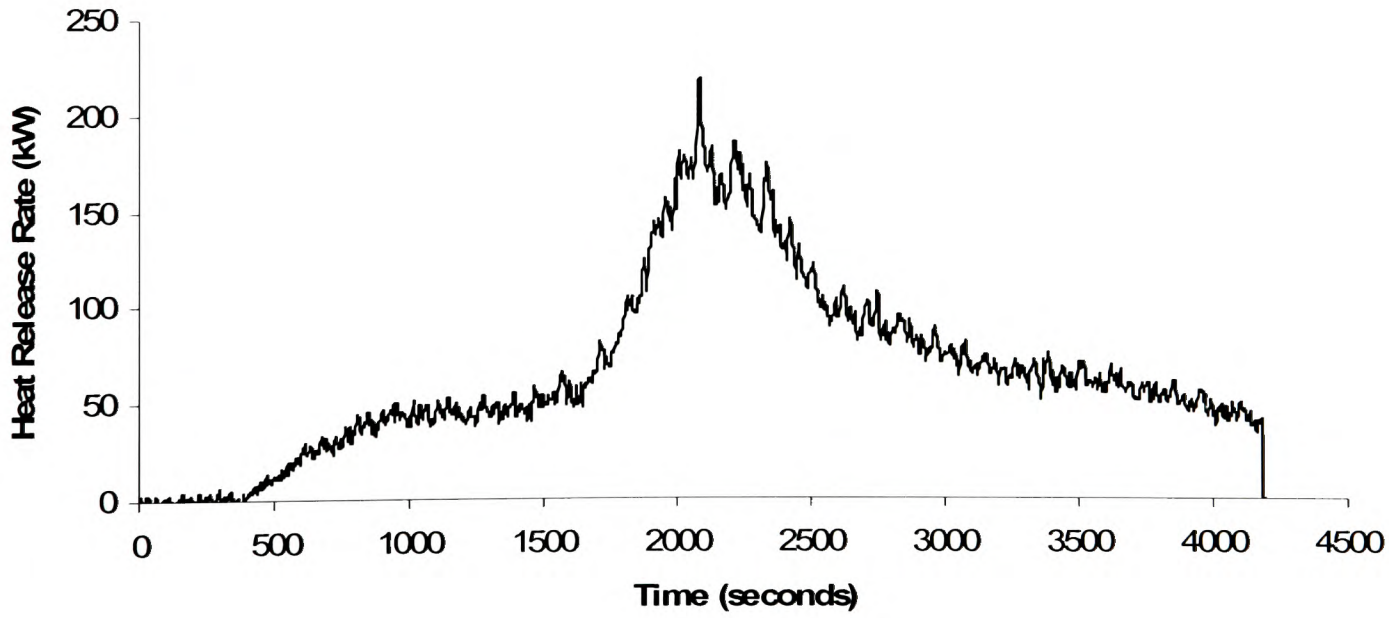

Figure A.6 Total Heat Release Rate measured at exhaust hood by oxygen calorimetry (Test 1)

A.2.2 NHMH Cable fire (Test 2) – Inlet open and No weir placed

Test 2 involved NHMH type cables (see Table 6.1 for its physical and chemical properties). Total 39 cables were burnt during the fire test which lasted up to 2000 seconds. The 1 m^2 vent in the floor level was kept opened during this test. The load cell data is shown in Figure A.7 and the total mass lost during the test was around 6.4 kg. Figure A.8 shows the temperature above the cable fire during the test. Two temperature peaks are observed from the temperature measurements (Figure A.8). The first temperature peak corresponds to the peak mass loss rate of the cables mounted on the vertical cable tray and the second peak corresponds to the peak mass loss rate of the cables mounted on the horizontal cable tray. The peak temperature above the horizontal cable tray and the vertical cable tray were around 750^0 C and 850^0C respectively. The time to reach peak temperature above the vertical cable tray was around 700 seconds. The total heat release rate (HRR) measured by the calorimeter system during the Test 2 is provided in Figure A.9 and the peak HRR was 334 kW.

As part of the test procedure, the instruments were checked and the sampling lines were cleaned. The thermocouple beads were also cleaned after each test. During this test also the load cell measurement was disturbed, probably due to thermal expansion of the cable tray and the support system.

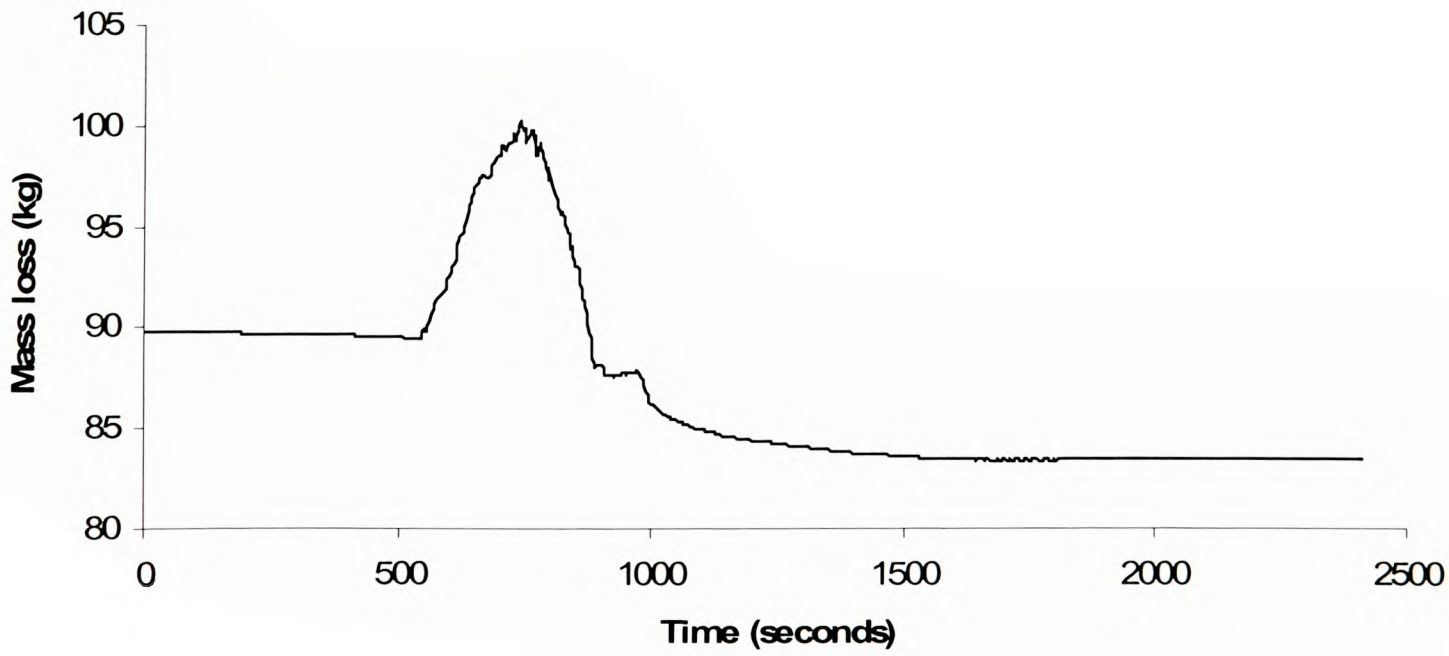

Figure A.7 Load cell measurement of mass loss in kg (Test 2)

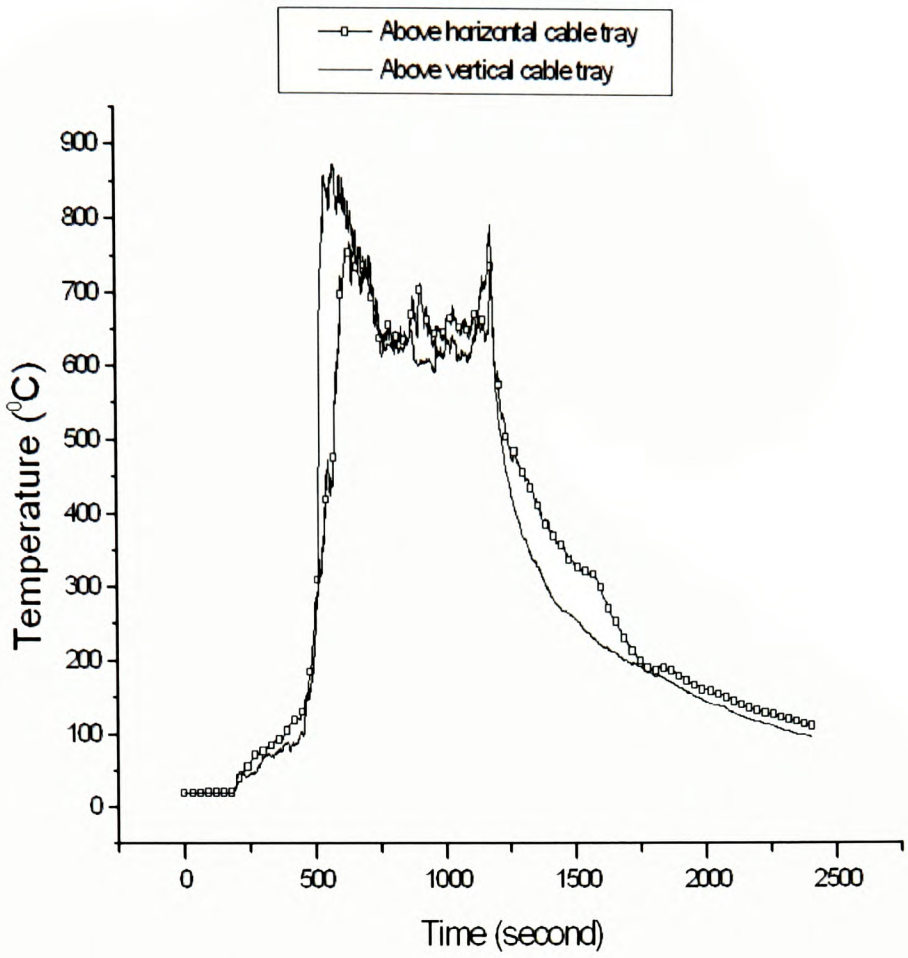

Figure A.8 Temperature above horizontal tray and vertical tray (Test 2)

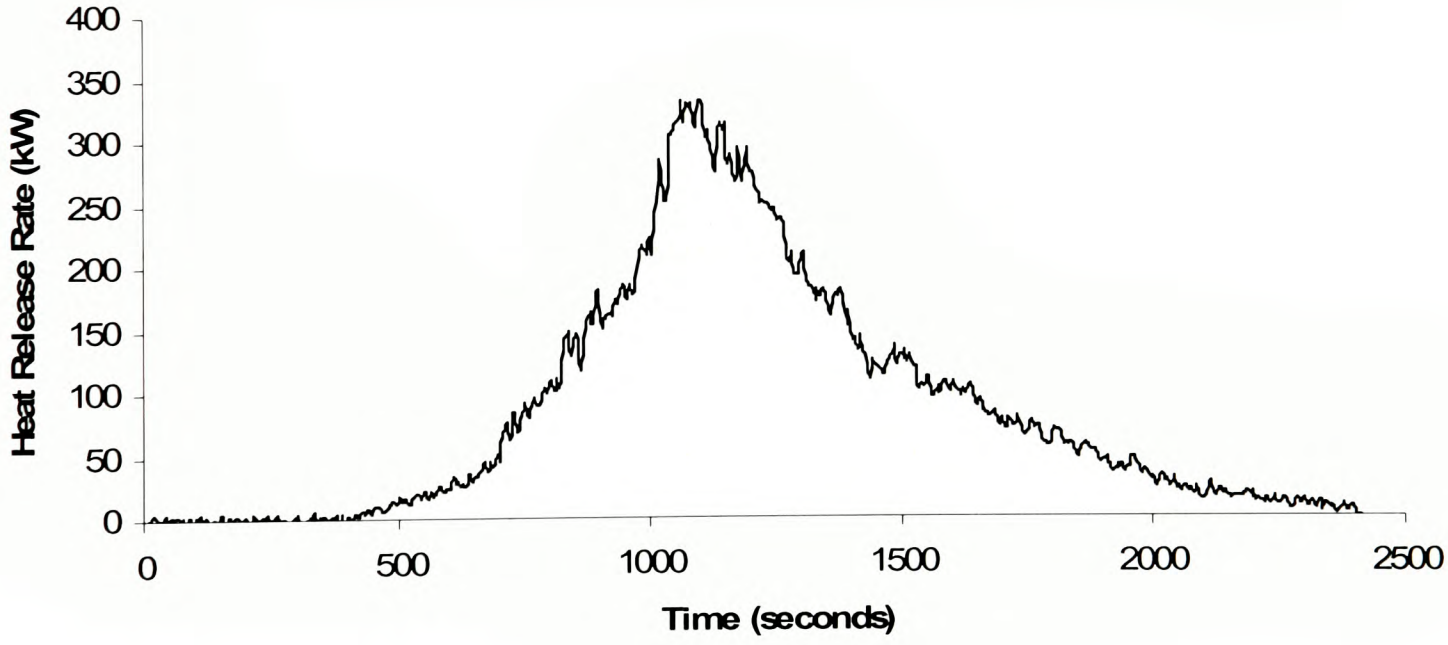

Figure A.9 Total Heat Release Rate measured at exhaust hood by oxygen calorimetry (Test 2)

A.2.3 NHMH Cable fire (Test 3) – Inlet closed and 1m weir placed

During the third test, NHMH type cables were burnt. Total 39 cables were involved during the test which lasted up to 1500 seconds. The 1 m^2 vent was closed and a weir of 1m height was placed at the end of the first corridor (see Figure 6.5) during the test. The load cell data is shown in Figure A.10 and the total mass lost during the test was around 6.48 kg. Figure A.11 shows the temperature above the cable fire during the test. The peak temperature above the horizontal cable tray and the vertical cable tray were around 800^0C. The time to reach peak temperature above the vertical cable tray was around 500 seconds. The total heat release rate (HRR) measured by the calorimeter system during test 3 is provided in Figure A.12 and the peak HRR was 323 kW. Both Test 2 and Test 3 involved burning of NHMH type power cables with the same amount of combustible material. The only difference between the two tests was the ventilation condition. Test 2 had the 1 m^2 vent opening making it more ventilated scenario than Test 3. This explains the reason for lower peak HRR during Test 3 than Test 2.

Even during this test, the weight loss measurement device was disturbed, probably due to thermal expansion of the cable tray and the support system. At around 600 seconds some plastic dripping from the horizontal cable tray to the floor was observed. At 700 seconds substantial dripping was taking place and a small pool fire on the floor was witnessed.

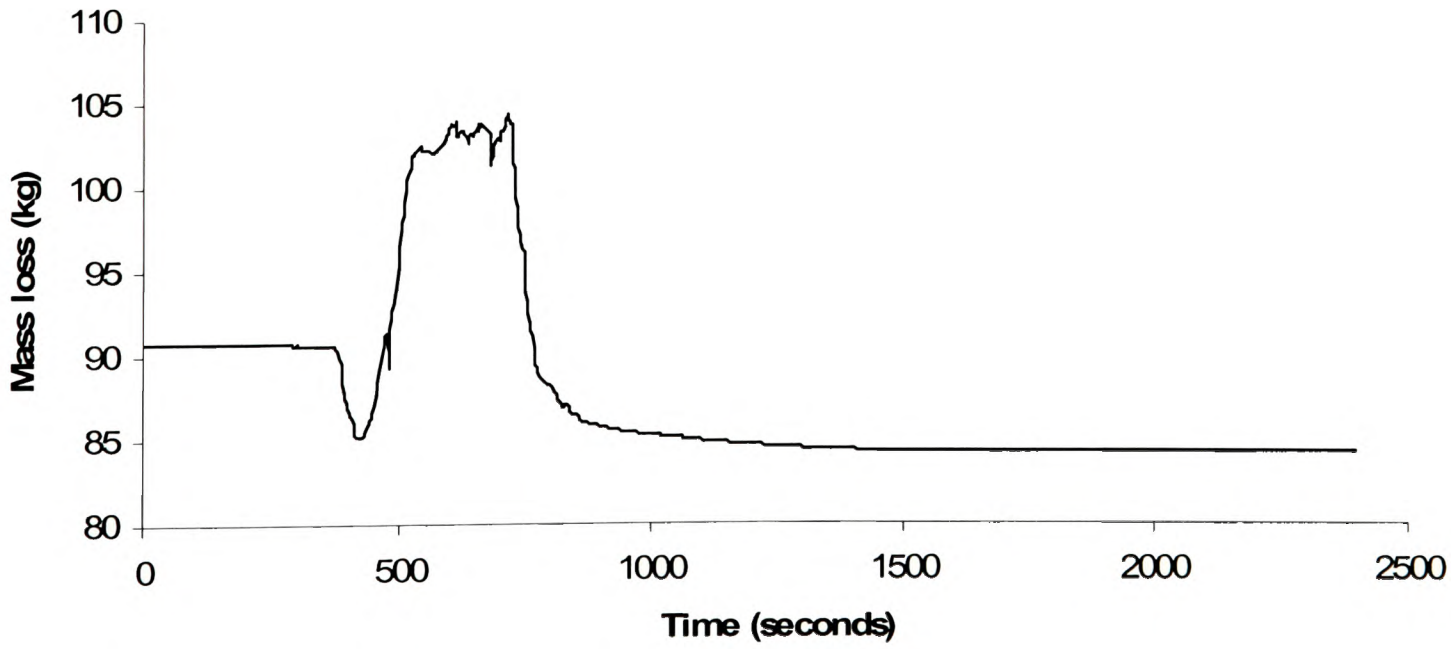

Figure A.10 Load cell measurement of mass loss in kg (Test 3)

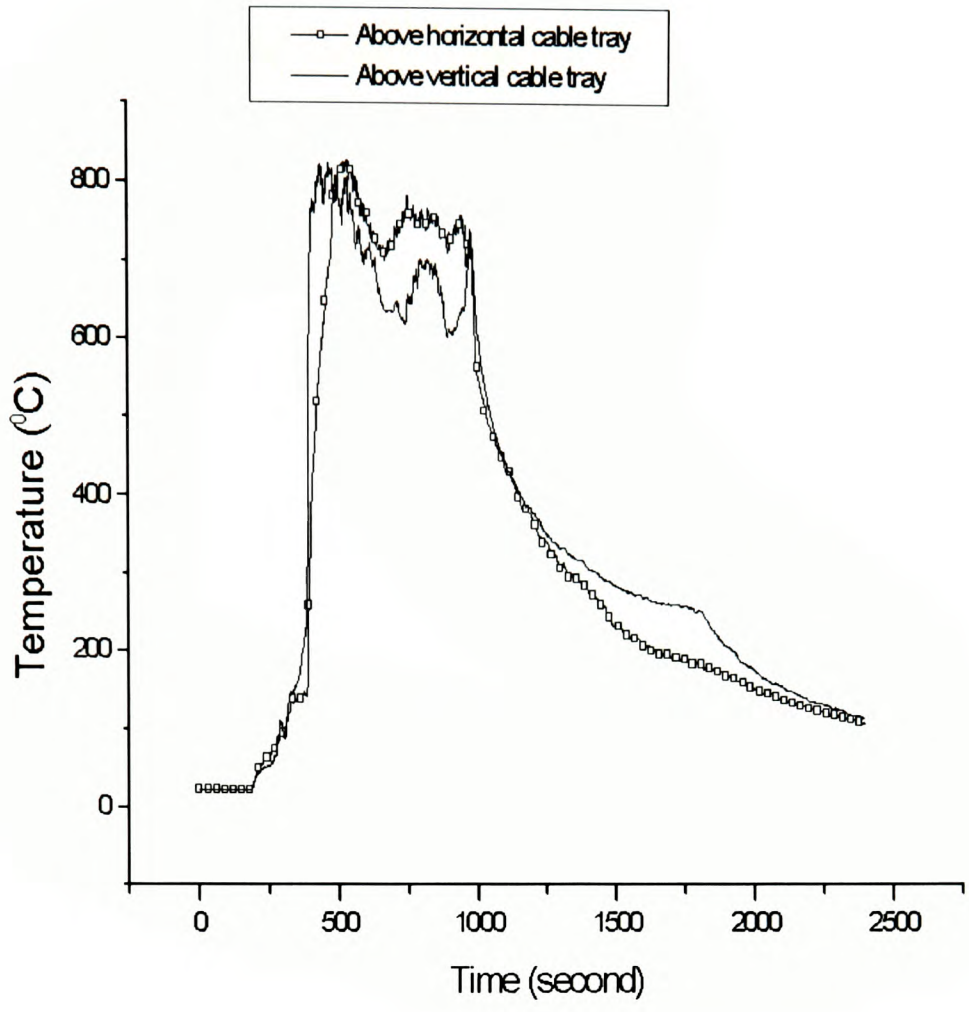

Figure A.11 Temperature above horizontal tray and vertical tray (Test 3)

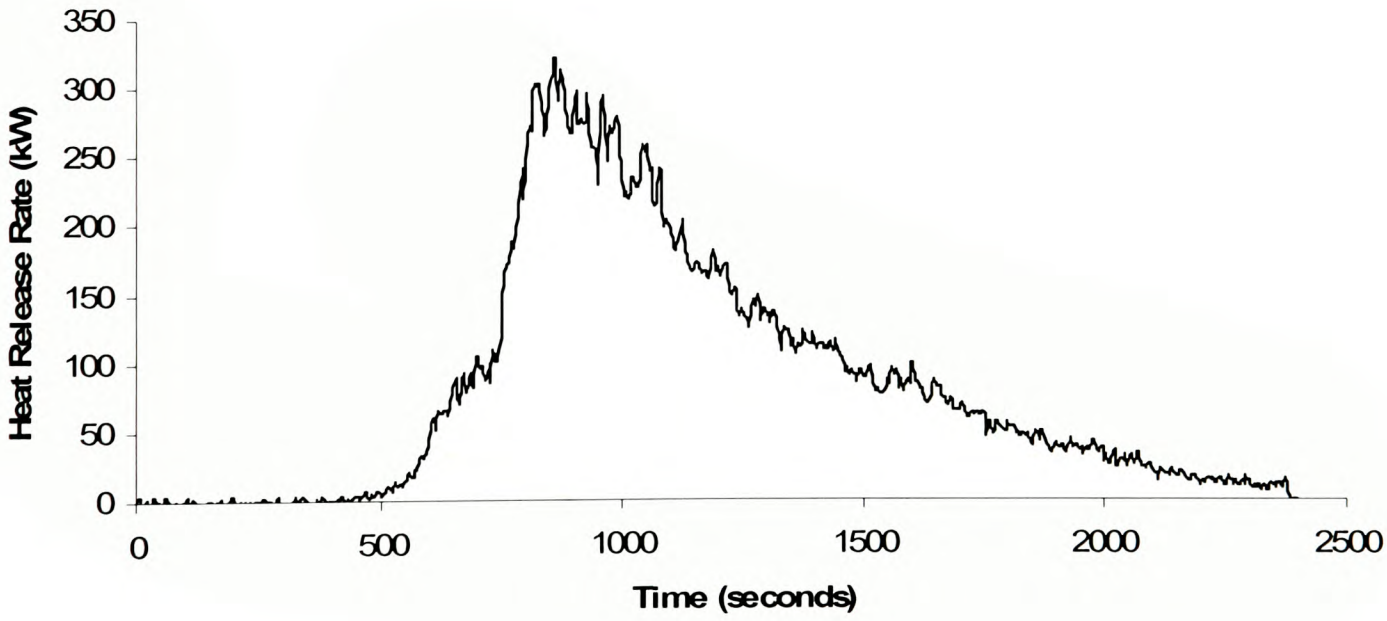

Figure A.12 Total Heat Release Rate measured at exhaust hood by oxygen calorimetry (Test 3)

A.2.4 RZ1-K Cable fire (Test 4) – Inlet closed and 1m weir placed

Test 4 involved RZ1-K type cables. Total 33 cables were involved during this test which lasted up to 4500 seconds. The 1 m^2 vent was closed and a weir of 1m height was placed at the end of the first corridor (see Figure 6.5) during the test. The load cell data is shown in Figure A.13 and the total mass lost during the test was around 7.89 kg. Figure A.14 shows the temperature above the cable fire during the test. The peak temperature above the horizontal cable tray and the vertical cable tray were around 820^0C and 1040^0C respectively. The time to reach peak temperature above the vertical cable tray was around 2800 seconds. The total heat release rate (HRR) measured by the calorimeter system during test 4 is provided in Figure A.15 and the peak HRR was 174 kW.

Both Test 4 and Test 1 involved burning of RZ1-K type power cables with the same amount of combustible material. The only difference between the two tests was the ventilation condition. Test 1 had the 1 m^2 vent opening making it more ventilated scenario than Test 4. This explains the reason for lower mass loss and peak HRR during Test 4 than Test 1.

During the test, less dripping of plastic was observed from the horizontal cable tray. The load cell arrangement was corrected and the weight loss measurement was improved.

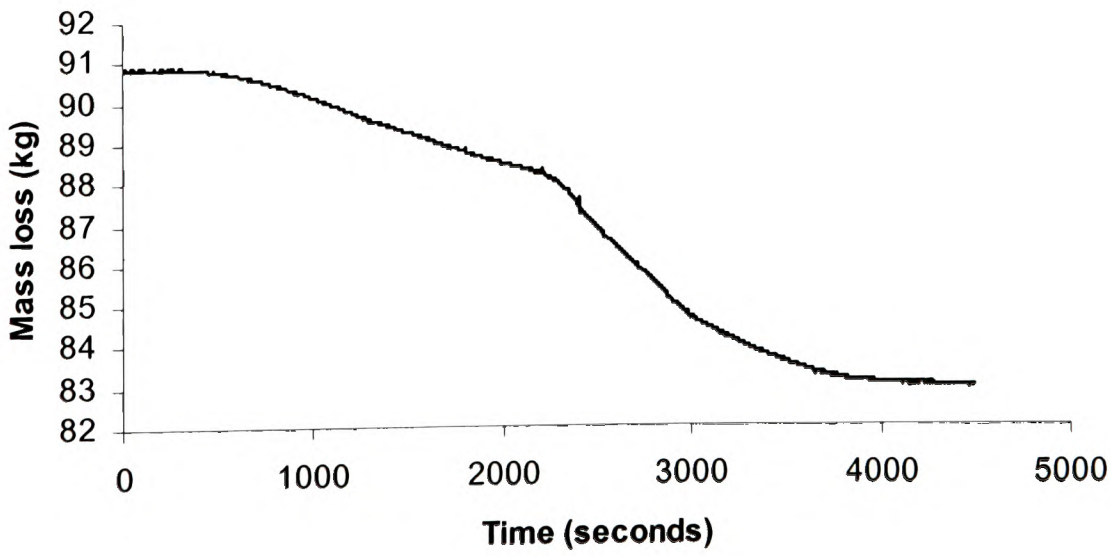

Figure A.13 Load cell measurement of mass loss in kg (Test 4)

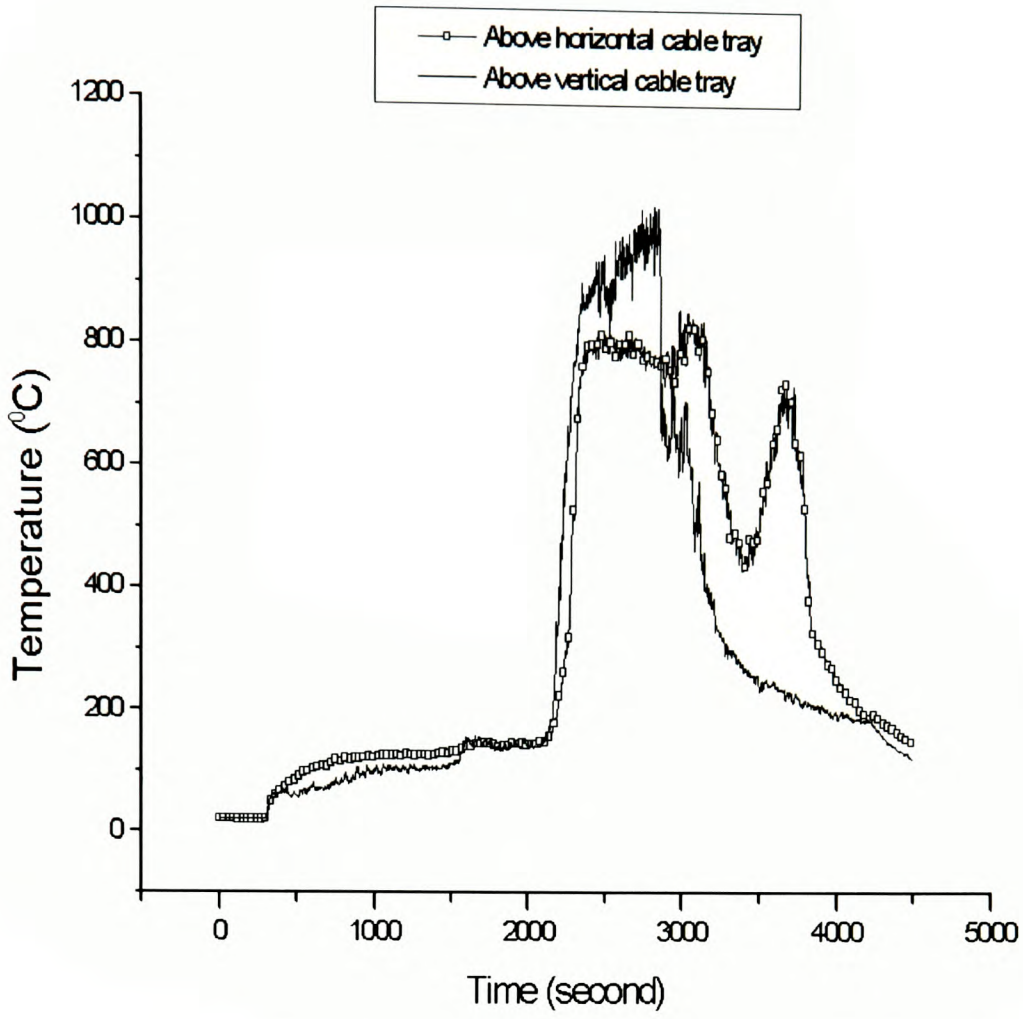

Figure A.14 Temperature above horizontal tray and vertical tray (Test 4)

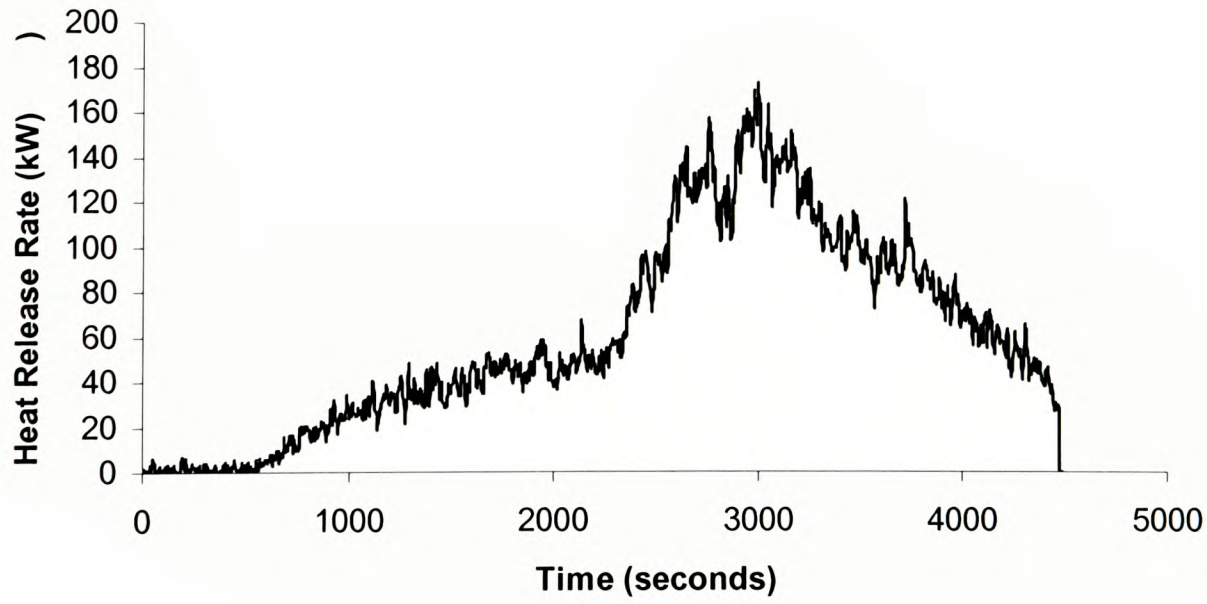

Figure A.15 Total Heat Release Rate measured at exhaust hood by oxygen calorimetry (Test 4)

A.2.5 NYM Cable fire (Test 6) – Inlet open and No weir placed

During the sixth test, NYM type cables were burnt. Total 35 cables were involved during the test which lasted up to 2000 seconds. The 1 m^2 vent was kept open during the test. The load cell data is shown in Figure A.16 and the total mass lost during the test was around 7.53 kg. Figure A.17 shows the temperature above the cable fire during the test. The peak temperature above the horizontal cable tray and the vertical cable tray was around 800^0C. The time to reach peak temperature above the vertical cable tray was around 700 seconds. The total heat release rate (HRR) measured by the calorimeter system during test 6 is provided in Figure A.18 and the peak HRR was 180 kW. Both Test 5 and Test 6 involved burning of NYM type power cables with the same amount of combustible material. The only difference between the two tests was the ventilation condition. Test 6 had the 1 m^2 vent opening making it more ventilated scenario than Test 5. This explains the reason for lower mass loss and peak HRR during Test 5 than Test 6.

Intensive smoke generation was witnessed at the very beginning of the fire similar to the previous test and the smoke layer was at 1.6 m height at around 300 seconds. During the test, there was no dripping of plastics from the horizontal cable tray was observed.

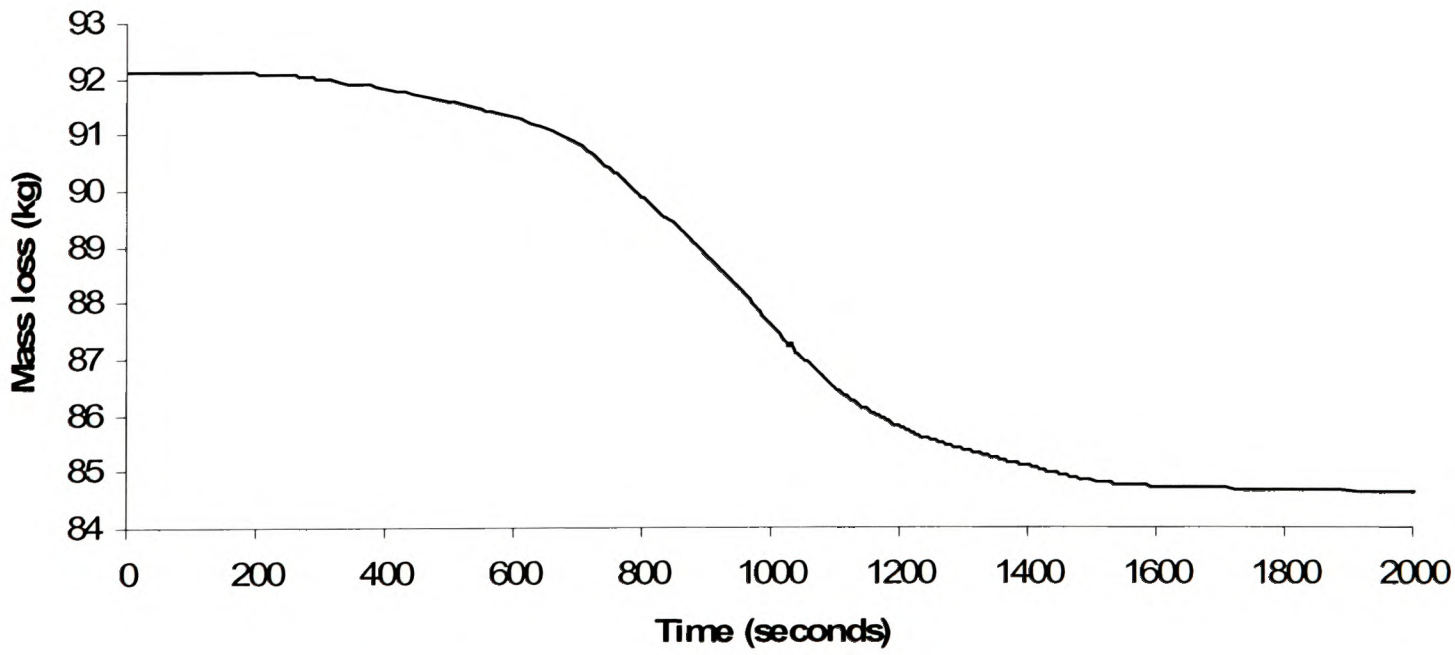

Figure A.16 Load cell measurement of mass loss in kg (Test 6)

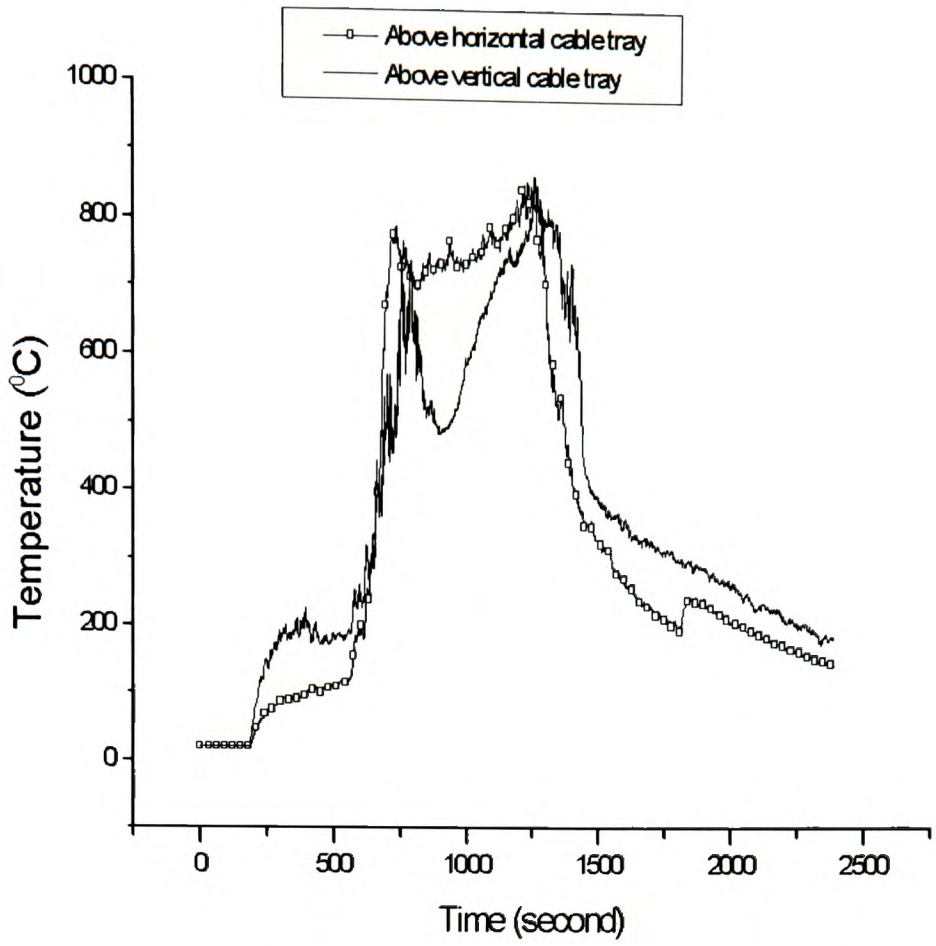

Figure A.17 Temperature above horizontal tray and vertical tray (Test 6)

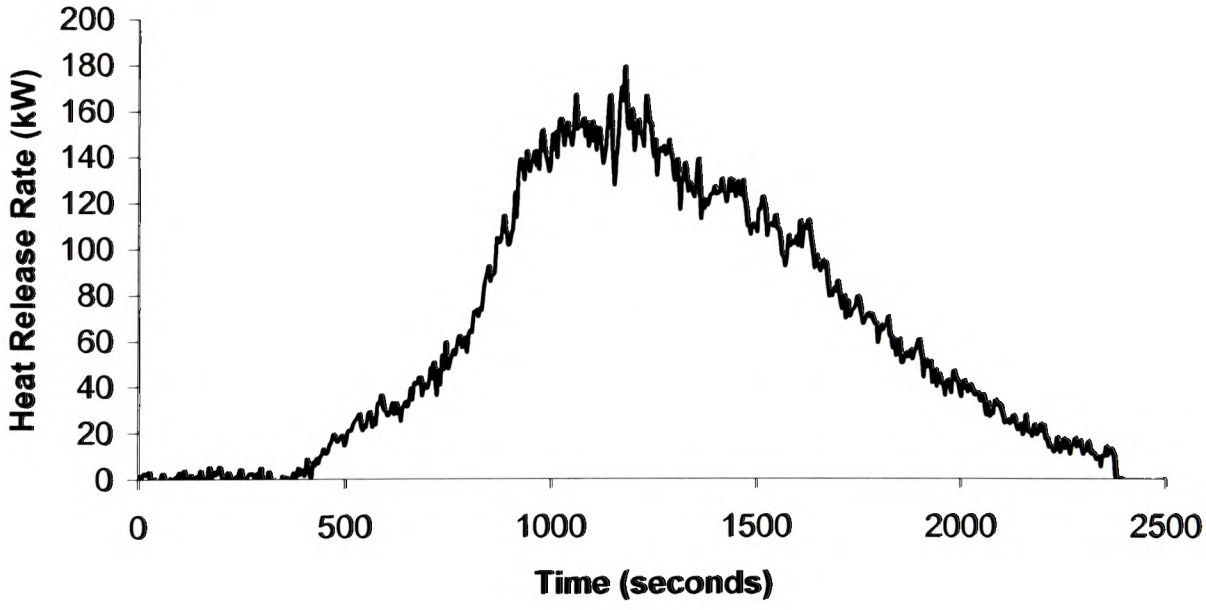

Figure A.18 Total Heat Release Rate measured at exhaust hood by oxygen calorimetry (Test 6)

A.2.6 NYM Cable fire (Test 9) – Inlet closed and 1m weir placed

Test 9, a repeat of Test 5 was carried out in order to verify the repeatability. During this test, NYM type cables were burnt. Total 35 cables were involved during the test which lasted up to 2000 seconds. The 1 m^2 vent was closed and a weir of 1 m height was placed at the end of the first corridor during the test. The load cell data is shown in Figure A.19 and the total mass lost during the test was around 7.55 kg. Figure A.20 shows the temperature above the cable fire during the test. The peak temperature above the horizontal cable tray and the vertical cable tray were around 900^0C and 950^0C respectively. The time to reach peak temperature above the vertical cable tray was around 900 seconds. The total heat release rate (HRR) measured by the calorimeter system during test 9 is provided in Figure A.21 and the peak HRR was 154 kW.

Intensive smoke generation was witnessed at the very beginning of the fire and the smoke layer was at 1.6 m height at around 300 seconds. During the test, there was no dripping of plastics from the horizontal cable tray was observed.

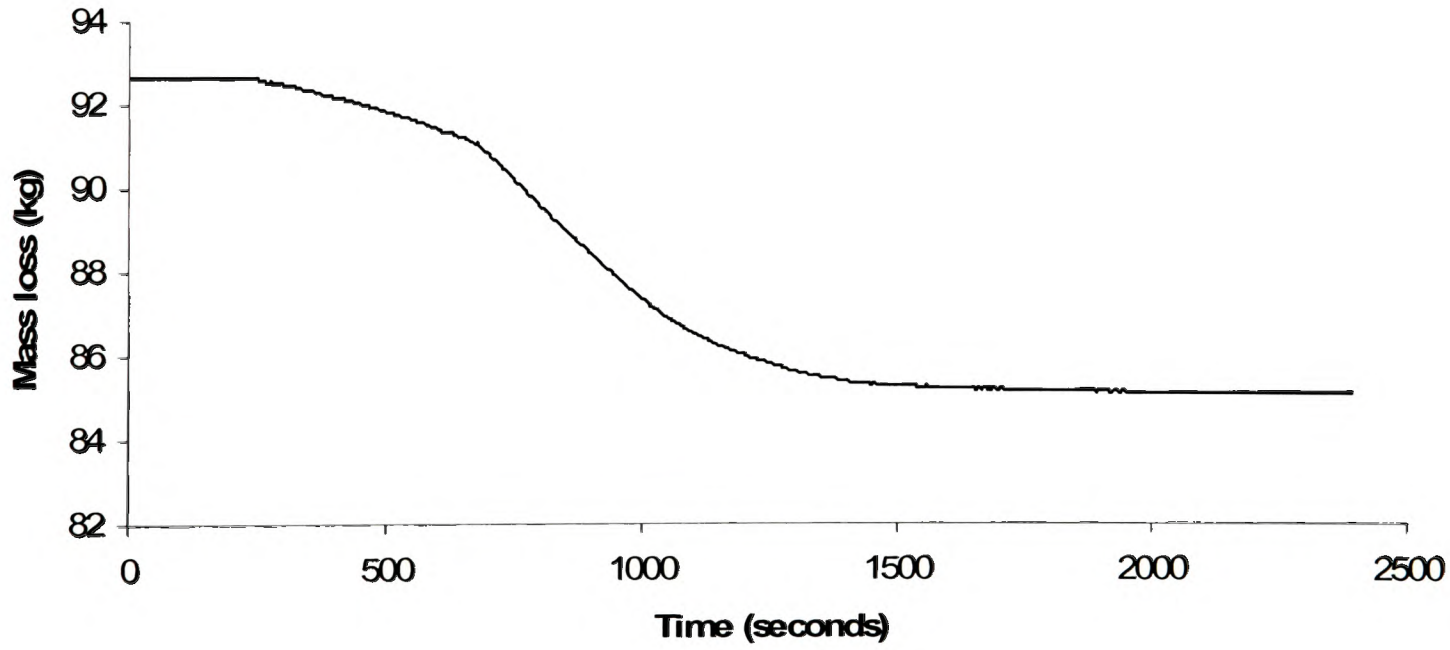

Figure A.19 Load cell measurement of mass loss in kg (Test 9)

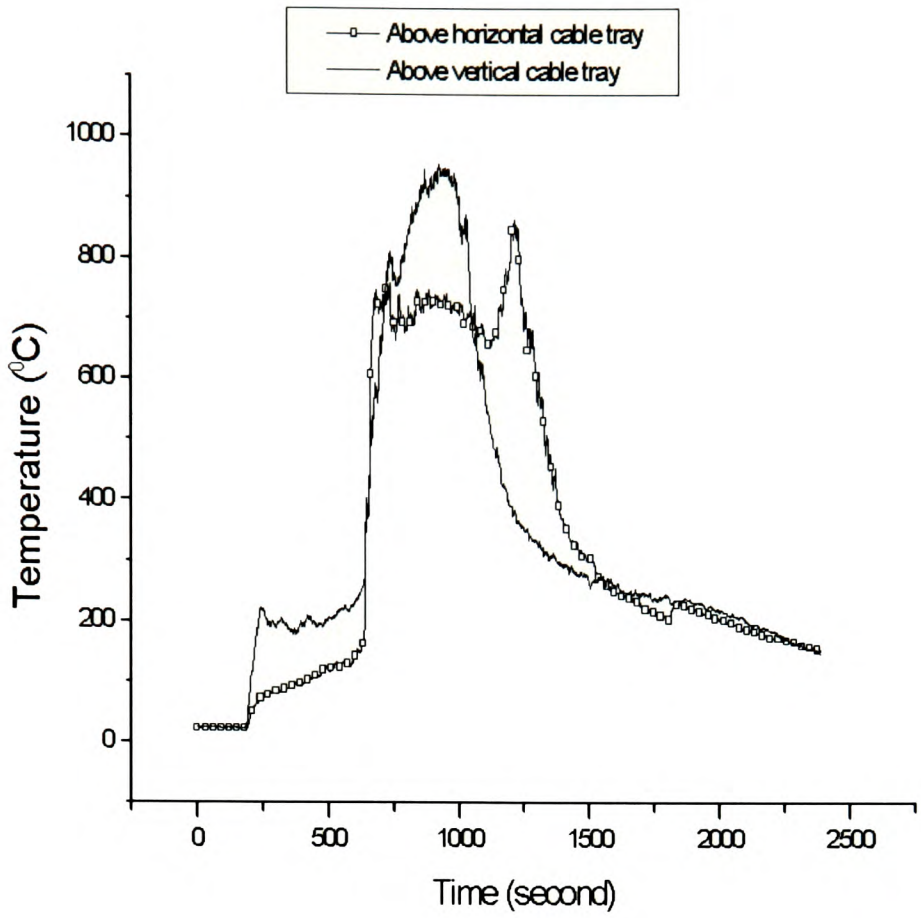

Figure A.20 Temperature above horizontal tray and vertical tray (Test 9)

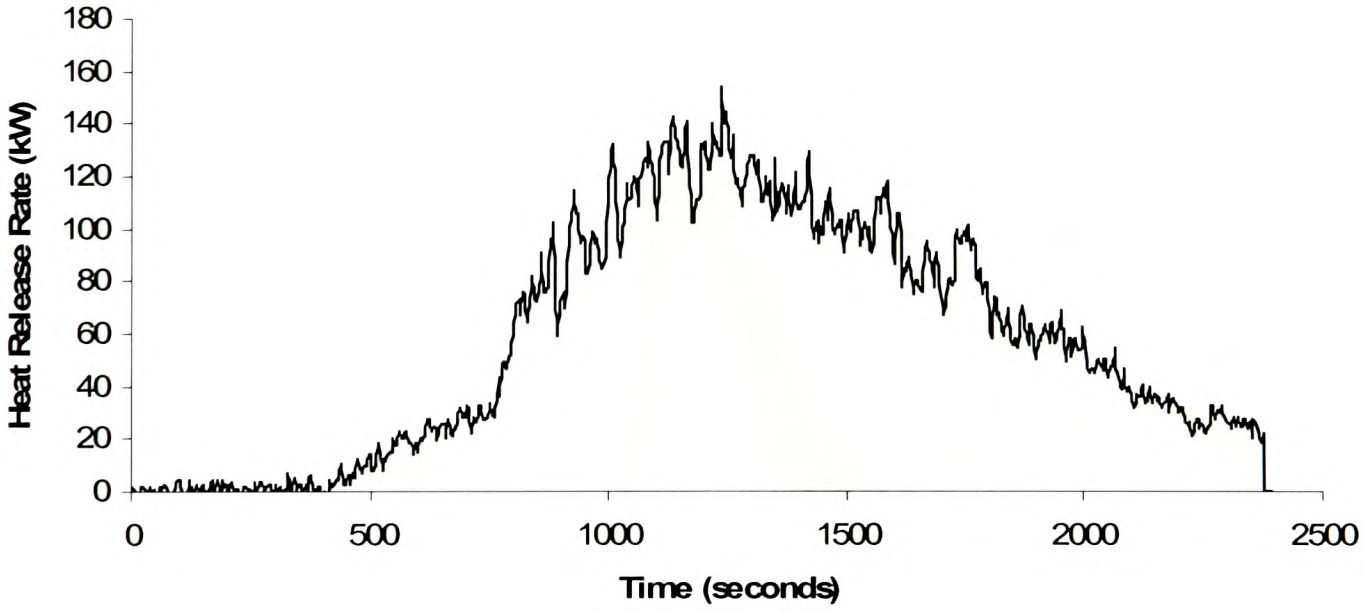

Figure A.21 Total Heat Release Rate measured at exhaust hood by oxygen calorimetry (Test 9)

A.3 Repeatability

During the experimental campaign, two tests were repeated in order to verify the repeatability. Test 1 with the RZ1 cable was repeated in test 7 and test 5 with the NYM cable was repeated in test 9. As can be seen from the Figures A.22- A.27, the repeatability was very good for test 5 and 9, and satisfactory for test 1 and 7. Some differences in peak values could be noted between the repeated tests, in particular between tests 1 and 7. One possible reason for the differences could be that the steel plate covering the vertical cable tray in test 1 opened up slightly due to heat expansion which might have changed the fire spread conditions. This metal cover was fastened with additional screws in the following tests to avoid this problem. As can be seen from the HRR graph shown in Figure A.22 and A.23, there is a significant time delay due to the low gas velocity inside the corridor. The mass loss and temperature measurements just above the fire source were, however, free from this influence and could be used to judge the time delay in the measuring system.

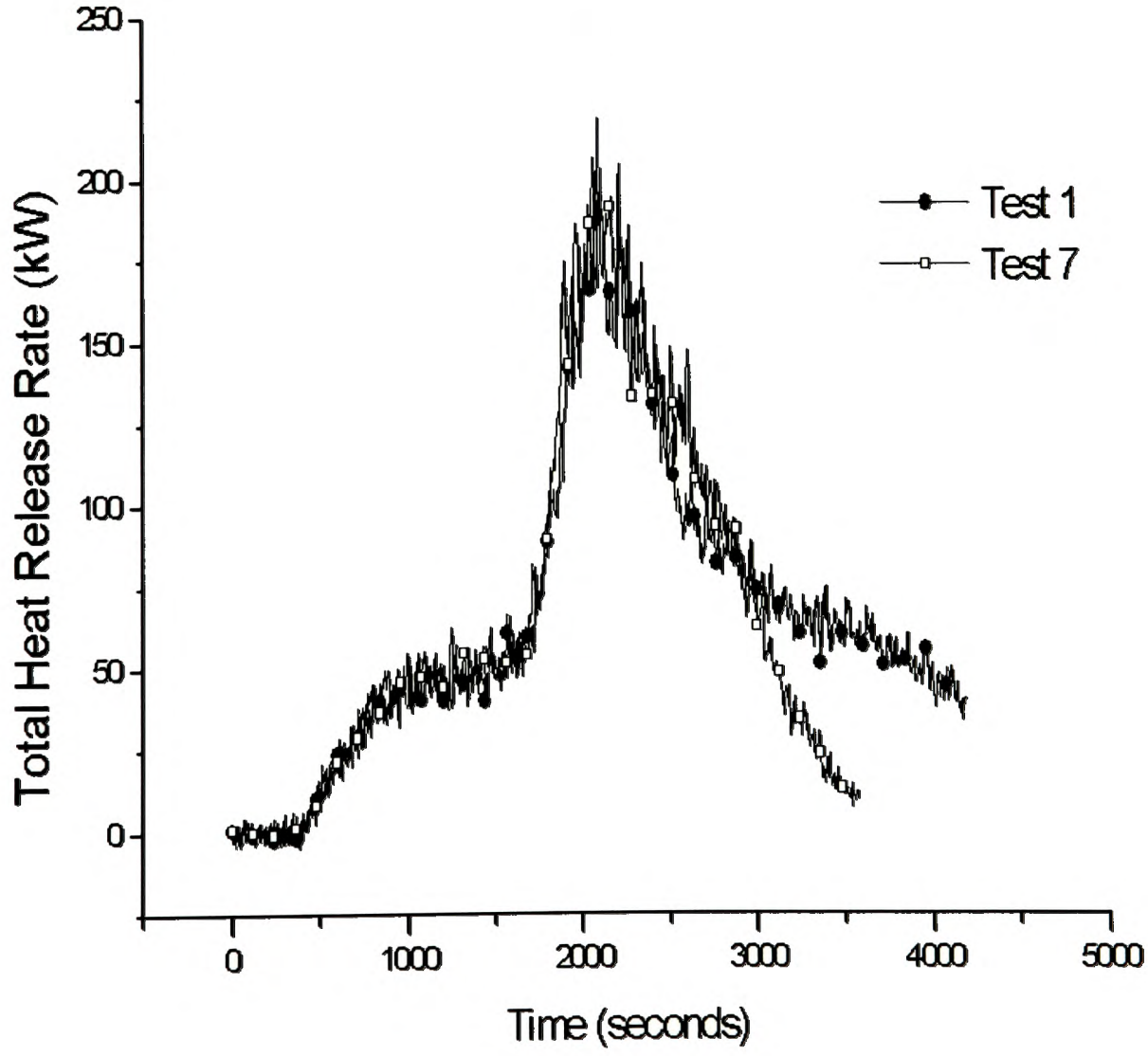

Figure A.22 Total Heat Release Rate for Test 1 and 7

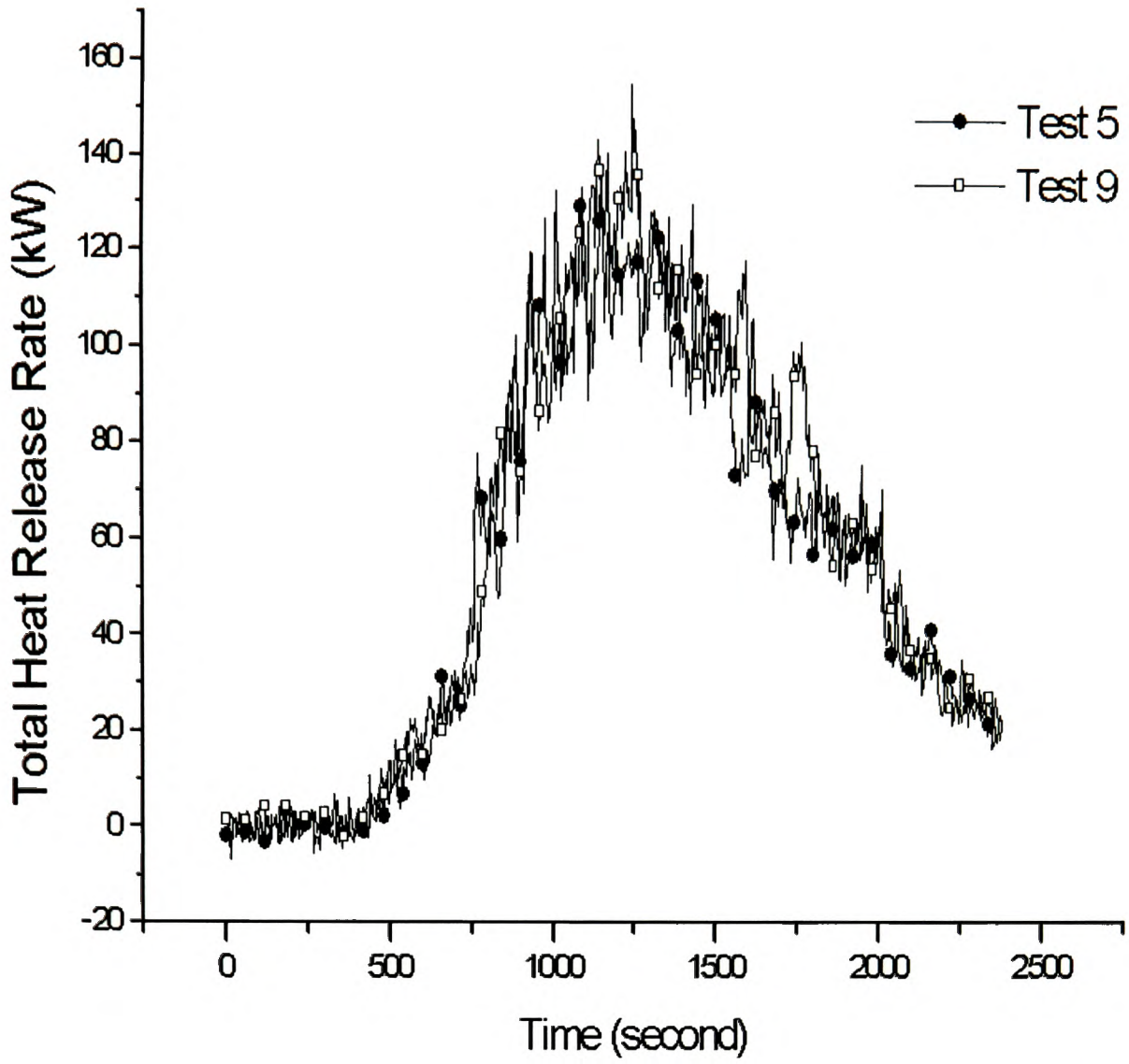

Figure A.23 Total Heat Release Rate for Test 5 and 9

As seen in Figure A.24, there was some problem with the weight loss measurements for the first three tests. Thermal expansion of the cable tray might have caused it to come into contact with the corridor wall which influenced the weight measurements during the most intensive part of the fire in tests 1-3 (see Figures 6.8, 6.11 and 6.14).

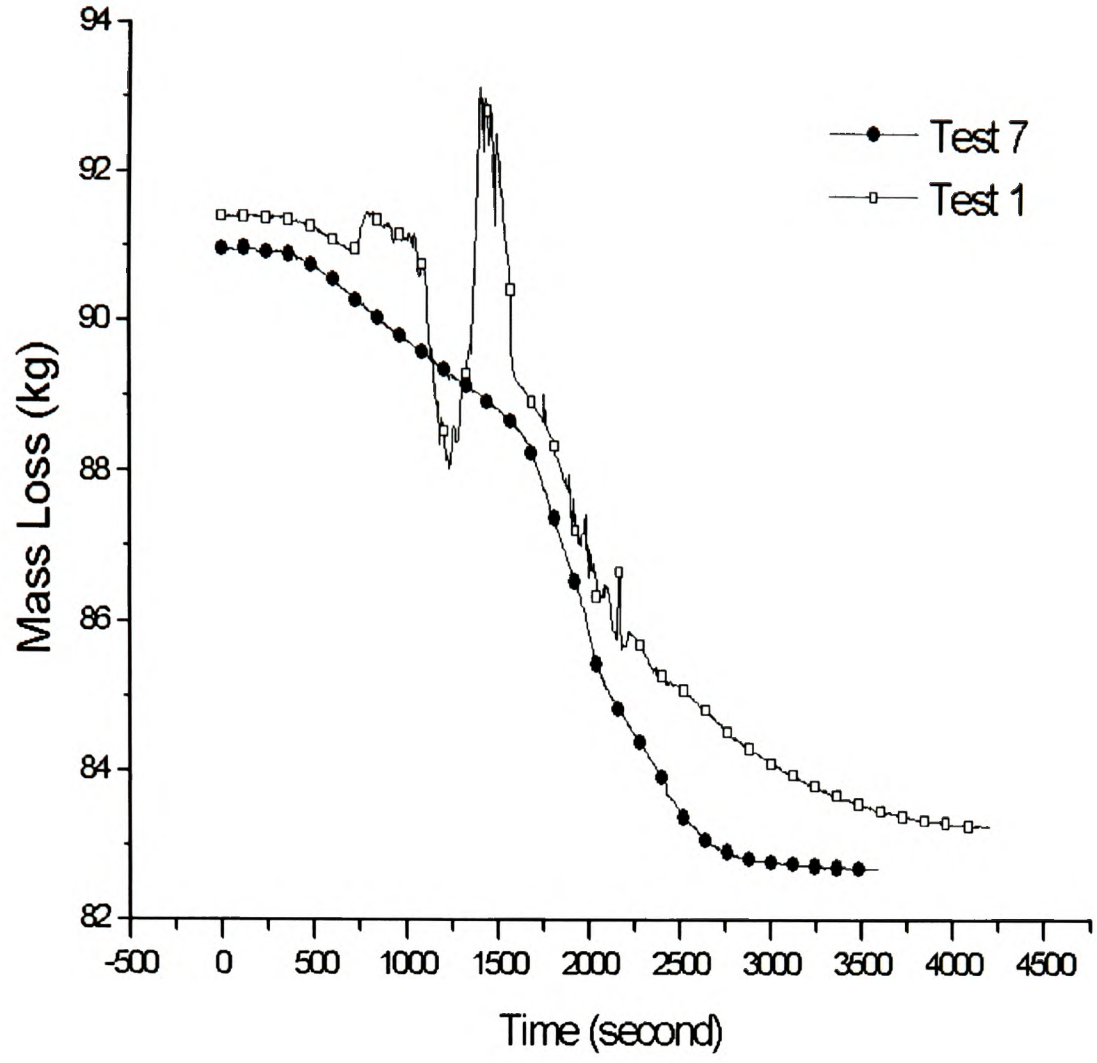

Figure A.24 Load Cell Measurements for Test 1 and 7

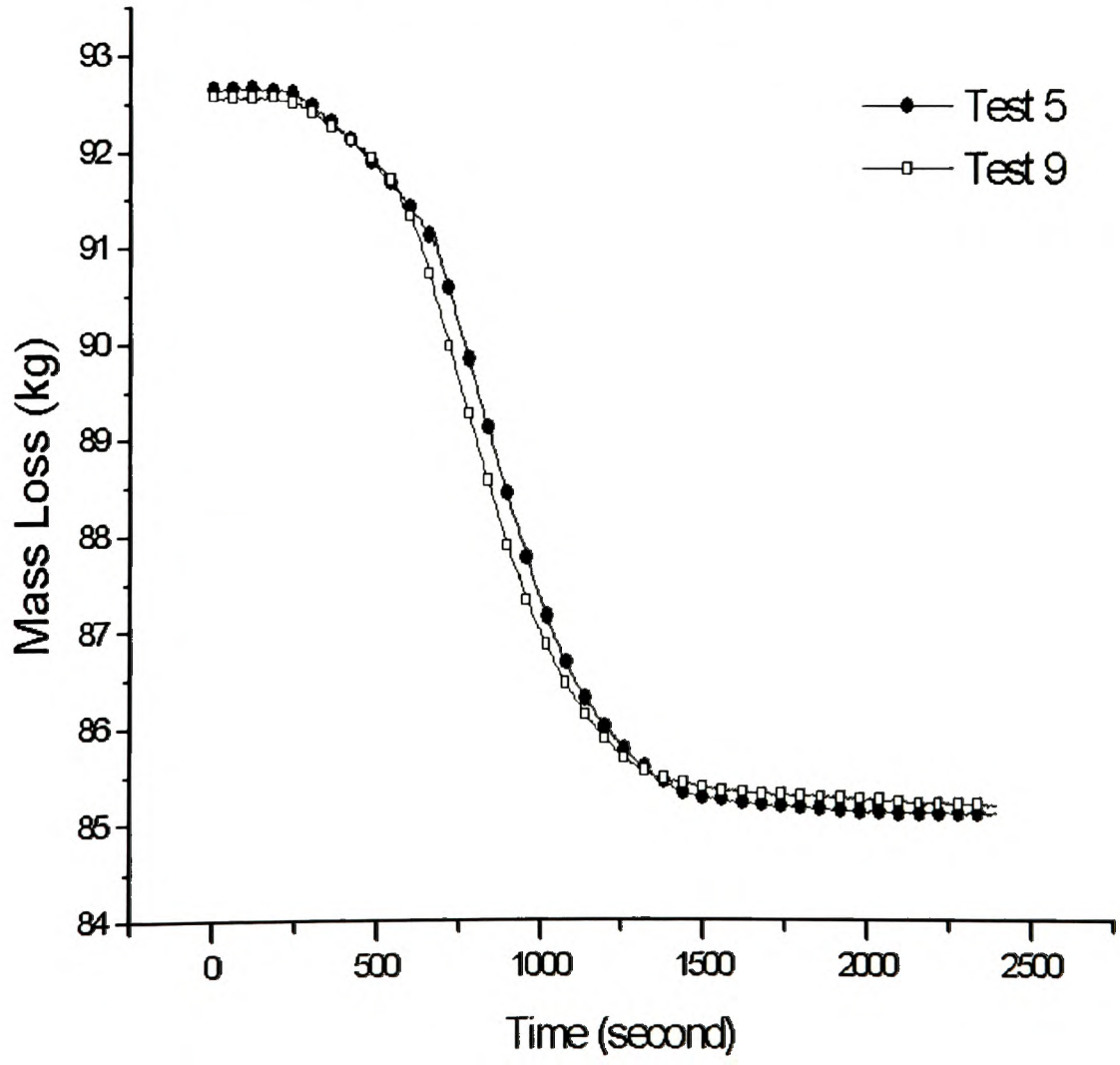

Figure A.25 Load Cell Measurements for Test 5 and 9

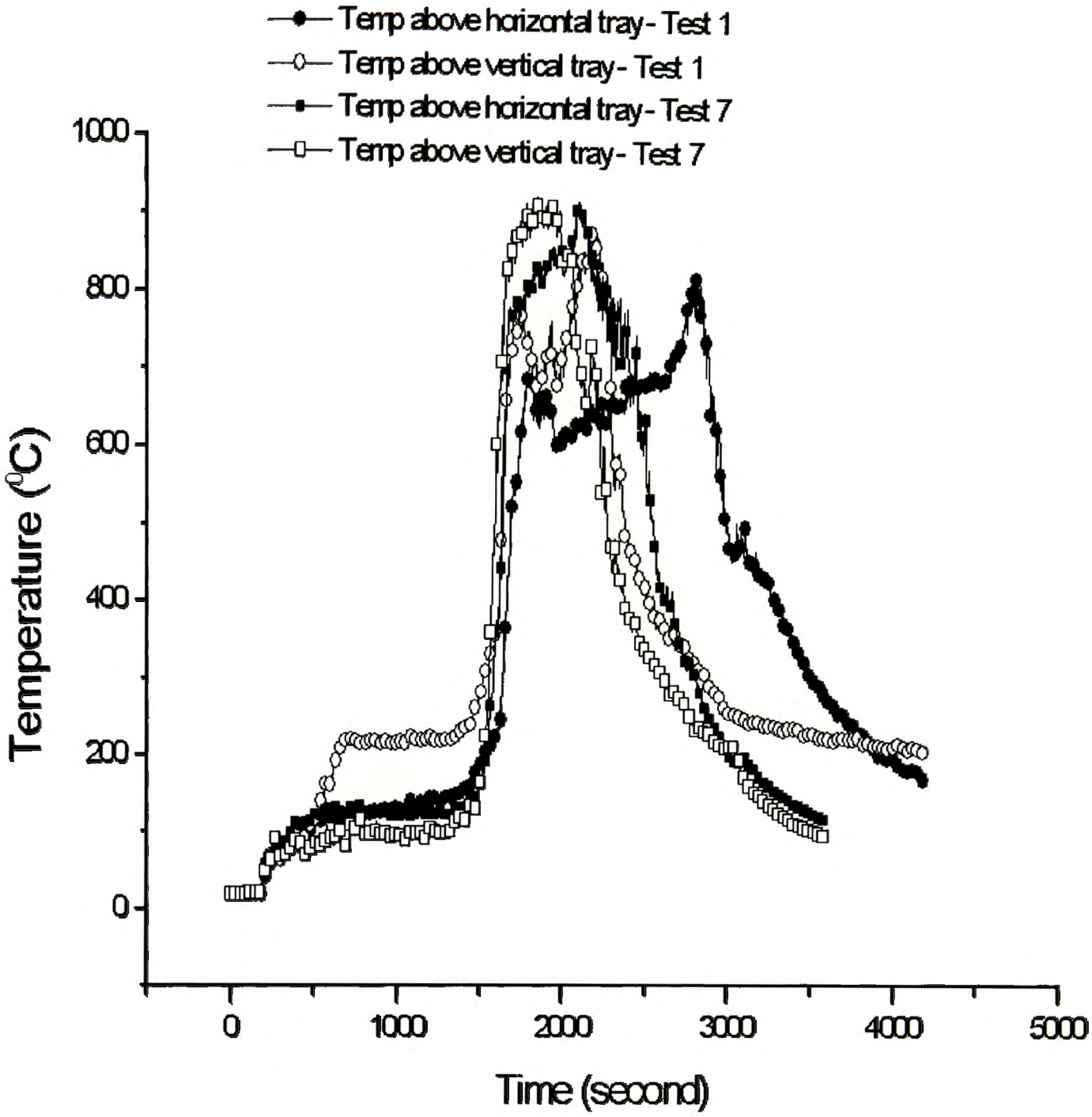

Figure A.26 Temperature above the fire for Test 1 and 7

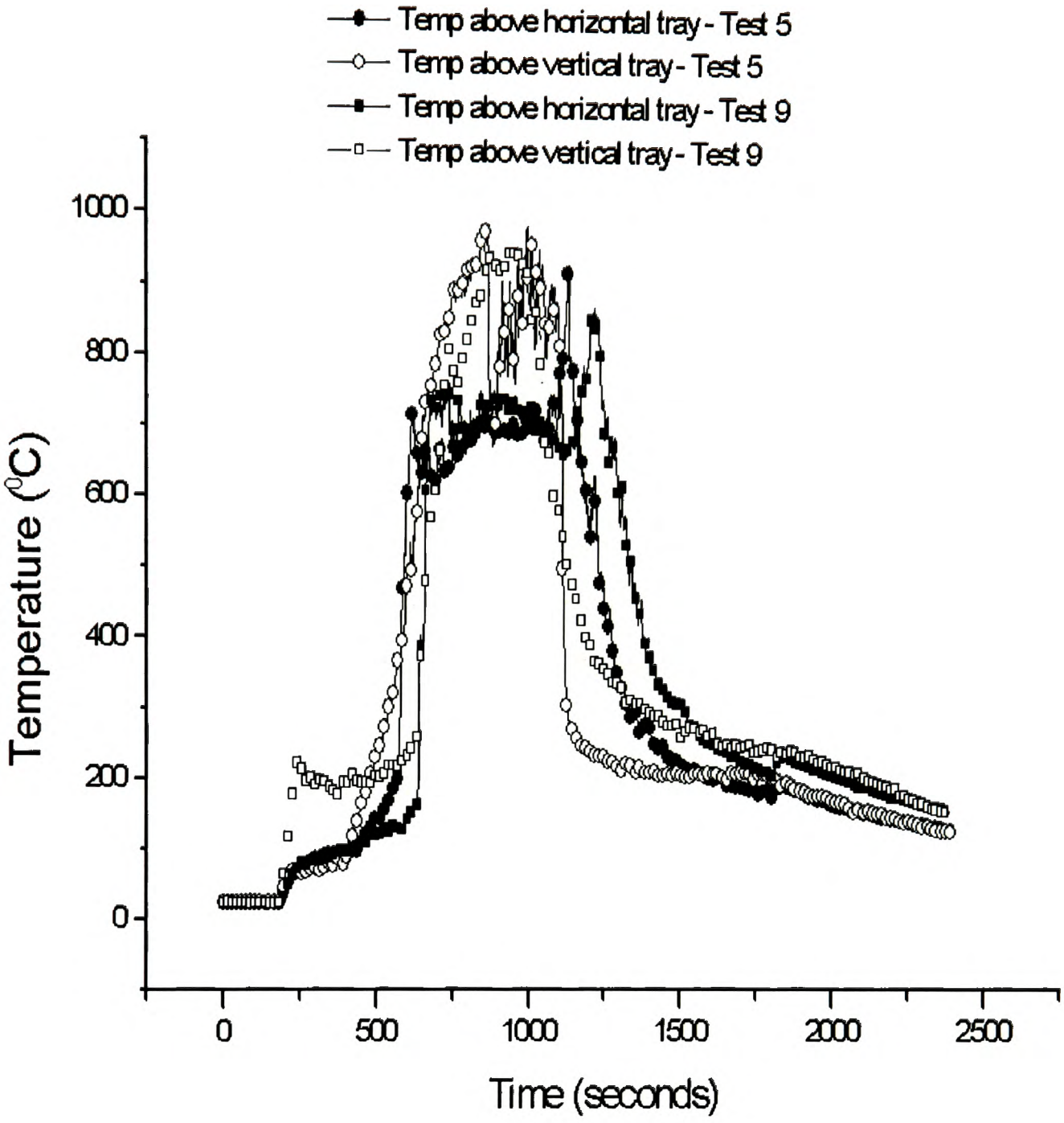

Figure A.27 Temperature above the fire for Test 5 and 9

References

1. Andersson, P., Rosell, L., and Simonson, M., "Small and large scale fire experiments with electric cables under well-ventilated and vitiated conditions", Fire Technology, Vol. 40, pp. 247-262, 2004.
2. Babrauskas, V., "Generation of CO in Bench-Scale Fire Tests and the Prediction for Real-Scale Fires," Interscience Communications Limited. Fire and Materials. International Conference, 1st. September 24-25, 1992, Arlington, VA, 155-177 pp, 1992.
3. Babrauskas, V., "The phi meter: A simple, fuel-independent instrument for monitoring combustion equivalence ratio," Rev. Sci. Instrumentation, 65(7), July 1994.
4. Beard, A., "Limitations of fire models," J. Applied Fire Sciences, Vol. 5, pp. 233-243, 1996.
5. Beyler, C., "Major species production by diffusion flames in a two-layer compartment fire environment," Fire Safety Journal, Vol. 10, pp. 47-56, 1986a.
6. Beyler, C., "Major species production by solid fuels in a two layer compartment fire environment," Fire Safety Science - Proceedings of the first international symposium, Hemisphere, Washington, D.C., pp. 431-430, 1986b.
7. Bilger, R. W., "The structure of diffusion flames," Combustion Science and Technology, Vol. 13, 1976.
8. Blomqvist, P., and Lönnermark, A., "Characterisation of the combustion products in large-scale fire tests: Comparison of three experimental configurations," Fire and Materials, Vol. 25, pp. 71-81, 2001.
9. Borealis Private communication – Experimental data, 2001.

10. Brohez, S., Marlair, G., Bertrand, J.P., and Delvosalle, C., "The effect of oxygen concentration on CO yields in fires," Interflam 2004, pp. 775-780, 2004.
11. Bryner, N. P., Johnsson, E. L., and Pitts, W. M., "Carbon monoxide production in compartment fires – Reduced-scale enclosure test facility," National Institute of Standards and Technology, NISTIR-5568, 1994.
12. Bryner, N. P., Johnsson, E. L., and Pitts, W. M., "Scaling compartment fires – Reduced and Full-scale enclosure burns," Proceedings of International Conference on Fire Research and Engineering (ICFRE), Boston, SFPE, pp. 9 – 14, 1995.
13. BS 7990: 2003, "Tube furnace method for the determination of toxic product yields in fire effluents".
14. Butler, K. M., Ohlemiller, T.J., and Linteris, G.T., "Progress report on Numerical modelling of experimental polymer melt flow behaviour," Interflam2004, Vol. 2, pp. 937-948, 2004.
15. Carman, J. M., Purser, D. A., Hull, R. T., Price, D., and Milnes, G. J., "Experimental parameters affecting the performance of the Purser furnace: a laboratory-scale experiment for a range of controlled real fire conditions," Polymer International, 49, pp. 1256-1258, 2000.
16. Cetegen, B.M., Zukoski, E. E. and Kubota, T., "Government Contractor's Report," GCR-82-402, National Bureau of Standards, August 1982.
17. Chow, W. K., "Use of computational fluid dynamics for simulating enclosure fires," Journal of Fire Science, Vol. 13, pp. 300-334, 1995.
18. Cox, G., "Compartment fire modelling," In: Cox, G., editor. Combustion fundamentals of fire. Academic Press, London, pp. 329-404, 1995.
19. Cullis, C. F., Hirschler, M. M., "The combustion of organic polymers," 1st ed. Oxford: Clarendon Press, 1981.
20. Dey, M., "Cable tray fires of redundant safety systems in nuclear power plants," Interflam 2001, 2, pp. 1117-1128, 2001.
21. Dryer, F.L., and Glassman, I., "High temperature oxidation of CO and CH_4," Proc. 14^{th} Int. Symp. on Combustion, The Combustion Institute, PA, USA, pp. 987-1003, 1973.
22. Drysdale, D.D., "An introduction to fire dynamics," John Wiley and sons (2^{nd} edition), 1998.

23. DuPont, V., Pourkashanian, M., and Williams, A., "Modelling of process heaters fired by natural gas," J. of Inst. of Energy, Vol. 66, pp. 20, 1993.
24. Emmons, H.W., "The prediction of fires in buildings," Seventeenth Symposium on Combustion (Int.), 1978.
25. Evans, G., "Progress on standards for the implementation of the Construction Products Directive," Fire Retardants '98, London, Feb 1998.
26. Ewens, D.S., Vandsburger, U., and Roby, R.J., "Transport and oxidation of compartment fires exhaust gases," 6, pp. 163-181, 1994.
27. Ewer, J., Jia, F., Grandison, A., Galea, E.R., and Patel, M.K., "SMARTFIRE V4.0 User Guide and Technical Manual," Fire Safety Engineering Group, University of Greenwich, UK, 2004.
28. Fardell, P. J., Murell, J. M., and Murell, J.V., "Chemical 'Finger print' studies of fire atmospheres," Fire and Materials, Vol. 10, pp. 21-28, 1986.
29. Fardell, P.J., Purser, D.A., Puser, J.A., Marshall, N.R., and Clark, P., "Fires in reduced oxygen conditions," Interflam 2004, pp. 129-142, 2004.
30. Fei, Y., Jianjun, Z., Yanghui, Z., Peide, L., Lin, J.Z., and Chow, T.T., "Preliminary real-scale experimental studies on cable fires in plenum," J. of Fire Sciences, Vol. 20, pp. 465-484, November 2003.
31. Ferziger, J. H., and Perić, M., "Computational methods for fluid dynamics," Springer-Verlag, 3rd Edition, Germany, 2002.
32. Fire Statistics and Social Research,"Fire statistics monitor up to 2005," Prepared by Fire Statistics & Social Research branch UK, Issue no. 03/06, 31 October 2006.
33. Fletcher, D. F., Kent, J. H., Apte, V. B., and Green, A. R., "Numerical simulation of smoke movement from a pool fire in a ventilated tunnel," Fire Safety Journal, Vol. 23, pp. 305-325, 1994.
34. Floyd, J. E., McGrattan, K. B., Hostikka, S., and Baum, H. R., "CFD fire simulation using mixture fraction combustion and finite volume radiative heat transfer," J. of Fire Protection Engineering, Vol. 13, pp. 11-36, 2003.
35. Galea, E.R., "On the field modelling approach to the simulation of enclosure fires," J. Fire Protection Eng., Vol. 1(1), pp. 11-22, 1989.
36. Galea, E.R., Gwynne, S., Lawrence, P.J., Filippidis, L., and Blackshields, D., "buildingEXODUS V4.0 – User guide and technical manual," 2004.

37. Galea, E.R., Knight, B., Patel, M., Ewer, J., Petridis, M., and Taylor, S., "SMARFIRE V 2.01 build 365, User Guide and Technical Manual," SMARTFIRE CD, 1999.
38. Gann R. G., "On the use of bench-scale smoke toxicity data in fire hazard and risk assessment," Interflam 2004, 10th Proceedings. Volume 2. July 5-7, 2004.
39. Gann, R.J., Babrauskas, V., and Peacock, R.D., "Fire conditions for smoke toxicity measurements," Fire and Materials, vol. 18 (3), pp. 193-199, 1994.
40. Gottuk, D. T., "The generation of carbon monoxide in compartment fires," National Institute of Standards and Technology, Report NBS-GCR-92-619, 1992b.
41. Gottuk, D. T., and Roby, R. J., "Effect of combustion conditions on species production," SFPE hand book, 2nd edition, Section 2/ Chapter 7, 1995.
42. Gottuk, D. T., Roby, R. J., and Beyler, C. L., "The role of temperature on carbon monoxide production in compartment fires," Fire Safety Journal, Vol. 24, pp. 315-331, 1995.
43. Gottuk, D. T., Roby, R. J., and Beyler, C. L., "A study of carbon monoxide and smoke yields from compartment fires with external burning," 24th Symp. (Int.) on Combustion, The Combustion Institute, Pittsburgh, PA, pp. 1729-1735, 1992c.
44. Gottuk, D.T., Roby, R.J., M.J. Peatross, and C.L. Beyler, "Carbon monoxide production in compartment fires," J. of Fire Protection Engineering, 4, pp. 133-150, 1992a.
45. Grayson, S.J., Van Hees, P., Vercellotti, U., Breulet, H., and Green, A., "Fire performance of electric cables," Final report on the European Commission SMT Programme Sponsored Research Project, SMT4-CT96-2059, 2000.
46. Green, A., "Development of a composite pyrolysis model for prediction of the heat release rate from cables by means of material testing in the cone calorimeter," Interflam 2001, 2, pp. 1107-1116, 2001.
47. Gwynne, S., Galea, E., R.,Lawrence, L. and Filippidis, L., "Modelling Occupant interaction with fire conditions using the buildingEXODUS evacuation model," Fire Safety Journal, 36, pp 327-357, 2001.
48. Gwynne, S., Galea, E.R., and Lawrence, P.J., "The Introduction of social adaptation within evacuation modelling," Fire and Materials, Vol 30(4), pp 285-309, 2006.

49. Gwynne, S., Galea, E.R., Owen, M., and Lawrence, P.J., "A review of the methodologies used in evacuation modelling," Fire and Materials, Vol 23(6), pp 383-389, 1999.
50. Hall, J.R., "Burns, Toxic gases, and other hazards associated with fires: Deaths and injuries in fire and non-fire situations," National Fire Protection Association, November 1997.
51. Hamaker, H.C., Philips Research Repts., 2: 55, 103, 112, 420, 1947.
52. Harlow, F. H. and Welch, J. E., "Numerical calculation of time-dependent viscous incompressible flow of fluid with free surface," Physics of Fluids, Vol. 8, pp. 2182-2189, 1965.
53. Hermansson, A., Hjertberg, T., and Sultan, B-A., "The flame retardant mechanism of polyolefins modified with chalk and silicone elastomer," Fire and Materials, 27, pp. 51-70, 2003.
54. Hirschler, M.M, Debanne, S.M., Larsen, J.B., and Nelson, G.L., "Carbon monoxide and human lethality: Fire and Non-fire studies," Elsevier Applied Science, New York, 1993.
55. Hossain, M. S., and Rodi, W., "A turbulence model for buoyant flows and its application to vertical buoyant flows," Turbulent Buoyant Jets and Plumes, Ed. Rodi, W., Pergamon UK, pp. 121-178, 1982.
56. Hull, T.R., Carman, J.M., and Purser, D.A., "Prediction of CO evolution from small-scale polymer fires," Polymer International, 49, pp. 1259-1265, 2000.
57. Hull, T. R., Lebek, K., and Paul, K. T., "Correlation of toxic combustion product yields from tube furnace tests and large scale fires," Fire Safety Science – Proc. of the 8th Int. Symp., pp. 1059-1070, 2005.
58. Hyde, S. M., "Field modeling of carbon monoxide production in vitiated compartment fires," PhD thesis, Cranfield University, 2000.
59. Hyde, S. M., and Moss, J. B., "Modelling of CO production in vitiated compartment fires," Fire Safety Science – Proc. of 7th Int. Symp., pp. 395-406, 2002.
60. IEC/ TS 60695-7-50, "Toxicity of fire effluent- Estimation of toxic potency – Apparatus and test method," 2002.
61. ISO/ IEC TR 9122-1, "Toxicity testing of fire effluents-Part 1," ISO, CP 56, 1989.

62. ISO, "Toxicity testing of fire effluents – Part 1," Technical Report, 9122-1, (E), 1989.
63. ISO/ DIS 19703, "Generation and analysis of toxic gases in fire – Calculation of species yields, equivalence ratios and combustion efficiency in experimental fires," 2004.
64. ISO 9705:1993(E), "Fire Tests – Full scale room tests for surface products," International Standards Organisation, Geneva, 1993.
65. Jason, E, F., Kevin, B, M., "Multiple parameter mixture fraction with two-step combustion chemistry for large eddy simulation," Interflam 2007, vol. 2, pp. 907-917, 2007.
66. Jia, F., Galea, E. R., and Patel, M. K., "The prediction of fire propagation in enclosure fires," Fire Safety Science – Proc. of 5th Int. Symp., pp. 345-354, 1997.
67. Jin, T., "Visibility through fire smoke," J of Fire and Flammability, 9, 135-155, 1978.
68. Jin, T. and Yamada, T., "Experimental Study of Human behaviour in smoke filled corridors," In: T. Wakamatsu, Y. Hasemi, A. Sekizawa, P. Seeger, P. Pagni and C. Grant (Eds.) Fire Safety Science Proceedings of the Second International Symposium, Hemisphere Publishing Company, New York, 561-570, 1989.
69. Karlsson, B., Quintiere, J., "Enclosure Fire Dynamics," CRC Press, 2001.
70. Karter, Jr., M. J., "Fire loss in the United States during 2005 – Full report," NFPA, USA, September 2006.
71. Kawagoe, K., "Fire behaviour in rooms," Technical Report 27, The buiding Research Institute (Japan), 1958.
72. Kee, R. J., Miller, J. A., and Jefferson, T. H., "CHEMKIN: A general purpose, problem-independent, transportable, Fortran Chemical Kinetics code package," Sandia National Laboratories, SAND80-8003, pp. 197, 1980.
73. Kee, R.J., Rupley, F.M. & Meeks, E., "CHEMKIN III: A Fortran chemical kinetics package for the analysis of gas-phase chemical and plasma kinetics," Sandia National Laboratories, SAND87-8215B (UC-4), 1996.
74. Kuo, K. K., "Principles of combustion," John Wiley & Sons, 1986.
75. Wells, L. K., "LabVIEW Student Edition : User's Guide", Prentice Hall, 1995.

76. Lattimer, B. Y., Vandsburger, U., and Roby, R. J., "The transport of high concentrations of carbon monoxide to locations remote from the burning compartment," NIST-GCR-97-713 Report, NIST, 1997.
77. Lattimer, B.Y., Vandsburger, U., and Roby, R.J., "Species transport from post-flashover fires," Fire Technology, 41, pp. 235-254, 2005.
78. Launder, B. E., and Spalding, D. B., "The numerical computation of turbulent flows," Computational Methods in Appl. Mech. Engg., Vol. 3, pp. 269-289, 1974.
79. Lebek, K., "Investigation of Fire Toxicity of Polymer Materials and Cables," PhD thesis, Fire Materials Laboratory, CMRI, Univ. of Bolton, UK, April 2007.
80. Leoz Arguelles, V., "Latest developments in the implementation of the construction products directive," 3rd Conf. Fire Safety and the use of Plastics in Buildings, Brussels, March 1999.
81. Leung, C. H., Staggs, J. E. J., Brindley, J., McIntosh, A. C., and Whiteley, R. H., "The effects of an inert central core on the thermal pyrolysis of an electrical cable," Fire Safety Journal, Vol. 34, pp. 143-168, 2000.
82. Lim, C., Masters Thesis, California Institute of Technology (1984). Also available as: Zukoski, E. E., Kubota, T., and Lim, C. S., Government Contractor's Report GCR-85-493, National Bureau of Standards, May 1985.
83. Liu, F., and Wen, J.X., "The effect of turbulence modelling on the CFD simulation of buoyant diffusion flames," Fire Safety Journal, Vol. 37, pp. 125-150, 2002.
84. Liu, Y., and Rogg, B., "Prediction of radiative heat transfer in laminar flames," Combustion Science and Technology, vol. 118, pp. 127-145, 1996.
85. Lönnermark, A., Blomqvist, P., Mansson, M., and Persson, H., "TOXFIRE – Fire characteristics and smoke gas analysis in under-ventilated large-scale combustion experiments: Tests in the ISO 9705 Room," SP Report 45, SP Swdish National Testing and Research Institute, Boras, Sweden, 1997.
86. Luo, M., and Beck, V., "The fire environment in a multi-room building – comparison of predicted and experimental results," Fire Safety Journal, Vol. 23(4), pp. 413-438, 1994.
87. Luo, M., and Beck, V., "A study of non-flashover and flashover fires in a full-scale multi-room building," Fire Safety Journal, Vol. 26, pp. 191-219, 1996.

88. Luo, M., and Beck, V., "Stoichiometric combustion model with oxygen threshold improved predictions for fire simulation using a CFD model," Fire Safety Science – Proc. of fifth int. symp., pp. 559-570, 1997.
89. Luo, M., He, Y., Beck, V., "Application of field and two-zone model to flashover fires in a full-scale multi-room single level building," Fire Safety Journal, 29, pp. 1-25, 1997.
90. Magnussen, B.F. and Hjertager, B.H., "On mathematical modelling of turbulent combustion with special emphasis on soot formation and combustion," 16th Int. symp. on combustion, The Combustion Institute, 1977.
91. Mahalingam, A., Jia, F., Patel, M.K., and Galea, E.R., "Modelling generation and transport of toxic combustion products in enclosure fires using bench-scale test data," Vol. 2, pp. 1631-1636, Interflam 2007.
92. Mitler, H.E., "Mathematical modelling of enclosure fires," Numerical Approaches to Combustion Modelling, AIAA, 1991.
93. Morehart, J.H., Zukoski, E.E and Kubota, T., "Species produced in fires burning in two-layered and homogeneous vitiated environments," Technical Report NBS-GCR-90-585, National Institute of standards and Technology, 1990.
94. Morikawa, T., Yanai, E., Okada, T., and Sato, K., "Toxicity of the atmosphere in an upstairs room caused by inflow of fire effluent gases rising from a burn room," Journal of Fire Sciences, Vol. 11, pp. 195-209, 1993.
95. Moss, B., "CFD simulation of cable tray fires," Interflam 2001, 2, pp. 1129-1140, 2001.
96. Mulholland, G.W., "Position paper regarding CO yield," Appendix C in Nelson, H.E., FPETOOL: Fire Protection Engineering Tools for Hazard Estimation, Technical Report NISTIR 4380, National Institute of standards and Technology, pp.93-100, 1990.
97. NFPA Report, "Carbon Monoxide Risks at Home Fact Sheet," National Fire Protection Association, 2000.
98. Nicol, D.G., Malte, P.C., Hamer, A. J., Roby, R. J., and Steele, R.C., "Development of a five-step global methane oxidation – NO formation mechanism for lean-premixed gas turbine combustion," Trans. of the ASME, vol. 121, pp. 272-280, April 1999.

99. Novozhilov, V., "Computational fluid dynamics modelling of compartment fires," Progress in Energy and Combustion Science, 27, pp. 611-666, 2001.

100. ODPM Report, "Fire statistics United Kingdom 2005," Office of the Deputy Prime Minister: London, March 2007.

101. Park J., Gwynne S., Galea E.R., and Lawrence P., "Validating the buildingEXODUS evacuation model using data from an unannounced trial evacuation," Proc 2nd Int Pedestrian and Evacuation Dynamics Conference, Ed: E.R.Galea, CMS Press, Greenwich, UK, ISBN 1904521088, pp295-306, 2003.

102. Patankar, S. V., "Numerical heat transfer and fluid flow," Hemisphere Publishing Corporation, Taylor & Francis Group, New York, 1980.

103. Patankar, S. V. and Spalding, D. B., "A calculation procedure for heat, mass and momentum transfer in three-dimensional parabolic flows," Int. J. Heat and Mass Transfer, Vol. 15, pp. 1787, 1972.

104. Patankar, S. V., and Spalding, D. B., "A computer model for three-dimensional flow in furnaces," 14th Symp. (Int.) on Combustion, pp. 605-614, 1973.

105. Peacock, R. D., Davis, S., and Babrauskas, V., "Data for room fire model comparisons," Journal of Research of the National Institute of Technology and Standards, Vol. 96(4), 1991.

106. Peters, N., "Lamina diffusion flamelet models in non-premixed turbulent combustion," Prog. Energy Combustion Sciences, 10, pp. 319-339, 1984.

107. Peters, N., "Reduced reaction mechanics," In: Peters, N., Rogg, B., editors, "Reduced mechanisms for applications in combustion systems," Berlin: Springer, [Chapter 3], 1992.

108. Pitts, W. M., "Reactivity of product gases generated in idealized enclosure fire enviroments," In 24th Int. Symp. On Combustion, The Combustion Institute, Pittsburgh, pp. 1737-1746, 1992.

109. Pitts, W. M., "The Global Equivalence Ratio concept and the prediction of carbon monoxide formation in enclosure fires," NIST Monograph 179, National Institute of Standards and Technology, 1994.

110. Pitts, W. M., "Application of thermodynamic and detailed chemical kinetic modeling to understanding combustion product generation in enclosure fires," Fire Safety Journal, Vol. 23, pp. 271-303, 1994.

111. Pitts, W. M., "The global equivalence ratio concept and the formation mechanisms of carbon-monoxide in enclosure fires," Progress in Energy and Combustion Science, 21, pp. 197-237, 1995.

112. Pitts, W. M., "An algorithm for estimating carbon monoxide formation in enclosure fires," Fire Safety Science, Proceedings of the 5th Int. Symp., pp. 535-546, 1997.

113. Pitts, W.M., "Toxicity yield - Technical Basis for Performance Based Fire Regulations," Proceedings of United Engineering Foundation Conference, United Engineering Foundation, Inc., San Diego, USA, January 7-11, 2001.

114. Purser, D. A., "Toxicity assessment of combustion products," The SFPE Handbook of Fire Protection Engineering, 2nd Edition, NFPA, 1995.

115. Purser, D.A., "People and Fire," Inaugural lecture series at The University of Greenwich, 17th February 1999.

116. Purser, D. A., Fardell, P. J., Rowley, S. Vollam, S., Bridgeman, B., and Ness, E. M., "An improved tube furnace method for the generation and measurement of toxic combustion products under a wide range of fire conditions Proceedings of the Flame Retardants '94 Conference, Interscience Communications, London, pp. 263-274, 1994.

117. Quintiere, J.G., "Fundamentals of enclosure fire zone models," J. of Fire Protection Engineering, 1, 1989.

118. Rhie, C.M., Chow, W.L., "Numerical study of the turbulent flow past an isolated airfoil with trailing edge separation," AIAA Journal, Vol. 21 No.11, pp.1525-32, 1982.

119. Richard Hull, T., Carman, J. M., and Purser, D. A., "Prediction of CO evolution from small-scale polymer fires," Polymer International, 49, pp. 1259-1265, 2000.

120. Richard Hull, T., Quinn, R. E., Areri, I. G., and Purser, D. A., "Combustion toxicity of fire retarded EVA," Polymer Degradation and Stability, 77, pp. 235-242, 2002.

121. Richard Hull, T., Lebek, K., and Paul, K. Y., "Correlation of toxic product yields from tube furnace tests and large scale fires," Fire Safety Science – 8th Int. Symp., pp. 1059- 1070, October 2005.

122. Robinson, J. E., "The Euroclassification of cables," Eurocable, 1999.

123. Robinson, J. E., "The impact of cable fires on building evacuation," Workshop on Impact of cable fires on building evacuation, BSI London, 17th October 2006.
124. Robinson, J. E., Samson, F., and Sultan, B., "The development of toxic gas yield in a format suitable for evacuation modelling," Interflam'04, pp. 781-786, 2004.
125. Rockett, J.A., "Fire induced gas flows in an enclosure," Combustion Science and Technology, 12, 1976.
126. Rodi, W., "Calculation of stably stratified shear layer flows with buoyancy extended k-ε turbulence model," Turbulence and Diffusion in Stable Environments, Ed. Hunt J.C.R., Oxford UK, Clarendon Press, pp. 111-140, 1985.
127. Rogg, B., RUN-1DL manual, 1998.
128. SP Report, "Labyrinth project full scale tests in a corridor arrangement," BRs 6119, SP Swedish National Testing and Research Institute, 2006.
129. Spalding, D.B., "Mixing and chemical reaction in steady confined turbulent flames," 13th Int. symp. on combustion, The Combustion Institute, 1971.
130. Steckler, K. D., Quintiere, J. G, and Rinkinen, W. J., "Flow induced by fire in a compartment," Technical Report NBSIR 82-2520, National Bureau of Standards, 1982.
131. Sultan, B-Å, and Paul, K. T., "Combustion atmosphere toxicity of polymeric materials intended for internal cables," FROCC Symposium, Koln, March 2002.
132. Sung, A. C. M., Chow, W. K., Han, S. S., Gao, Y., Dong, H., and Zou, G. W., "Preliminary full-scale burning tests of electric cables," Journal of Applied Fire Science, Vol. 121(4), pp. 335-352, 2004.
133. Takeda, H., and Yung, D., "Simplified fire growth models for risk-cost assessment in apartment buildings," J. Fire Protection Engg., vol. 4, pp. 53-66, 1992.
134. Tewarson, A., "Fully developed enclosure fires of wood cribs," 20th Symposium (International) on Combustion, pp. 1555-1566, 1984.
135. Tewarson, A., "Generation of heat and chemical compounds in fires," SFPE Handbook of Fire Protection Engineering, pp. 3.53 – 3.124, 1995.

136. Tewarson, A., Chu, F., and Jiang, F.H., "Combustion of Halogenated Polymers," Fire Safety Science – Proc. of the fourth int. symp., pp. 563-574, 1994.

137. Tewarson, A., Jiang, F.H., and Morikawa, T., "Ventilation controlled combustion of Polymers," Combustion and Flame, 95, pp. 151-169, 1993.

138. Toner, S. J., Zukoski, E. E. and Kubota, "Entrainment, Chemistry, and Structure of Fire Plumes," Technical Report NBS-GCR-87-528, National Institute of standards and Technology, 1987.

139. Tsuchiya, Y., "CO/CO_2 ratios in fire," Fire Safety Science – Proc. of fourth int. symp., pp. 515-528, 1994.

140. Tsuchiya, Y., "Chemical modelling of fire gases," J. Fire Science, vol. 13, pp. 214-223, 1995.

141. Tuovinen, H., "Simulation of combustion and fire-induced flows in enclosure," Report LUTVDG/(TVBB-1010), Lund University, 1995.

142. Van Doormal, J. P. and Raithby, G. D., "Enhancements of the SIMPLE method for predicting incompressible fluid flows," Numerical Heat Transfer, Vol. 7, pp. 147-163, 1984.

143. Versteeg, H. K., and Malalasekera, W., "An introduction to computational fluid dynamics," Prentice Hall, UK, 1995.

144. Wang, Z., "Predicting toxic gas concentrations resulting from enclosure fires using the local equivalence ratio concept linked to fire field models," PhD Thesis, School of Computing and Mathematical Sciences, The University of Greenwich, London, UK, 2006.

145. Wang, Z., Jia, F., Galea, E.R., "Applying the local equivalence ratio concept to fire field models," Interflam 2001, 2, pp. 1409-1414, 2001.

146. Wang, Z., Jia, F., Galea, E.R., "Predicting toxic gas concentrations resulting from enclosure fires using local equivalence ratio concept linked to fire field models," Fire and Materials, Vol. 31(1), pp. 27-51, 2007.

147. Wang, Z., Jia, F., Galea, E.R., and Ewer, J., "Predicting HCl concentrations in fire enclosures using an HCl decay model coupled to a CFD-based fire field model," Fire and Materials, Vol. 31(1), pp. 27-51, 2007.

148. Warnatz, J., "Combustion Chemistry," Edited by Gardiner, W. C., Springer-Verlag, New York, pp. 224-232, 1984.

149. Welch, S., "Development and validation of a comprehensive model for flame spread and toxic products in full-scale scenarios Proceedings of Workshop on Fire Growth and Spread on Objects," 4-6 March, 2002, National Institute of Standards and Technology, Gaithersburg, Maryland, USA.
150. Wen, J.X., and Huang, L.Y., "CFD modelling of confined jet fires under ventilation-controlled conditions," Fire Safety Journal, Vol. 34, pp. 1-24, 2000.
151. Wen, J.X., and Huang, L.Y., and Roberts, J.J., "The effect of microscopic and global radiative heat exchange on the numerical predictions of compartment fires," Fire Safety Journal, Vol. 36(2), 2001.
152. Wieczorek, C.J., "Carbon Monoxide generation and transport from compartment fires," PhD thesis, Virginia Polytechnic Institute and State University, 2003.
153. Woodburn, P.J., and Britter, R.E., "CFD simulations of a tunnel fire – Part II," Fire Safety Journal, Vol. 26, pp. 63-90, 1996.
154. Woolley, W. D., and Fardell, P. J., "Basic aspects of combustion toxicology," Fire Safety Journal, vol. 5(1), pp. 29-48, 1982.
155. Yeoh, G. H., Yuen, R.K.K., Chueng, S.C.P., and Kwok, W.K., "On modelling combustion, radiation and soot process in compartment fires Building and Environment," Vol. 38, pp. 771-785, 2003.
156. Yeoh, G. H., Yuen, R. K. K., Lo, S. M., and Chen, D. H., "On numerical comparison of enclosure fire in a multi-compartment building," Fire Safety Journal, Vol. 38, pp. 85-94, 2003.
157. Zukoski, E. E., Kubota, T., and Lim, T., "Experimental study of environment and heat transfer in a room fire," National Bureau of Standards Government Contractor's Report, GCR-83-493, April, 1987.
158. Zukoski, E. E., Morehart, J. H., Kubota, T., and Toner, S. J., Combustion and Flame, Vol. 83, pp. 324 – 332, 1991.
159. Zukoski, E. E., "The growth of fire-ignition to full involvement," Combustion Fundamentals of Fire, Chapter 3, Academic Press, 1995.
160. Zukoski, E. E., Toner, S. J., Morehart, J. H, and Kubota, T., "Combustion processes in two-layered configurations," Fire Safety Science – Proceedings of the 2nd Int. Symp., Hemisphere, Washington, D. C., pp. 295-304, 1989.